

INVESTIGATIONS ON BROADBAND PLANAR DIPOLE ANTENNAS

A THESIS SUBMITTED BY
SUPRIYO DEY
IN PARTIAL FULFILMENT OF THE REQUIREMENTS
FOR THE DEGREE OF
DOCTOR OF PHILOSOPHY

DEPARTMENT OF ELECTRONICS
FACULTY OF TECHNOLOGY
COCHIN UNIVERSITY OF SCIENCE AND TECHNOLOGY
KOCHI 682 022
INDIA

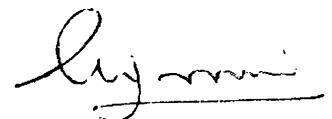
DECEMBER 1993

*"Education is a progressive discovery
of our own ignorance"*

Will Durant

CERTIFICATE

This is to certify that the thesis entitled "**Investigations on Broadband Planar Dipole Antennas**" is a bona fide record of the research work carried out by Mr. Supriyo Dey under my supervision in the *Department of Electronics, Cochin University of Science and Technology*. The results embodied in this thesis or part of it have not been presented for any other degree.



(Dr. K. G. NAIR)
(Supervising Teacher)
Professor & Head
Dept. of Electronics
Cochin University of Sci. & Tech.

KOCHI 682 022
28th December 1993

DECLARATION

I hereby declare that the work presented in the thesis entitled "**Investigations on Broadband Planar Dipole Antennas**" is based on the original work done by me under the supervision of Dr. K. G. Nair, in the *Department of Electronics, Cochin University of Science and Technology*, and that no part thereof has been presented for the award of any other degree.

KOCHI 682 022
28th December 1993


(SUPRIYO DEY)

ACKNOWLEDGEMENTS

1

First and foremost I would like to express my profound gratitude to my research guide Dr. K. G. Nair, Professor and Head, Department of Electronics, Cochin University of Science and Technology, for his invaluable help in the course of this study. This thesis is the outcome of education, able guidance, encouragement and inspiration I received from him.

Sincere thanks are due to Dr. C. S. Sridhar, Dr. K. G. Balakrishnan, Professors of Department of Electronics, for their valuable suggestions and encouragements during the tenure of this work.

I am particularly indebted to Dr. P. Mohanan, Reader of this department, for his inestimable suggestions and invaluable help during the course of this work. Special thanks are due to Dr. K. Vasudevan and Dr. K. T. Mathew, Readers of this department for the keen interest they have shown in my work.

My acknowledgement would be incomplete if a mention is not made of the kind cooperation and valuable suggestions I received from Dr. C. K. Aanandan, Lecturer, Department of Electronics.

I owe special debt to Dr. K. A. Jose, Research Associate, PennState University, USA, Dr. K. K. Narayanan, Research Associate, Department of

Electronics and Mr. V. Ajaikumar, USA, for their help and encouragement in various ways.

I take this opportunity to express my sincere thanks to all the members of faculty, laboratory and non-teaching staffs and research scholars of the department, who served as beacon and made my stay in Kochi a memorable one. While expressing my gratefulness to all of them, I would also like to place on record the splendid cooperation I received from my enjoyable colleagues Mr. J. Jagannath Bhat, Mr. U. Ravindranath, Mr. T. K. Mathew, Mr. S. Stephen, Mr. J. George and Mr. P. V. John, research scholars and Mrs. B. Aanandan, Librarian of this department, who sustained me with their encouragement and their affection during the period of my research work.

Thanks are also due to Dr. S. Rodrigues and Mr. W. Gomez, Lectures, St. Paul's College, Kochi, Dr. P. M. Joseph, Lecturer, Karunya Institute of Technology, Coimbatore, Mr. P. P. Thomson, Project associate, New South Wails University, Australia, Mr. Sreemoolanathan, Research scholar, Regional Research Laboratory, Trivandrum, Dr. P. V. Hunagund, Reader, Department of Applied Electronics, Gulberga University, Gulberga and Dr. P. Vanugopal, Scientist-C, NPOL, Kochi.

In the course of my research work I was enjoying UGC research fellowship. This financial support provided by UGC is greatly acknowledged.

I am indebted to one and all, who have enlightened me, in this short, but crucial period of life.

INVESTIGATIONS ON BROADBAND
PLANAR DIPOLE ANTENNAS

Contents

Chapter 1	Introduction	1
1.1	Waveguide antennas	2
1.1.1	Slot element design and development	3
1.1.2	Waveguide arrays	3
1.1.3	Dielectric waveguide arrays	5
1.2	Triplate antennas	5
1.2.1	Design of slot element	5
1.2.2	Triplate slotted arrays	6
1.3	Cavity backed printed antennas	6
1.3.1	Printed dipole elements	6
1.3.2	Cavity backed printed arrays	8
1.4	Microstrip antennas	10
1.4.1	Microstrip dipole antenna	12
1.5	Motivation for the present work	14
1.6	Brief sketch of the present work	15

Chapter 2	Review of past work in the field	16
2.1	Printed dipole antenna	16
2.1	Microstrip dipole antenna	27
Chapter 3	Methodology	42
3.1	Design and fabrication of antennas	42
3.1.1	Printed dipole	43
3.1.2	Microstrip dipole	47
3.2	Antenna feeding	47
3.3	Facilities utilised	50
3.3.1	Anechoic chamber	50
3.3.2	Network Analyser	52
3.3.3	Antenna positioner and controller	56
3.4	Method of measurements	57
3.4.1	Impedance	57
3.4.2	Radiation pattern	58
3.4.3	Gain	60
Chapter 4	Experimental results I: Printed dipoles	64
4.1	Flared printed dipole	66
4.1.1	Flaring angle	70
4.1.2	Arms overlapping	72
4.1.3	Arm width at feed point	72
4.1.4	Main arm to ground arm ratio	77
4.1.5	Design details	79
4.2	Triangular end-loaded printed dipole	83
4.2.1	Triangle dimensions	90
4.2.2	Arm width at feed point	90
4.2.3	Main arm to ground arm ratio	98
4.2.4	Flaring angle	98
4.2.5	Cavity backed triangular end-loaded printed dipole	106
4.2.6	Design details	112
4.3	Parallelogram end-loaded printed dipole	113
4.3.1	Cavity backed parallelogram end-loaded printed dipole	123
4.3.2	Design details	127

Chapter 5	Experimental results II: Microstrip dipoles	131
5.1	Triangular end-loaded microstrip dipole	132
5.1.1	Main arm length	134
5.1.2	Height of triangle	137
5.1.3	Apex angle	139
5.1.4	Design details	144
5.2	Triangular microstrip dipole	146
5.2.1	Balun length	148
5.2.2	Feed point location	148
5.2.3	Arms separation	151
5.2.4	Flaring angle	153
Chapter 6	Theoretical analysis	159
6.1	Rectangular microstrip patch	160
6.1.1	Derivation of the Green's function	160
6.1.2	Calculation of complex power	163
6.1.3	Space wave radiation	164
6.2	Rectangular printed dipole	165
6.3	Flared printed dipole	170
6.4	Triangular end-loaded printed dipole	172
6.4.1	Q of the triangle	173
6.4.2	Q of the remaining dipole	173
6.4.3	Q of the complete structure	175
Chapter 7	Conclusions	177
7.1	Inferences from the experimental studies	177
7.1.1	Printed dipole	178
7.1.2	Microstrip dipole	181
7.2	Conclusions from the theoretical analysis	183
7.3	Some practical applications of the present antennas	183
7.4	Scope of further work in the field	184
Appendix A	Development of an input impedance tunable circular patch antenna	186
A.1	Introduction	186

A.2	Antenna geometry and experimental set-up	187
A.3	Experimental results and discussions	187
A.4	Conclusions	189
Appendix B Performance study of YBCO superconducting wire loop antenna		192
B.1	Introduction	192
B.2	Antenna fabrication	194
B.2.1	Preparation of YBCO powder	194
B.2.2	Fabrication of antenna	194
B.3	Experimental set-up	195
B.4	Experimental results	195
B.5	Conclusions	199
References		200
Index		211
List of publications of the author		214

Introduction

An antenna is a device ordinarily used for both transmitting and receiving electromagnetic energy. It is an integral part of the radio communication system and accounts for a good deal of progress that has been made in this field during the last few decades.

The part of electromagnetic spectrum suitable for communication is limited. Although it is extended day-by-day, even with global allocation and system management, the problem of spectrum congestion continues to present formidable, if not unsurmountable, difficulty. Thus, many new designs of antennas/arrays are being developed to meet this challenge. Basically the spectral expansion is dominated by human motivation and different antenna configurations with various techniques have gradually been evolved, guided by multifarious technological needs. J. D. Kraus [1], the father of helical antennas rightly said,

"With mankind activities expanding into space, the need for antenna will grow to an unprecedented degree. Antennas will provide the vital link to and from everything out there. The future of antenna reaches to the stars."

Though the basic philosophy of antennas/arrays of transmitting or receiving electromagnetic energy remains unchanged, the characteristics, performance, shape and structure, may be drastically different and solely depend on the application. In recent years, due to rapid miniaturisation of electronic components, the antenna system is left out as the most bulky device in the equipment; the demand for smaller and light-weight antenna systems is thus evident. A commonly occurring requirement is, antennas with flat profile, that can be made conformal with the vehicle and aircraft bodies, or alternatively, ideally suited to manpack microwave systems. Typical applications include intruder alarm, aircraft radio altimeter, portable radar, microwave telecommunication and telemetry links. Now-a-days, light-weight flat arrays are being employed in missile guidance system. Ways of making antenna arrays flat and thin have featured strongly as a research area embracing both conventional waveguide components and newer printed assemblies. These types of antennas can be subdivided into four groups; *waveguide, stripline, printed cavity backed assembly* and finally *microstrip*.

1.1 WAVEGUIDE ANTENNAS

A suitably oriented slot in waveguide radiates and a linear array can be formed by placing several slots periodically along the waveguide run. A narrowband resonant array can be made by terminating the waveguide with a short. Alternatively, if the residue of the incident wave is absorbed by a load, a broadband travelling wave array is produced. Waveguide flat

profile array consists of several slotted waveguide sections placed in parallel and fed by either a bunched system of waveguides or more compact series waveguide feeds.

1.1.1 Slot element design and development

Some basic slot arrangements, together with their equivalent circuits are shown in Fig. 1.1. Stevenson [2] derived the equivalent R and G values using Babinet's principle assuming very thin waveguide walls. Oliner [3] extended the treatment to obtain Z and Y for finite wall thickness. The basic nature of the slot pattern is that of a Hertzian magnetic dipole element embedded in a conducting plane. Various modifications in fundamental slot design, *eg.*, V-slot, cross-slot, dielectric coating *etc.*, have been done by numerous researchers to improve the antenna performance or to modify the radiation characteristics.

1.1.2 Waveguide arrays

For resonant type arrays, the radiating elements are normally placed $\lambda_g/2$ apart and are arranged to produce alternately antiphase radiation. Here λ_g is the wavelength in the waveguide. Such an array shows very narrow bandwidth, typically less than 1%, but with a broadside beam [4]. Bandwidth constrain can be removed by using travelling wave type array, sketched in Fig. 1.2, by spacing the radiating slots slightly different from $\lambda_g/2$ so that in a long array, a stable cycle is set up in which reflected waves from the slot conductances are essentially cancelled by the effect of spacing. However, in this type of array the main beam squints with frequency which is a disadvantage in most applications, except in the case of frequency scanning antennas.

1.1.3 Dielectric waveguide arrays

The recent requirement for millimeter wave radar equipment has triggered the interest in the design of new type of antennas for this frequency range, where metal waveguides exhibit unacceptable losses. New type of dielectric waveguide structure with periodic metallic perturbations has been investigated by many researchers [5,6], which also allows some degree of beam scanning.

1.2 TRIPLATE ANTENNAS

A triplate transmission line, often referred to as *stripline*, consists of a flat conducting strip sandwiched between two grounded dielectric substrates. The guided wave is confined between the ground planes in the vicinity of the central conductor and the basic mode of propagation is a *transverse electric magnetic wave* [7]. Stripline is thinner, lighter and low cost guiding structure than the conventional waveguide and can be made to radiate in a similar fashion by creating slots in one of the ground planes.

1.2.1 Design of the slot element

Oliner [8] derived an approximate expression for the calculation of a slot in a ground plane fed by a symmetrically placed strip. Berthaupt [9] extended this to include asymmetrically fed slots. An accurate calculation of slot susceptance is difficult due to the presence of higher order modes; in particular so called *parallel plate mode*. In practice, higher order modes are undesirable if several slots have to be fed from one single stripline. A technique to reduce it is to place metal pins around the slot, as shown in Fig. 1.3. This technique makes the slot element design reliant on trial and error method.

1.2.2 Triplate slotted arrays

Despite the empirical nature of design method for triplate slot elements, several useful antenna arrays have been developed using dielectric filled triplate structure [10,11]. To improve the array performance, various multilayered triplate assemblies have also been developed. For arrays operating above 10 GHz, minimum attainable side-lobe level is -25 dB.

Another feed arrangement that dispenses with symmetrically dielectric loaded triplate is the microstrip fed slot antenna, shown in Fig. 1.4, used as radiating element in array configuration [12]. In such elements, feed losses and side-lobe level control seem to have severe constraints.

1.3 CAVITY BACKED PRINTED ANTENNAS

Much expertise on conventional wire antenna has accumulated over some fifty years, and it is well known that the wires need not be cylindrical but can be flattened into strips. The idea of printing dipoles as flat conducting strips on a substrate then follows logically. This concept has produced some very important light weight planar arrays and bandwidth obtained are comparable with those of conventional antennas.

1.3.1 Printed dipole elements

There are numerous versions of printed dipoles available in the literature and two basic approaches are sketched in Fig. 1.5. One design (Fig. 1.5a) attributed to Wilkinson [13], uses metallisation on two sides of a microstrip line to produce a complete dipole, fed by

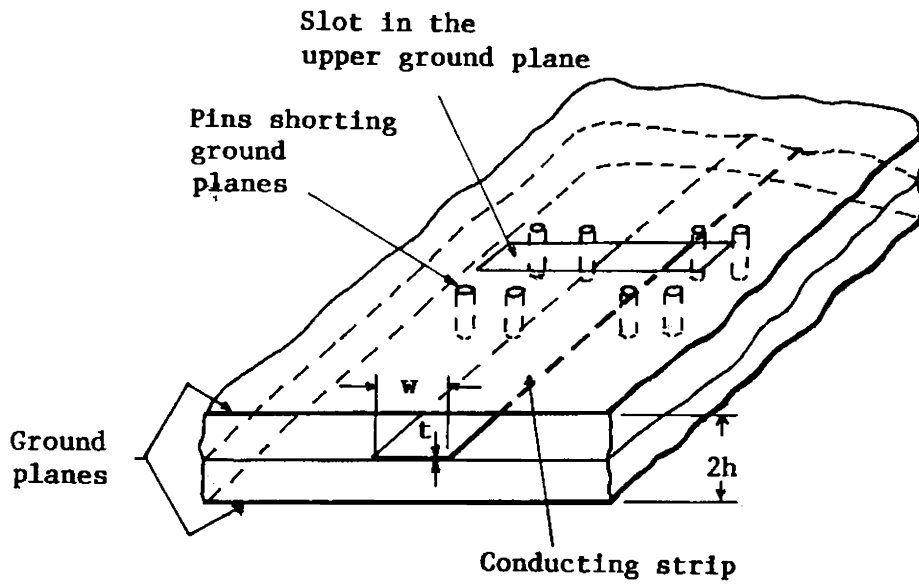


Fig. 1.3 Stripline slot radiator and feed arrangement showing shorting pins

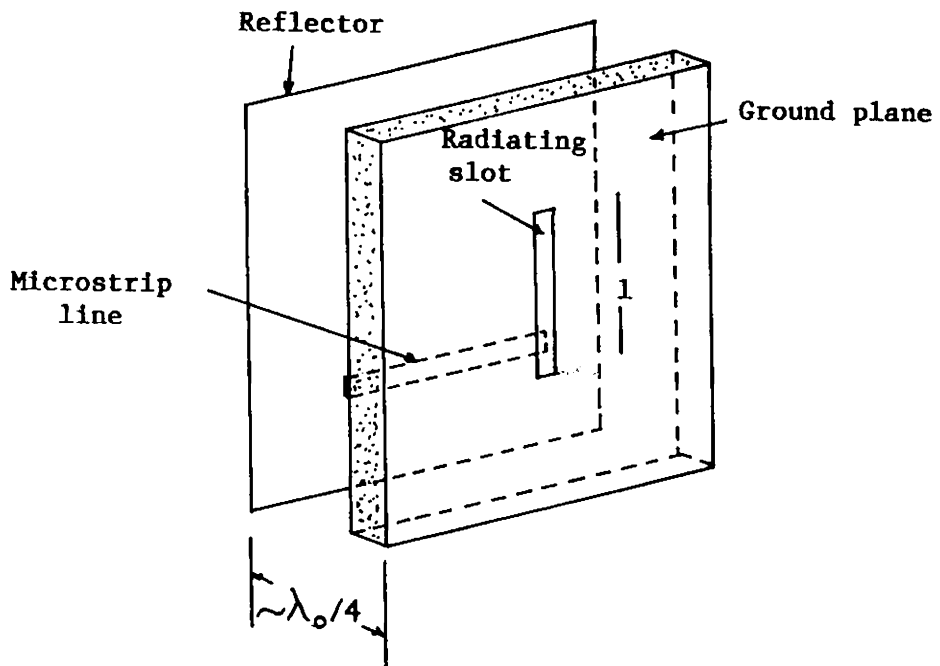


Fig. 1.4 Ground plane slot radiator

two-wire strip line in the plane of the dipole. This dipole and printed circuit distribution network are fabricated by two photographic exposures on a double side copper cladded dielectric sheet, and so, is a good example of low cost technology. Another convenient circuit for dipole design, shown in Fig. 1.5b, is a printed stripline folded dipole with Schiffman balun [14]. One major advantage of this antenna is that, it is printed in a single process, all on one side of the substrate and so is relatively inexpensive to produce. The only difference between these two antennas is in the near-field polarisation.

Some earlier attempts of printing dipole structures included a printed version of the conventional Franklin antenna, shown in Fig. 1.6a, by Fubini *et al.* [15] and a capacitively coupled dipole array by McDonough *et al.* [16], shown in Fig. 1.6b. These antennas were found to be of very narrow band.

Much of the recent efforts have been concentrated on evolving printed dipole elements that have wider bandwidth and a thinner structure. A successful design was created by Sidford [17] and is illustrated in Fig. 1.7; a printed dipole is placed within a coplanar slot to produce circular polarisation. A bandwidth of 5% for a VSWR < 2 was obtained together with 2 dB ellipticity. The antenna was very thin with substrate to ground plane spacing of $\lambda_v/12$. Dubost [18] modified this design to obtain linear polarisation and proposed various other wideband dipole designs, shown in Fig. 1.8, capable of producing linear as well as circular polarisation with very large bandwidth.

1.3.2 Cavity backed printed arrays

The main disadvantage of using printed dipole as radiating element in large array is radiation from feed network. To overcome this problem, travelling wave approach has been

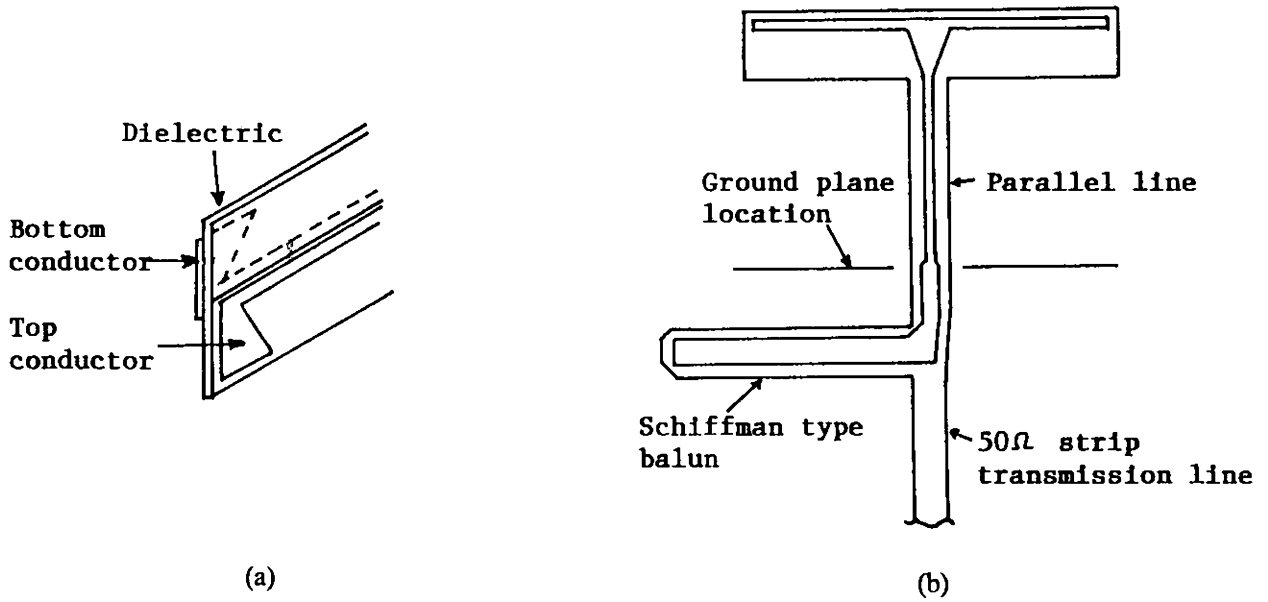


Fig. 1.5 Printed dipole antennas

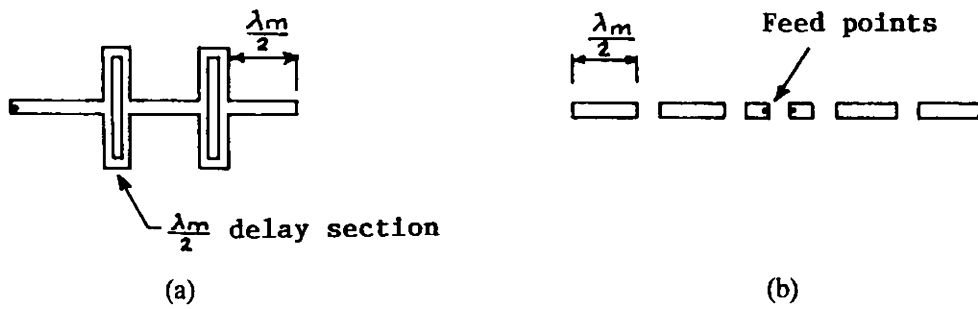


Fig. 1.6 Printed collinear dipole arrays
(a) Franklin antenna array
(b) Capacitively coupled array

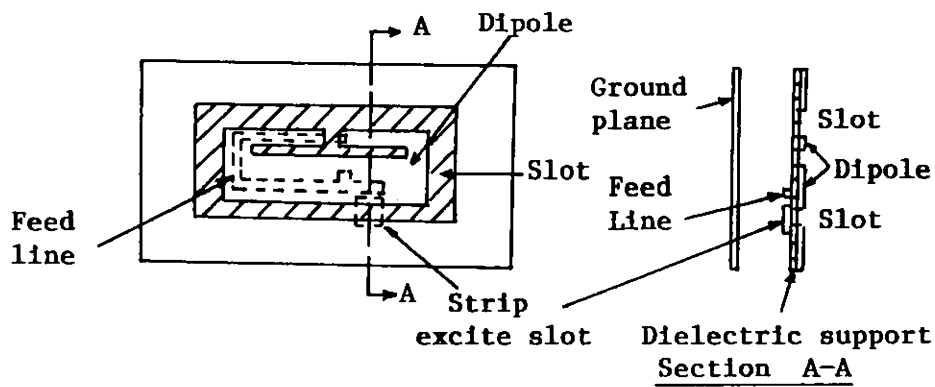


Fig. 1.7 Flat hybrid arrangement of slot radiator and embedded dipole element

coupled to sandwich wire antenna [19]. Later design improvement has been introduced by Graham [20] in the development of a monopulse array, shown in Fig. 1.9, having bandwidth of 40% and side-lobe level of -27 dB.

1.4 MICROSTRIP ANTENNAS

There is no doubt that viable alternatives to metal waveguide slotted arrays can now be constructed using the slotted stripline or cavity backup technique as cited above. Compared with waveguide antennas, these new types have the advantages in weight, thickness and cost but do involve a number of manufacturing processes. The ideal arrangement would allow the conductors together with the feed to be printed on a single substrate directly backed with ground plane. Such an assembly would show further saving of space, weight and cost and the resulting thin structure can be mounted conformally on the surface of a vehicle or a missile. In essence, this takes the cavity backed printed radiator to the extreme case when there is no air gap and the printed antenna and the feed line are on the upper surface of the substrate, while the lower surface is the ground plane. This leads directly to the microstrip antenna concept presented by Deschamps [21] in 1953 and separately by Gulton and Baissinot [22] in 1955. Except in few other papers, the interest in microstrip antenna concept did not emerge until around 70's. It was probably the need for conformal missile and spacecraft antennas that provide the impetus rather than the good selection of microwave substrates that were becoming available. First practical microstrip radiator was constructed by Byron [23] and shortly thereafter, a microstrip element was patented by Munson [24] in 1973. These remarkable achievements by Byron and Munson gave birth to

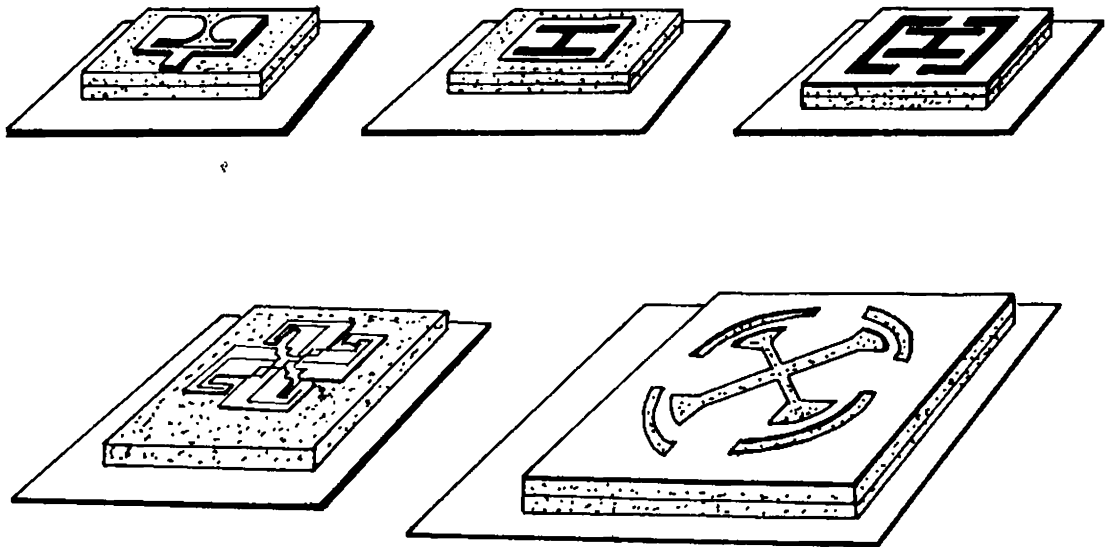


Fig. 1.8 Usual wideband printed dipoles

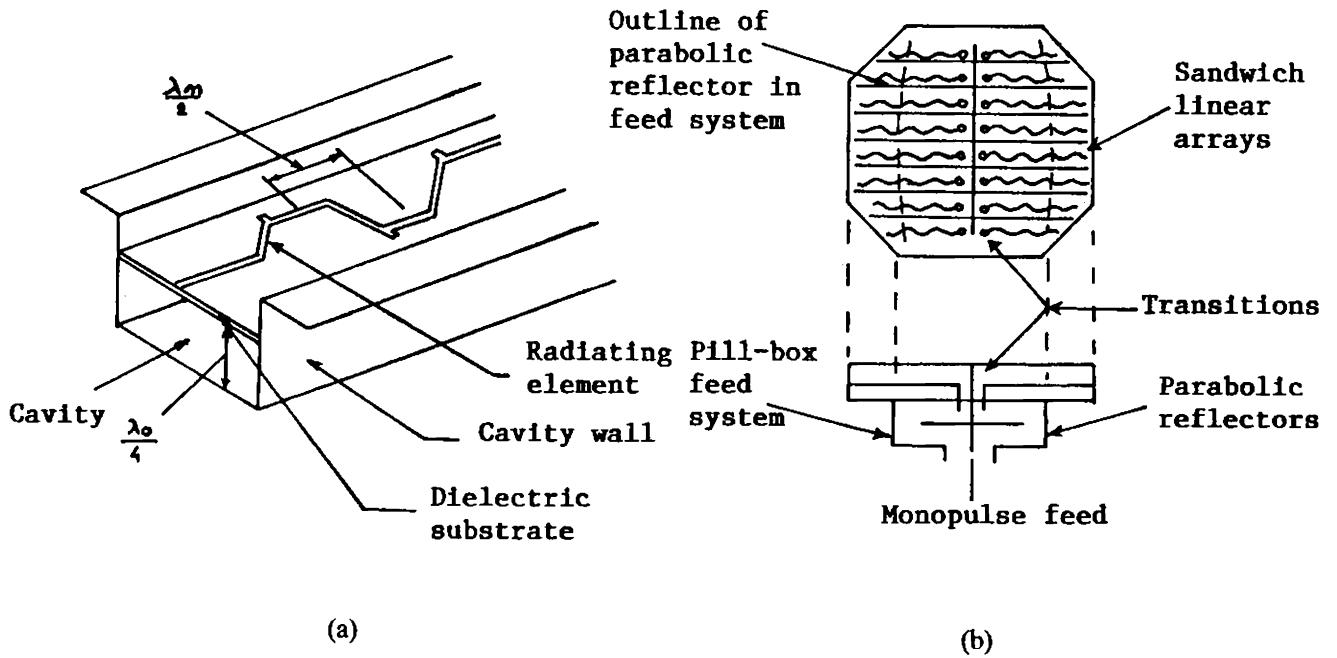


Fig. 1.9 Sandwich wire antenna
 (a) Basic configuration
 (b) Monopulse array showing pill-box feed in section

a new antenna industry and a number of research papers on various aspects of microstrip antennas were published in the succeeding years.

Microstrip antennas can be broadly classified into two categories; 1. *resonant type*, 2. *travelling wave type*. Travelling wave type antennas show large bandwidth compared to resonant type antennas but their radiation efficiency is relatively poor.

1.4.1 Microstrip dipole antenna

The microstrip dipole antenna is a resonant type antenna and is essentially same as rectangular patch antenna in the sense that it possesses almost all the characteristics of rectangular patch, like extremely narrow bandwidth and broad E and H-plane radiation patterns *etc.* The basic difference of microstrip dipole from rectangular patch is in terms of their dimensions. For, the latter, both side dimensions are comparable to wavelength while for the former, one side length is resonant and the other side is very thin. Also, the first resonance of printed dipoles, is a series type resonance, while that of a rectangular patch is parallel type. Fig. 1.10 shows microstrip dipole with different excitation mechanism. Microstrip dipole resembles the free space cylindrical dipoles in the sense that radiation results from a harmonically varying dipole moment. But the main difference of microstrip dipole from ordinary dipole near the ground is that impedance level is much higher in the case of microstrip dipoles. This higher impedance level is attributed to the fact that the microstrip dipole radiates power as space wave and also launches surface waves in the dielectric surface guide.

Microstrip dipoles are attractive elements in large array environment owing to their desirable properties such as design simplicity and smaller size compared to rectangular patch

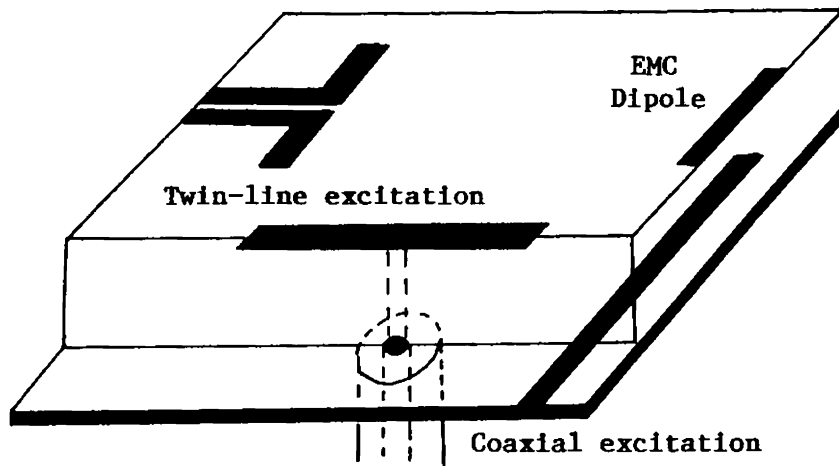


Fig. 1.10 Different excitation mechanisms for microstrip dipole

antennas. They are well suited for higher frequency operations, particularly in high millimeter wave range (> 100 GHz) where microstrip patch can not be used. Also at higher frequencies, the bandwidth is fairly good for thick substrates. It is also possible to alter the radiation properties by the use of a superstrate layer, making microstrip dipole a possible competitor in superstrate-substrate configuration.

1.5 MOTIVATION FOR THE PRESENT WORK

As discussed earlier, the impedance bandwidth of printed version of cylindrical dipole is not very broad and maximum bandwidth reported is around 37% by Baily [25]. Although considerable improvement in the impedance bandwidth of printed dipole is achieved by Dubost and others [18], it is at the expense of increase in design complexity. The motivation behind the present work is to optimise the printed cylindrical dipole structure for maximum impedance bandwidth while keeping the antenna design as simple as possible.

In the case of microstrip dipole, as explained in the preceding section, the impedance bandwidth is extremely narrow, around 1% - 2%. A design proposed by Oltman [26] shows considerable improvement in impedance bandwidth. But the feeding is done through electromagnetic coupling which decreases the radiation efficiency of the dipole. Work has also been carried out to improve the bandwidth of microstrip dipoles directly coupled to feedline.

1.6 BRIEF SKETCH OF THE PRESENT WORK

The scheme of the work presented in this thesis is given below:

A review of the important research work done in the field of planar dipoles is presented in Chapter 2. Special emphasis is given on various bandwidth enhancement techniques.

The methodology adopted for the experimental investigation is highlighted in Chapter 3. The details of fabrication of various antennas and the instruments utilised are described. The measurement techniques of various antenna characteristics are also discussed in detail.

The experimental procedure and the experimental results for printed dipoles and microstrip dipoles are presented in Chapter 4 and Chapter 5 respectively.

Chapter 6 extensively presents the theoretical analysis used to explain the experimental results. Comparison between theoretical and experimental results is also given.

The conclusions drawn from the investigations on planar dipole antennas, their various applications and the scope of further work in this field are discussed in Chapter 7.

The experimental results of a few investigations in the related field done by the author are incorporated in this thesis as two appendices. Appendix A deals with the design and development of a new type of circular microstrip antenna, matched with a 50Ω feedline. Fabrication and evaluation of superconducting circular wire loop antenna is discussed in Appendix B.

Planar dipole as a single isolated radiating element or as a radiating element in an array environment was studied, both theoretically and experimentally, by many researchers. In this chapter an overview of important works in the field of printed dipole and microstrip dipole is presented in chronological order.

2.1 PRINTED DIPOLE ANTENNA

The idea of printing dipole as a flat conducting strip on dielectric substrate was first utilised by Fubini *et al.* [15]. He fabricated a 6×5 element array of conventional Franklin antenna. The phase reversing sections were also printed along with the dipole elements. But the array was found to be narrow band.

A five-element capacitive-coupled printed dipole array was developed by McDonough *et al.* [16]. In this design, the center element was connected to the feed directly and the other elements were capacitively coupled to the driven element.

Stark [27] was the first to analyse the dipole array printed on a dielectric substrate, protruding over a ground plane. He calculated the active element impedance of such an infinite array by using appropriate Floquet mode expansions in a unit cell with one element. The theoretical active impedance was found to be a good approximation of a practical large array.

Kahrilas [28] used printed dipole as radiating element in the thinned aperture computed lens, in HAPDAR multi-functional phased array radar. The dipole arms were of rectangular shape and were etched on both sides of a thin dielectric substrate. The total number of elements in the array was 4300.

A printed dipole configuration, that can be fed with stripline, was developed and used by Hersch [29] to make a two element array. The VSWR of the array was less than 1.5 over a 5% bandwidth.

Klensch [30] developed an antenna array, consisting of 16 dipole elements and a corporate feed, for automatic vehicle identification system. The dipoles were of half wavelength. Half of the dipole patterns were etched on the top side of the board and the other half was etched on the bottom side of the board. To achieve unidirectional pattern, a cavity was placed behind the array.

The deployment of 256 printed dipoles in a X-band uniformly illuminated array was described by Wilkinson [13]. The elements along with the feed network were in the same plane. The array was mounted a quarter wavelength above the ground plane to produce

unidirectional radiation pattern. The losses in the radiating elements and the feed system was 3 dB and VSWR was less than 1.3 over a 5% bandwidth.

Sidford [17] used printed dipole placed within a coplanar slot and separated from ground plane by $\lambda_0/4$ to produce circular polarisation. The antenna showed a bandwidth of 5% for VSWR < 2 together with 2 dB ellipticity.

The transition from the balanced strip feeding for double sided printed S-band dipole to the coaxial line has been investigated in detail by Singh *et al.* [31]. They have also reported the optimum transition design, which gives minimum VSWR.

Othius [32] used thin rectangular dipoles printed on both sides of a substrate to form an array. The array was backed by a ground plane kept at quarter wavelength away, to produce unidirectional radiation pattern. He used this antenna array as a Doppler module for radar altimeter.

The concept of using printed dipoles at its first anti-resonance stage to achieve large bandwidth was introduced by Dubost [33]. Utilising this idea, he fabricated an array of symmetric dipoles. The dipole arms were etched on both sides of a substrate and fed by twin wire parallel strip line. The 2:1 VSWR bandwidth of the array was 5% with a maximum gain of 18 dB.

A Doppler module, where the oscillator and the radiating elements both fabricated on a single substrate, was successfully developed by Nanbu [34]. The radiating element was a printed dipole with its arms etched on both sides of the substrate and having a built-in reflector. The 2:1 VSWR bandwidth of the antenna was 1.5 GHz with central frequency at 11.05 GHz. The half-power beam-width was 60° and the gain was 10 dB.

Newman [35] developed a technique to analyse electrically thin strip antennas on an electrically thin dielectric substrate. He used moment method solution of the integral equation with a modification in the piecewise sinusoidal reaction formulation for the thin wire radiators in a homogenous medium. The theory was verified by fabricating a number of dipoles.

Dubost [36] modified the design proposed by Sidford [17]. He used capacitive coupling in between the dipole and the microstrip line, instead of connecting directly by a shorting pin. He achieved the same results as that was published by Sidford earlier. Using this design, he fabricated a cylindrical four element array producing circular polarisation and omnidirectional radiation pattern [37]. At the same time, he has proposed a new dipole design [38] consisting of a short circuited dipole printed on a thin dielectric substrate and separated from ground by a shorting plate. The 3:1 VSWR bandwidth of this new dipole was found to be more than 30%. He has also given the theoretical explanation for this large bandwidth.

A new printed dipole antenna design was described in a report by Hanley and Perini [14]. The dipole is a printed stripline folded dipole etched on one side of a dielectric substrate and matched to 50Ω strip transmission line using Schiffman balun. Main advantage of this design is that the antenna element and the feed network all are on the same side of the substrate and thus can be made with a single photographic exposier.

Keen [39] used printed dipole as a feed for a small axially symmetric paraboloidal reflector at an operational frequency of just over 1 GHz. The feed consists of a broad-side array of two dipoles printed on a printed circuit board and joined by a common planar two wire transmission line. Each dipole was backed by a strip reflector. With this simple array,

H-plane pattern can be varied independently of the E-plane patterns. In addition to this, the aperture blockage of this feed was also very small.

Explicit formulas have been derived by Dubost and Rabbaa [40] for the mutual impedance and coupling between two parallel and collinear short circuited flat dipoles etched on a thin dielectric substrate and kept at a finite distance away from the ground plane. The experimental results were in good agreement with theory. They have also concluded that the radiating dipoles are particularly uncoupled and therefore suitable for incorporation in short arrays for which superdirectivity can be achieved.

Rutledge and Muha [41] developed an imaging antenna for millimetre wave application employing seven element bow-tie dipole antenna array interfaced with Schockly detector diodes in planar configuration. The array was capable of capturing 50% of the available power. The system cross-talk level was 19 dB.

Dubost and Vinatier [42] used flat folded dipoles as radiating elements to construct a 32×32 array to receive radio-broadcasting signals from geostationary satellites. The array operates between 11.7 and 12.4 GHz with a maximum gain of 37 dB and the efficiency was better than 48%. The cross-polar level was less than -30 dB.

Assuming a quasi-TEM mode of wave propagation and using conformal transformation technique, accurate and simple analytic expressions for the input impedance and effective dielectric constant of the rectangular printed dipole antenna in the mixed dielectric medium have been derived by Subhnani and Rao [43]. The theoretical values were in good agreement with the experimental results.

Ito [44] has presented a design of circularly polarised six element linear array, fed electromagnetically by microstrip feedline. The radiating elements consist of a strip dipole

and a slot. A window, behind the strip dipole, was etched in the ground plane to increase the gain and bandwidth of strip dipole.

A theoretical model equivalent to several lossy transmission lines acting together at quasi-TEM mode has been given by Dubost and Beauquat [45], to explain the bandwidth and radiation admittance of the flat symmetrical folded dipole. The theoretical results were compared with a flat folded dipole array and the comparison was found to be satisfactory.

An ultra high frequency (UHF) fan-dipole was optimised by Baily [25] for wideband applications near the first resonance, in order that the antenna could be used in a planar array of half wavelength spaced elements operating over a conducting ground plane. The resultant VSWR of the optimised dipole was less than 2 over 37% of frequency band.

The problem of a dipole above an inhomogeneous half-space was solved by Mohsen [46] in terms of field elements rather than Hertz potential, so that the boundary conditions can be applied directly. He solved the second order differential equation by transforming it to canonical form *via* proper transformations.

Lampe [47] used the transmission line technique to solve the asymmetric coplanar strip folded dipole problem. He has shown that the input impedance of such an antenna depends on three factors; the impedance of the transmission line mode, the impedance of dipole mode and the impedance of the step-up ratio. He derived the design formula for the planar folded dipole by solving these three parameters.

Agrawal and Powell [48] designed a Ku-band monopulse planar array. The cylindrical antenna consists of sixteen 90° flared triangular dipoles etched on RT-Duriod board, placed over a 0.2λ spaced ground plane. The antenna shows 20 dB sidelobe sum-pattern in the azimuth plane at an operating frequency of 12 GHz.

Dubost [49] proposed a flat radiating source consisting of two folded dipoles with orthogonal electric moments. This antenna can simultaneously transmit or receive two frequencies of orthogonal linear polarisations and subsequently a circularly polarised wave of either the right hand or left hand sense.

An easy to use simplified network representation for internal multiple reflection model for feed-through phased array lens antenna element was presented by Chu *et al.* [50]. The model makes use of readily available active radiation impedance of an infinite array rather than the self and mutual impedances between the array elements, which are not easy to obtain. Using this theory, they have analysed a large planar dipole lens array and showed that the lens internal multiple reflections have large effect on the amplitude and the phase variations of the lens aperture and the antenna gain fall off as a function of frequency.

The radiation impedance of a dipole printed on a periodic dielectric slab protruding over a ground plane in an infinite phased array was calculated by Chu and Lee [51], using model expansion in terms of longitudinal section electric and longitudinal section magnetic modes. Firstly these hybrid modes and model expansions were calculated and then the impedance of the dipole was derived by a method based on complex power relations with the aid of Poynting theorem. Results, calculated using this theory in the limiting case of no dielectric slab loading, have been compared with the results calculated by the method of ordinary plane wave expansions. They have also verified this approach by fabricating three dipole arrays.

A new formulation for the calculation of the radiation pattern of a bow-tie dipole antenna of finite length and infinitesimal thickness, placed on a loss-less dielectric substrate was discussed by Compton *et al.* [52]. The analysis is based on a representation of the current density on the metal surface of the antenna as a sum of imposed (quasi-static) term

and a set of current modes with unknown amplitudes. Free space fields that are expressed in terms of continuous spectra of symmetrised plane waves are matched to the current modes using the method of moments. The resulting set of equations are solved for the unknown current amplitudes. The pattern measurements at 94 GHz shows to agree well with theoretical predictions.

A new feeding technique for double sided printed dipoles enabling the realisation of flat array on foam like substrate with bandwidth up to 25% was developed by Levine *et al.* [53]. They have also experimentally shown that the gain of double sided printed dipole array is equal to the gain of a thin single layer microstrip array, while the bandwidth of such an array is much larger than the microstrip array. Data useful for fabricating such an array was also given.

Khamas *et al.* [54] fabricated a superconducting short dipole using $\text{YBa}_2\text{Cu}_3\text{O}_{7-x}$ rare-earth superconducting material. The dipole was fixed over a substrate and operated at 550 MHz. The gain of the superconducting dipole at liquid nitrogen was compared with an antenna of same size, fabricated using copper and was found to be 10.56 dB more.

Athanasas [55] presented an analysis of the parasitic coupling between a printed circuit dipole and a coplanar feedline. The dipole was centred over and perpendicular to the transmission line. The analysis was done using moment method for various dipole lengths and separation between the dipole and transmission line.

A cavity backed circularly polarised conical beam antenna consisting of slots and strip dipoles, having an axial ratio of less than 3 dB and impedance bandwidth of 9.5% was designed by Ito *et al.* [56]. They have also compared experimental patterns with theoretical patterns.

A single wire fed dipole on a dielectric substrate was developed by Parfitt and Griffin [57] to use it as a radiating element in MMIC phased array module. Their reported test dipole on alumina substrate showed 2:1 VSWR bandwidth of 10% at the central frequency of 4.2 GHz and maximum gain of 6 dB.

Skalar *et al.* [58] developed a planar antenna structure consisting of two half wave dipoles etched on a dielectric substrate, backed by metallic reflector, to create an image of two more elements. The array along with a dielectric lens shows cross-polar level better than -20 dB and sidelobe below -13 dB.

Maddocks and Smith [59] developed a flat plate steerable antenna array in X-band, for DBS television reception system. The radiation elements consist of folded dipoles printed on low cost foam substrate. The resultant antenna system was capable to steer in both azimuth and elevation. The range of azimuth angle was $\pm 45^\circ$.

A theoretical method to analyse the radiation characteristics of infinite phased array of horizontal dipoles printed on thin dielectric substrate in the presence of vertical wires protruding out of the ground plane was presented by Lee and Chu [60]. They obtained the dipole current distribution using method of moments. The theoretical model was verified with and without wire by taking measurements of the radiation impedance of waveguide simulator. The theoretical predictions matched well with the experimental results.

Bayard *et al.* [61] presented a full wave approach to analyse a variety of radiating elements printed on one side of a protruding substrate in infinite array environment. They used the equivalence principle to create a unit cell model that was then solved by Green's function - moment method technique. Validity of the approach was shown by fabricating a dipole element on a coplanar line. In another paper [62], they have extended the same

theory to predict the input impedance of waveguide simulator. The measured values were in good agreement with theory. They have also discussed the scan blindness in E-plane for several arrays due to dielectric thickness and permittivity of the substrate.

Parfitt *et al.* [63] solved the problem of radiation by a narrow metal strip dipole antenna contiguous with the edge of a dielectric substrate. They modified the technique for computing the scattered fields from composite conducting and dielectric bodies of arbitrary shape and finite size to determine the near-field and far-field patterns. The comparison of experimental results with theoretical values, for input impedance and far-field radiation patterns show excellent agreement. They have also analysed the co-planar strip transmission line feed antenna and the folded strip dipoles.

Lancaster *et al.* [64] analysed various properties of superconducting electric and magnetic (loop antenna) dipoles and discussed their respective matching networks. The superconducting loop and dipole antennas are fabricated from YBCO wire and placed over a dielectric substrate. The gain of the antennas are compared with corresponding identical loop and dipole antenna made up of copper wire. The gain of superconducting loop shows 5 dB improvement while dipole shows 6 dB improvement corresponding to super-cooled copper antenna.

Pratt *et al.* [65] analysed the mutual coupling between metal strip antennas which are contiguous with the ends of finite size, electrically thick dielectric substrate. They used electric field integral equation method with a volume formulation for the polarisation currents in the dielectric to calculate the self and mutual impedance of the antennas in array configuration. The results were verified by fabricating a three element folded dipole array. They have also discussed the effect of electrically thick, finite size dielectric substrate on the mutual coupling between the elements of the array.

Clapp [66] presented a new design of wideband resistively loaded triangular dipole. The input VSWR of the antenna is better than 2:1 over a 4:1 frequency band when mounted in front of a conducting ground plane. He has also fabricated a two element array using this triangular dipole.

Eleftheriades and Rebeiz [67] analysed a planar antenna structure in array environment for millimeter wave applications. The radiating element consisting of a cavity-backed strip dipole printed on Si or GaAs wafer. They used closely spaced metallised *via* holes technique to provide required isolation between adjacent dipoles in phased array applications for avoiding severe scan blindness effects. To analyse the structure, firstly they determined the Green's function for 2D array, which enabled them to construct the integral equation. Solution of the integral equation, using Galarkin's method gives the active input impedance.

The problem of cross-polarised radiation from electrically thick substrate supporting metal strip antenna was analysed by Prafitt *et al.* [68]. They have shown that good polarisation purity can be achieved by proper designing of the feed structure and fabricated an antenna having cross-polar level below 30 dB throughout the entire angular range.

Nesic and Radnovic [69] developed three different types of wideband printed dipoles - triangular, triangular with cap and trapezoidal. The VSWR of these antennas are below 2 with $Z_0 = 75\Omega$ in the frequency range of one octave (4 - 8 GHz). They have also developed a trapezoidal slot fed by coplanar waveguide antenna structure. VSWR of this antenna is also less than 2 in the frequency range of one octave.

2.2 MICROSTRIP DIPOLE ANTENNA

The difference of microstrip dipole antenna from the rectangular microstrip patch antenna is that in the latter case both sides dimensions are appreciable fraction of wavelength, while in the former case one side length is resonant and the other dimension is kept very thin.

James and Wilson [70,71] used microstrip dipole as radiating element in array configuration. The array consisted of a line sequence on a planar matrix of (unbroken) horizontal dipoles end-fed by high impedance microstrip lines. Both the resonant and the travelling wave type arrays were fabricated and performance was evaluated. For resonant type array, beam maximum was along bore-sight direction whereas the travelling wave array radiated in an angle against the bore-sight and the main beam scanned with frequency.

Williams [72] designed a 16×16 element center-fed microstrip dipole array with diagonal layout of feed system, operating at 36 GHz. The array gain was 25 dB and sidelobe levels and cross-polarisation levels were below 20 dB. The bandwidth, corresponds to 3 dB reduction in gain, was 700 MHz.

Ito *et al.* [73] proposed a travelling wave type circularly polarised array consisting of inclined half wave microstrip dipoles arranged along both sides of a microstrip feedline terminated to a matched load.

Oltman [26] pointed out that thin resonant microstrip dipole can be efficiently excited by electromagnetic proximity coupling to a microstrip transmission line embedded in the substrate. Huebner [74] successfully used this technique in the development of a 24 element X-band monopulse array. The array elements were distributed in three rings and a separate corporate feed was used to excite each quadrant. Measured gain was 19.7 dB and sidelobe level was below -17.5 dB.

A rigorous analysis of thin wire printed microstrip dipole and coupled dipole has been reported by Rane and Alexopoulos [75]. Numerically they have shown that the input impedance has no critical dependence on the gap length so long as the length is less than $0.1\lambda_0$. They have extended the same technique to compute the mutual impedance between parallel, collinear and echelon microstrip dipoles.

The input impedance and radiation properties of a microstrip dipole having finite width was analysed by Uzunoglu *et al.* [76] using variational method. The method developed by them relies on employing dyadic Green's function for Hertzian dipole printed on a grounded dielectric substrate together with an assumed current distribution. The input impedance of the dipole was calculated and the results were found to be well-matched with the experimental values when the dielectric thickness was much smaller than the wavelength in the dielectric. The far field patterns were computed by evaluating the Green's function for far field using a stationary phase integration. It was also shown that the efficiency of surface wave modes is a function of antenna dimensions.

The configuration for an infinitely long cylindrical array of printed dipoles, etched on thin dielectric sheet and covering a large radius cylinder, was analysed by Lee and Eichmann [77]. The two dimensional Green's function for a single column was evaluated in the near zone of the cylinder using Watson transformation method and the poles of the Green's function were traced on a complex plane using perturbation technique. The active input impedance of the dipole as a function of the beam direction was also derived from Green's function and based on this, elementary pattern cuts at different elevation angles were discussed.

The radiation resistance of half wave microstrip dipole antenna was solved by Panchenko and Shabunin [78], by writing the Green's function in the form of a finite sum

of natural wave functions of discrete spectrum and the integral with respect to the functions of the continuous part of the spectrum. They have also investigated separate contribution of the surface and spatial waves to the antenna radiation impedance. Numerical computations were given for the radiation impedance and radiation patterns of the surface wave and spatial waves of dipoles for different substrates.

The current distribution, input impedance and radiation patterns of printed wire dipoles on grounded dielectric substrate were computed by Rane and Alexopoulos [79]. The current distribution was obtained by solving Pocklington's equation by moment method. In order to solve Pocklington's equation, appropriate Green's function was obtained by considering a Hertzian dipole printed on the substrate. The resulting Green's function was in terms of improper Sommerfeld type integrals. These integrals were then computed using real axis integration techniques which involve analytical and numerical steps. Finally, the effect of surface wave modes on the current distribution and on the input impedance were determined. Numerical computations were also given to show the effect of one surface wave and two surface waves modes.

The mutual impedance between thin microstrip dipoles printed on grounded dielectric substrate was also analysed by the same authors [80]. For this, the integral equation was formed for the unknown currents over two printed dipoles and was solved by moment method. Numerical computations were shown for three configurations; 1. broadside, 2. collinear and 3. echelon. They have also shown that the surface wave enhances the mutual coupling in collinear arrangement and have a significant contribution even when the array elements are several wavelength apart.

Experimental investigations on various configurations of electromagnetically coupled microstrip dipole were done by Oltman and Huebner [81], using two different methods.

They used transmission line model to explain the coupling mechanism from circuit view point, while a moment method solution was used to provide the inside from field view point. Using the optimised configuration, a monopulse array was formed which showed a gain of 26 dB. Experimental results for a few linear arrays and circularly polarised arrays were also presented by them.

A rigorous theory to explain the behaviour of electromagnetically coupled dipoles was developed by Elliott and Stern [82]. They obtained relations involving the active input impedance of the individual dipoles and then solved them iteratively. Using this theory, they developed an eight element array [83]. The performance of the array was measured against the design data and was found to be quite satisfactory.

Hansen [84] derived simple approximate equations for microstrip dipoles, starting from the exact equation for the field components, consisting of integrals of Sommerfeld type. Numerical calculations has been done for two examples and were compared with those obtained by combined numerical and analytical techniques from the exact formulation.

The effects of substrate thickness and relative permittivity on the radiation properties of microstrip dipoles were investigated by Katehi and Alexopoulos [85]. They developed the Sommerfeld integral equation for unknown current distribution with dyadic Green's function and introduced a new method [86] to solve it. The technique is based on the combination of analytical - numerical real axis method and was combined with piece-wise sinusoidal expansions to solve the Fredholm integral equation for the unknown current density. Using this approach, they have presented a trade-off between substrate thickness and resonant input resistance, bandwidth and radiation efficiency for PTFE substrate and achieved a radiation efficiency of 80% for a bandwidth of 18%.

Pozar [87] used dyadic Green's function for grounded dielectric substrate to calculate the performance of microstrip dipole on electrically thick substrate. He has also included the effect of exterior fields making the calculation for surface wave excitation and mutual coupling possible. The numerical data were presented for various antenna characteristics at millimeter wave range on various substrates. He has also given an optimisation procedure.

A fast approach to analyse large microstrip dipole phased arrays was given by Wright and Lo [88]. The analysis presented by them is based on two steps. First is to derive periodic electric field Green's function for the grounded dielectric substrate and second is to evaluate the generalised impedance matrix using moment method. A numerical result for the reflection coefficient against the scan angle was also given for a typical array.

The dipoles printed on semi-infinite grounded dielectric substrate was investigated using moment method in the Fourier Time Domain by Masanobu and Rokushima [89]. Using this formulation they calculated the input impedance, resonant length and radiation patterns of a dipole.

A slow wave periodically modulated type of millimeter wave array has been presented by Birand and Williams [90]. The structure consist of an array of printed dipoles on a dielectric substrate of low dielectric constant and fed by an insular guide. They use the simple array theory along with effective dielectric constant to determine the radiation characteristics. A prototype in Ku band was fabricated and the experimental results were compared with the theory.

Pozar and Schaubert [91] analysed the infinite phased array of microstrip array of dipoles by generalising the Green's function for dielectric slab in its spectral domain form and then applied moment method on unit cell to solve the integral equation to find out the

current distribution. Using this theory, they explained the scan blindness in terms of a forced surface wave response of dielectric slab. Also a simple theory based on the array grid spacing and surface wave propagation constant of the dielectric slab was given, which allowed to predict the occurrence of blind spots. This theory was compared with the waveguide simulator model for the prediction of scan blindness.

The effect of superstrate on microstrip dipole antenna was analysed by Alexopoulos and Jackson [92], by solving the problem of Hertzian dipole. Firstly, Green's function for the infinitesimal dipole was derived using Sommerfeld's method. Then a contour integration was used to compute the surface wave power in the transverse electric and transverse magnetic surface waves. Subsequently, they obtained the radiation resistance by reciprocity theorem and then calculated the efficiency. Using this method, numerically they have shown the possibility of achieving 100% radiation efficiency. The criteria for nearly omnidirectional radiation pattern for E and H-planes were also given.

At the same time, the same problem of the effect of superstrate cover on the current distribution and input impedance of microstrip dipoles were analysed independently by Soares *et al.* [93]. They obtained the Hertz vector potential for a horizontal current element located in the stratified medium with four layers and calculated the current distribution and input impedance of the dipole as a function of dielectric cover parameter after solving the Pocklington's equations by moment method. Validity of the approach was shown by calculating the input impedance of the dipole without dielectric cover.

Katehi and Alexopoulos [94] developed a theoretical model for electromagnetically coupled microstrip dipole by obtaining the current distribution along the dipole and the transmission line, including all mutual interactions. The method of moment was applied for the determination of the current distribution in the longitudinal direction. The current in

transverse direction was selected, so as to satisfy the boundary conditions. Then the self impedance of the dipole was calculated using transmission line theory. This approach was experimentally verified by fabricating a number of dipoles and comparing the experimental data with the theoretically predicted values.

Tsulamengas and Uzunoglu [95] used matrix method in conjunction with Fourier transformation technique to analyse the radiation patterns of microstrip dipoles in the presence of a gyromagnetic-electric (gyrotropic) layer. Numerical computations were given for the far-field pattern for dipoles on different types of substrates and the substrate effect on radiation patterns due to anisotropy was also discussed.

The design criteria for producing nearly omnidirectional E and H-plane radiation patterns for microstrip dipoles were given by Alexopoulos *et al.* [96]. The existence of non-zero radiation along the horizon in either E or H-plane was explained theoretically by the coincidence of a pole and a branch point in Sommerfeld type integral. A ray optics interpretation was also given to aid the physical understanding of the phenomenon.

Simple and general relations, characterising the behaviour of infinite phased array of microstrip dipoles were derived by Pozar [97] from a model based on infinite current sheet. The Green's function of an electric current source on a grounded substrate was used in various limiting forms to treat the array in free space, array above ground plane, array on a semi-infinite substrate and array on a grounded dielectric substrate. The current sheets were selected using orthogonal properties of the Floquet modes of the infinite array. He compared the results of this idealised model with rigorous moment method solutions for microstrip dipoles and patch antennas and showed that the scan blindness and grating lobe effects are primarily decided by factors such as element spacing and substrate parameters rather than by the particular element itself.

The microstrip dipoles and slot antennas on a semi-infinite substrate and in infinite phased array configuration were also investigated by Kominami *et al.* [98]. They obtained the current distribution by employing moment method to solve the spectral domain algebraic equations corresponding to Pocklington's integral equations in the space domain and then calculated the resonant length, resistance and the radiation pattern for isolated element. Further they extended the theory to calculate the reflection coefficient and broadside power division for infinite phased array.

The microstrip dipoles with superstrate were analysed by Jackson and Alexopoulos [99] using transmission line analogy to determine the resonance condition, which allows for large gain. Asymptotic formula for gain, beamwidth and bandwidth were given and bandwidth limitations were discussed. They also extended the method to produce narrow patterns about the horizon and directive patterns at two different angles.

The same authors [100] also investigated the radiation properties of microstrip dipoles on electrically thick substrate and made comparison with dipoles printed on dielectric half-space. The conclusion drawn by them was that the microstrip dipole radiation properties are sensitive to substrate-loss as the substrate thickness increases. Asymptotic formulas were given for the radiated power and efficiency. They extended this analysis for center-fed strip dipoles and discussed a method to improve the gain and efficiency using superstrate cover.

Jackson [101] proposed two configurations for feeding microstrip dipoles with coplanar waveguide transmission lines. One design produces the circular polarisation and the other, the linear polarisation.

Jackson and Alexopoulos [102] investigated the effect of superstrate layer on microstrip line, center fed dipole, mutual impedance between two dipoles and on EMC dipoles. Analysis were carried out by plane wave spectral formulation for the reaction between two arbitrary x -directed current sources, together with a Galarkin's moment method formulation. For mutual coupling, they used a real space evaluation technique [103] to improve the efficiency of moment method, used for finding the electric field.

Katehi *et al.* [104] developed a new technique to enhance the impedance bandwidth of electromagnetically coupled dipoles by adopting one or two parasitic metallic strips either in stacked fashion or coplanar to the radiating dipole. The maximum bandwidth achieved was 10.4%. They have also given a theoretical analysis for all these configurations.

A rigorous and complete analysis of electromagnetically coupled microstrip dipoles were done by Lepeltier *et al.* [105]. The theory given by them was based on the resolution of electric field integral equations, which was then transformed into a matrix potential (scalar and vector) integral equations. The surface current densities were calculated using method of moments by solving the integral equations. They compared the theoretical results for experimental data with input impedance and radiation patterns.

Yang and Alexopoulos [106] have used reciprocity and transmission line model to determine the radiation properties of microstrip antennas in a multilayered configuration. They have shown that, an extremely high directive gain may result at any scan angle, with practical substrate materials, if the thickness of the substrate and multiple substrate layers are chosen properly. The approach was verified by fabricating dipoles over various dielectric substrates.

Griffin and Kara [107] have experimentally showed that the radiation characteristics of rectangular patches were same to microstrip dipoles when etched on thick dielectric substrate.

An efficient and fast analysis of a finite phased array of microstrip dipoles using closed form asymptotic representation for the planar microstrip Green's function was presented by Barkeshli and Pathak [108]. They have also shown that this new method considerably reduces the computational time compared to the older methods.

Blischke *et al.* [109] developed a theoretical model for obtaining the scattering characteristics of a two dimensional infinite array of microstrip dipoles printed on a dielectric coated conductor, using dyadic Green's function and Galarkin's method. Numerical results were also given by them.

The cross-polar level of a small horizontal electric dipole (HED) on flat grounded dielectric substrate was analysed by Hoofar *et al.* [110]. Numerical calculations have been presented for two cases, HED along the array direction and HED perpendicular to the array direction. They showed that there is a limitation in achieving the minimum cross-polar level and low value of dielectric constant and thick substrates give better cross-polar level.

Russo and Ruggieri [111] fabricated large number of electromagnetically coupled microstrip dipole arrays for linear and circular polarisation, in the frequency range of 11.7 to 12.5 GHz. They also compared the experimental results with the theoretically predicted values.

An analysis of mutual coupling between finite phased array of microstrip dipole elements and its feed network were given by Lee and Chu [112]. They used an iterative method to solve the scattering matrix problem of feed network instead of formulating a

large scattering matrix. Using this model, they fabricated a 14×28 element array. The experimental design well satisfied the theoretical predictions.

Katehi [113] presented an integral equation approach to calculate the mutual coupling of electromagnetically coupled dipoles with superstrate, in the array environment. She also evaluated the mutual impedance and scattering coefficients by transmission line theory.

An accurate analysis of microstrip dipole element, electromagnetically coupled to a covered microstrip line running perpendicularly under it in a superstrate-substrate configuration, using the principle of reciprocity along with full wave spectral domain Green's function for multilayered dielectric substrate, was done by Das and Pozar [114]. They also included the mutual coupling effect and using the result of element analysis, a series-fed array was successfully designed, built and tested.

The effect of radome on input impedance and radiation pattern of EMC dipoles was calculated by Gaouyer *et al.* [115], using integral equation technique, solved by moment method, associated with single one port model. They showed that the presence of radome has effect only on dyadic Green's function, which can analytically be determined in space domain. They compared the theoretical results with the experimental data.

Yang *et al.* [116] have presented the design equations for transversely coupled EMC dipoles from rigorous integral equation solution, which include the mutual coupling between the elements. They fabricated a seven element standing wave linear array and compared the experimental results with the calculated values.

At the same time Jackson *et al.* [117] developed another design procedure for EMC dipoles based on moment method analysis. In their method, only one pair of dipole was needed to analyse at a time in order to develop necessary coupling coefficients. These

coupling coefficients were then used for array designing. Using this design approach, they fabricated a four element array and the performance was found to be satisfactory.

The discrete natural resonance modes of microwave patch devices were identified with simple pole singularities in the temporal transformation plane by Hanson and Nyquist [118]. Coupling coefficients relating the amplitude of resonant current to impressed current relations were found out from an integral-operator description of the patch device. Then the solution was obtained from Hallen type integral equation. Using this theory, they analysed thin microstrip dipole.

The use of printed microstrip dipole array for the treatment of tumours by microwave hyperthermia was presented by Dvoark [119]. The main advantage of such an array is to create the hot spot only at the tumour.

A rigorous analysis of the electromagnetically coupled microstrip dipole based on potential integral equation and its solution using moment method was presented by Lipeltier *et al.* [120]. They discussed the steepest descent technique for far-field computation and compared the theoretical data with the experimental results.

Paul and Gupta [121] analysed log-periodic dipole array. They solved the wave equation for Hertz potential in rectangular coordinates by applying boundary conditions on flat strip dipole. Using this model, they compared the various antenna characteristics with the experimental results.

A three port S-parameter model for the isolated inclined dipole was introduced by Clate and George [122]. The model uses an iterative design procedure for linear array of strip dipoles which are proximity coupled to a continuous microstrip feedline. Numerical computations were done for 45° inclination of the dipole.

Brennan [123] designed a low cost steerable phased array radar for land mobile satellite communication system. The array consists of six subarrays, each having three cross-dipoles etched on glass-epoxy printed board. The array works at 1.59 GHz in $\pm 45^\circ$ range of beam deflection from zenith.

Alder *et al.* [124] developed a monolithic microwave receiver in the frequency range of 10 to 35 GHz. The receiving antennas were integrated with a balance mixer and IF amplifier on the common substrate. The antenna array consists of dipoles and a lens to produce a high gain beam.

System eigen modes of N-coupled, nearly degenerate microstrip dipoles were investigated by Hanson and Nyquist [125] through singularity expansion based on perturbation technique. They used rigorous dyadic Green's function for the layered microstrip environment. A comparison of this technique with full wave solution was also give by them.

Design details of electromagnetically coupled linear dipole array were presented by Hong and Alexopoulos [126]. They designed a 5 - element equi-spaced array of 20 dB Dolph-Chebyshev pattern to illustrate the design procedure.

Hong [127] analysed mutual impedance between two side coupled asymmetric microstrip dipoles using spectral domain method. He compared the results for a special case of symmetrical structure with odd-mode feeding with that for a microstrip dipole calculated by moment method. He has also discussed the open end effect of the dipoles.

The analysis of arbitrary periodic conducting structures embedded in layered medium was performed by Montgomery and Wilton [128], using triangular basis function and the

mixed potential formulation. Numerical computations were given on microstrip dipole array and reflection-coefficient vs scan angle was presented by them.

Design procedures of a leaky wave antenna, consisting of microstrip feedline on a substrate and an array consisting of printed dipoles etched on other substrate to form EMC dipoles perpendicular to the microstrip line over it were presented by Potharazu and Jackson [129]. They analysed the antenna from leaky wave point of view and provided an easy design procedure for large array. A comparison was also given with simple Bloch-wave analysis of the periodic structure.

Crzybowski *et al.* [130] presented the design and characterisation of a number of travelling wave microstrip dipoles of various lengths from one quarter-wavelength to two wavelengths long.

Hassan *et al.* [131] developed a method to evaluate the performance of log periodic microstrip dipole antenna. Based on this method, they studied the behaviour of a log periodic microstrip dipole array and concluded that the anomalous back-lobe peaks can be eliminated by optimising the spacing factor and by selecting small dipole lengths.

Seaux *et al.* [132] described a new type of microstrip antenna which used a double resonance phenomenon to radiate as a short dipole. The working wavelength of the antenna was approximately eight times the maximum dimension of the antenna.

Das and Pozar [133,134] used a full wave spectral domain moment method approach and a new generalised multiport scattering formulation to model the excitation from the multiport feed lines. They formulated a general solution to a class of printed antenna geometry composed of multiple dielectric layers and ground planes, radiating patches, dipoles or slots and an arbitrary configuration of multiple transmission lines proximity

coupled or aperture coupled to the radiating elements. Further they analysed various configurations, which includes dipoles inclined or perpendicularly coupled to different feedlines. The experimental results were also given to validate the approach.

Tulintseff [135] has developed a dipole and slot series-fed-type linear array, transversely coupled to microstrip line, using transmission line theory with equivalent circuit model for radiating elements. The antenna radiates a fixed beam, 46° above the horizon, transmitting in horizontal polarisation and receiving in vertical polarisation at 30 and 20 GHz respectively.

The input impedance of a center fed microstrip dipole having finite conductor thickness was analysed by MacPhic [136]. He used Poynting vector method to determine the complex power leaving the surface and then obtained the input impedance.

2.3 PRESENT WORK

From the above review of the past work in the field, it is clear that although various researchers have tried to enhance the impedance bandwidth of planar dipole antennas using numerous techniques, no sincere attempt has been made so far to improve the impedance bandwidth through end-loading of the dipole arms. This thesis is the outcome of the investigations carried out to achieve a large impedance bandwidth by loading the dipole arms at the ends.

This chapter describes in detail the design and fabrication procedures, the facilities utilised and the measurement techniques of various antenna characteristics.

3.1 DESIGN AND FABRICATION OF ANTENNAS

The work presented in this thesis is on antennas operating in the frequency range of 800 - 2500 MHz. This low frequency band is selected mainly due to the ease and convenience in fabrication of the antennas. It is well-known that the size of printed antennas become smaller as we go to higher frequencies. The physical dimension of the printed antennas will further be reduced by the use of high dielectric constant substrate.

The substrate used for the antenna fabrication is double-side copper cladded glass-epoxy, having dielectric constant 4.5 and thickness 1.6 mm, which is readily available in the market. Selection of such a substrate, for the above frequency band gives the freedom to neglect the fabrication tolerance, which will be a very small fraction of wavelength. Also this frequency band is of particular interest because it is most commonly used in land mobile satellite communication systems and for IFF applications.

The antennas are fabricated using photolithographic technique. The chart shown in Fig. 3.1 describes the step-by-step procedure of photolithographic etching technique.

3.1.1 Printed dipole

Experiments are started with the fabrication of ordinary rectangular printed dipoles, as shown in Fig. 3.2. The arm shown by dotted line is etched on the other side of the substrate.

As a modification of this structure, flaring is given to the dipole arms. Fig. 3.3 shows the sketch of such an antenna. Experimental observations indicate that the impedance bandwidth can be improved considerably by this modification. Optimisation of the design is done by exhaustive experimental observations.

Further investigations revealed that enhancement of impedance bandwidth is possible by end-loading of dipole arms. A number of printed dipoles with different end-load shapes, like triangular, circular, parallelogram, square *etc.* are fabricated. The conclusions drawn from these experiments are that the triangular and parallelogram shapes are most suitable for bandwidth optimisation of the printed dipoles. Fig. 3.4 and Fig. 3.5 show the antennas with triangular and parallelogram end-loading respectively.

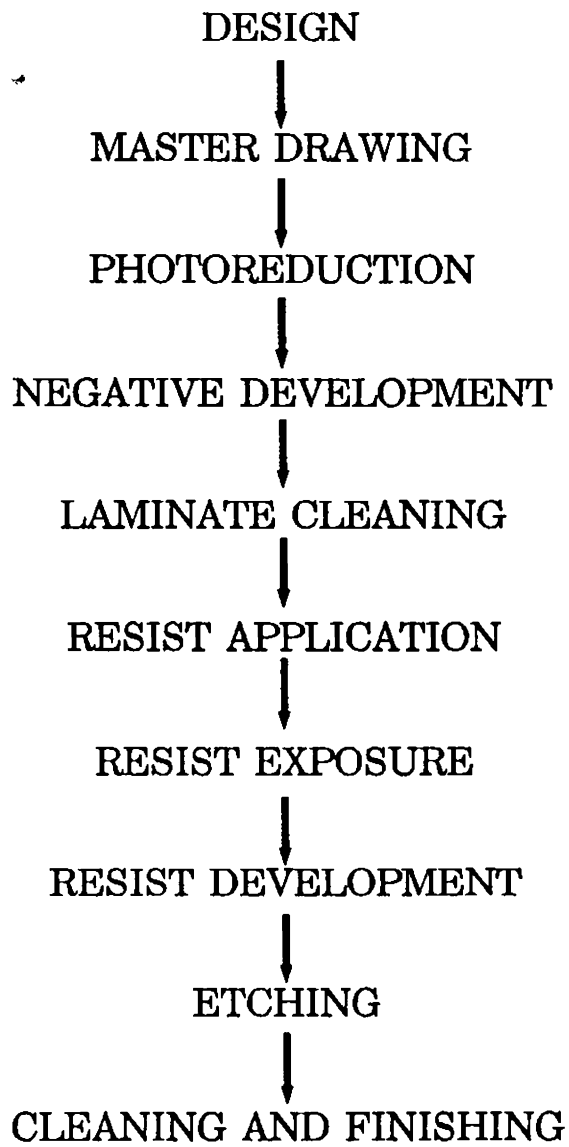


Fig. 3.1 Photolithographic design procedure

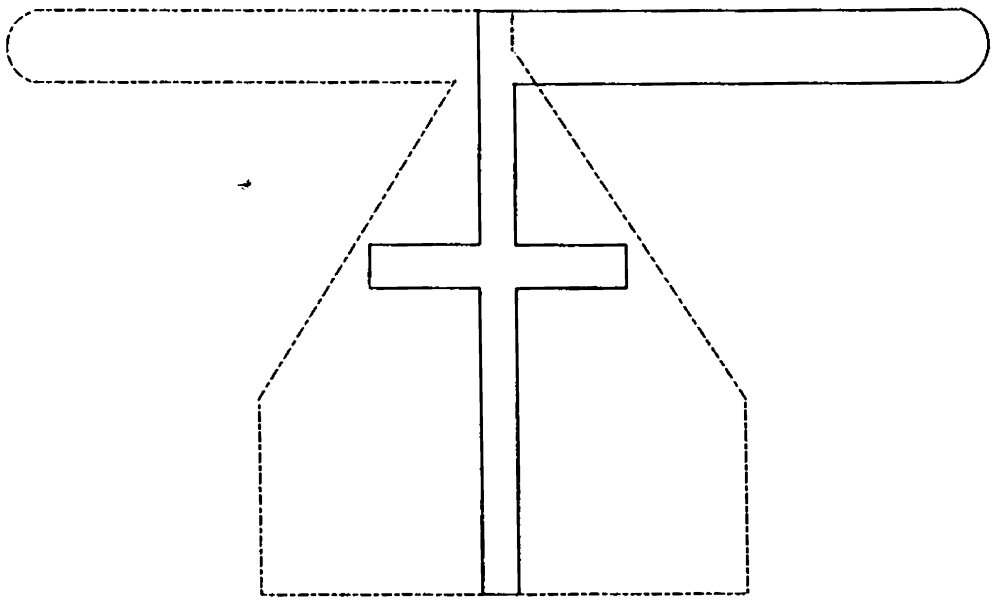


Fig. 3.2 Ordinary rectangular printed dipole

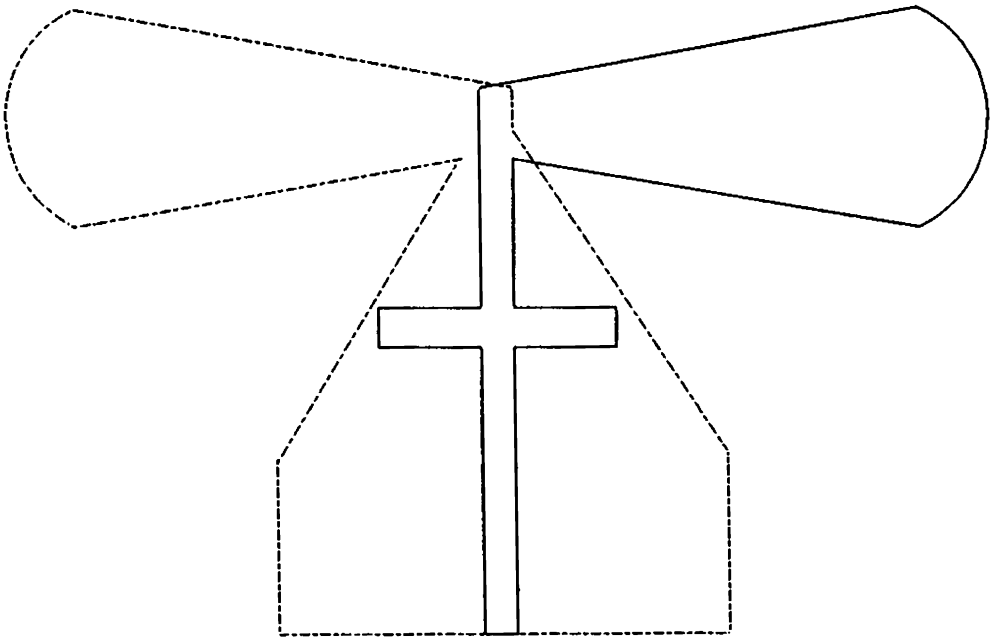


Fig. 3.3 Flared printed dipole

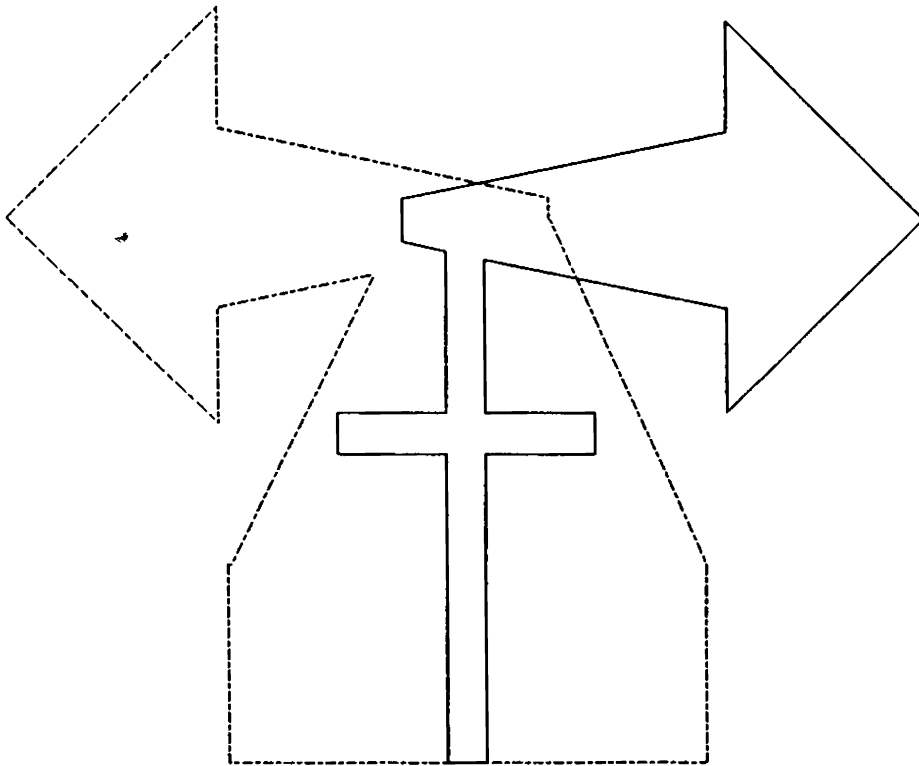


Fig. 3.4 Triangular end-loaded printed dipole

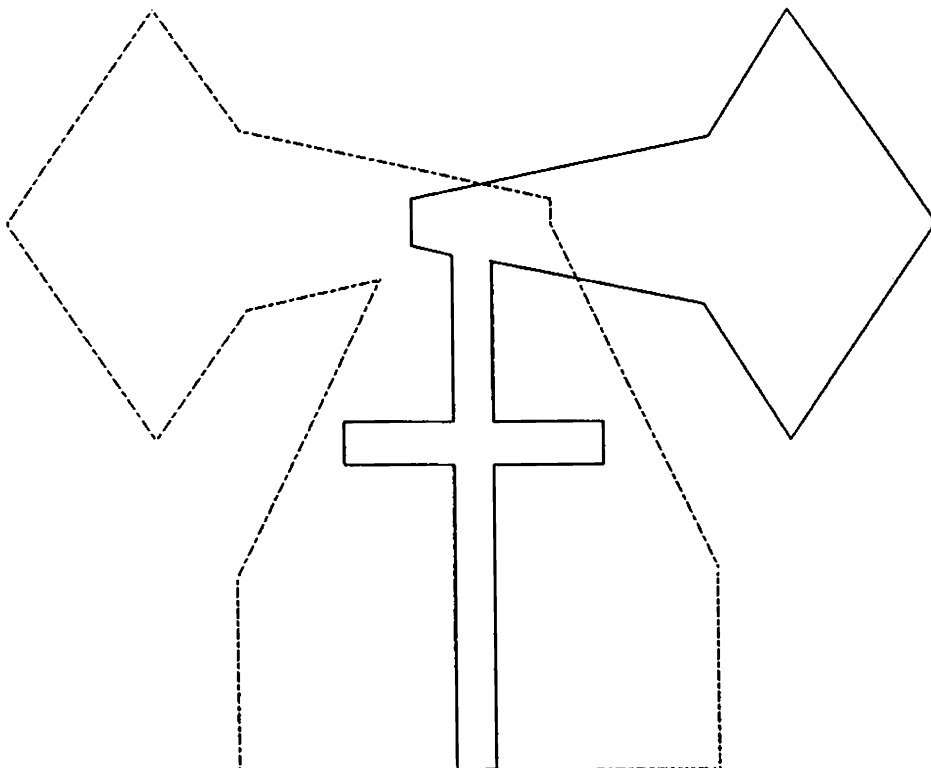


Fig. 3.5 Parallelogram end-loaded printed dipole

Apart from this, studies are carried out to optimise the triangular and parallelogram end-loaded dipoles with cavity backup. This is done by placing a large ground plane at the optimum distance from the dipole.

3.1.2 Microstrip dipole

The triangular end-loaded printed dipole antenna design is extended to develop a wideband microstrip dipole antenna. The design requires two dielectric substrates. In one substrate, the dipole structure is etched as discussed in Section 3.1.1. The other substrate, which acts as the ground plane, is a single-side copper cladded glass-epoxy. The substrate having the dipole structure is placed on the other substrate in such a way that the dipole arm connected to the main feedline is sandwiched between the two substrates. Fig. 3.6 shows the complete structure. The interfacing layer is made air-tight by means of four screws at the corners of the substrate. The feedline for this dipole is stripline because the main feedline is in between the two substrates with top and bottom metallised.

To avoid double photographic exposure and the requirement of two substrates, a new type of triangular microstrip dipole antenna, shown in Fig. 3.7, is developed and optimised. Here both arms are etched on the same side of the substrate and the other side of the substrate is kept completely metallised. This design gives almost the same impedance bandwidth as that of the previous design.

3.2 ANTENNA FEEDING

It is clear from Fig. 3.2 to 3.5 that the electromagnetic energy is fed to the arms of the printed dipoles through microstrip line. To match the low input impedance of the antenna

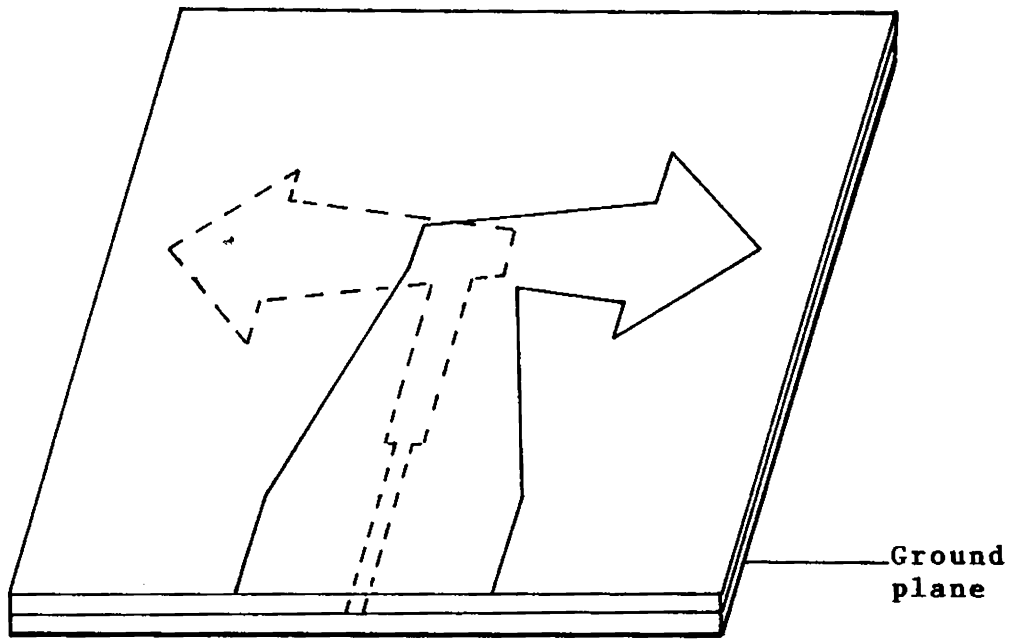


Fig. 3.6 Triangular end-loaded microstrip dipole

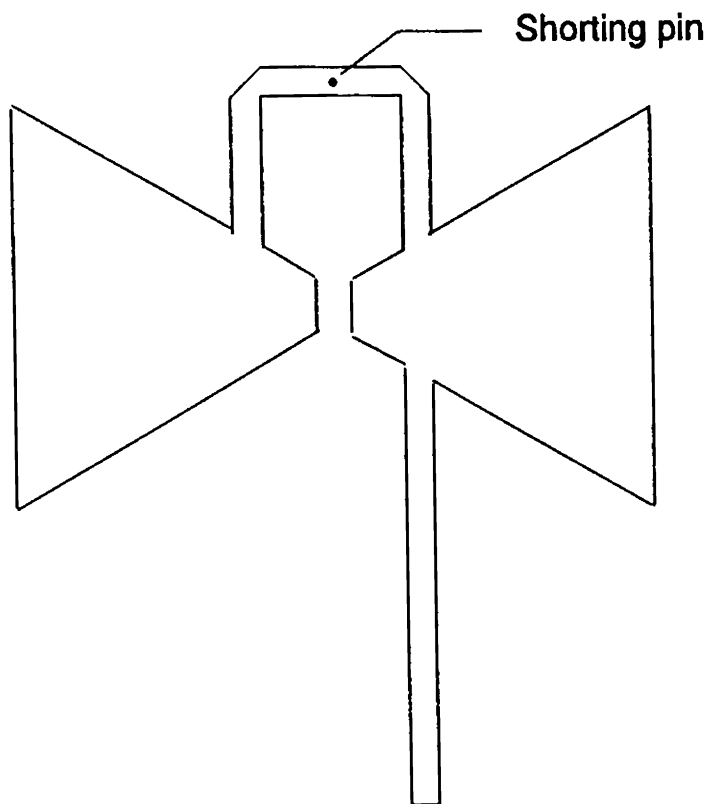


Fig. 3.7 Triangular microstrip dipole

with system impedance (*ie.* 50Ω), an impedance transformer and a stub is used. Initial studies showed that the 42Ω line impedance for impedance transformer is the best choice. Thus, for all further designs the line impedance of the impedance transformer is kept 42Ω . To optimise the impedance bandwidth for a particular antenna, the stub is not etched along with the dipole and the impedance transformer, rather they are cut from thin copper foil and pasted using very thin layer of conducting flux, so that the length, width and position of the stub from the antenna, can be varied easily.

For microstrip dipoles, shown in Fig. 3.6, the feedline is stripline. Like printed dipoles, the input impedance of microstrip dipole is less than the system impedance. Here matching is achieved with a single impedance matching transformer. The dipole arms are etched along with 50Ω stripline and the optimisation of impedance transformer is done by cutting and pasting thin copper foil of different length and width.

In the case of triangular microstrip dipoles with microstrip feed (Fig. 3.7), antennas are etched along with 50Ω line. Matching is achieved by adjusting the matching balun length.

The planar transmission lines, for printed and microstrip dipoles are coupled to coaxial line through SMA connectors. The SMA connector is screwed to a rectangular aluminum block. Four holes are made in the block to tighten it with the antenna substrate. Fig. 3.8 shows the side - view of the same.

For printed dipoles, the microstrip line is soldered to the center conductor of the SMA connector and the antenna substrate plate is screwed with the aluminum block. Thus, the outer conductor of SMA connector is coupled to the other dipole arm.

The same connector and the base is used for feeding triangular end-loaded microstrip dipole antenna. The center conductor of the SMA connector is soldered to the center-line of the stripline. Then the other substrate is placed over it and both the substrates are screwed together with the base block. Thus, the ground plane and the top metallised portion are electrically coupled to the outer conductor of the SMA connector.

The feeding mechanism for triangular microstrip dipole is entirely different from the earlier ones. The outer conductor of the SMA connector is connected to the ground plane and the inner conductor comes out through a hole made in the substrate and is soldered to the microstrip feedline. The side-view is shown in Fig. 3.9.

3.3 FACILITIES UTILISED

The main facilities used for antenna characterisation are :

1. Anechoic chamber
2. HP 8510B Network Analyser
3. Scientific Atlanta positioner-controller

3.3.1 Anechoic chamber

The most important antenna characteristics are the radiation patterns. Hence, proper care has to be taken while plotting the radiation patterns. For indoor pattern measurements, the reflections from the surrounding walls, objects and external radiations may create errors in the measurements. Hence the resultant pattern may deviate from the actual one. For avoiding such spurious reflections during pattern measurements, *anechoic (no-echo) chamber*

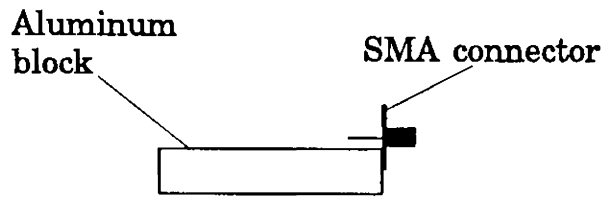


Fig. 3.8 Side-view of the SMA connector and the base

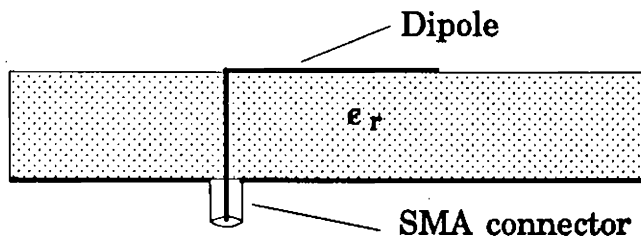


Fig. 3.9 Cross-sectional view of triangular microstrip dipole with feed mechanism

is used. The philosophy is to have a non-reflecting environment like the outer space except that the walls are at ambient (~ 300 K) temperature instead of 3 K.

The walls of the chamber are covered with good RF absorbers. Instead of flat sheet absorbers, pyramidal and wedge shaped absorbers are used to reduce the reflection further [137]. To avoid external electromagnetic signal interference, a metallic lining is also provided in between the absorbers and the walls of the chamber. The measured return-loss of the chamber is found to be better than -35 dB.

Out of two basic types (rectangular and tapered) of anechoic chamber design, the tapered one is preferred for radiation pattern measurement, because it straighten the E-field faster than rectangular chamber.

In the present test set-up, the test antenna, whose radiation characteristics have to be measured, is mounted on a Scientific Atlanta turn-table which is kept in the quiet zone of the chamber. The antenna is aligned in such a way that the plane of the radiating edge is exactly along the axis of rotation of the turn-table. The turn-table is controlled from outside the chamber, through the controller, which can be automated using HP 9000/300 series computer. A schematic representation of the anechoic chamber is shown in Fig. 3.10.

3.3.2. Network Analyser

All antenna measurements have been taken using HP 8510B Vector Network Analyser. In this section, a brief description of microwave network analyser is given.

The description of parameters like impedance or transfer function of both the active and passive networks through stimulus response testing is referred as network analysis. Thus, using network analyser, the transmission and reflection characteristics of a test device

CONVERTIBLE MICROWAVE ANECHOIC CHAMBER

[view from the top]

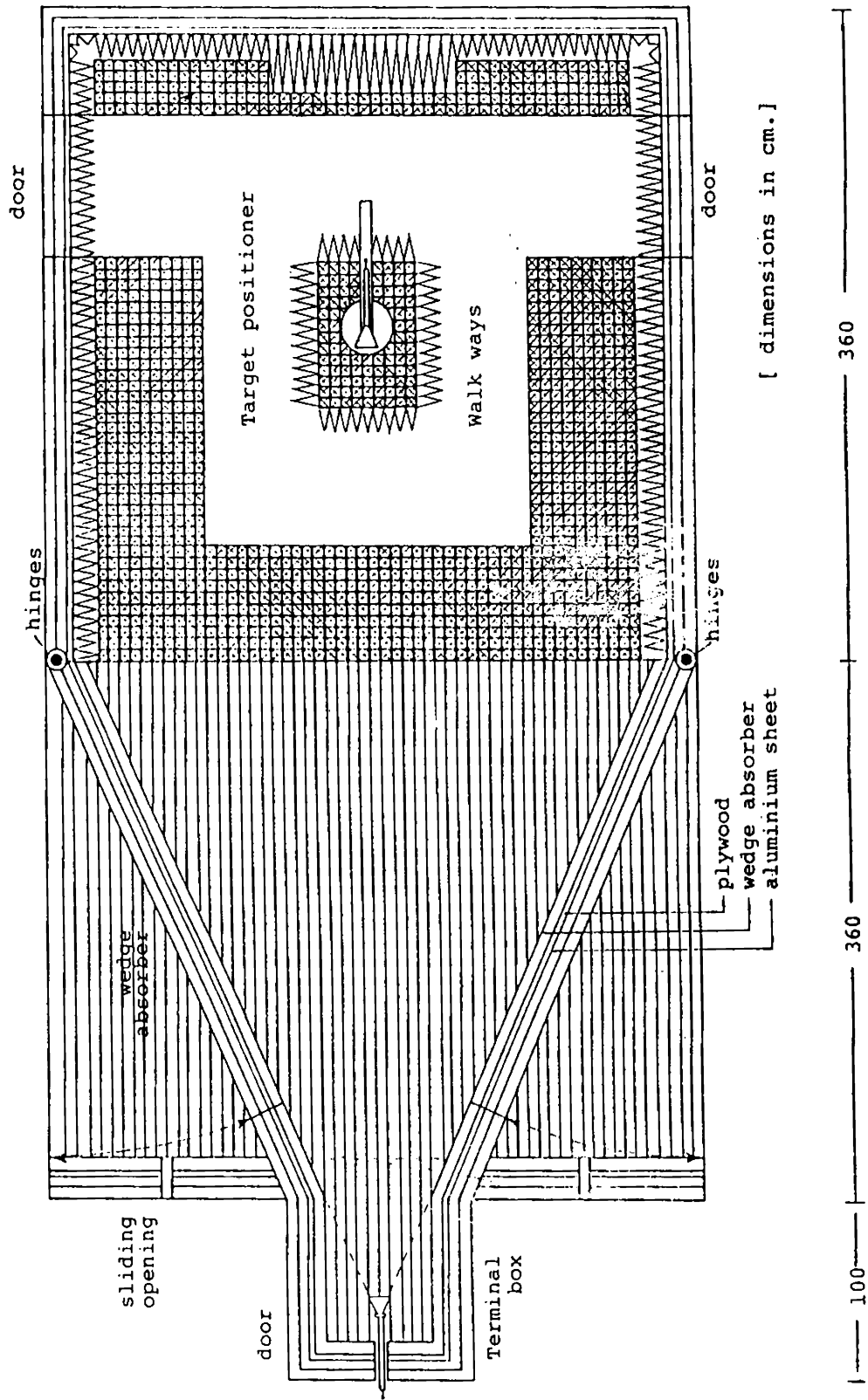


Fig. 3.10 Schematic representation of the microwave anechoic chamber

can be measured. A network analyser consists of a *sweep oscillator*, a *transducer*, a *harmonic frequency converter (receiver)* and a *display unit*, as shown in Fig. 3.11.

The transducer, which is the transmission/reflection test unit, is connected between the signal source and the receiver. It has a three-fold function. The first is to split the incoming signal into the reference and test signals. Secondly, it provides an extension capability for the electrical length of the reference channel, so that the distance travelled by the test and the reference signal are equal. Finally, it connects the system properly for transmission or reflection measurements.

In the receiver, the harmonic frequency converter mixes the RF signal with the output of a local oscillator and the resulting signal is given to the display unit.

The present configuration of HP 8510B Network Analyser is capable of measuring the transmission and reflection characteristics of active and passive networks in the form of gain, reflection coefficient, S-parameters and normalised impedance over 110 dB spurious free dynamic range in the frequency band of 10 MHz to 26.5 GHz. The measurements can be executed in any one of the two independent channels. The channels can be displayed individually or simultaneously in coupled or uncoupled channel mode. This provides the facility of simultaneously observing both transmission and reflection characteristics of the network under test. The measured results can be presented in logarithmic or linear magnitude, phase or group delay format on rectangular or polar coordinates. Direct measurement of normalised impedance or admittance is possible with Smith-Chart or Inverted Smith-Chart format. The value and frequency of any data can be read directly with the help of one of the five independent markers. The measurement can be done either in Ramp mode or in Step mode. In Step mode, measurements can be performed in 801 points with a maximum averaging of 4 K. The sweep rate can also be adjusted depending upon

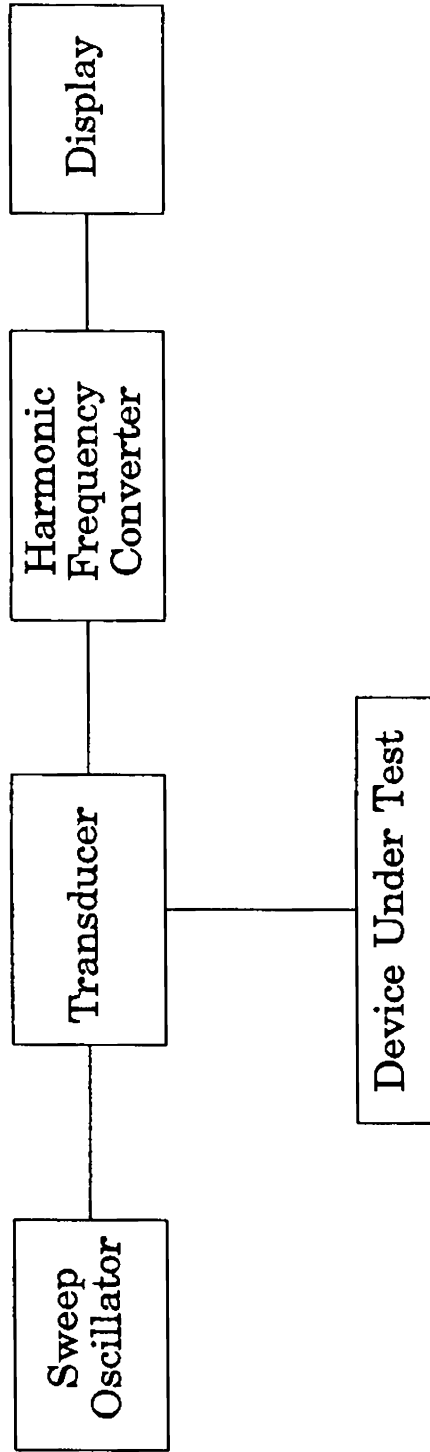


Fig. 3.11 Block diagram of a network analyser

with a maximum averaging of 4 K. The sweep rate can also be adjusted depending upon the need. The main advantage of HP 8510B Network Analyser from its earlier versions is its capability of *time domain measurements*. This gives more accuracy in measurement by knowing the precise point of reflection and by removing it (if unwanted) using *time domain gating* technique.

In the present measurement set-up, HP 8510B is interfaced with HP 9000/300 series computer and a HP 7475A plotter, so that depending upon the need, the displayed output can be saved in floppy through computer or the hard copy can be taken out directly using the plotter.

3.3.3 Antenna positioner and controller

For plotting the radiation patterns, the test antenna can be used either as a receiver or as a transmitter, whichever is convenient. In the present work, the radiation patterns are measured in the receiving mode. In this mode of pattern measurement, the test antenna has to be rotated about a vertical axis in the azimuth plane. For this, an antenna positioner (turn-table) with remote control facility is required.

The positioner-controller used for the measurement is Scientific Atlanta 4131 positioner-controller. The model 4131 is a microprocessor based unit designed to move about a single axis and simultaneously display the angular position. The controller can be interfaced to a computer and various setting parameters like range, speed of rotation, direction of rotation *etc.*, can be controlled from the front panel of the controller or through the computer. The accuracy of the system is 0.01 degree.

3.4 METHOD OF MEASUREMENTS

The various antenna characteristics measured are:

1. Impedance
2. Radiation pattern
3. Gain

3.4.1 Impedance

The knowledge of input impedance of an antenna is of prime importance, because input impedance directly effects the efficiency with which the energy is transferred to and from the antenna. When the microwave signal is fed to the antenna, if the antenna input impedance is not properly matched with the source impedance, part of the signal will be reflected back towards the source. This results in a standing wave pattern in the transmission line. The reflection is accounted by the parameter *reflection coefficient* (ρ) and is defined as the voltage/current ratio of the energy reflected to the incident energy. The mismatch of the device can be measured by another parameter called VSWR. It is related to ρ by the relation, $VSWR = (1 + \rho) / (1 - \rho)$. For perfect match, the VSWR is unity which is an ideal case.

The input impedance measurement of the antennas are carried out using HP 8510B Vector Network Analyser. Before taking any measurement, one port calibration has been done using 3.5 mm cal-kit and the calibration is stored in the memory, so that it can be revoked at any time. Recalling the proper calibration, the test antenna is connected to Port 1 of the S-parameter test set. Using FORMAT menu, the measured values can be

displayed in any one of the numerous possible formats. In the present investigation, plots are taken in Smith-Chart and VSWR formats.

Since the characteristic impedance of the network analyser is set to 50Ω , the center of the Smith-Chart corresponds to 50Ω . The trace shows the variation of complex input impedance of the test antenna with frequency. By selecting the MARKER, the complex impedance in $R + jX$ format can be read directly from the display for any frequency value.

In VSWR format, the trace represents the variation of VSWR with frequency. In this format, value of VSWR for a particular frequency can be displayed using MARKER. The impedance bandwidth of the antenna can be obtained directly by noting the frequency band over which the VSWR value is less than 2. Then the percentage bandwidth is given by $(\Delta f / f_0) \times 100\%$, where f_0 is the central frequency of the band and Δf is the frequency band where VSWR is less than 2.

3.4.2 Radiation pattern

The radiation pattern of an antenna is the spatial variation of the received/transmitted field intensity/power by the antenna. A complete representation of the radiation pattern requires a three dimensional plot. For simplicity, the radiation pattern can often be described in terms of principal E and H-planes. According to the reciprocity theorem, the radiation pattern can be measured by either of the two methods: (i) test antenna as receiver and (ii) test antenna as transmitter. In the present investigation, the radiation pattern measurements of the antennas are carried out inside an anechoic chamber, using the first method. The set-up used for pattern measurement is shown in Fig. 3.12.

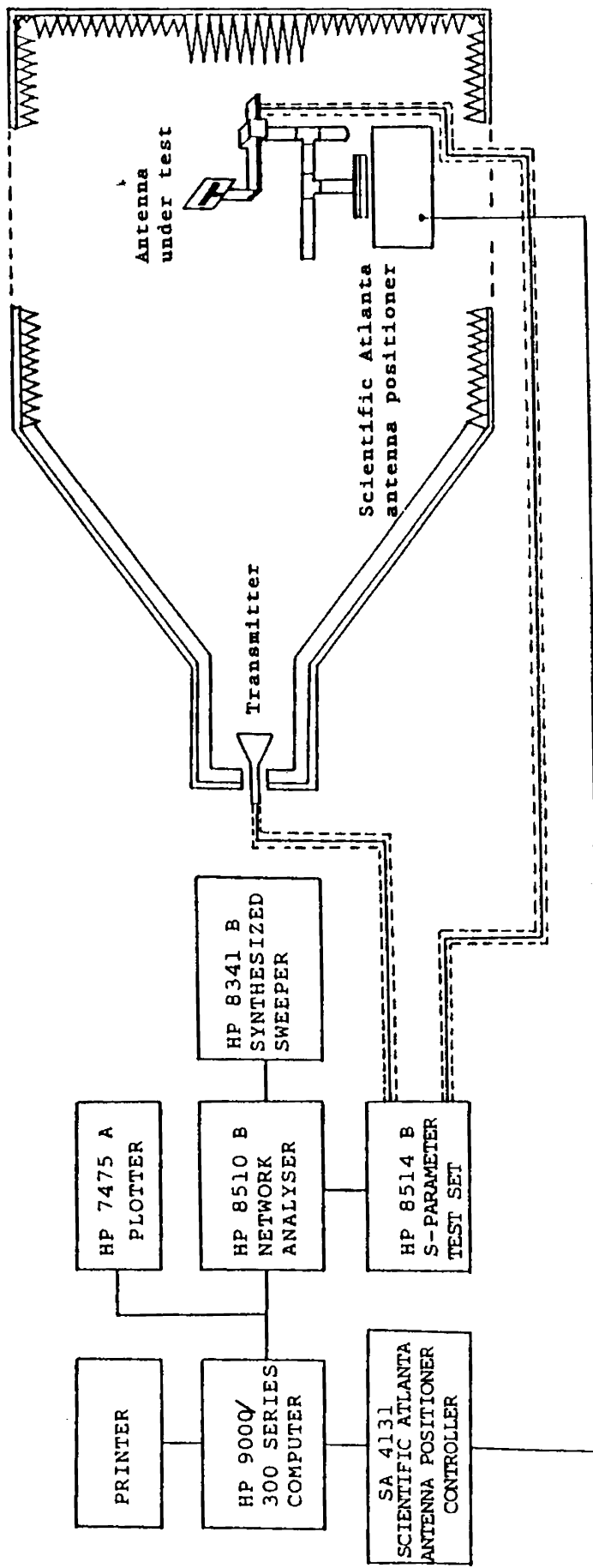


Fig. 3.12 Experimental set-up used for radiation pattern measurement

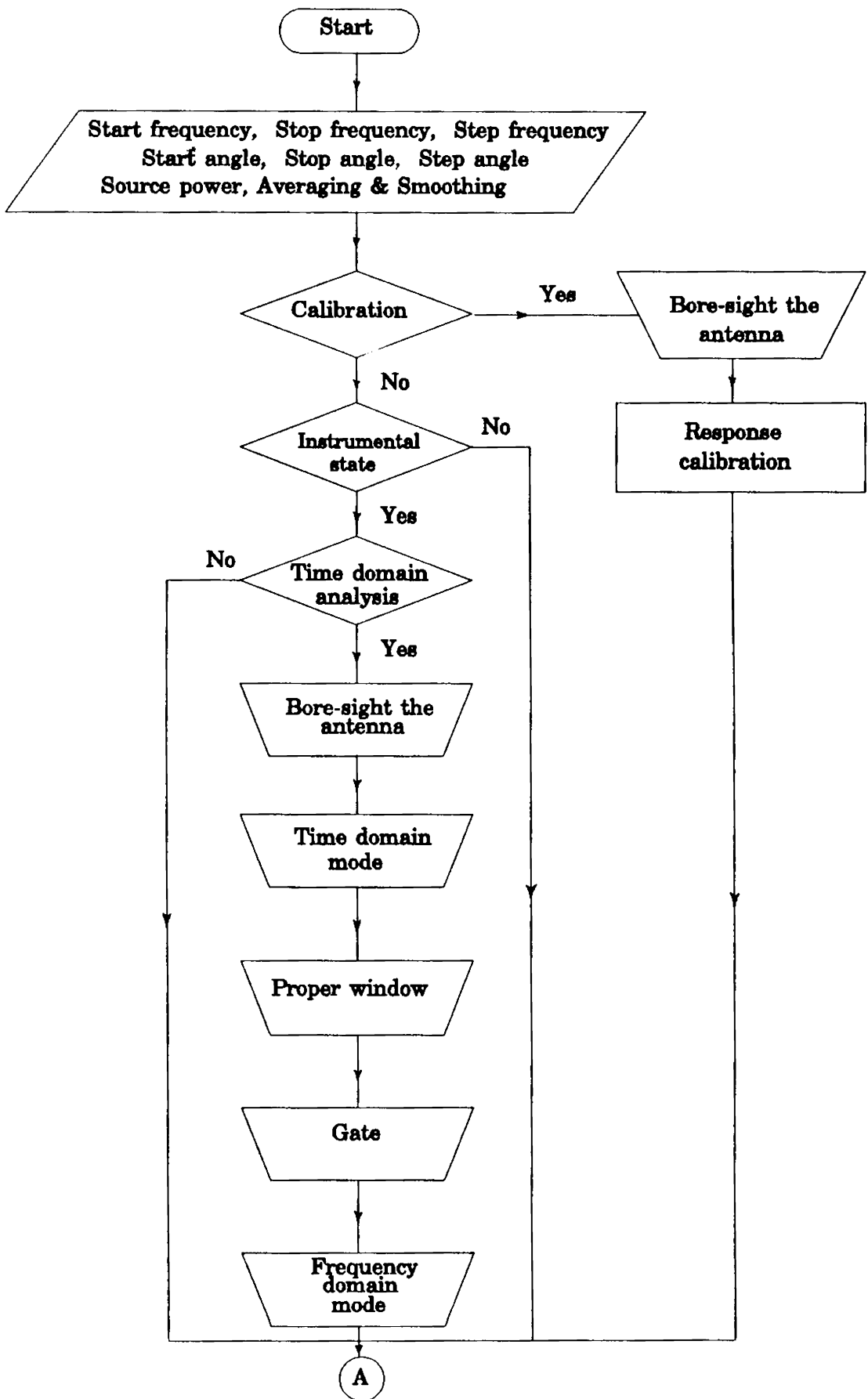
The HP 8510B Network Analyser system is used for pattern measurement. The network analyser is interfaced to HP 9000/300 series computer and Scientific Atlanta positioner-controller. An automatic pattern measurement software [138] is used for measuring and plotting the radiation patterns of the test antennas. The software incorporates all the facilities of network analyser like averaging, time domain capabilities *etc.* Flow chart of the programme is given in Fig. 3.13.

In the experimental set-up, the standard transmitting antenna (wideband ridged horn, 1 GHz - 18 GHz) is connected to Port 1 and the test antenna is connected to Port 2 of the network analyser. The test antenna can be rotated along the azimuth plane using a Scientific Atlanta positioner-controller, which is also connected to the computer. The computer automatically controls both the network analyser and the positioner-controller and acquires and stores data in it. In sweep mode, it can collect information about 801 frequency points in one rotation itself. The HP 7475A plotter, interfaced with the computer, gives the hard copy of the radiation pattern.

3.4.3 Gain

The ability of the antenna to concentrate radiated power in a direction, or conversely to absorb the incident power efficiently from that direction is termed as its gain.

In this thesis, a comparative measurement of gain of new antennas is made with standard antennas. For printed dipoles, gain is compared with standard half wave wire dipole resonating at the central frequency of the band of interest. The gain of microstrip dipoles is compared with standard rectangular patch etched on same dielectric substrate and resonating at the central frequency of the band of interest of test antenna.



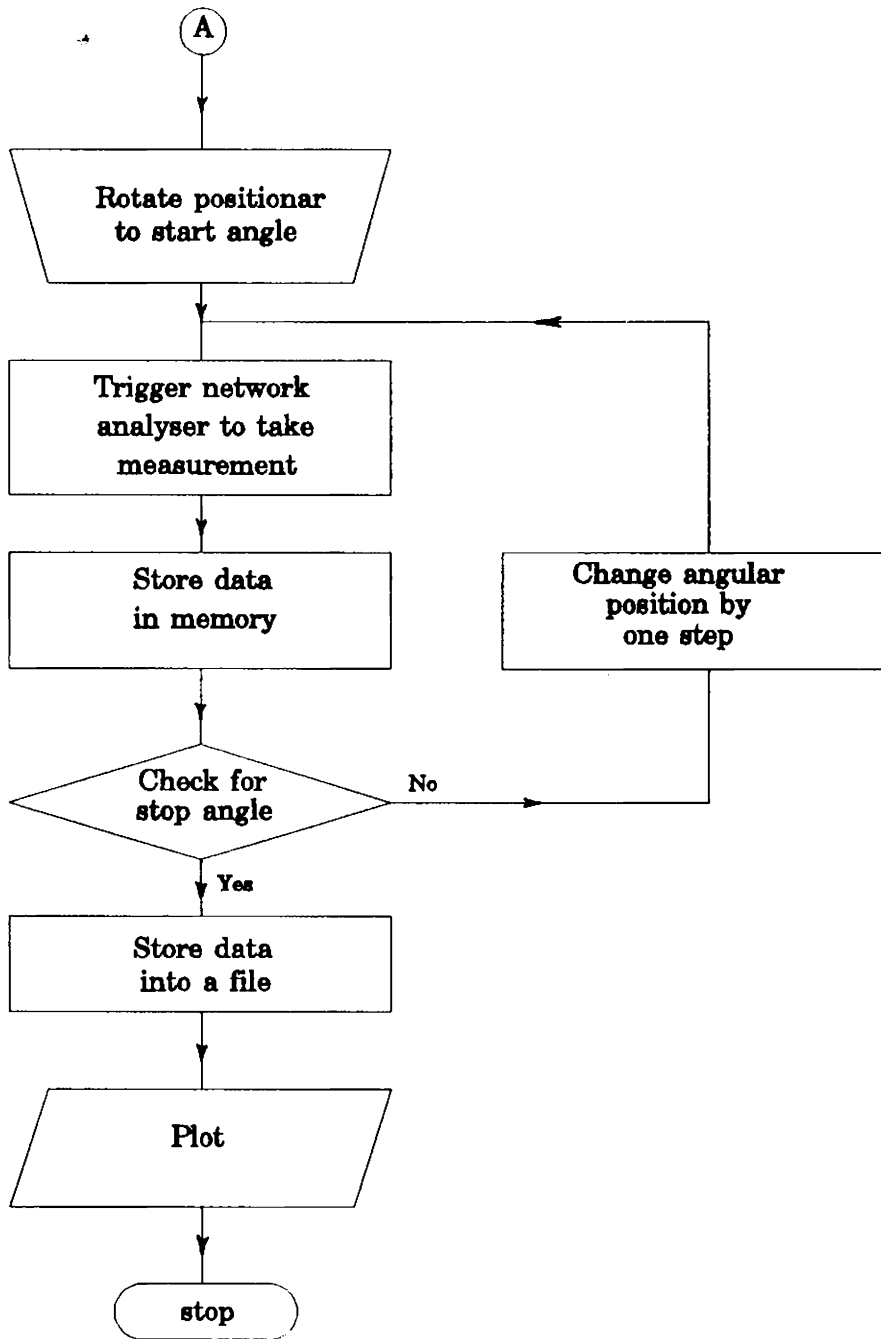


Fig. 3.13 Flow chart for radiation pattern measurement procedure using HP 8510B network analyser

For measurement, the reference antenna (wire dipole for printed dipole and rectangular microstrip patch for microstrip dipole) is kept on the turn-table and connected to the Port 2 of the network analyser. The Port 1 is connected to a wideband transmitting horn. The turn table is rotated so as to receive maximum power. Then the network analyser is calibrated *ie.*, the $|S_{21}|$ is made 0 dB in the frequency band of interest. Now, the reference antenna is replaced by the test antenna and the trace of $|S_{21}|$ gives the gain of test antenna with respect to the reference antenna.

Experimental results I: Printed dipoles

4

In this chapter, the experimental results obtained for various types of printed dipoles are presented. The studies are conducted in the frequency range of 800 - 2000 MHz. The chapter is divided into three sections as follows:

1. Flared printed dipole
2. Triangular end-loaded printed dipole
3. Parallelogram end-loaded printed dipole

Due to non-availability of proper design criteria of printed dipoles in open literature, a rectangular printed dipole is optimised for maximum impedance bandwidth (2:1 VSWR bandwidth) through experimental iterations. Schematic representation of the dipole is given in Fig. 4.1. The dotted line shows the arm etched on the other side of the substrate. The

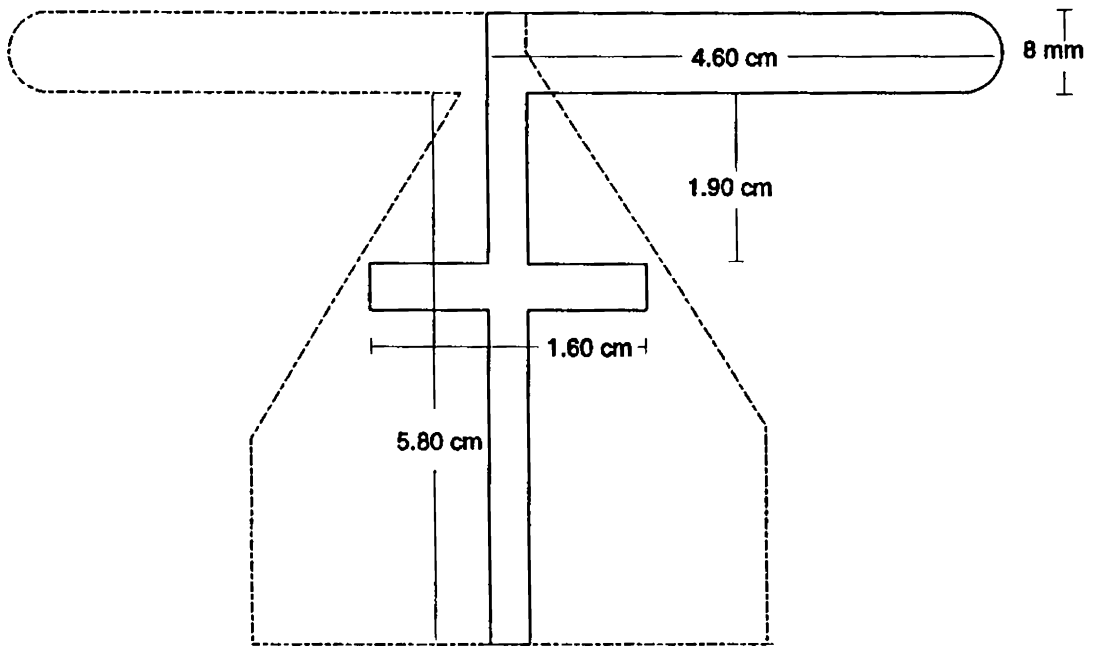


Fig. 4.1 Schematic representation of rectangular printed dipole

dipole is matched to 50 Ω feed using a stub and an impedance transformer. The line length and impedance of the stub and transformer are 1.60 cm and 33.5 Ω and 5.80 cm and 42 Ω respectively.

The impedance chart along with the VSWR plot of the dipole are shown in Fig. 4.2. The central frequency of the antenna is 1.498 GHz and the 2:1 VSWR bandwidth is 27%. The co and cross-polar patterns of the principal planes at the central and two end frequencies are given in Fig. 4.3. From this figure, it is clear that the E-plane patterns are broad, similar to that of wire dipole antennas. The deviation in the H-plane patterns from the conventional omnidirectional shape may be due to the finite size of the dielectric substrate and the radiation from the feed structure.

As already mentioned, throughout the experimentation on printed dipoles, the parameters of matching transformer, such as its length and line impedance are kept the same as that in the case of optimised rectangular printed dipole. The optimisation of matching of various dipoles are done by adjusting the length, position and line impedance of the stub.

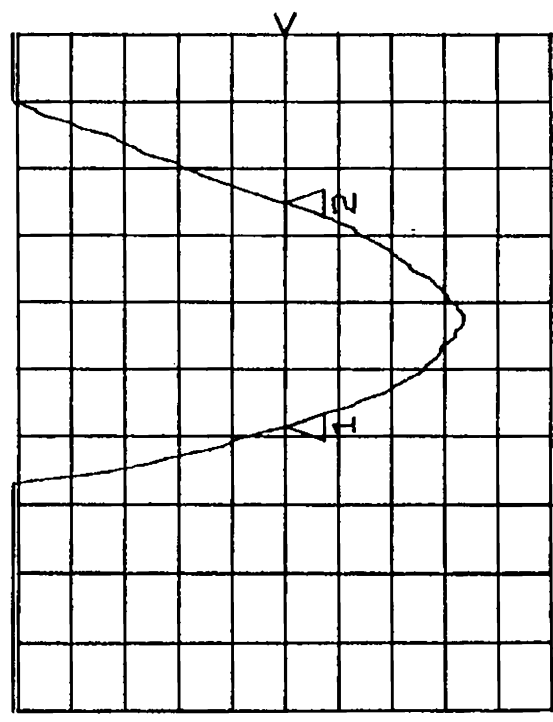
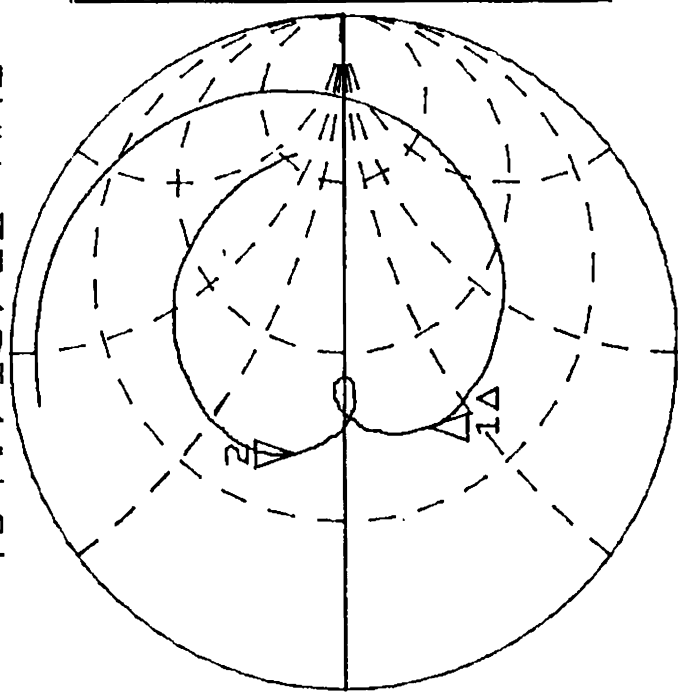
4.1 FLARED PRINTED DIPOLE

The effect of flaring the dipole arms are studied by providing flaring to the arms of the optimised rectangular printed dipole. The sketch of the antenna is given in Fig. 4.4. Here, all the initial design values are same as that of the optimised rectangular printed dipole. An experimental study of the impedance characteristics with the following antenna parameters has been done:

S_{11} REF 1.0 Units
 Z REF 2.0
 ∇ 200.0 mUnits/
 Δ 250.0 m /
 ∇ -2.6639 Ω 25.082 Ω 2 -0.0000
 hp

* C

MARKER 2-1
 404.719712 MHz



START 0.79500000 GHz
 STOP 2.00437500 GHz

Fig. 4.2 Impedance loci and VSWR plot of rectangular printed dipole

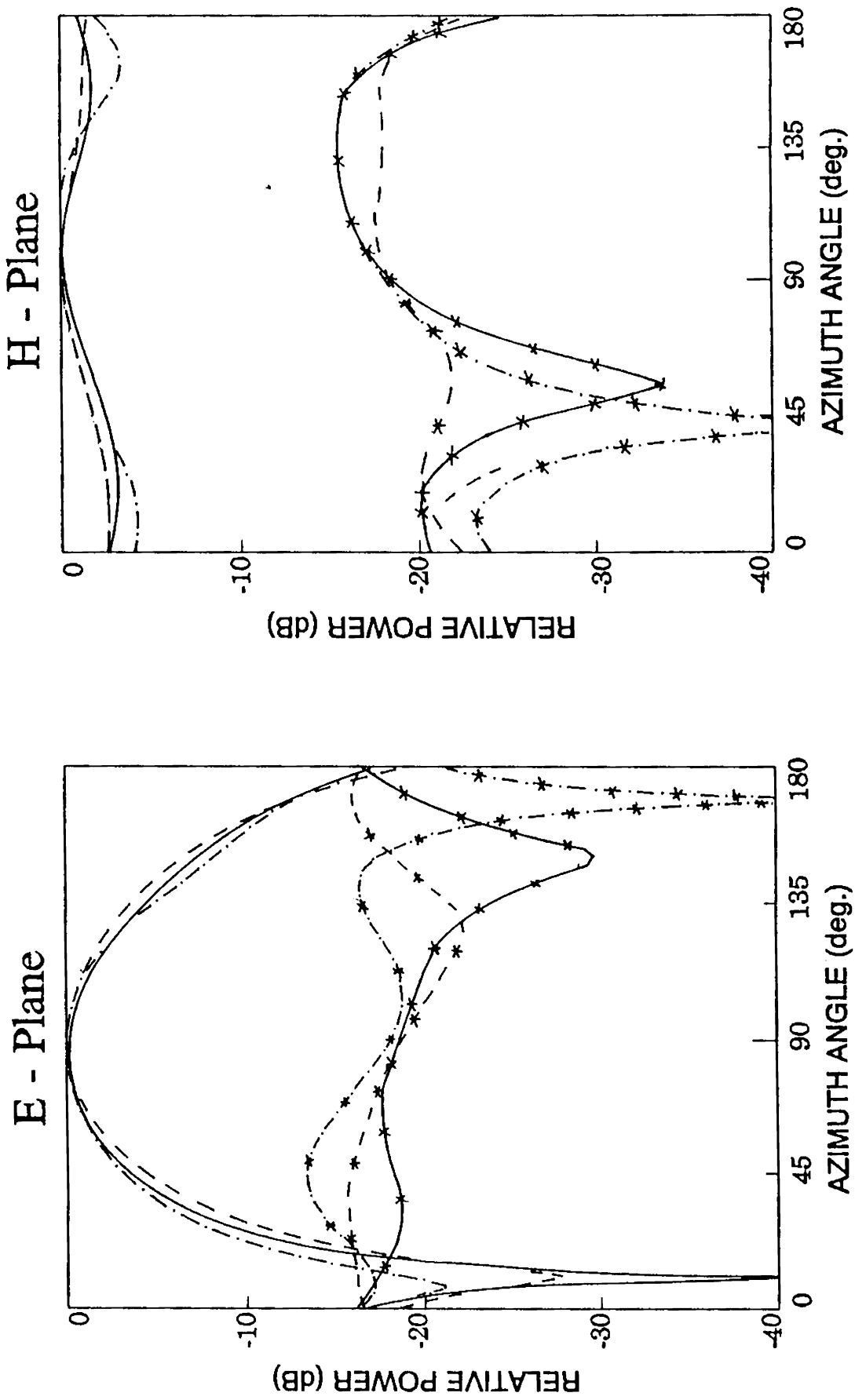


Fig. 4.3 Radiation patterns of rectangular printed dipole

co-polar : - - - - - 1.296 GHz, ——— 1.498 GHz, - - - - - 1.700 GHz
 cross-polar : - - * - - 1.296 GHz, ——— * ——— 1.498 GHz, - - - * - - 1.700 GHz

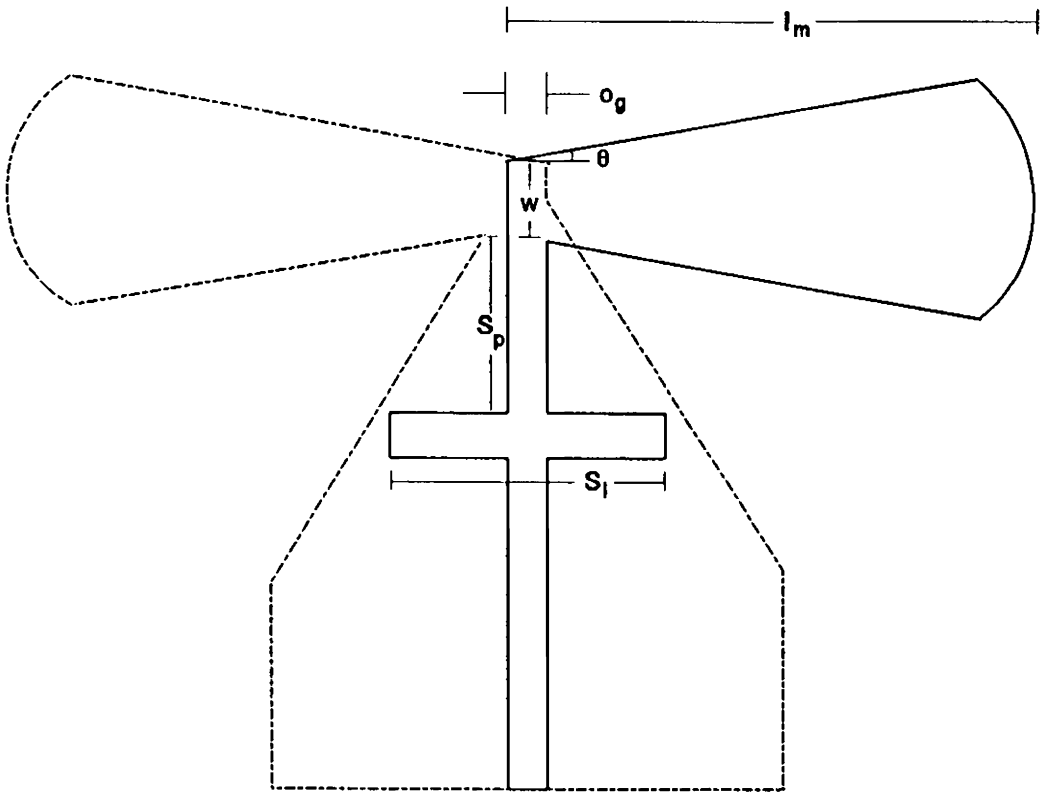


Fig. 4.4 Schematic representation of flared printed dipole

1. Flaring angle θ
2. Arms overlapping O_s
3. Arm width at feed point w
4. Main arm to ground arm ratio R

4.1.1 Flaring angle

The flaring angle θ is varied from 0° to 20° , keeping the remaining parameters constant. The VSWR plots of the dipoles of various flaring angles are given in Fig. 4.5. The Δf value in the plots shows the 2:1 VSWR bandwidth. The percentage bandwidths and the central frequencies with optimised stub parameters are given in Table 4.1. It is quite evident from the table that there is considerable improvement in impedance bandwidth with flaring. Although the optimum value of θ is 10° , there is little change in percentage bandwidth in the range 5° to 15° . Thus, it can be concluded that the value of θ is not that critical. Also, with increase in the flaring angle there is a decrease in the central frequency.

Table 4.1

Percentage bandwidths and central frequencies of flared printed dipoles of various flaring angles with optimised stub parameters

Flaring angle θ	Stub			Percentage bandwidth	Central frequency (GHz)
	position (cm)	length (cm)	impedance (Ω)		
0°	1.90	1.60	33.5	27.01	1.498
5°	1.95	2.00	33.5	32.99	1.459
10°	2.15	1.90	36.0	33.85	1.442
15°	2.30	1.60	32.0	32.89	1.407
20°	2.15	1.05	32.0	30.15	1.396

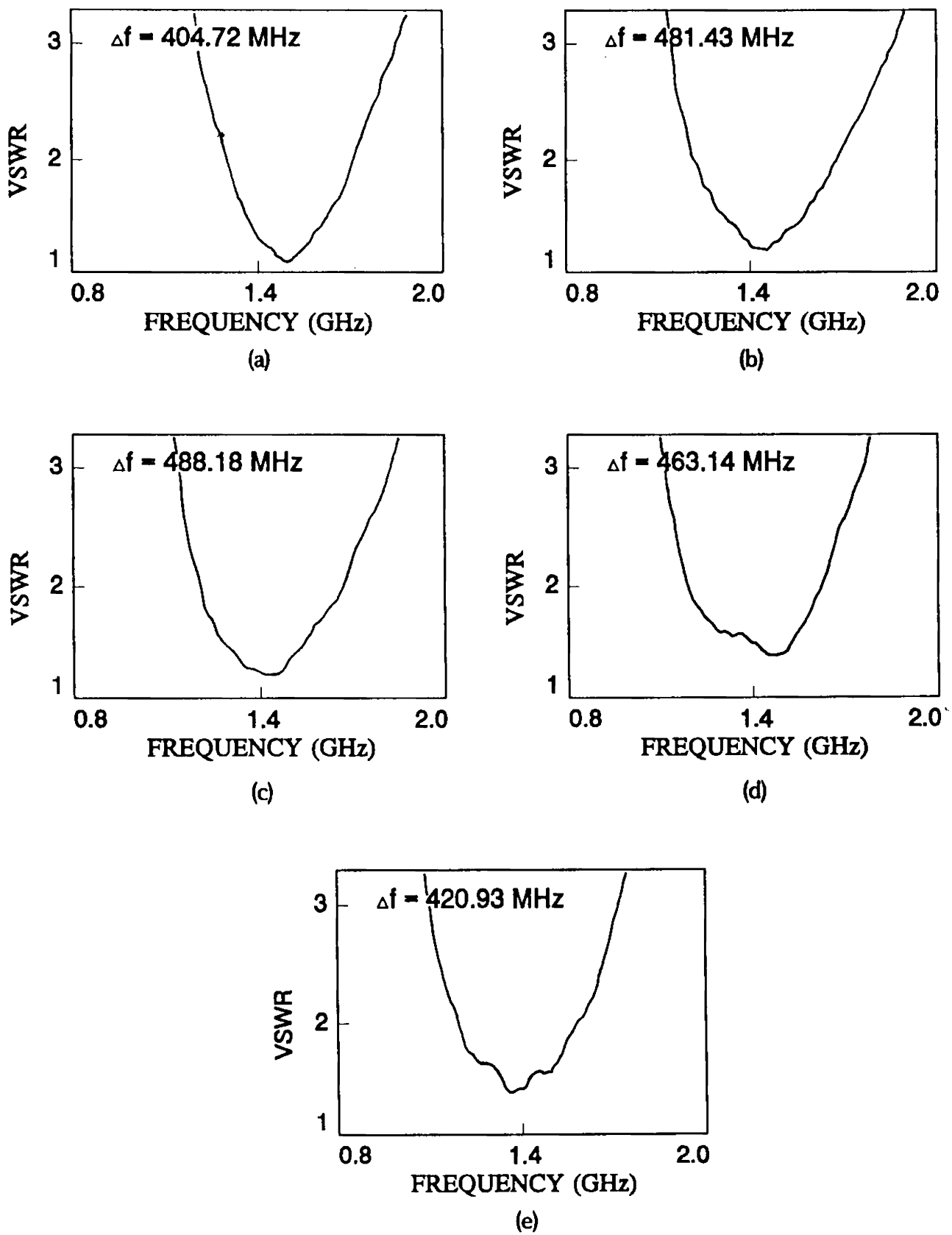


Fig. 4.5 VSWR plots of flared printed dipoles for different flaring angles
a) $\theta = 0^\circ$ b) $\theta = 5^\circ$ c) $\theta = 10^\circ$ d) $\theta = 15^\circ$ e) $\theta = 20^\circ$

Since the introduction of flaring to the dipole arms brings a structural modification to the dipole design, its effect on the radiation characteristics is observed in the band of interest. The E and H-plane radiation patterns of the dipole with $\theta = 10^\circ$ are plotted in Fig. 4.6. A comparison with the patterns of the dipole with no flaring (Fig. 4.3) reveals that there is no significant change in the co-polar patterns; but the cross-polar level is high for the flared dipole.

4.1.2 Arms overlapping

As a next step towards design optimisation, the flaring angle is selected as $\theta = 10^\circ$ and dipoles are fabricated with different overlapping lengths O_s . For this, only the position of main arm, with respect to ground arm is varied; so that other parameters can be kept constant. Thus, along with the overlapping length, the feed point also changes for different dipoles. The VSWR plots of various antennas are given in Fig. 4.7. The percentage bandwidths and the central frequencies along with the optimised stub parameters of different antennas are given in Table 4.2. Although the optimum value of O_s is 9 mm, the effect of change in the arms overlapping length O_s on percentage bandwidth is very small. This is due to the fact that variation in O_s brings only a very little change in the input impedance characteristics of the antenna and is easily compensated by proper selection of stub.

4.1.3 Arm width at feed point

The next parameter studied is the width of arms at the feed point. Like previous cases, width w is varied around 8 mm (the value of w for the optimised rectangular printed dipole) in steps of 1 mm, while other parameters are kept constant. The different VSWR plots, and

the percentage bandwidths and the central frequencies are given in Fig. 4.8 and Table 4.3 respectively. Except for $w = 10$ mm, effect of w on the percentage bandwidth is very little. Also the central frequency is shifted towards higher value with increase in w . The optimum value of arm width at feed point is $w = 9$ mm.

Table 4.2

Percentage bandwidths and central frequencies of flared printed dipoles of various arms overlapping with optimised stub parameters

Arms overlapping O_s (mm)	Stub			Percentage bandwidth	Central frequency (GHz)
	position (cm)	length (cm)	impedance (Ω)		
6	2.35	1.40	38.5	34.70	1.464
7	2.20	1.40	28.5	34.96	1.453
8	2.15	1.90	36.0	35.85	1.442
9	1.95	2.00	33.5	36.85	1.484
10	1.75	2.00	33.5	35.99	1.528

Table 4.3

Percentage bandwidths and central frequencies of flared printed dipoles of various arm widths at feed point with optimised stub parameters

Arm width at feed point w (mm)	Stub			Percentage bandwidth	Central frequency (GHz)
	position (cm)	length (cm)	impedance (Ω)		
6	2.25	1.60	32.0	36.34	1.475
7	1.80	1.60	33.5	36.71	1.502
8	1.95	2.00	33.5	36.85	1.484
9	1.55	2.40	32.0	37.72	1.508
10	1.40	2.00	33.5	33.80	1.556

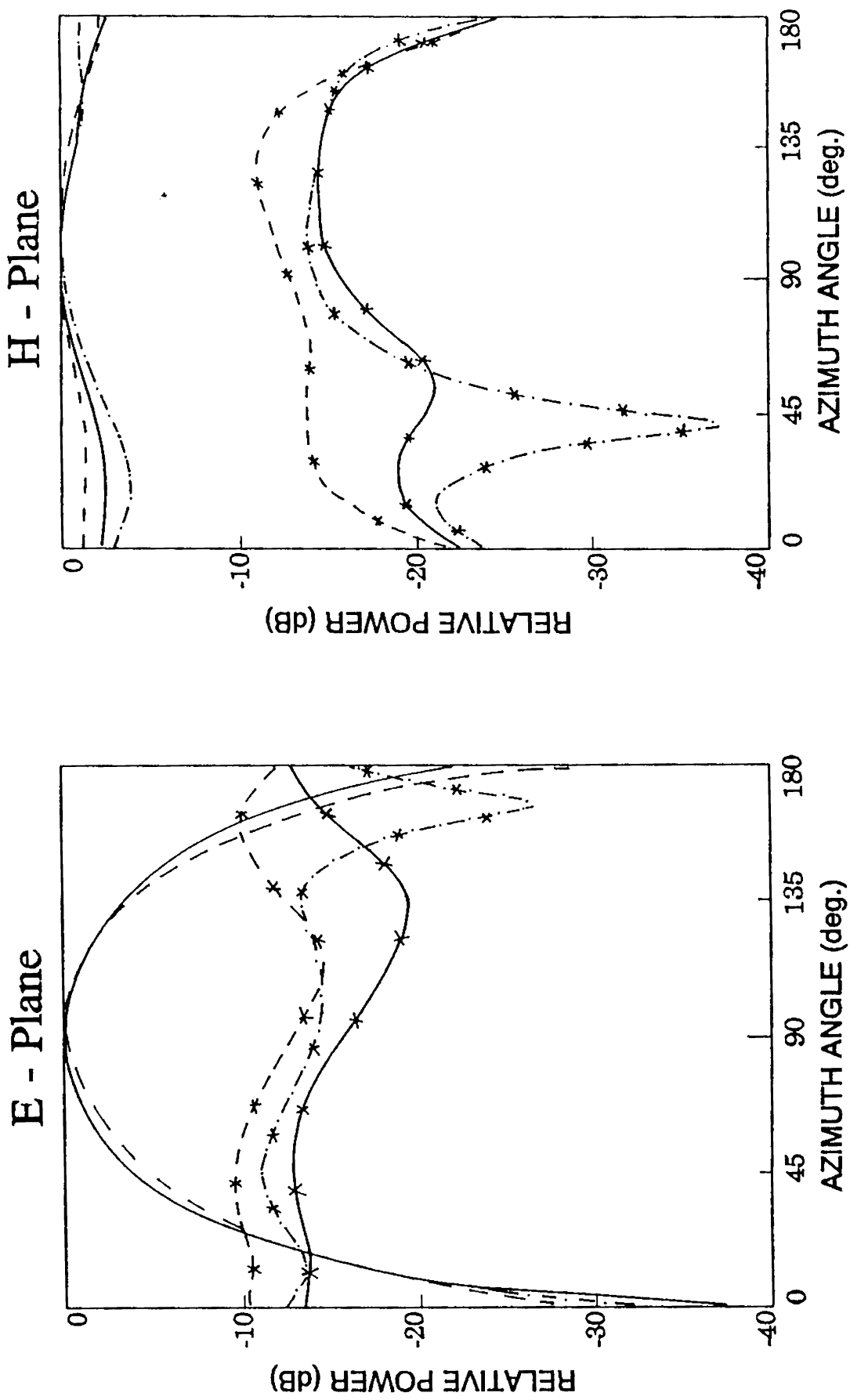
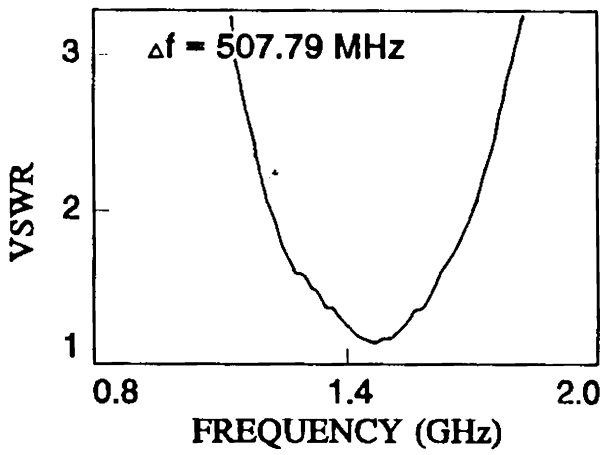
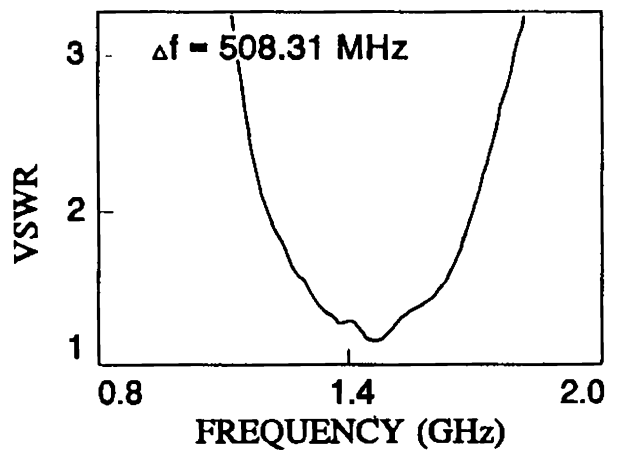


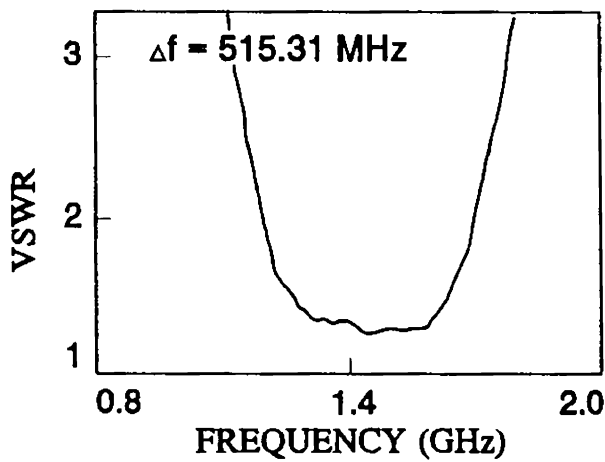
Fig. 4.6 Radiation patterns of flared printed dipole
 co-polar : ——— 1.197 GHz, ——— 1.441 GHz, ——— 1.686 GHz
 cross-polar : - - - * - - - 1.197 GHz, - - - * - - - 1.441 GHz, - - - * - - - 1.686 GHz



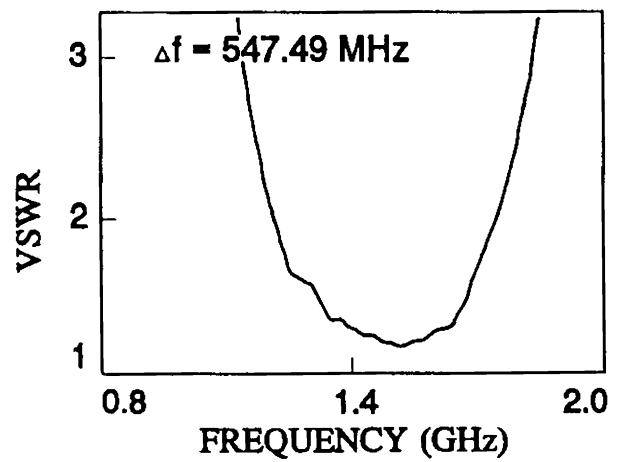
(a)



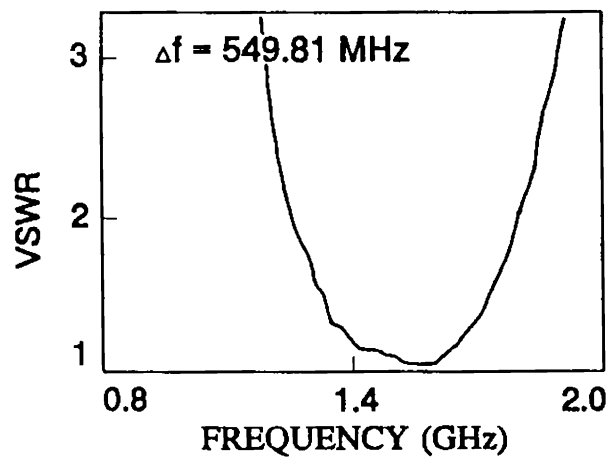
(b)



(c)

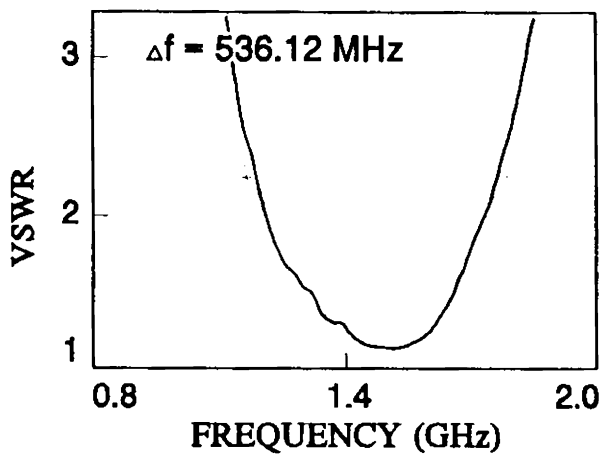


(d)

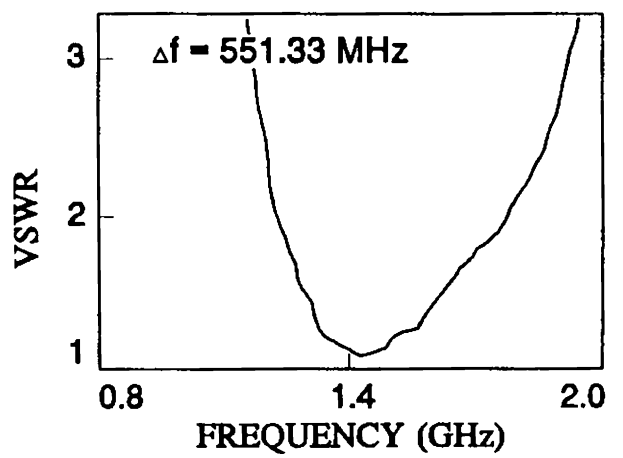


(e)

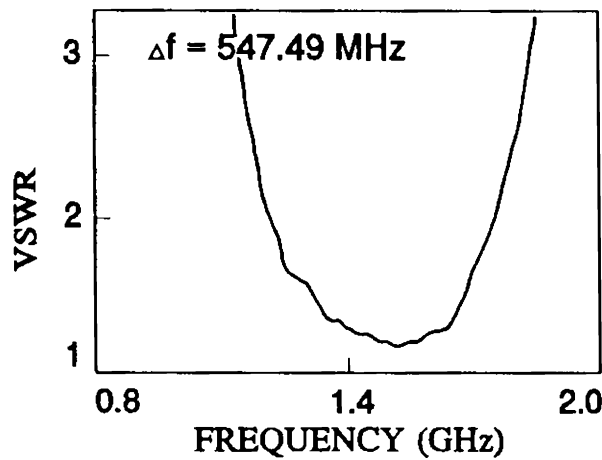
Fig. 4.7 VSWR plots of flared printed dipoles for different arms overlapping
 a) $O_g = 6 \text{ mm}$ b) $O_g = 7 \text{ mm}$ c) $O_g = 8 \text{ mm}$ d) $O_g = 9 \text{ mm}$ e) $O_g = 10 \text{ mm}$



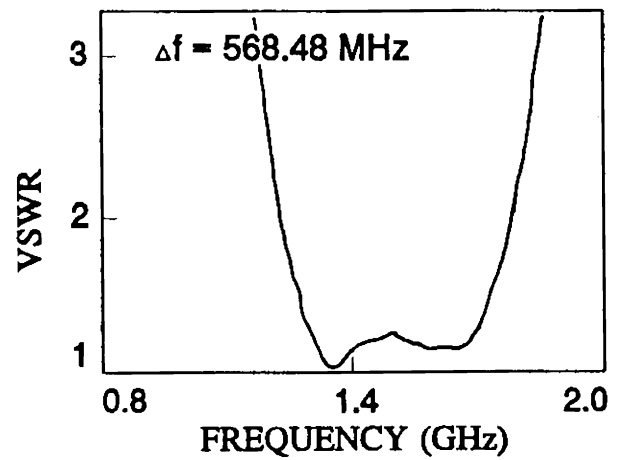
(a)



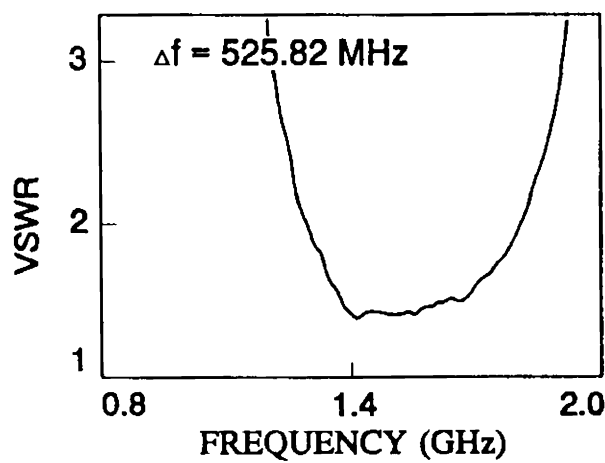
(b)



(c)



(d)



(e)

Fig. 4.8 VSWR plots of flared printed dipoles for different arm widths at the feed point
 a) $w = 6 \text{ mm}$ b) $w = 7 \text{ mm}$ c) $w = 8 \text{ mm}$ d) $w = 9 \text{ mm}$ e) $w = 10 \text{ mm}$

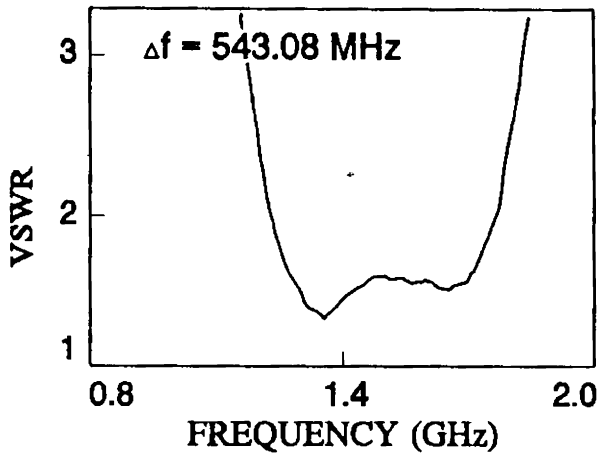
4.1.4 Main arm to ground arm ratio

To properly match the balanced dipole to unbalanced microstrip feedline, the dimensions of the ground arm are varied while keeping the main arm dimensions constant. Experiments are conducted for different main arm to ground arm ratio like 1:0.90, 1:0.95, 1:1.00, 1:1.05 and 1:1.10. The corresponding VSWR plots, and the percentage bandwidths and the central frequencies are given in Fig. 4.9 and Table 4.4 respectively. From the table, it is clear that the percentage bandwidth is better for ground arm dimensions larger than the main arm dimensions and increases with the increase in arms ratio. The percentage bandwidth is maximum for the arms ratio 1:1.10, but the difference from the value of percentage bandwidth for ratio 1:1.05 is only 0.41%. It is also well-known that any asymmetry in the arms structure creates asymmetry in the radiation pattern. Thus, as a compromise between the two, the ratio 1:1.05 is selected as the final design value.

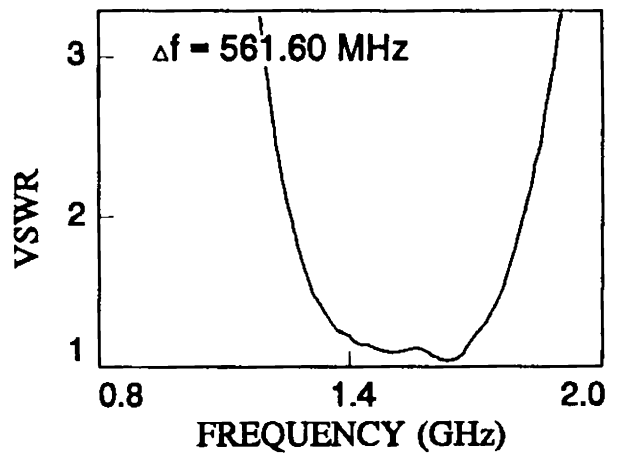
Table 4.4

Percentage bandwidths and central frequencies of flared printed dipoles of various main arm to ground arm ratio with optimised stub parameters

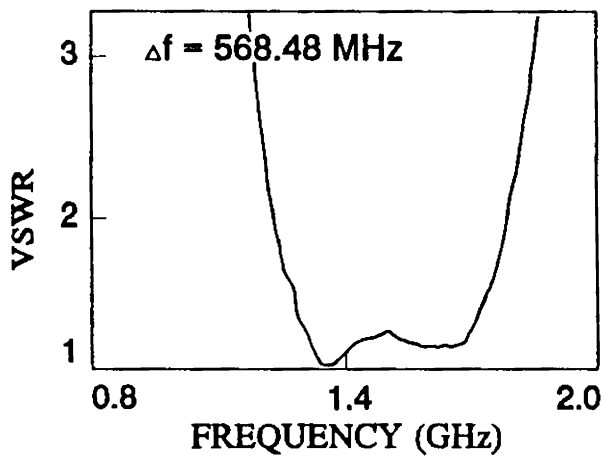
Main arm to ground arm ratio R	Stub			Percentage bandwidth	Central frequency (GHz)
	position (cm)	length (cm)	impedance (Ω)		
1:0.90	1.75	2.40	33.5	36.20	1.499
1:0.95	1.60	2.40	33.5	36.47	1.540
1:1.00	1.55	2.40	32.0	37.72	1.508
1:1.05	1.30	2.20	33.5	39.04	1.588
1:1.10	1.50	2.40	33.5	39.45	1.526



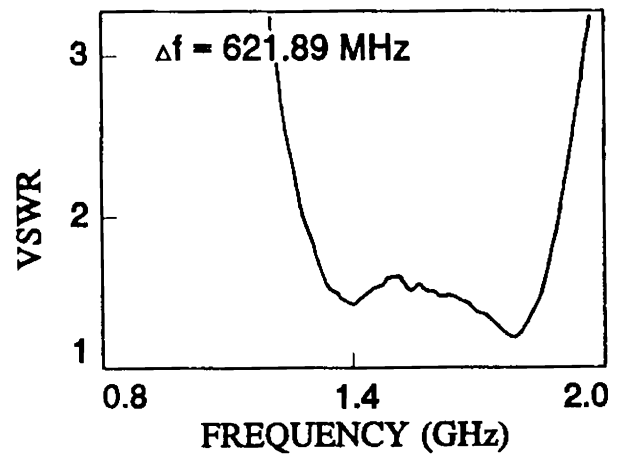
(a)



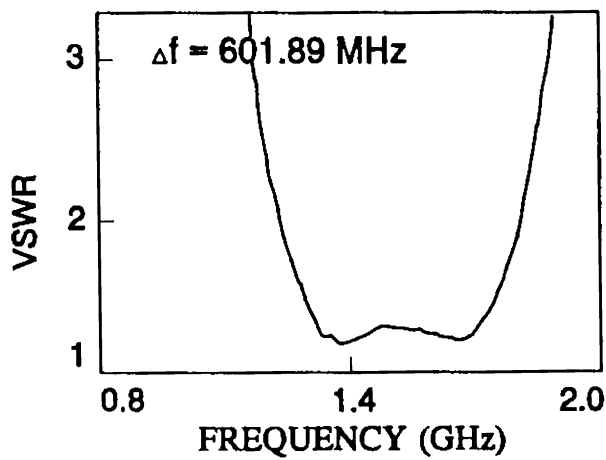
(b)



(c)



(d)



(e)

Fig. 4.9 VSWR plots of flared printed dipoles for different main arm to ground arm ratio
 a) $R = 1:0.90$ b) $R = 1:0.95$ c) $R = 1:1.00$ d) $R = 1:1.05$ e) $R = 1:1.10$

From the above results, the optimum parameters of Flared Printed Dipole Antenna (FPDA), shown in Fig. 4.10, are as follows:

Main arm length l_m	= 4.60 cm
Flaring angle θ	= 10°
Arms overlapping O_s	= 0.90 cm
Arm width at feed point w	= 0.90 cm
Feed point location l_f	= 0.45 cm
Stub length S_l	= 2.20 cm
Stub position S_p	= 1.30 cm
Stub line impedance	= 33.5 Ω

The ground arm dimensions are 1.05 times larger than the corresponding main arm values.

The impedance plot of FPDA is given in Fig. 4.11. The 2:1 VSWR bandwidth of the antenna is 621.79 MHz with central frequency at 1.588 GHz. Thus, the percentage bandwidth of the antenna is 39.04%.

The E and H-plane radiation patterns of FPDA are given in Fig. 4.12. It can be seen that these patterns do not show significant changes from those of rectangular printed dipole. Thus, it can be stated that the bandwidth enhancement is achieved without any degradation in the radiation characteristics of the dipole.

4.1.5 Design details

The design criteria for Flared Printed Dipole Antenna in terms of wavelength (λ_0), corresponding to the central frequency, has been developed by fabricating a large number of dipoles of various dimensions. The design details of the antenna, shown in Fig. 4.10, are given below:

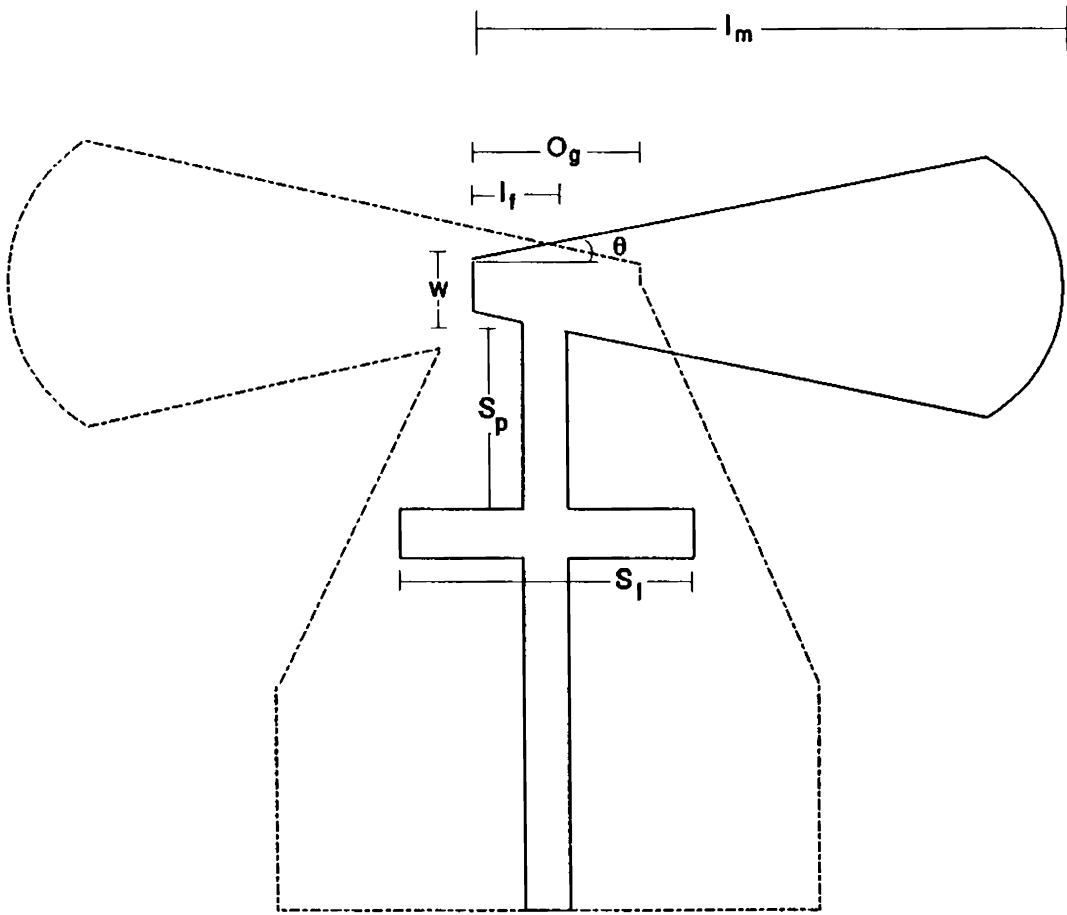
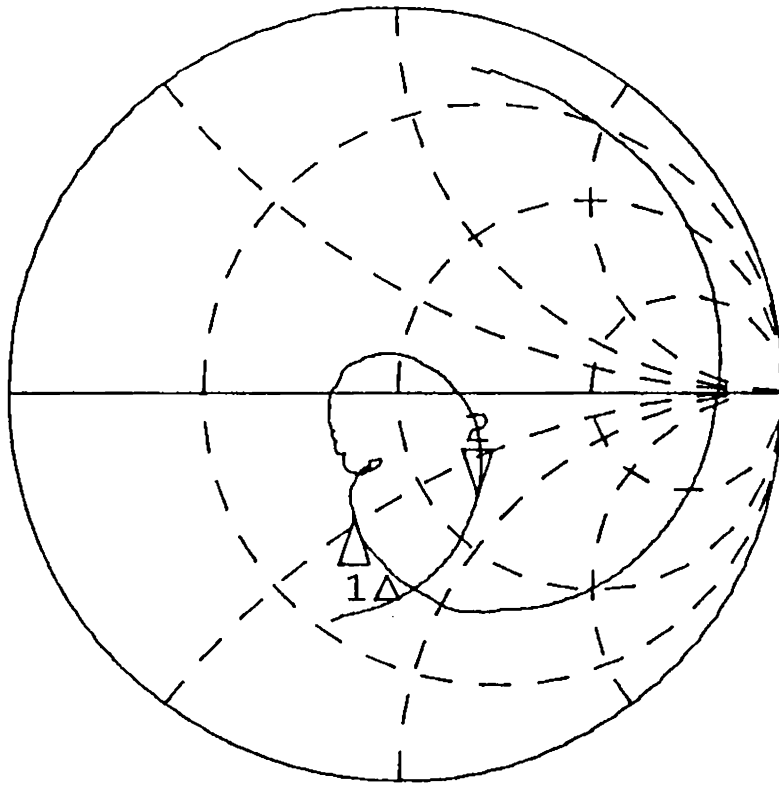


Fig 4.10 Schematic representation of optimised flared printed dipole

MARKER 2-1
621.793435 MHz



START 0.795000000 GHz
STOP 2.004375000 GHz

Fig. 4.11 Impedance loci of FPDA

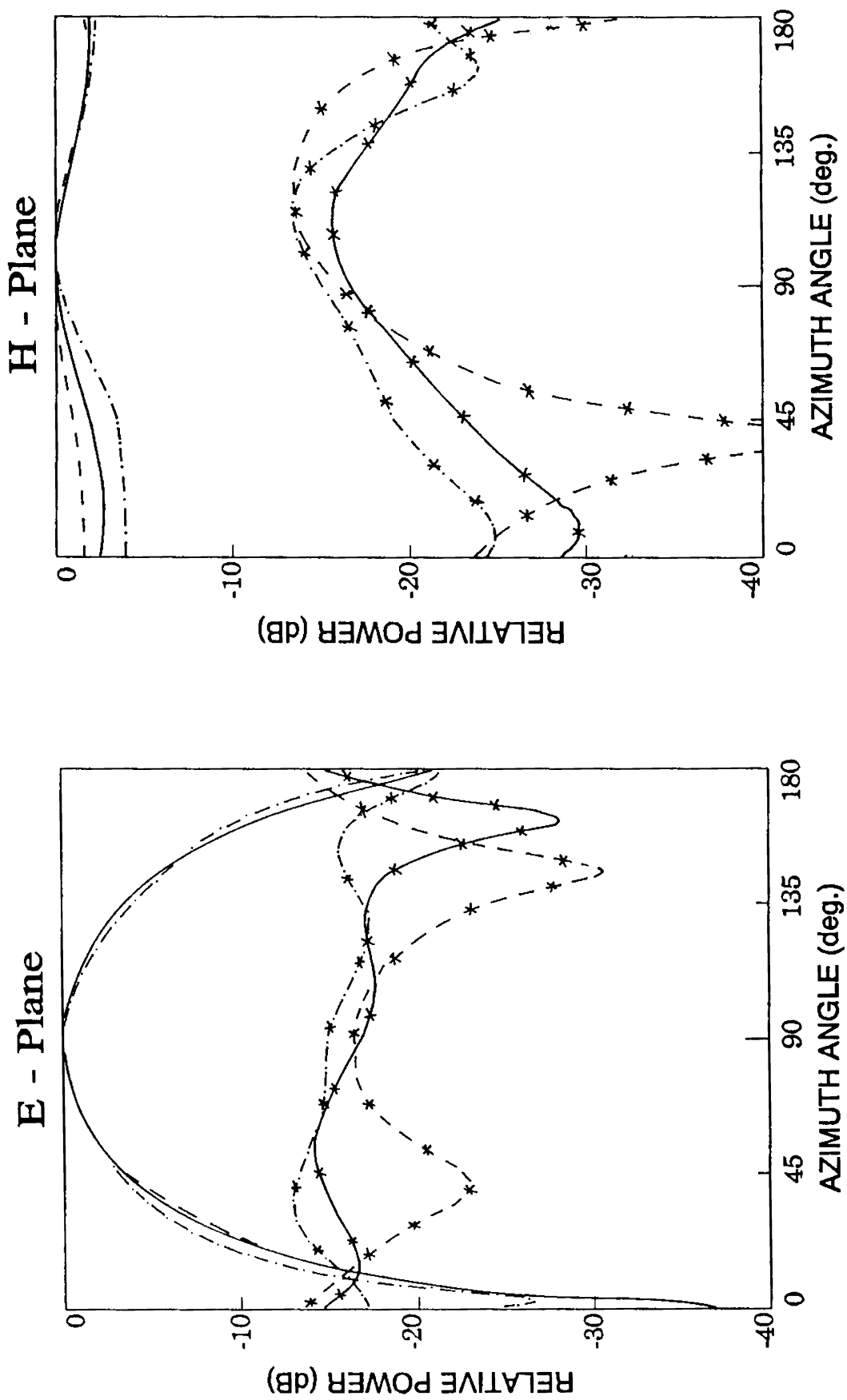


Fig. 4.12 Radiation patterns of FPDA
 co-polar : ——— 1.278 GHz, ——— 1.588 GHz, - - - - - 1.898 GHz
 cross-polar : - - - * - - 1.278 GHz, - - - * - - 1.588 GHz, - - - * - - 1.898 GHz

Main arm length l_m	= $0.243 \lambda_0$
Arm width at feed point w	= $0.048 \lambda_0$
Feed point location l_f	= $0.024 \lambda_0$
Arms overlapping O_s	= $0.048 \lambda_0$
Flaring angle θ	= 10°
Stub length S_l	= $0.225 \lambda_d$
Stub position S_p	= $0.133 \lambda_d$
Stub line impedance	= 33.5Ω
Transformer length l_t	= $0.57 \lambda_d$
Transformer line impedance	= 42Ω

All the ground arm parameters are 1.05 times larger than the corresponding main arm values. Here, $\lambda_d = \lambda_0 / \sqrt{\epsilon_{eff}}$ and the effective dielectric constant ϵ_{eff} can be calculated using the formula [139] given below:

$$\epsilon_{eff} = \frac{\epsilon_r + 1}{2} + \frac{\epsilon_r - 1}{2} \cdot \frac{\ln \left[\frac{\pi}{2} \right] + \left[\frac{1}{\epsilon_r} \right] \ln \left[\frac{4}{\pi} \right]}{\ln \left[\frac{8h}{w} \right]} \quad (1)$$

where, ϵ_r is the dielectric constant, h is the thickness of the substrate and w is the width corresponding to the line impedance.

4.2 TRIANGULAR END-LOADED PRINTED DIPOLE

As mentioned in the earlier chapter, investigations are also carried out on the effect of different shapes of end-loading on the impedance bandwidth of flared printed dipole antenna. For this, the design values of FPDA are used along with various shapes of loads like triangular, circular, parallelogram *etc.* The VSWR plots of different antennas are given

in Fig. 4.13 and the corresponding percentage bandwidths and the central frequencies are given in Table 4.5. It can be seen from the table that the central frequency is much higher for the triangular and parallelogram loads compared to the rest of the shapes. Also, percentage bandwidth is maximum for the triangular shape.

To observe the effect of triangular shaped loads at the dipole arms' ends, on the radiation characteristics, radiation patterns of the antenna are measured and plotted in Fig. 4.14. From the E and H-plane patterns, it is clear that there is no significant change in the co-polar patterns with respect to optimised rectangular printed dipole antenna (Fig. 4.3). Only 3-dB beamwidth for the triangular end-loaded printed dipole is slightly more than that of the rectangular dipole. Also the cross-polar level is slightly higher for the triangular end-loaded dipole. From the above observations it can be concluded that end-loading of dipole arms does not adversely effect the radiation properties of the printed dipoles.

The sketch of triangular end-loaded printed dipole is given separately in Fig. 4.15. To optimise the impedance bandwidth of triangular end-loaded printed dipole, the design values of FPDA are used as initial design values and the effect of the following parameters on the impedance bandwidth of the antenna is studied.

1. Triangle dimensions
2. Arm width at feed point w
3. Main arm to ground arm ratio R
4. Flaring angle θ

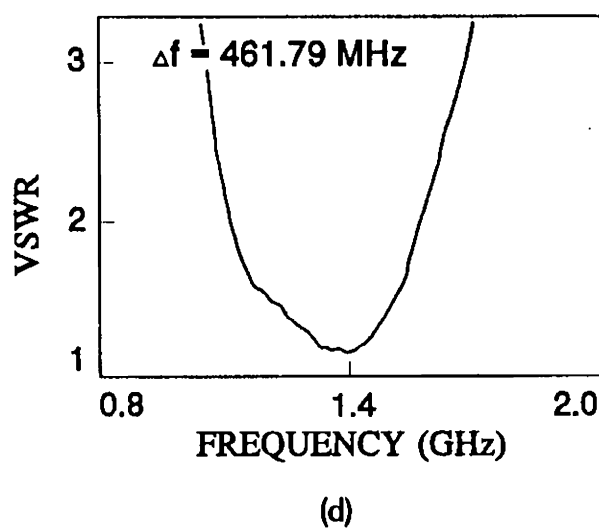
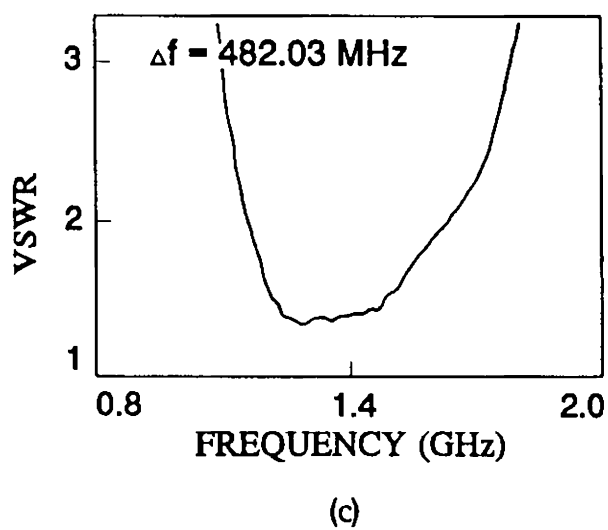
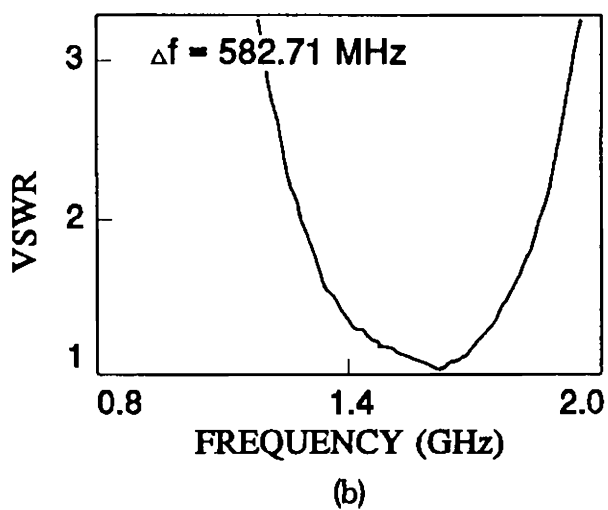
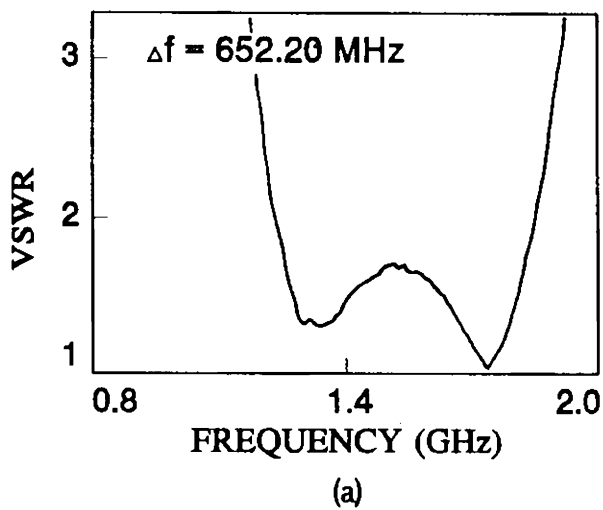
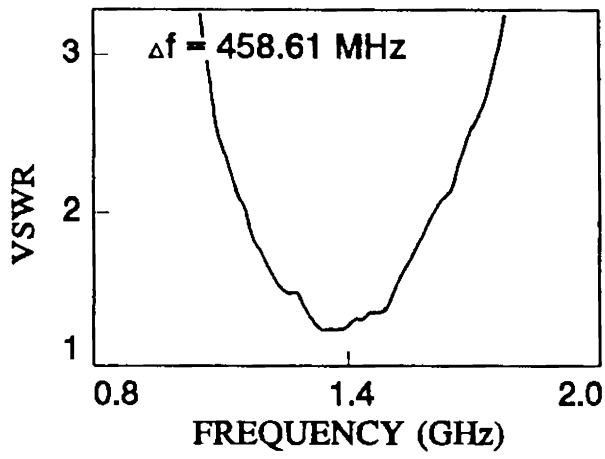
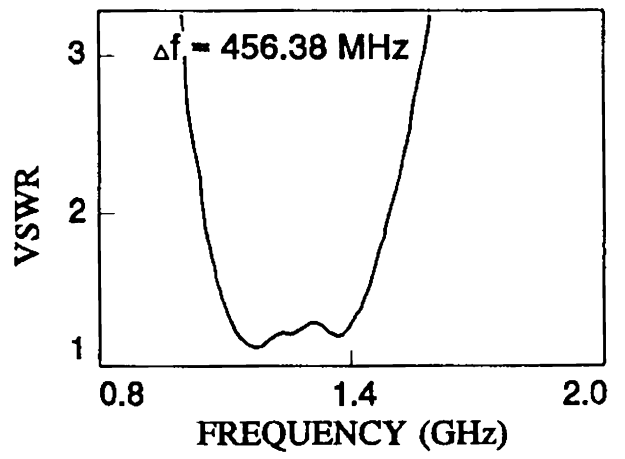


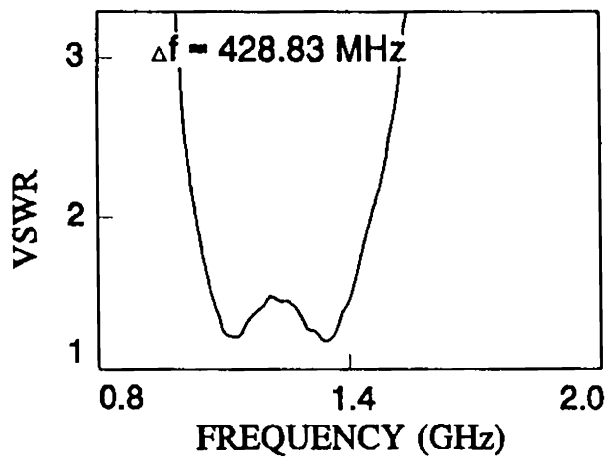
Fig.4.13 VSWR plots of FPDA with different shapes of end-loads
 a) Triangular b) Parallelogram c) Circular d) Semi-circular



(e)



(f)

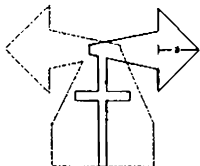
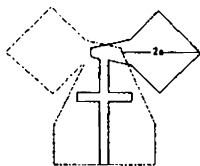
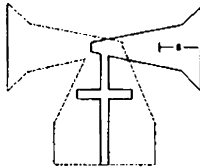
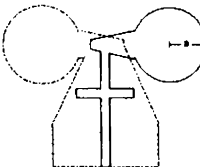
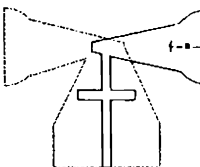
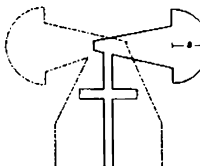
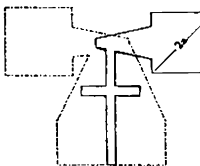


(g)

Fig.4.13 VSWR plots of FPDA with different shapes of end-loads
 e) Square f) Rev-triangular g) Rev-semi-circular

Table 4.5

Percentage bandwidths and central frequencies of FPDA with various load shapes and optimised stub parameters ($a = 1.75 \text{ cm}$)

Antenna Loading	Antenna structure	Stub			Percentage bandwidth	Central frequency (in GHz)
		position (cm)	length (cm)	impedance (Ω)		
Triangle		1.40	2.50	36.0	42.09	1.547
Parall- elogram		1.60	2.50	39.0	36.96	1.577
Rev- triangle		2.25	2.70	39.0	35.74	1.276
Circle		1.70	2.55	33.5	34.48	1.398
Rev-semi- circle		2.20	2.25	36.0	34.38	1.245
Semi-circle		2.00	2.25	36.0	34.35	1.345
Square		1.95	2.50	42.0	32.84	1.385

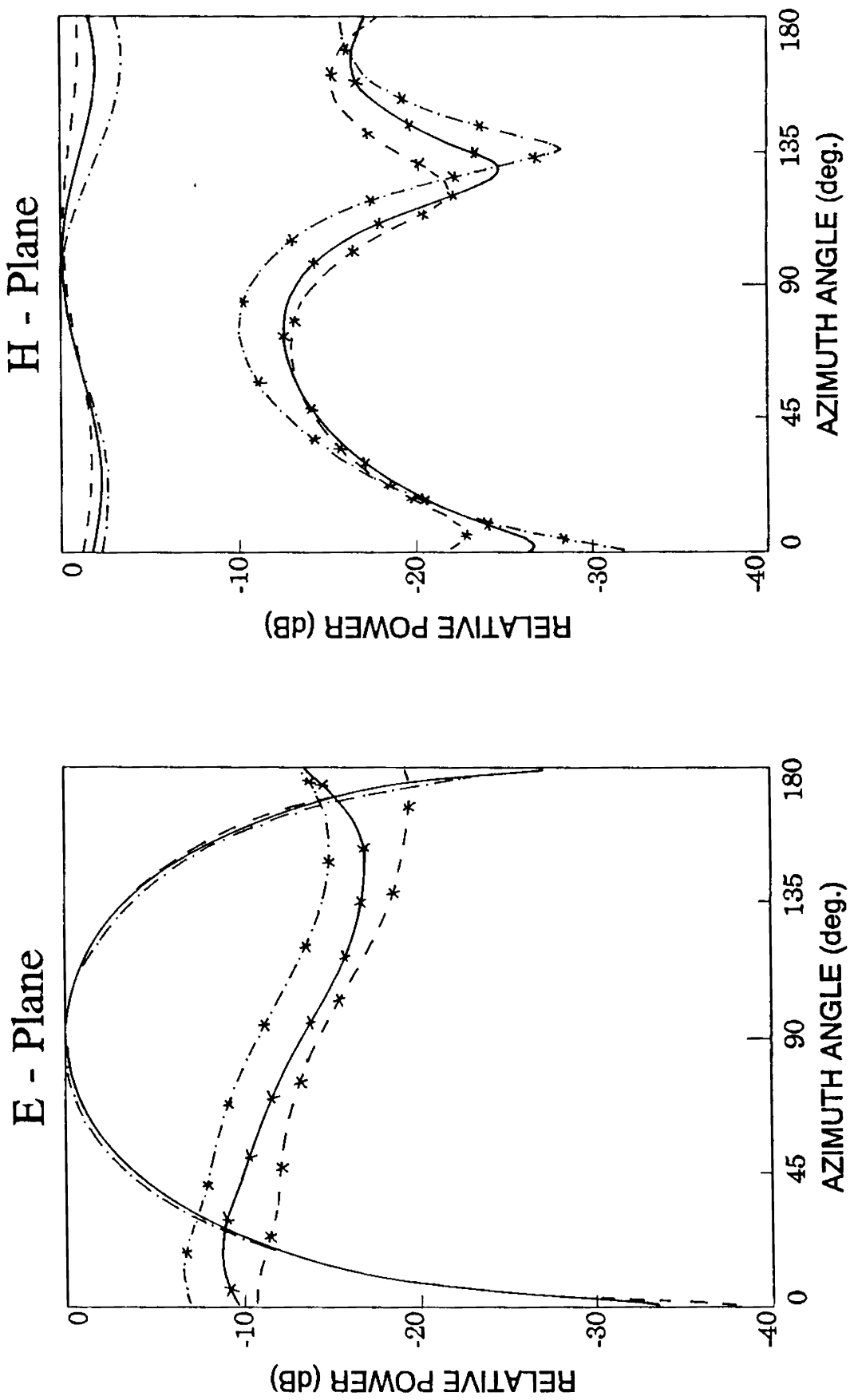


Fig. 4.14 Radiation patterns of triangular end-loaded printed dipole
 co-polar : — 1.221 GHz, — 1.546 GHz, — 1.872 GHz
 cross-polar : - - * - - 1.221 GHz, - - * - - 1.546 GHz, - - * - - 1.872 GHz

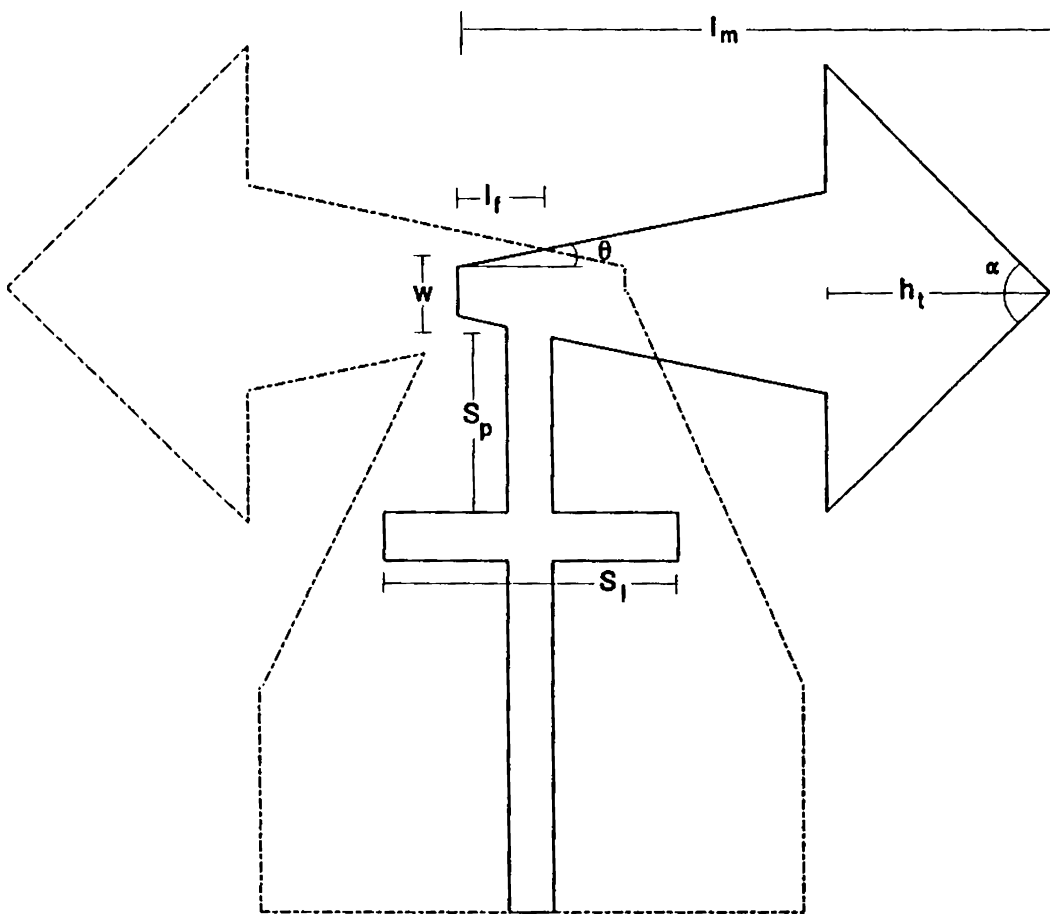


Fig 4.15 Schematic representation of triangular end-loaded printed dipole

In the optimisation procedure of FPDA, it was observed that the effect of change in arms overlapping O_g on the impedance bandwidth is very small. Therefore this parameter is not considered here for investigation.

4.2.1 Triangle dimensions

To optimise the dimensions of the triangle, the triangle height h_t is varied from 1.50 cm to 2.50 cm in steps of 0.25 cm and the apex angle α is varied from 80° to 120° in steps of 10° . The VSWR plot, and percentage bandwidth and the central frequency along with optimised stub parameters of each antenna are given in Fig. 4.16(i) - (v) and Table 4.6 respectively. From the table, it can be seen that except for very large and very small load size, the percentage bandwidth is improved considerably compared to FPDA. For smaller size of the triangle, the effect of loading is less, hence no improvement is observed in the impedance bandwidth. Conversely, for large size of the triangle, the loading effect is very prominent which considerably alters the input impedance of the dipole and results in drastic reduction in the percentage bandwidth of the antenna. Also from the table, percentage bandwidth is maximum for the triangle height $h_t = 2.00$ cm and the apex angle $\alpha = 100^\circ$.

4.2.2 Arm width at feed point

Keeping the apex angle and the triangle height at their optimum values, the main arm width is varied around 9 mm (the design value of FPDA) in steps of 0.5 mm. The VSWR plots of different antennas are given in Fig. 4.17. The percentage bandwidths and central frequencies along with the optimised stub parameters are given in Table 4.7. From the table, it is clear that the main arm width at the feed point as 9 mm is still the best choice.

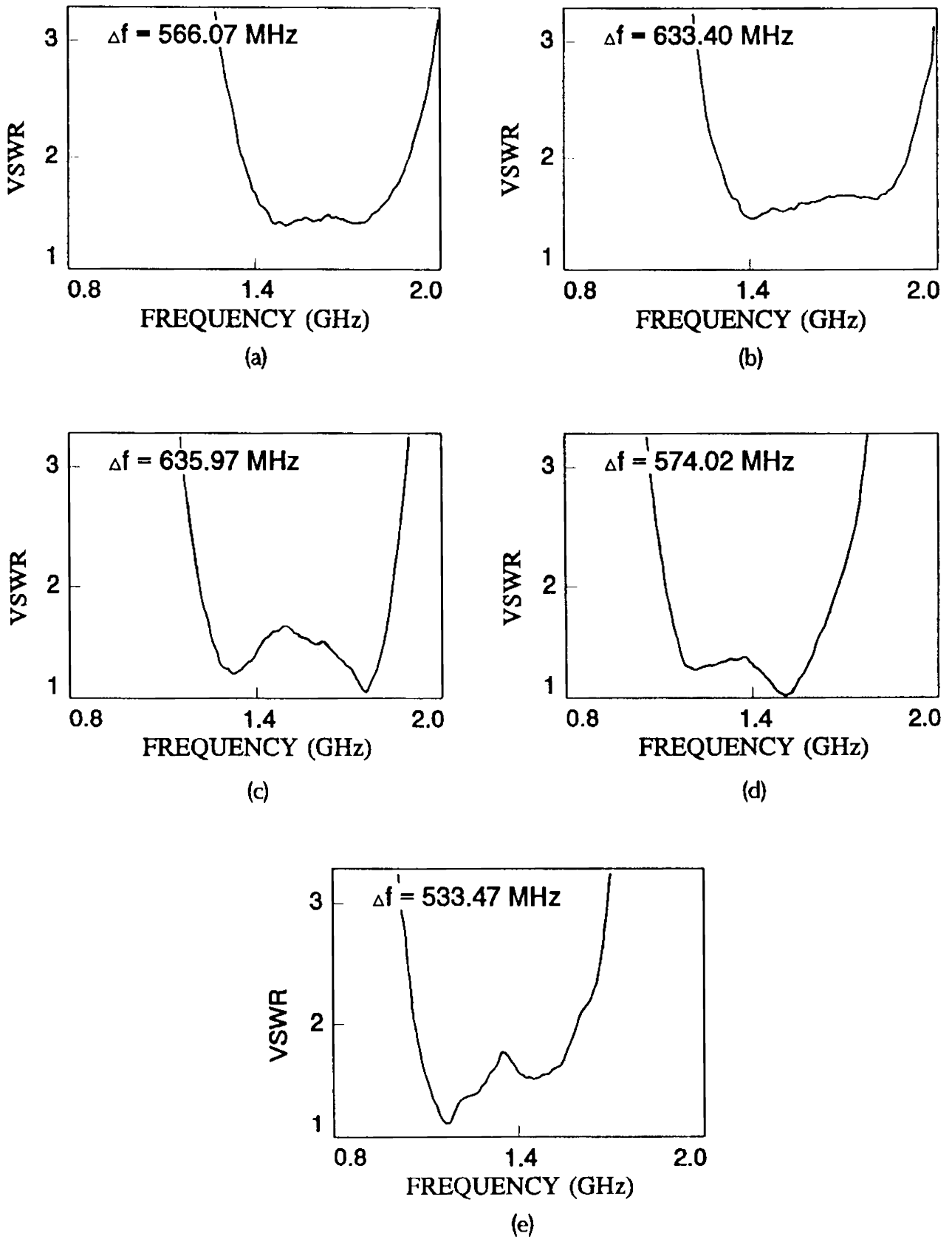


Fig. 4.16(i) VSWR plots of triangular end-loaded printed dipoles for different apex angles ($h_t = 1.50$ cm)
 a) $\alpha = 80^\circ$ b) $\alpha = 90^\circ$ c) $\alpha = 100^\circ$ d) $\alpha = 110^\circ$ e) $\alpha = 120^\circ$

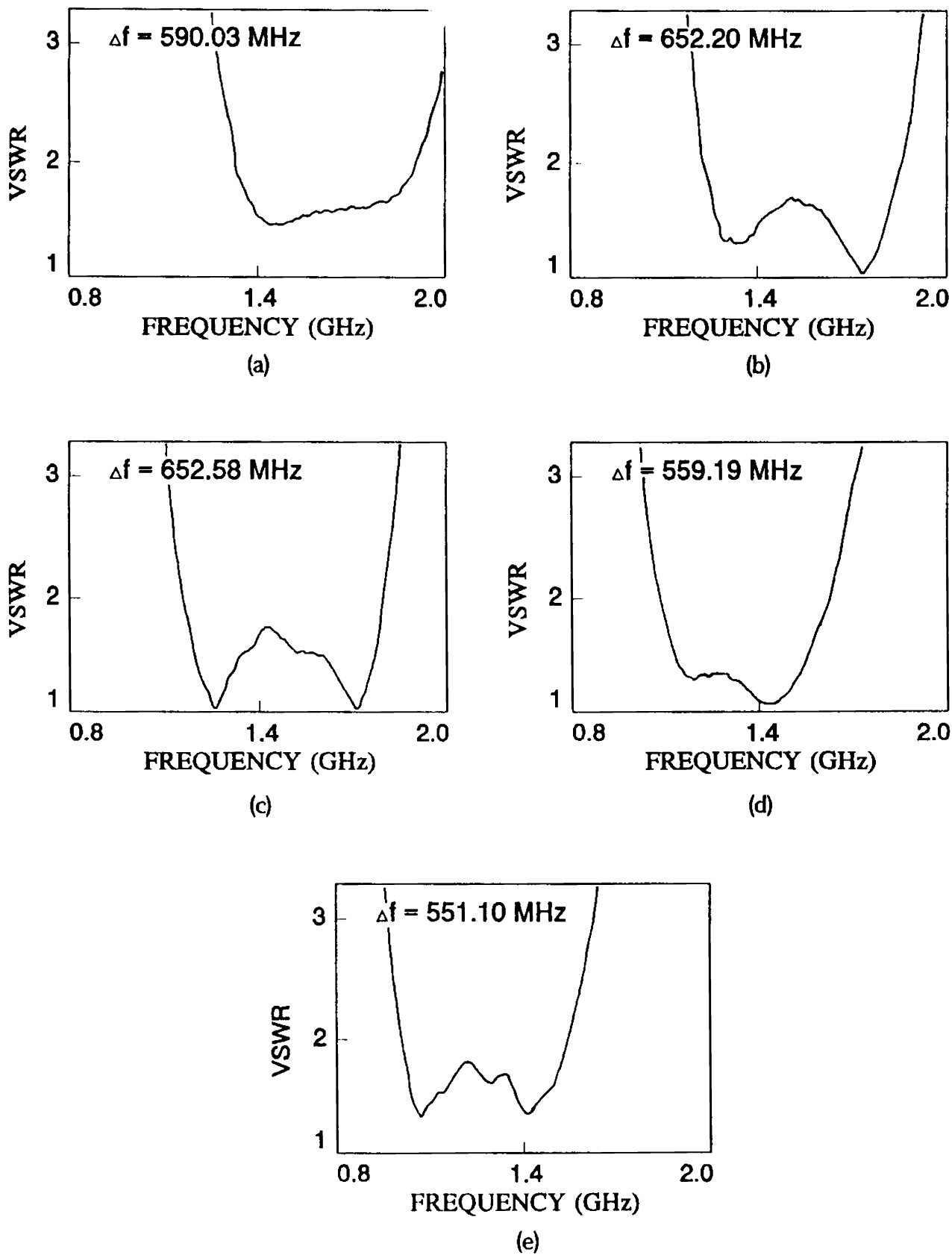
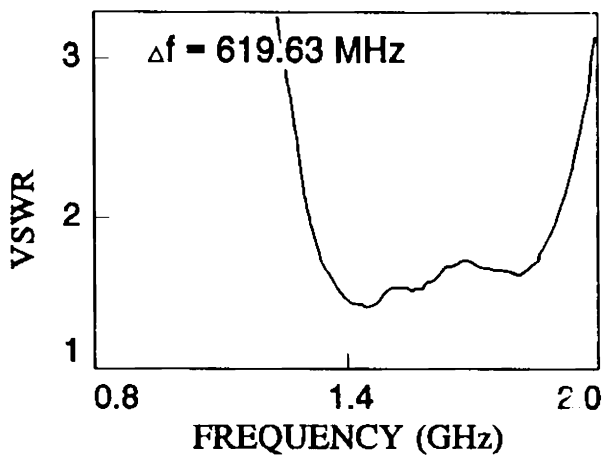
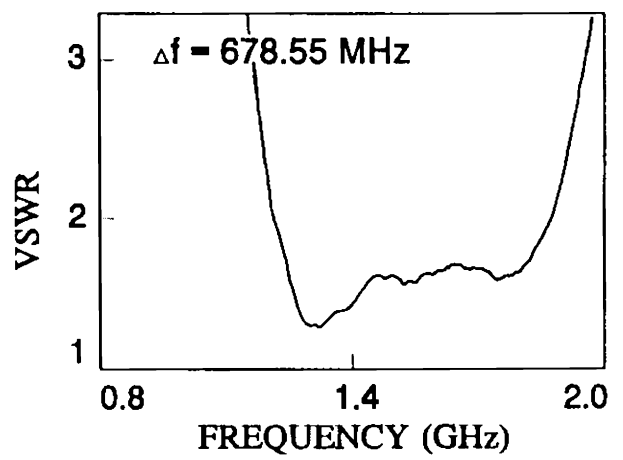


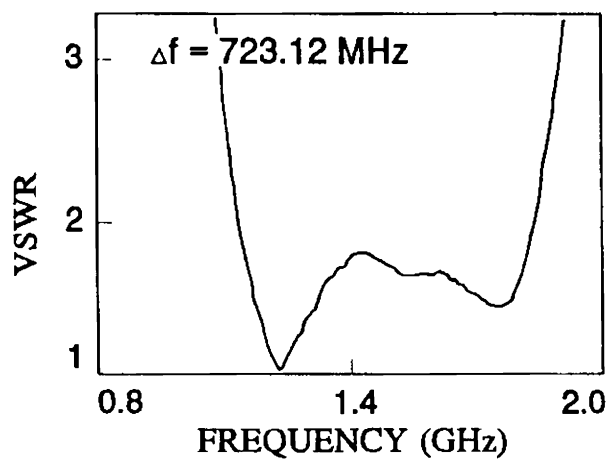
Fig. 4.16(ii) VSWR plots of triangular end-loaded printed dipoles for different apex angles ($h_1 = 1.75 \text{ cm}$)
 a) $\alpha = 80^\circ$ b) $\alpha = 90^\circ$ c) $\alpha = 100^\circ$ d) $\alpha = 110^\circ$ e) $\alpha = 120^\circ$



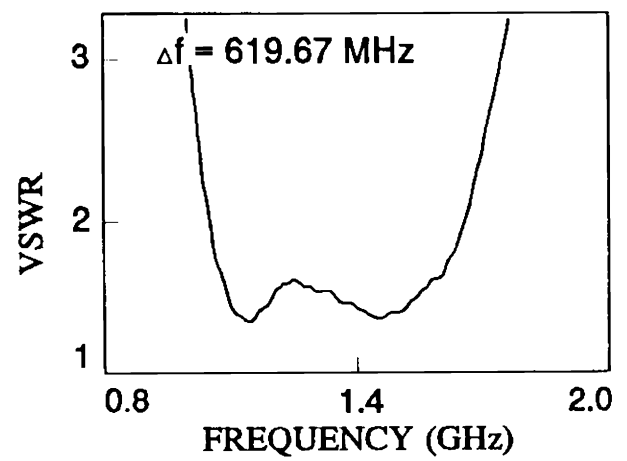
(a)



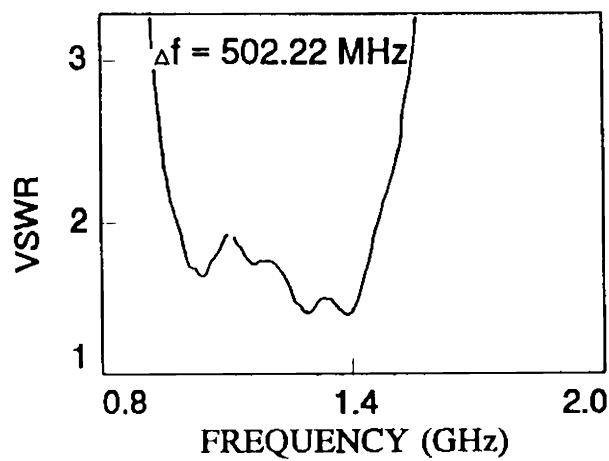
(b)



(c)



(d)



(e)

Fig. 4.16(iii) VSWR plots of triangular end-loaded printed dipoles for different apex angles ($h_r = 2.00$ cm)
 a) $\alpha = 80^\circ$ b) $\alpha = 90^\circ$ c) $\alpha = 100^\circ$ d) $\alpha = 110^\circ$ e) $\alpha = 120^\circ$

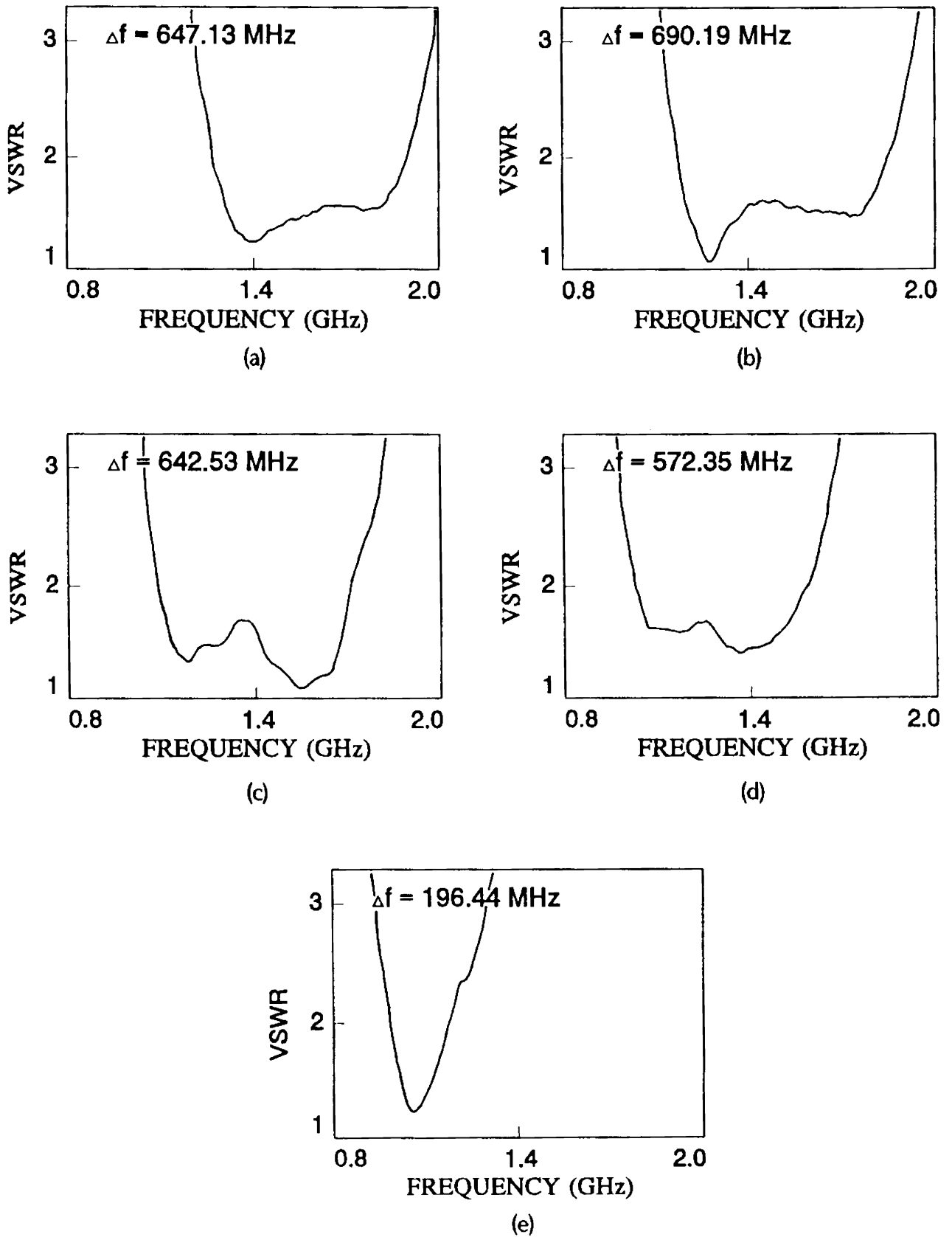
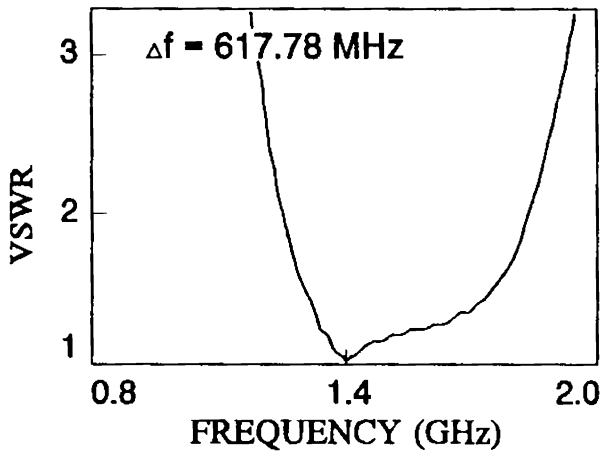
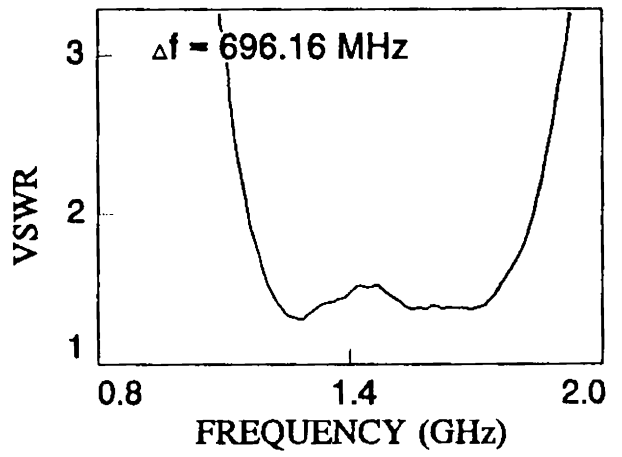


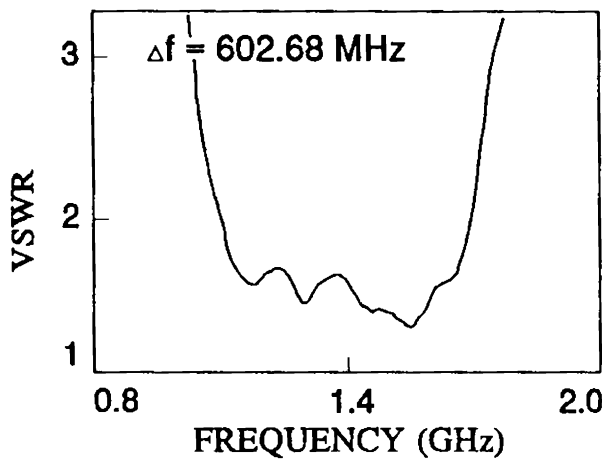
Fig. 4.16(iv) VSWR plots of triangular end-loaded printed dipoles for different apex angles ($h_t = 2.25$ cm)
 a) $\alpha = 80^\circ$ b) $\alpha = 90^\circ$ c) $\alpha = 100^\circ$ d) $\alpha = 110^\circ$ e) $\alpha = 120^\circ$



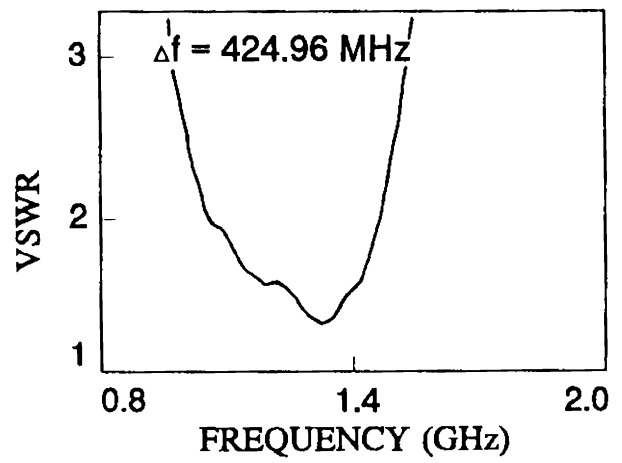
(a)



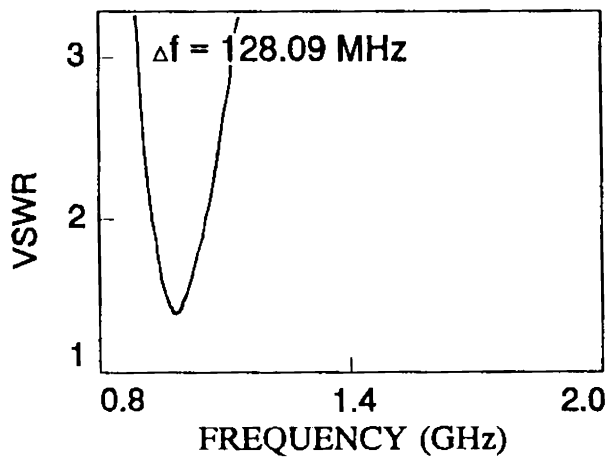
(b)



(c)



(d)



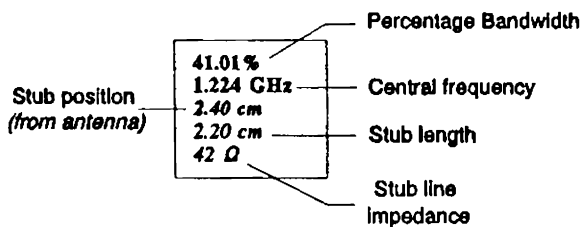
(e)

Fig. 4.16(v) VSWR plots of triangular end-loaded printed dipoles for different apex angles ($h_r = 2.50$ cm)
 a) $\alpha = 80^\circ$ b) $\alpha = 90^\circ$ c) $\alpha = 100^\circ$ d) $\alpha = 110^\circ$ e) $\alpha = 120^\circ$

Table 4.6

Percentage bandwidths and central frequencies of triangular end-loaded printed dipoles of various apex angles and heights of triangle with optimised stub parameters

Triangle height h_t Apex Angle α	1.50 cm	1.75 cm	2.00 cm	2.25 cm	2.50 cm
80°	34.71% 1.631 GHz 1.35 cm 1.90 cm 36 Ω	36.42% 1.620 GHz 1.30 cm 1.90 cm 36 Ω	38.37% 1.616 GHz 1.30 cm 1.90 cm 36 Ω	40.60% 1.593 GHz 1.40 cm 1.90 cm 36 Ω	39.74% 1.552 GHz 1.55 cm 2.00 cm 42 Ω
90°	39.30% 1.613 GHz 1.35 cm 2.15 cm 42 Ω	42.09% 1.547 GHz 1.40 cm 2.25 cm 36 Ω	43.66% 1.553 GHz 1.50 cm 2.20 cm 42 Ω	46.80% 1.517 GHz 1.50 cm 2.15 cm 42 Ω	46.25% 1.505 GHz 1.80 cm 2.15 cm 42 Ω
100°	41.51% 1.532 GHz 1.35 cm 2.35 cm 32 Ω	43.94% 1.485 GHz 1.40 cm 2.35 cm 32 Ω	48.55% 1.488 GHz 1.55 cm 2.70 cm 42 Ω	45.81% 1.403 GHz 1.85 cm 2.40 cm 42 Ω	43.12% 1.398 GHz 1.90 cm 2.00 cm 42 Ω
110°	40.88% 1.404 GHz 1.70 cm 2.35 cm 32 Ω	41.18% 1.357 GHz 1.90 cm 2.40 cm 42 Ω	45.89% 1.351 GHz 1.90 cm 2.40 cm 42 Ω	43.89% 1.305 GHz 2.05 cm 2.15 cm 42 Ω	33.53% 1.297 GHz 2.20 cm 2.00 cm 42 Ω
120°	40.18% 1.329 GHz 1.95 cm 2.20 cm 42 Ω	43.07% 1.278 GHz 2.10 cm 2.40 cm 42 Ω	41.01% 1.224 GHz 2.40 cm 2.20 cm 42 Ω	18.23% 1.080 GHz 1.40 cm 1.70 cm 42 Ω	12.92% 0.991 GHz 0.95 cm 1.60 cm 32 Ω



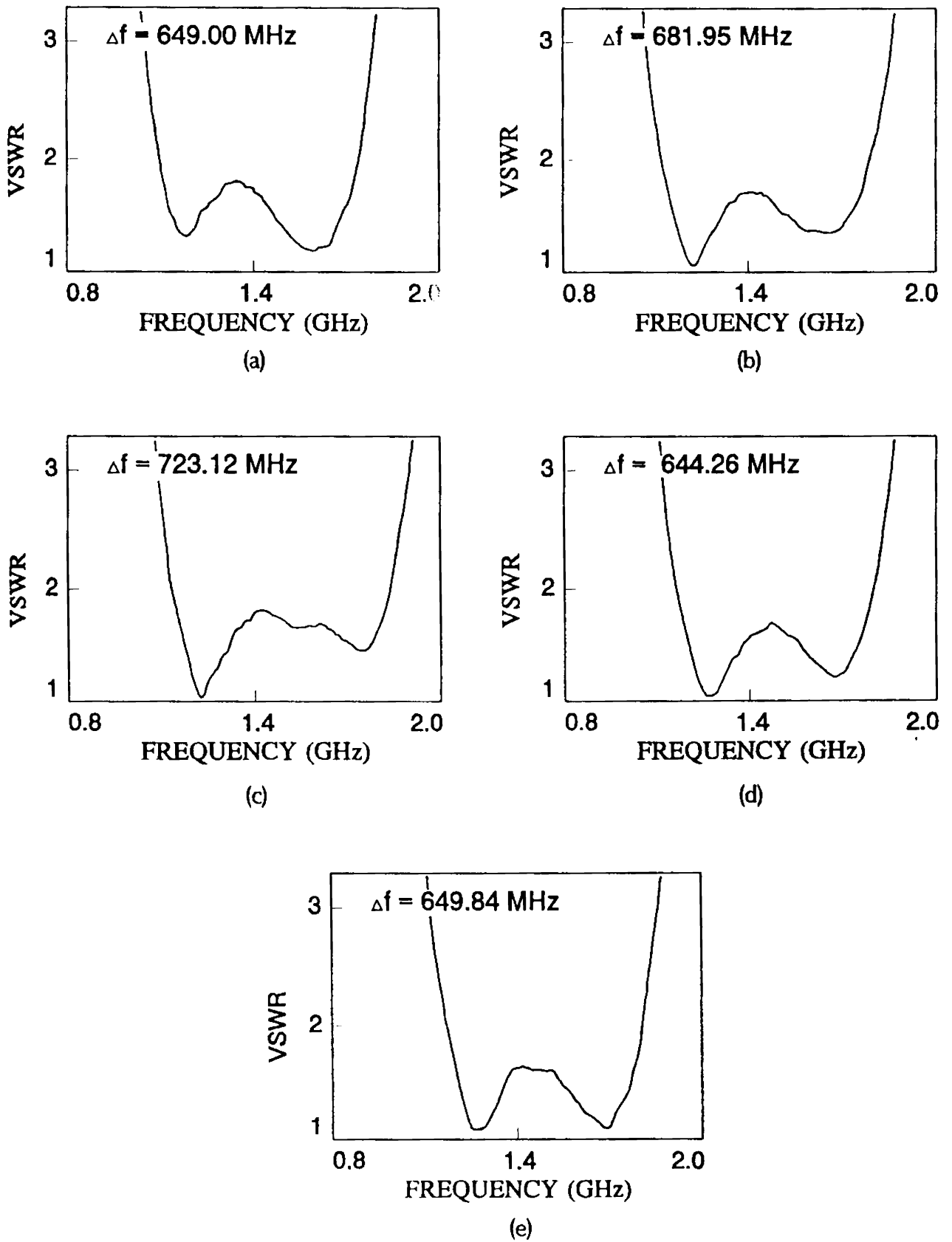


Fig. 4.17 VSWR plots of triangular end-loaded printed dipoles for different arm widths at the feed point
a) $w = 8.0$ mm b) $w = 8.5$ mm c) $w = 9.0$ mm d) $w = 9.5$ mm e) $w = 10.0$ mm

Table 4.7

Percentage bandwidths and central frequencies of triangular end-loaded printed dipoles of various main arm widths at feed point with optimised stub parameters

Main arm width at feed point w (mm)	Stub			Percentage bandwidth	Central frequency (GHz)
	position (cm)	length (cm)	impedance (Ω)		
8.0	1.85	2.75	42.0	45.37	1.430
8.5	1.70	2.40	42.0	46.77	1.457
9.0	1.55	2.70	42.0	48.55	1.488
9.5	1.40	2.50	36.0	43.51	1.480
10.0	1.50	2.50	36.0	43.77	1.485

4.2.3 Main arm to ground arm ratio

The ratio of main arm to ground arm is varied from 1:0.90 to 1:1.10 as in the case of flared printed dipole antenna and the corresponding VSWR plots are given in Fig. 4.18. The percentage bandwidths and the central frequencies of different antennas are given in Table 4.8. Here, the percentage bandwidth is maximum for the ratio 1:1.05; whereas for the flared printed dipole, it is maximum for the ratio 1:1.10.

4.2.4 Flaring angle

As a last step towards the design optimisation, the flaring angle θ is varied from 5° to 15° in steps of 2.5° . The VSWR plot of each antenna and the corresponding percentage bandwidth and the central frequency are given in Fig. 4.19 and Table 4.9 respectively. As in the case of flared printed dipole, the effect of change in the flaring angle on the

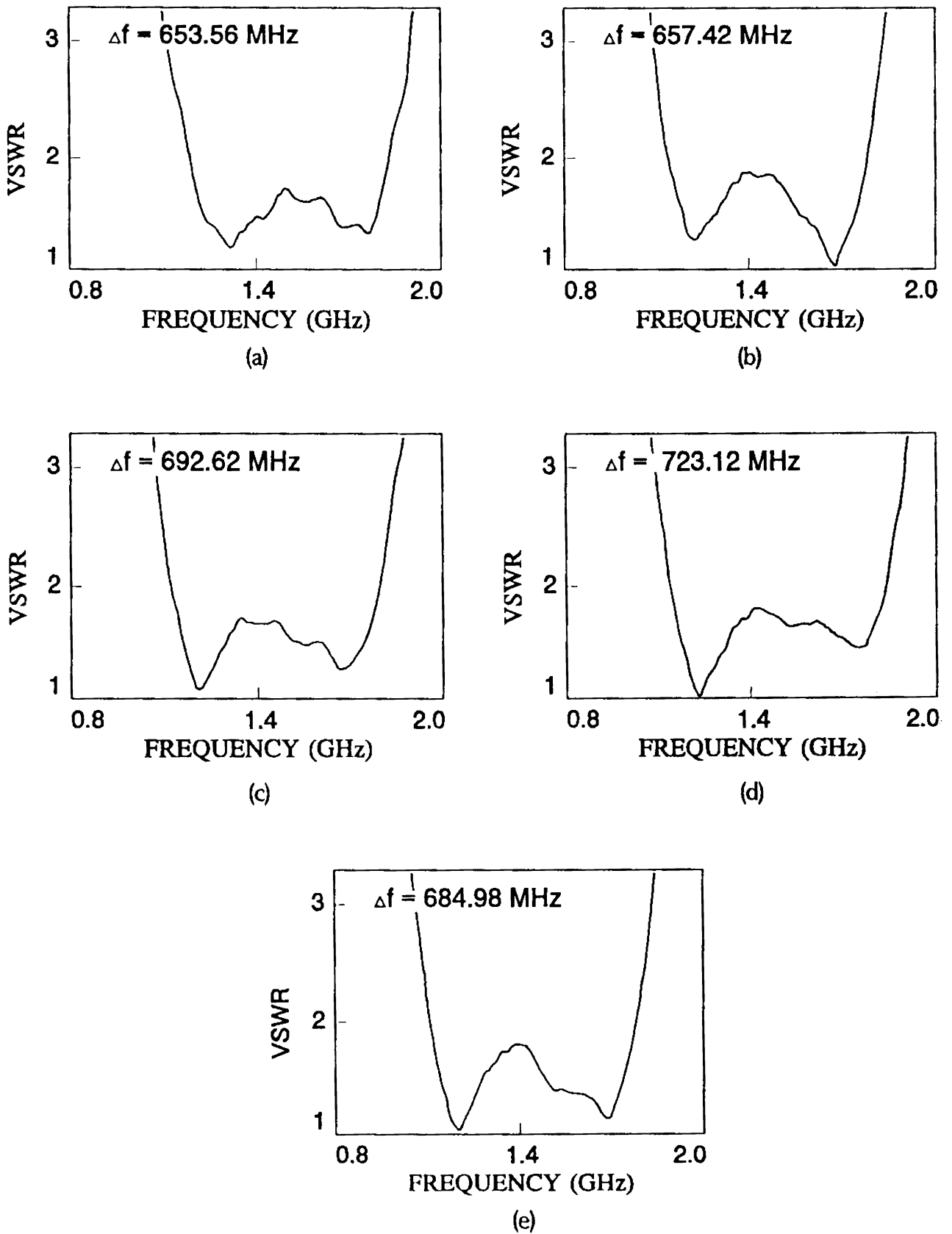


Fig. 4.18 VSWR plots of triangular end-loaded printed dipoles for different main arm to ground arm ratio
a) R = 1:0.90 b) R = 1:0.95 c) R = 1:1.00 d) R = 1:1.05 e) R = 1:1.10

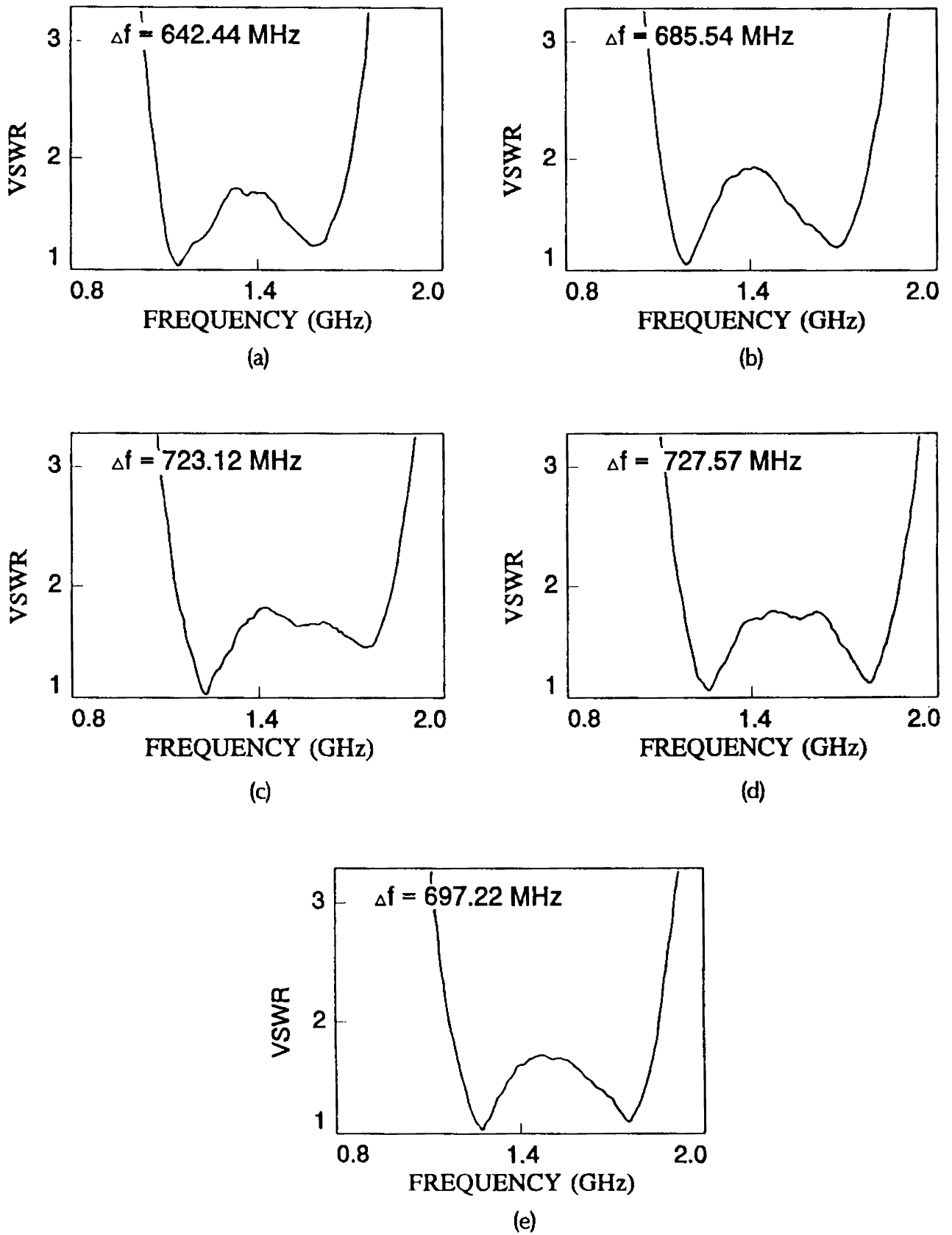


Fig. 4.19 VSWR plots of triangular end-loaded printed dipoles for different flaring angles
 a) $\theta = 5.0^\circ$ b) $\theta = 7.5^\circ$ c) $\theta = 10.0^\circ$ d) $\theta = 12.5^\circ$ e) $\theta = 15.0^\circ$

impedance bandwidth is very small. Also from the table, the percentage bandwidth is maximum for $\theta = 10^\circ$.

Table 4.8

Percentage bandwidths and central frequencies of triangular end-loaded printed dipoles of various main arm to ground arm ratio with optimised stub parameters

Main arm to ground arm ratio R	Stub			Percentage bandwidth	Central frequency (GHz)
	position (cm)	length (cm)	impedance (Ω)		
1:0.90	1.65	2.40	36.0	43.23	1.513
1:0.95	1.65	2.50	36.0	45.05	1.458
1:1.00	1.70	2.40	42.0	47.51	1.458
1:1.05	1.55	2.70	42.0	48.55	1.488
1:1.10	1.65	2.70	42.0	47.45	1.443

Table 4.9

Percentage bandwidths and central frequencies of triangular end-loaded printed dipoles of various flaring angles with optimised stub parameters

Flaring angle θ	Stub			Percentage bandwidth	Central frequency (GHz)
	position (cm)	length (cm)	impedance (Ω)		
5.0°	1.70	2.50	36.0	46.08	1.393
7.5°	1.55	2.50	36.0	47.44	1.446
10.0°	1.55	2.70	42.0	48.55	1.488
12.5°	1.35	2.50	36.0	47.83	1.522
15.0°	1.45	2.50	36.0	45.94	1.515

From the above results, it is clear that all the design values of FPDA are still valid for triangular end-loaded printed dipole antenna. Thus, it can be stated that the optimisation of the dimensions of the triangular load is related to the other design parameters.

The design data for optimised Triangular End-Loaded Printed Dipole Antenna (TELPDA) are as follows:

Height of the triangle h ,	= 2.00 cm
Apex angle α	= 100°
Stub length S_t	= 2.70 cm
Stub position S_p	= 1.55 cm
Stub line impedance	= 42Ω

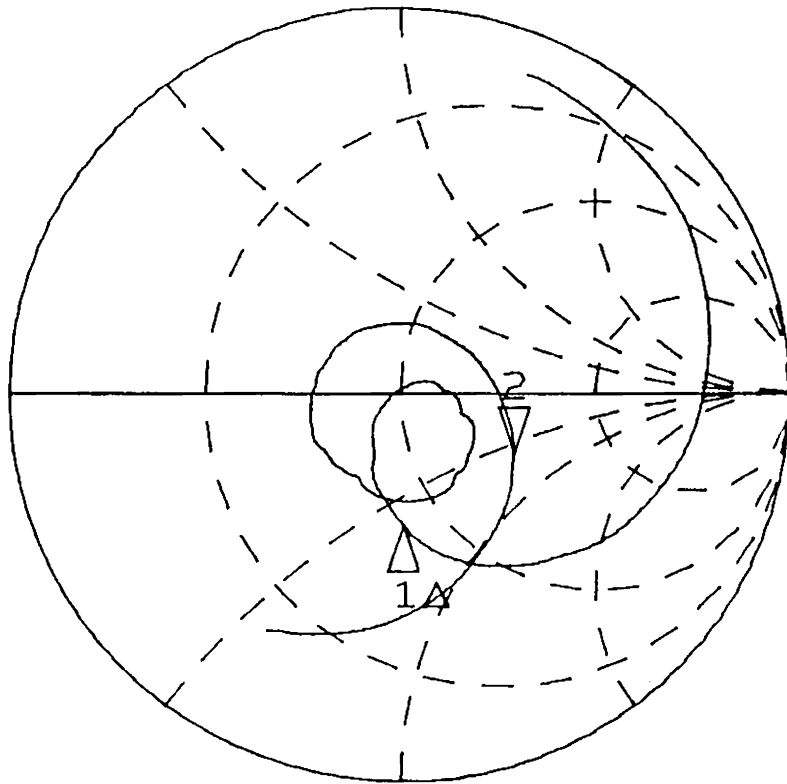
The remaining design parameters are having the same values as that of FPDA.

The impedance plot of the antenna is given in Fig. 4.20. The 2:1 VSWR bandwidth is 723.12 MHz and the central frequency is 1.488 GHz. This corresponds to 48.55% impedance bandwidth. It is interesting to note that the central frequency of FPDA is 1.588 GHz. That is, for the same arms length, there is considerable decrease in the central frequency of TELPDA. This can be attributed to the loading effect of the dipole.

The radiation patterns of the antenna at start, end and central frequencies are given in Fig. 4.21. The co-polar patterns are almost identical to that of the previous dipole patterns but the cross-polar level is slightly high and increases with frequency. This may be due to the fact that, at higher frequencies, sides of the triangle become appreciable fraction of wavelength.

As described in Chapter 3, a comparative gain measurement of TELPDA is done with a standard half wave wire dipole antenna, resonating at 1.496 GHz, which is approximately at the center of the frequency band of TELPDA. Fig. 4.22 shows the $|S_{21}|$ of the antenna with respect to the wire dipole. From the figure, the gain of TELPDA is only 0.55 dB less than the wire dipole at the resonating frequency of the wire dipole (*ie.* at 1.496 GHz). This is obvious because of large impedance bandwidth of TELPDA as

MARKER 2-1
723.117237 MHz



START 0.795000000 GHz
STOP 2.004375000 GHz

Fig. 4.20 Impedance loci of TELPDA

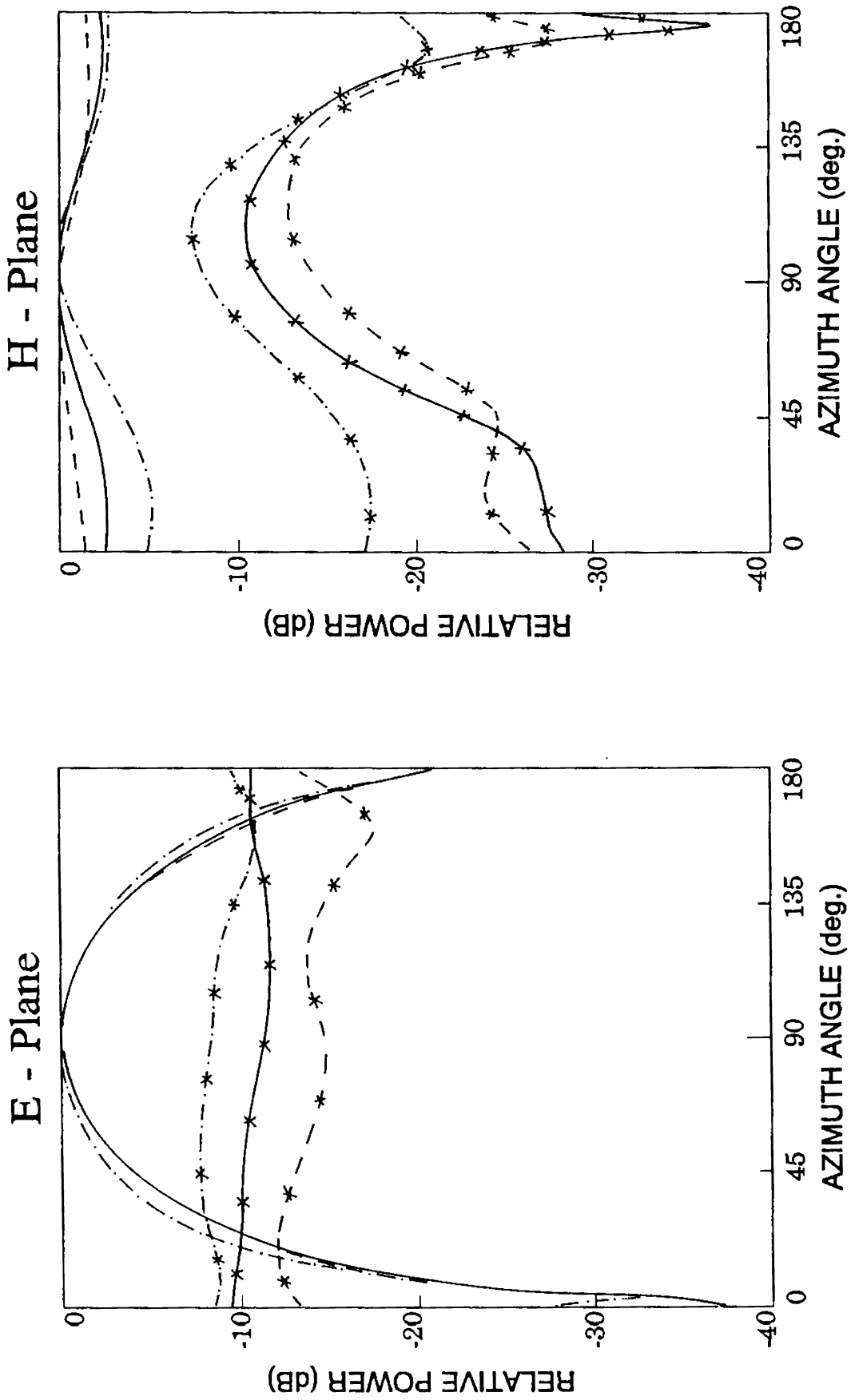


Fig. 4.21 Radiation patterns of TELPDA
 co-polar : --- 1.127 GHz, — 1.488 GHz, -·-·- 1.849 GHz,
 cross-polar : - - - 1.127 GHz, - - - 1.488 GHz, ···· 1.849 GHz

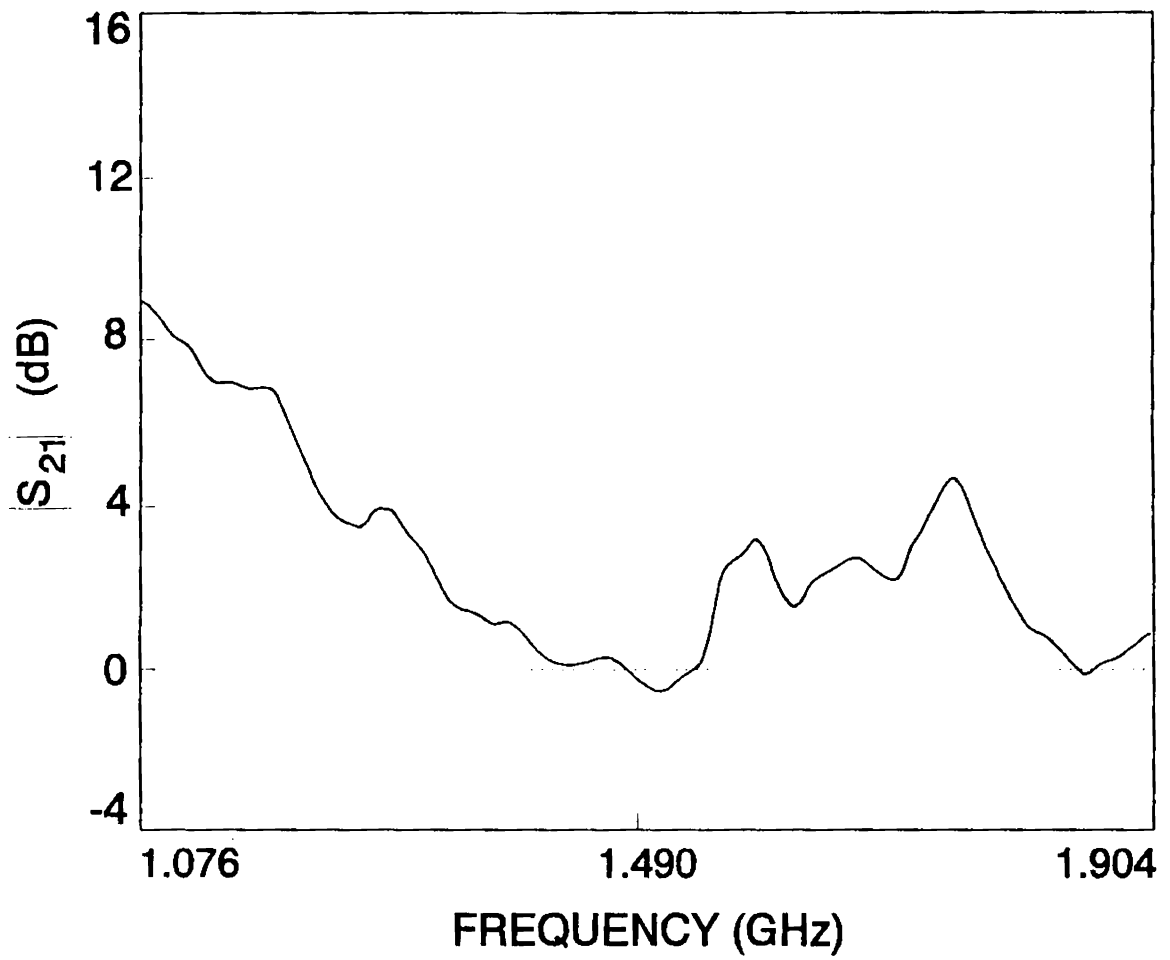


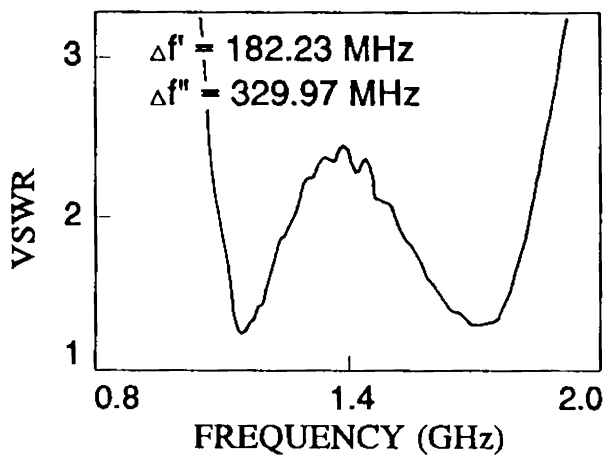
Fig. 4.22 $|s_{21}|$ of TELPDA with respect to half wave wire dipole resonating at 1.496 GHz

compared to the wire dipole. Thus, it can be stated that the bandwidth enhancement of the triangular end-loaded printed dipole is achieved without much sacrifice of the gain of the antenna.

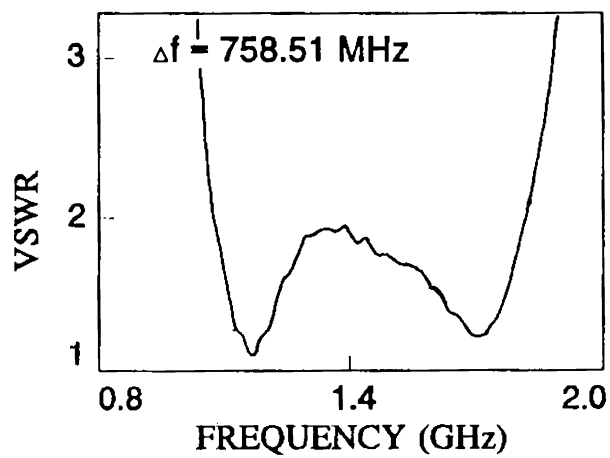
4.2.5 Cavity backed triangular end-loaded printed dipole

To produce an unidirectional radiation pattern, dipoles are often used with a reflector plate placed at finite distance away from it, thus forming a cavity backed structure. The effect of reflector plate on the impedance bandwidth of TELPDA is studied by varying the separation h between the reflector plate and the dipole. The VSWR plots for different separations are given in Fig. 4.23. From the plots, it can be seen that VSWR of the antenna increases in the middle portion of the frequency band with decrease in separation between the reflector plate and the dipole and it is more than 2 for separation $h = 4.0$ cm. The change in the percentage bandwidth and the central frequency with separation are given in Table 4.10. From the table, it can be seen that the central frequency increases with separation. Also, percentage bandwidth is maximum for $h = 6$ cm and is selected as the design value.

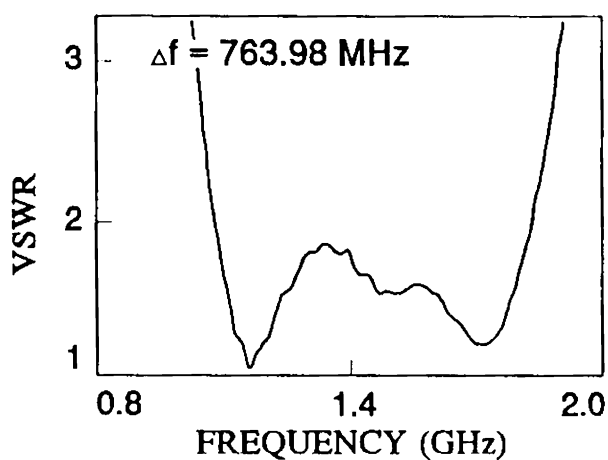
The impedance plot of Cavity Backed Triangular End-Loaded Printed Dipole Antenna (CBTELPDA) with optimum separation ($h = 6$ cm) is plotted in Fig. 4.24. The impedance bandwidth of the antenna is 786.02 MHz and the central frequency is 1.469 GHz. Thus, the central frequency of CBTELPDA is almost equal to the central frequency of TELPDA. The impedance bandwidth of the antenna is 53.51%. This is nearly 5% more than TELPDA.



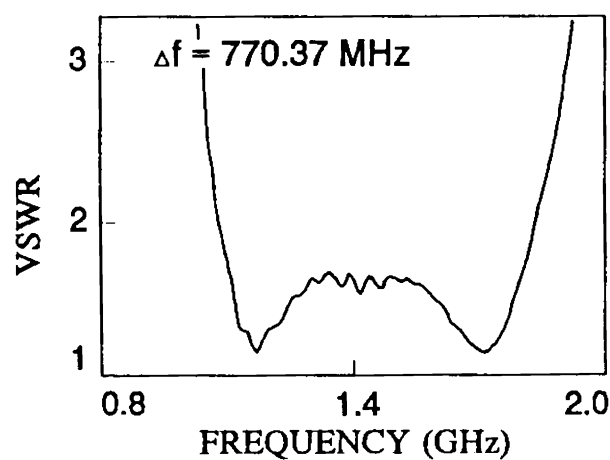
(a)



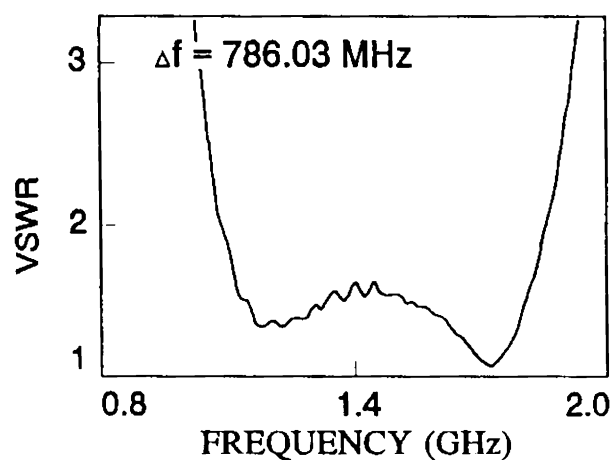
(b)



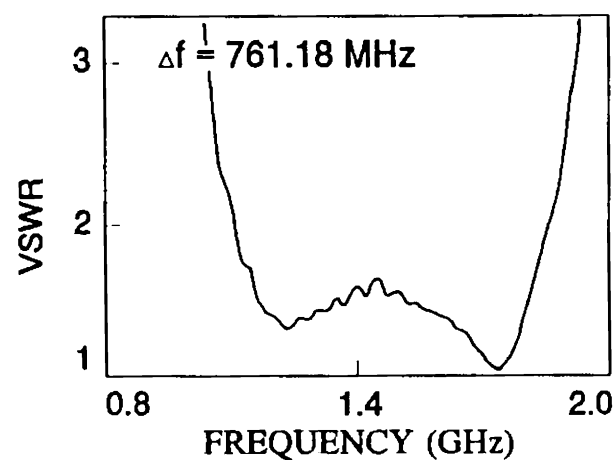
(c)



(d)



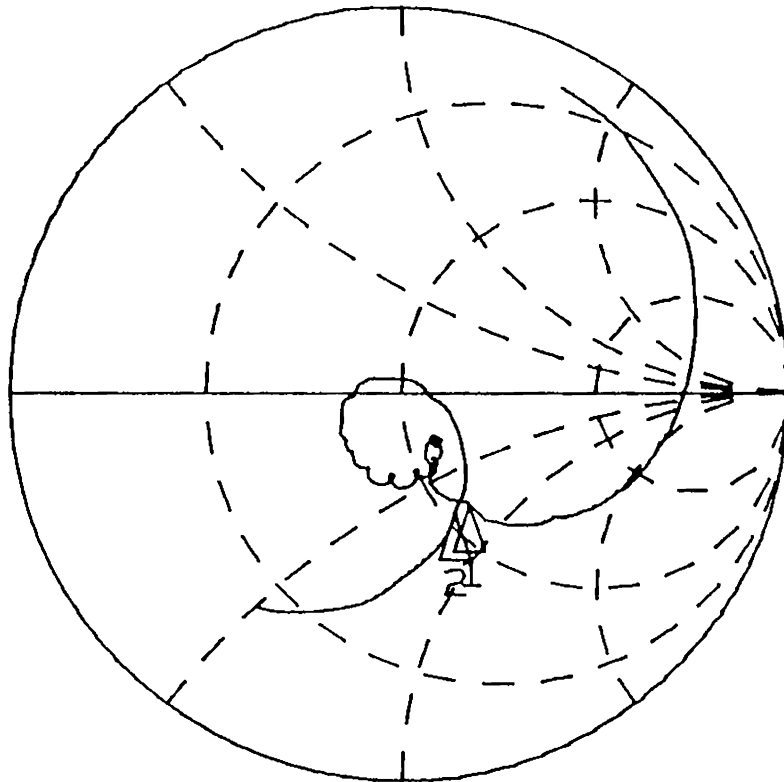
(e)



(f)

Fig. 4.23 VSWR plots of cavity backed TELPDA for different separations between the reflector and the dipole
 a) $h = 4.0 \text{ cm}$ b) $h = 4.5 \text{ cm}$ c) $h = 5.0 \text{ cm}$ d) $h = 5.5 \text{ cm}$ e) $h = 6.0 \text{ cm}$
 f) $h = 6.5 \text{ cm}$

MARKER 2-1
786.024598 MHz



START 0.800000000 GHz
STOP 2.000000000 GHz

Fig. 4.24 Impedance loci of CBTELPDA

Table 4.10

Percentage bandwidths and central frequencies of cavity backed triangular end-loaded printed dipole for different separations between the dipole and the reflector plate

Separation h (cm)	Percentage bandwidth	Central frequency (GHz)
4.0	15.41 / 19.74	1.181 / 1.672
4.5	52.25	1.452
5.0	52.40	1.458
5.5	52.83	1.459
6.0	53.51	1.469
6.5	51.26	1.485

The radiation patterns of CBTELPDA are given in Fig. 4.25. Like TELPDA, the cross-polar level is higher at the upper frequency side of the band of interest. The co-polar patterns of the antenna are almost similar to that of TELPDA. Only at higher frequency side, E-plane patterns show a dip of around 0.5 dB at the bore-sight direction. This is due to effective increase in the separation between the dipole and the reflector with the increase in frequency.

Like the case of TELPDA, gain of CBTELPDA is compared with the same standard wire dipole antenna, resonating at 1.496 GHz. The $|S_{21}|$ of the antenna with respect to the standard wire dipole is given in Fig. 4.26. The gain of CBTELPDA is 4.43 dB more than the standard wire dipole at 1.496 GHz. This increase in gain of CBTELPDA is due to the presence of reflector, which enhances the gain of the antenna by making the radiation unidirectional from bidirectional and narrowing the beamwidth compared to TELPDA.

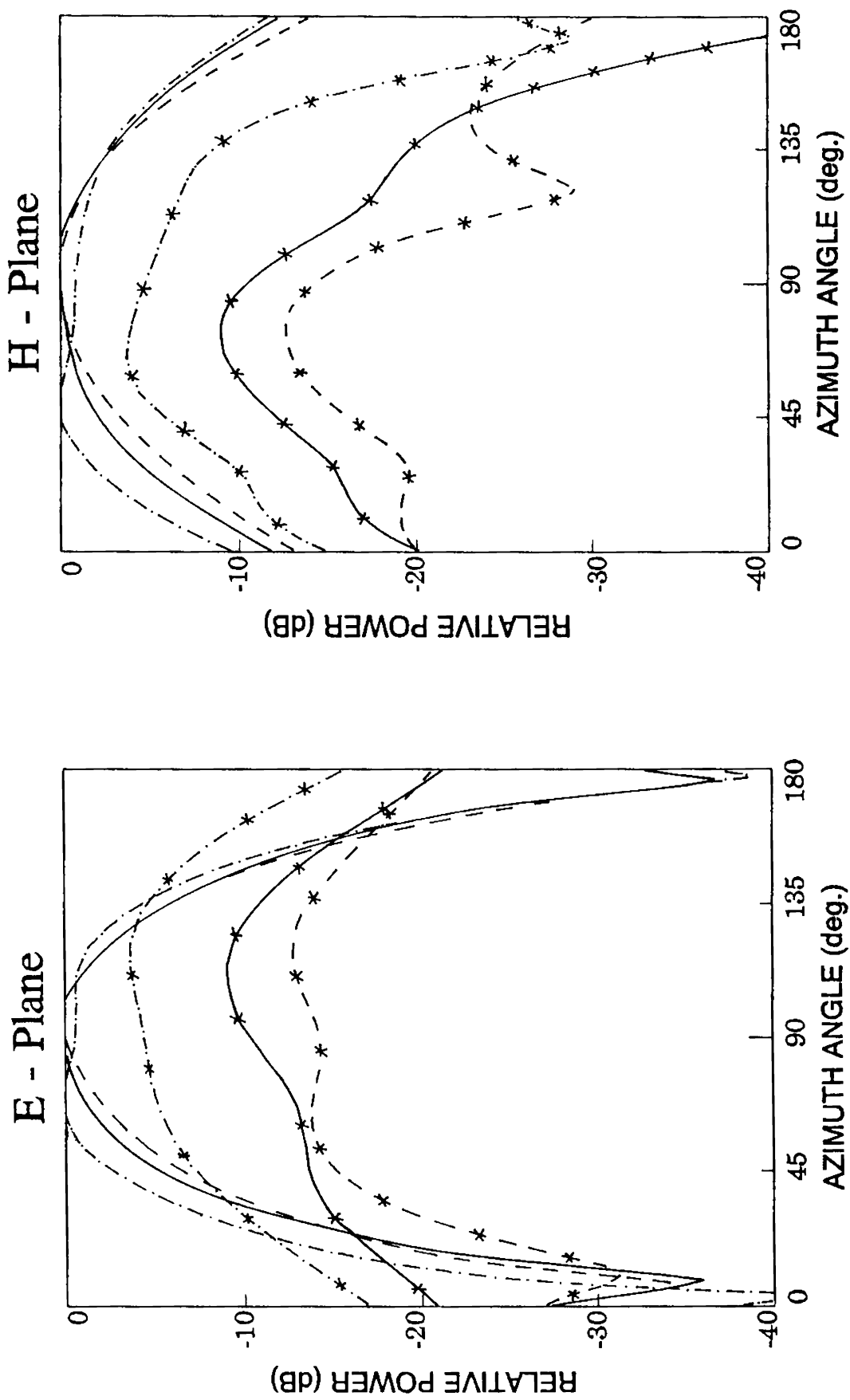


Fig. 4.25 Radiation patterns of CBTELPDA
 co-polar : ——— 1.076 GHz, ——— 1.469 GHz, ——— 1.862 GHz
 cross-polar : - - - * - - - 1.076 GHz, - - - * - - - 1.469 GHz, - - - * - - - 1.862 GHz

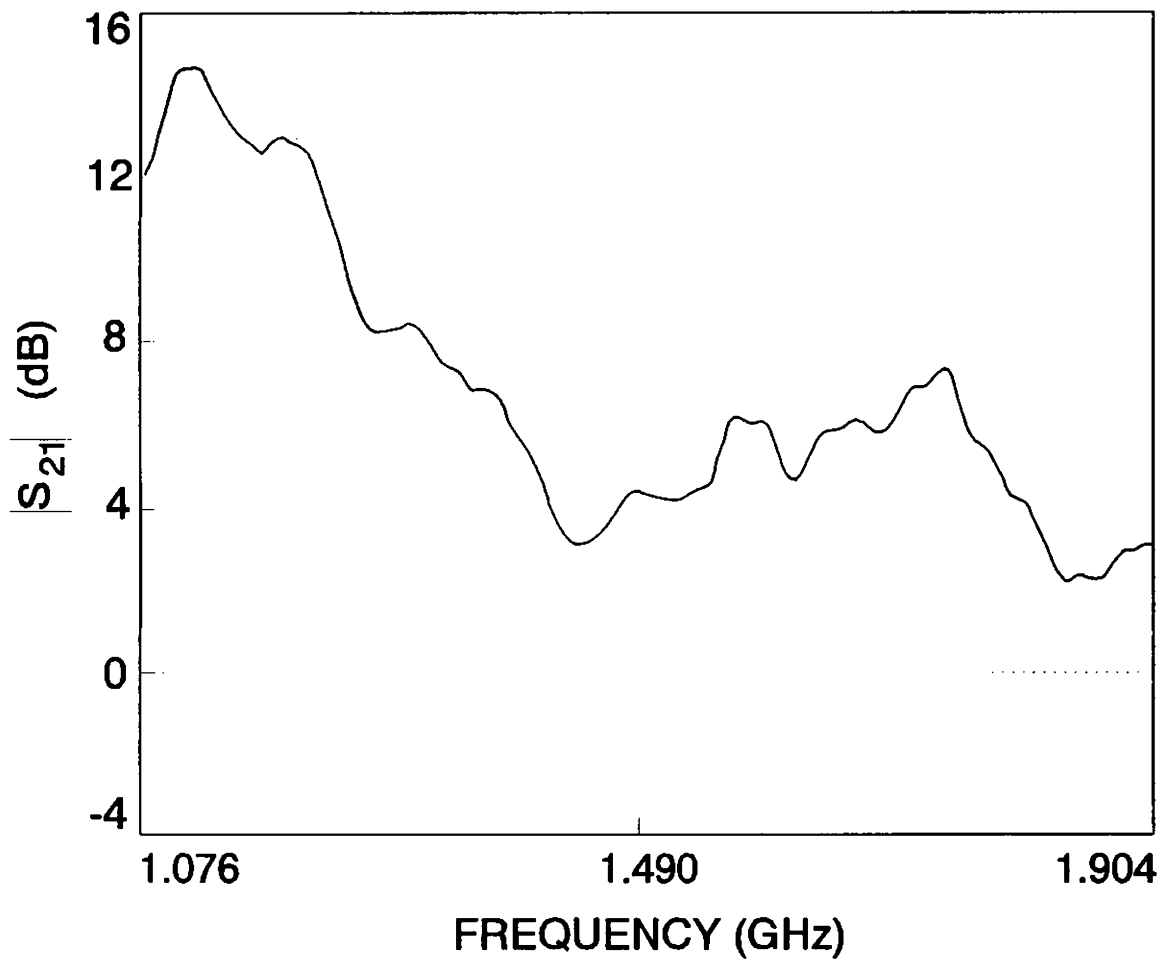


Fig. 4.26 $|s_{21}|$ of CBTELPDA with respect to half wave wire dipole resonating at 1.496 GHz

4.2.6 Design details

The empirical design criteria for Triangular End-Loaded Printed Dipole Antenna has been developed through experimental iterations. The design details of the antenna, shown in Fig. 4.15, are given below in terms of the wavelength (λ_0) corresponding to the central frequency.

Main arm length l_m	=	$0.228 \lambda_0$
Height of the triangle h_t	=	$0.099 \lambda_0$
Arm width at feed point w	=	$0.045 \lambda_0$
Feed point location l_f	=	$0.022 \lambda_0$
Flaring angle θ	=	10°
Apex angle α	=	100°
Stub length S_t	=	$0.25 \lambda_d$
Stub position S_p	=	$0.143 \lambda_d$
Stub line impedance	=	42Ω
Transformer length l_t	=	$0.54 \lambda_d$
Transformer line impedance	=	42Ω

All the dimensions of ground arm are 1.05 times larger than the corresponding main arm values. Here, $\lambda_d = \lambda_0 / \sqrt{\epsilon_{eff}}$ and the effective dielectric constant ϵ_{eff} can be calculated using the formula given in (1).

From the experimental results of TELPDA and CBTELPDA, it can be seen that the difference in the central frequency of the antennas is negligible compared to the bandwidth of the antennas. Thus, all the design criteria of Triangular End-Loaded Printed Dipole Antenna are valid for Cavity Backed Triangular End-Loaded Printed Dipole Antenna with a separation between the dipole and the reflector of $0.3 \lambda_0$.

4.3 PARALLELOGRAM END-LOADED PRINTED DIPOLE

From Table 4.5, the next choice of the shape of end-load, after triangle, is parallelogram. Attempts made to enhance the impedance bandwidth of flared printed dipole by parallelogram shaped end-loads are described in this section.

Initial attempts for improving the bandwidth just by changing the size of the parallelogram do not yield much improvement in impedance bandwidth from the value given in Table 4.5. Thus, the design parameters of FPDA are thoroughly modified through experimental iterations.

The schematic diagram of parallelogram end-loaded printed dipole is given in Fig. 4.27 and different initial design values are given below:

Main arm length l_m	=	4.90 cm
Main arm width at feed point w_m	=	1.00 cm
Ground arm width at feed point w_g	=	1.10 cm
Arms overlapping O_g	=	1.25 cm
Feed point location l_f	=	0.50 cm
Flaring angle θ	=	10°

The ground arm length and the load dimensions are 1.05 times larger than the corresponding main arm values.

The parallelogram dimensions are optimised by varying the bisecting length l_p from 3.00 cm to 3.75 cm and the angle β from 80° to 120° , while keeping the other parameters constant. The VSWR plots of different antennas are given in Fig. 4.28(i) - (iv) and the corresponding percentage bandwidths and the central frequencies with optimised stub parameters are given in Table 4.11. It is clear from the table that the percentage bandwidth increases with the increase in the size of the parallelogram. The bisecting length

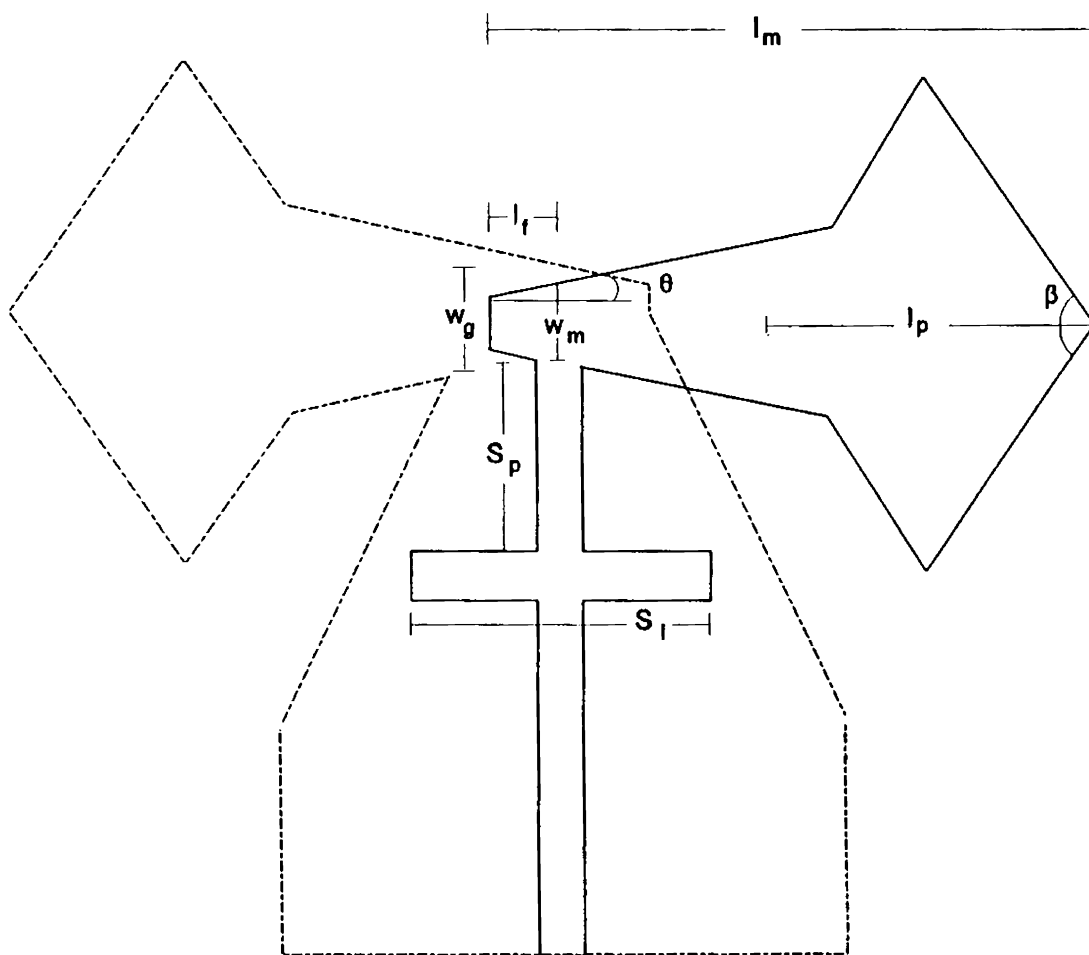
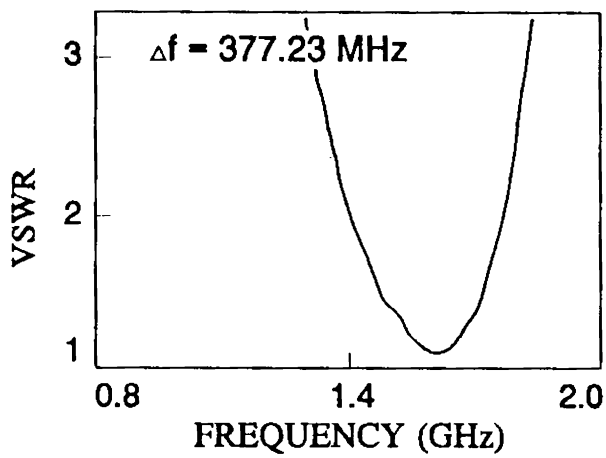
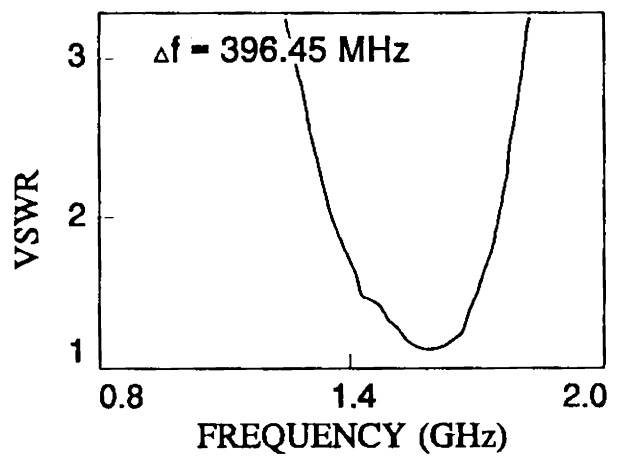


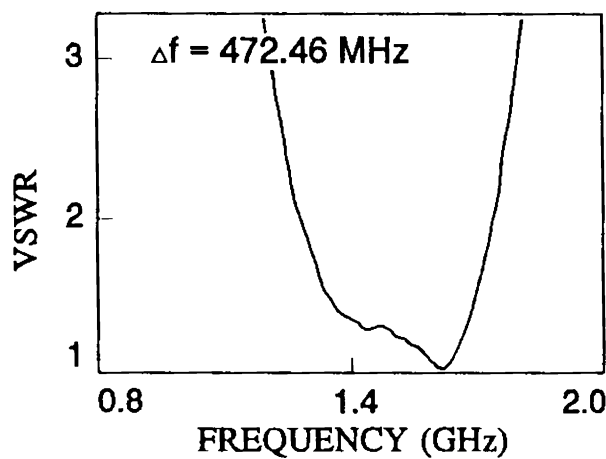
Fig. 4.27 Schematic representation of parallelogram end-loaded printed dipole



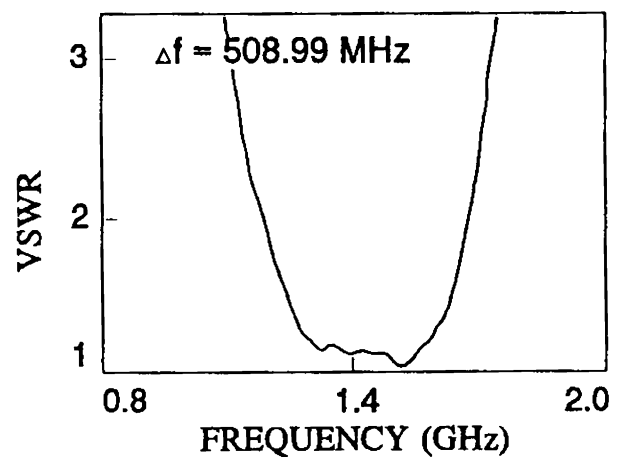
(a)



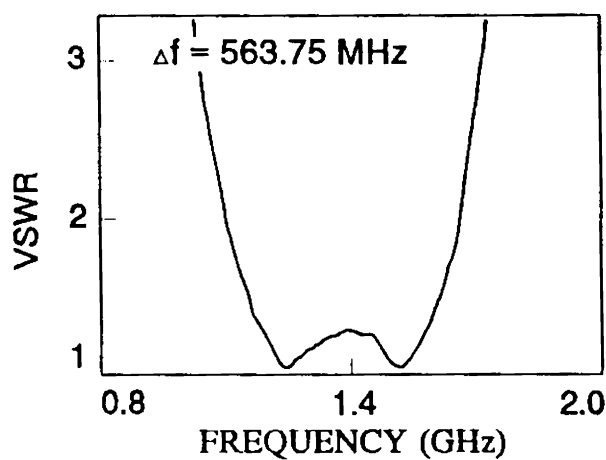
(b)



(c)

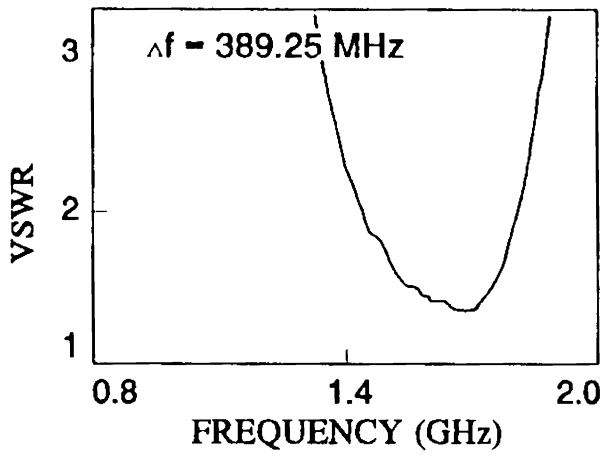


(d)

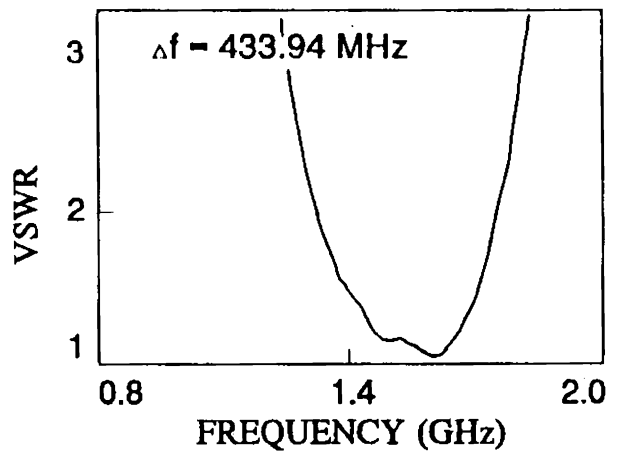


(e)

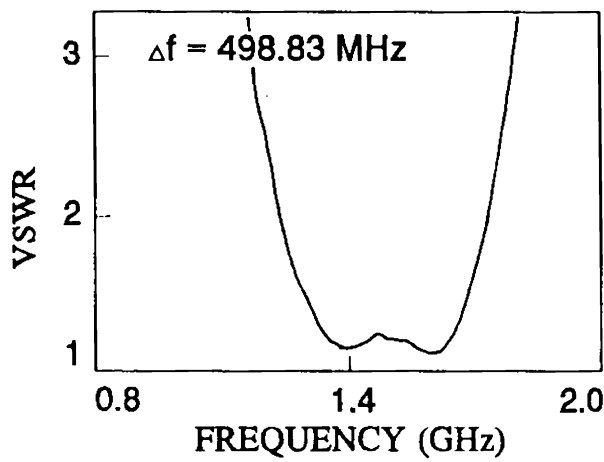
Fig. 4.28(i) VSWR plots of parallelogram end-loaded printed dipoles for different angles ($l_p = 3.00 \text{ cm}$)
 a) $\beta = 80^\circ$ b) $\beta = 90^\circ$ c) $\beta = 100^\circ$ d) $\beta = 110^\circ$ e) $\beta = 120^\circ$



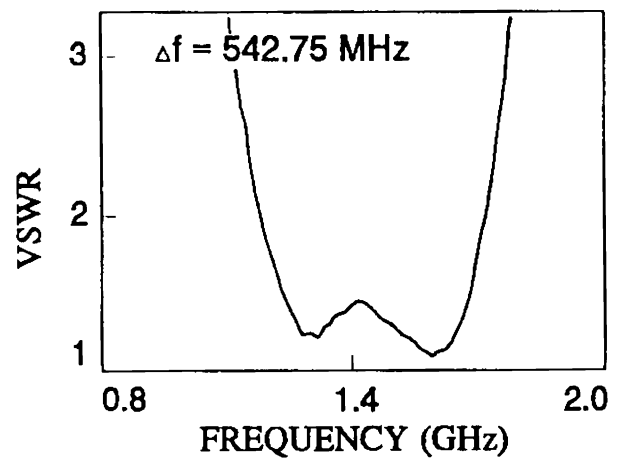
(a)



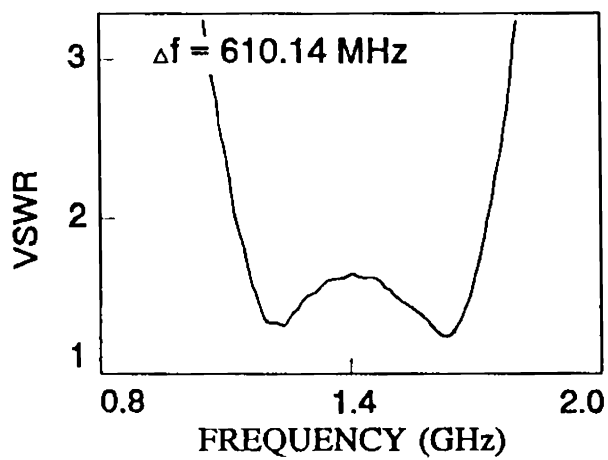
(b)



(c)



(d)



(e)

Fig. 4.28(ii) VSWR plots of parallelogram end-loaded printed dipoles for different angles ($l_p = 3.25 \text{ cm}$)
 a) $\beta = 80^\circ$ b) $\beta = 90^\circ$ c) $\beta = 100^\circ$ d) $\beta = 110^\circ$ e) $\beta = 120^\circ$

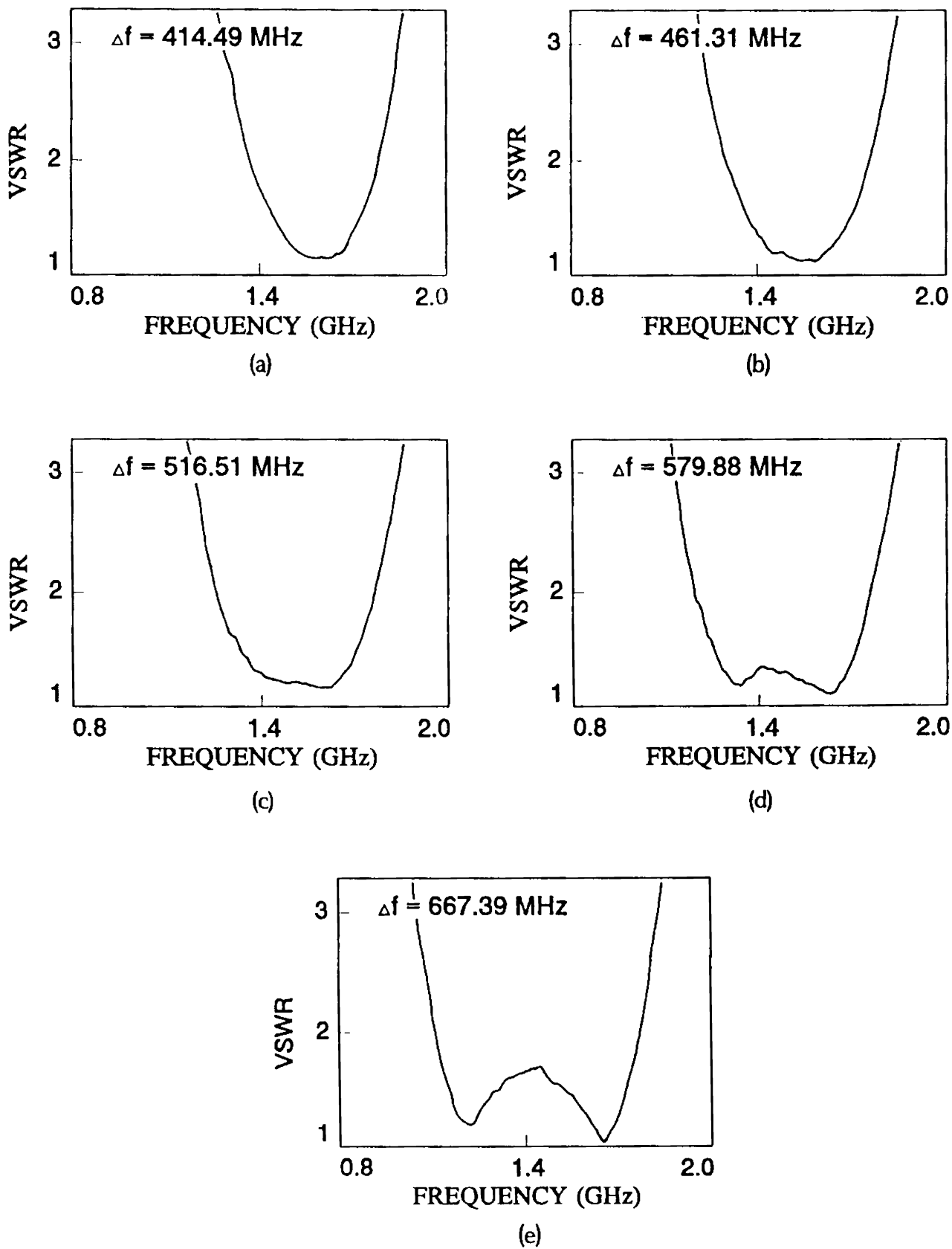


Fig. 4.28(iii) VSWR plots of parallelgram end-loaded printed dipoles for different angles ($l_p = 3.50$ cm)
a) $\beta = 80^\circ$ b) $\beta = 90^\circ$ c) $\beta = 100^\circ$ d) $\beta = 110^\circ$ e) $\beta = 120^\circ$

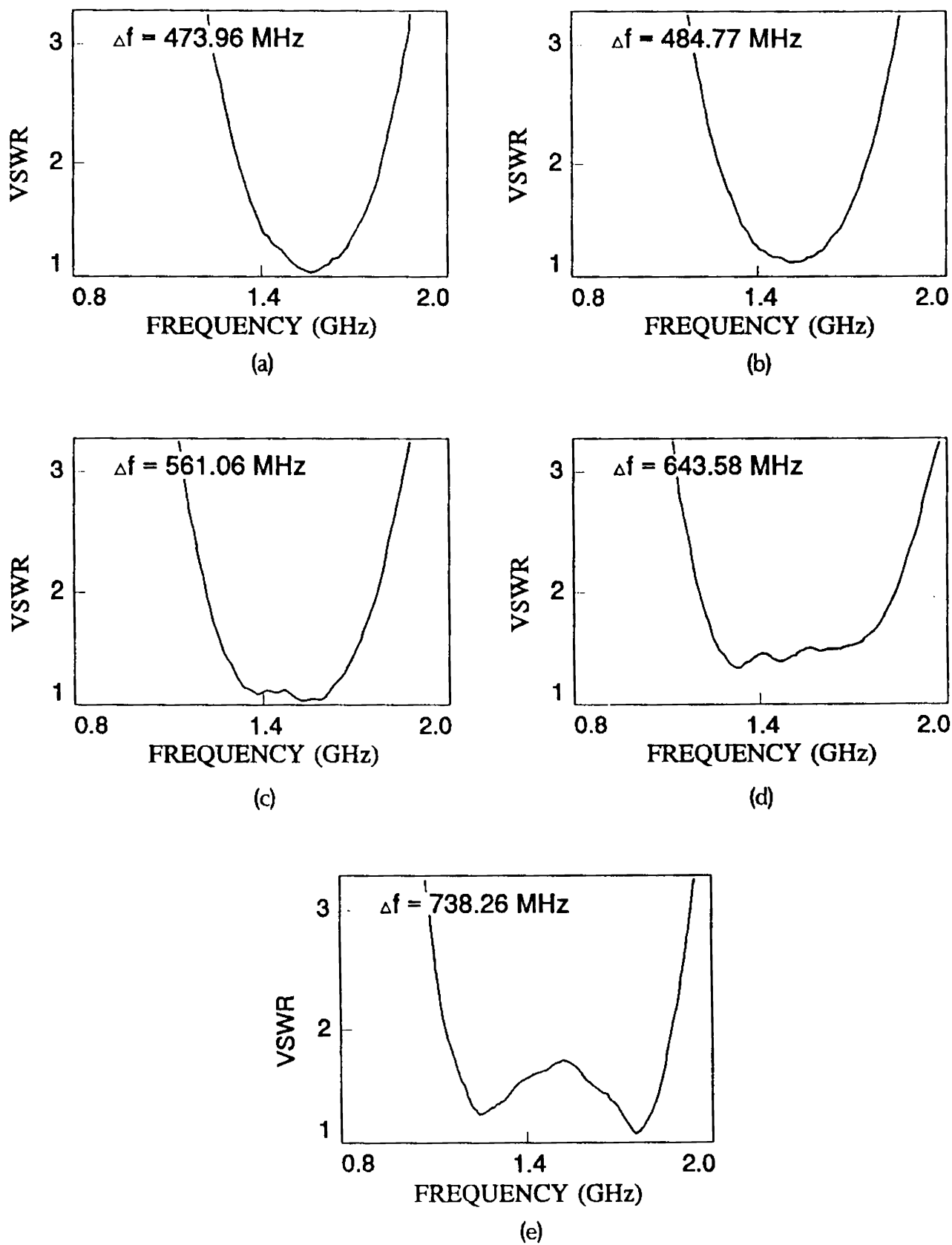
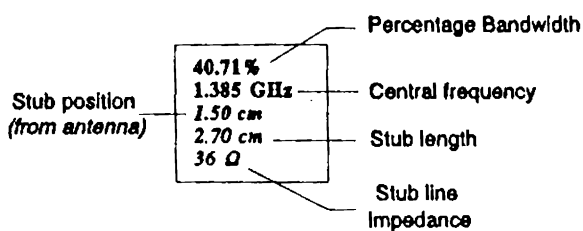


Fig. 4.28(iv) VSWR plots of parallelogram end-loaded printed dipoles for different angles ($l_p = 3.75$ cm)
 a) $\beta = 80^\circ$ b) $\beta = 90^\circ$ c) $\beta = 100^\circ$ d) $\beta = 110^\circ$ e) $\beta = 120^\circ$

Table 4.11

Percentage bandwidths and central frequencies of parallelogram end-loaded printed dipoles of various angles and bisecting lengths with optimised stub parameters

Bisecting length l_p Angle β	3.00 cm	3.25 cm	3.50 cm	3.75 cm
	80°	23.67% 1.594 GHz 1.40 cm 2.50 cm 39 Ω	23.93% 1.627 GHz 1.40 cm 2.30 cm 42 Ω	26.35% 1.573 GHz 1.40 cm 2.50 cm 42 Ω
90°	25.28% 1.568 GHz 1.40 cm 2.50 cm 39 Ω	28.18% 1.540 GHz 1.40 cm 2.50 cm 39 Ω	30.14% 1.530 GHz 1.45 cm 2.25 cm 36 Ω	31.90% 1.519 GHz 1.45 cm 2.50 cm 42 Ω
100°	31.23% 1.513 GHz 1.40 cm 2.50 cm 36 Ω	33.73% 1.482 GHz 1.35 cm 2.50 cm 36 Ω	34.14% 1.511 GHz 1.45 cm 2.25 cm 36 Ω	37.44% 1.498 GHz 1.40 cm 2.25 cm 36 Ω
110°	35.48% 1.434 GHz 1.50 cm 2.70 cm 36 Ω	37.45% 1.449 GHz 1.45 cm 2.50 cm 36 Ω	39.48% 1.469 GHz 1.45 cm 2.25 cm 36 Ω	42.21% 1.525 GHz 1.40 cm 2.30 cm 42 Ω
120°	40.71% 1.385 GHz 1.50 cm 2.70 cm 36 Ω	42.55% 1.434 GHz 1.45 cm 2.50 cm 42 Ω	46.52% 1.435 GHz 1.40 cm 2.55 cm 36 Ω	48.74% 1.514 GHz 1.25 cm 2.50 cm 42 Ω



$l_p = 3.75$ cm and the angle $\beta = 120^\circ$ are the maximum possible values of the parallelogram. Further increase in the values of these parameters means overlapping of the loading structure with the feed structure, which will completely change the impedance characteristics of the antenna. Thus, $l_p = 3.75$ cm and $\beta = 120^\circ$ are taken as the optimum design parameters.

While optimising the triangular end-loaded printed dipole, it was observed that the optimisation of the dimensions of the end-load is related to other design parameters. Thus, no attempt has been made to reconfirm the optimisation of other parameters.

The final design values of optimised Parallelogram End-Loaded Printed Dipole Antenna (PELPDA) are as follows:

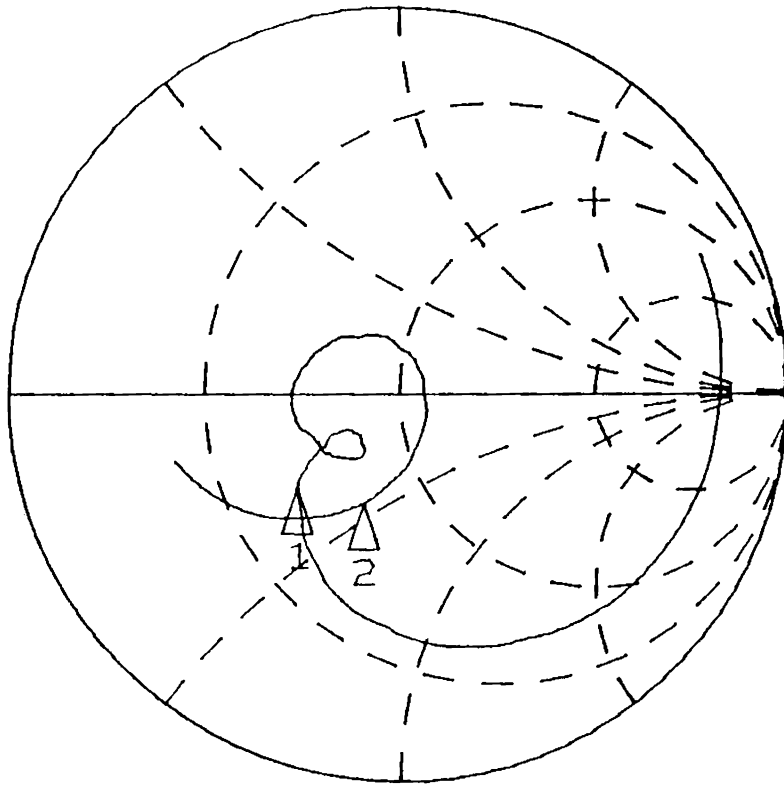
Bisecting length l_p	= 3.75 cm
Angle β	= 120°
Stub length S_l	= 2.50 cm
Stub position S_p	= 1.25 cm
Stub line impedance	= 42 Ω

The remaining design values are same as that given earlier.

The impedance plot of the antenna is given in Fig. 4.29. The 2:1 VSWR bandwidth is 738.26 MHz and the central frequency is 1.514 GHz. Thus, the percentage bandwidth is 48.74%, which is almost the same as that of TELPDA.

The radiation patterns of the antenna at start, stop and central frequencies are given in Fig. 4.30. The radiation patterns are almost identical to that of TELPDA. The only difference is that the cross-polar level is higher in this case. This may be due to the large size of the end-loads.

MARKER 2-1
738.26295 MHz



START 0.800000000 GHz
STOP 2.000000000 GHz

Fig. 4.29 Impedance loci of PELPDA

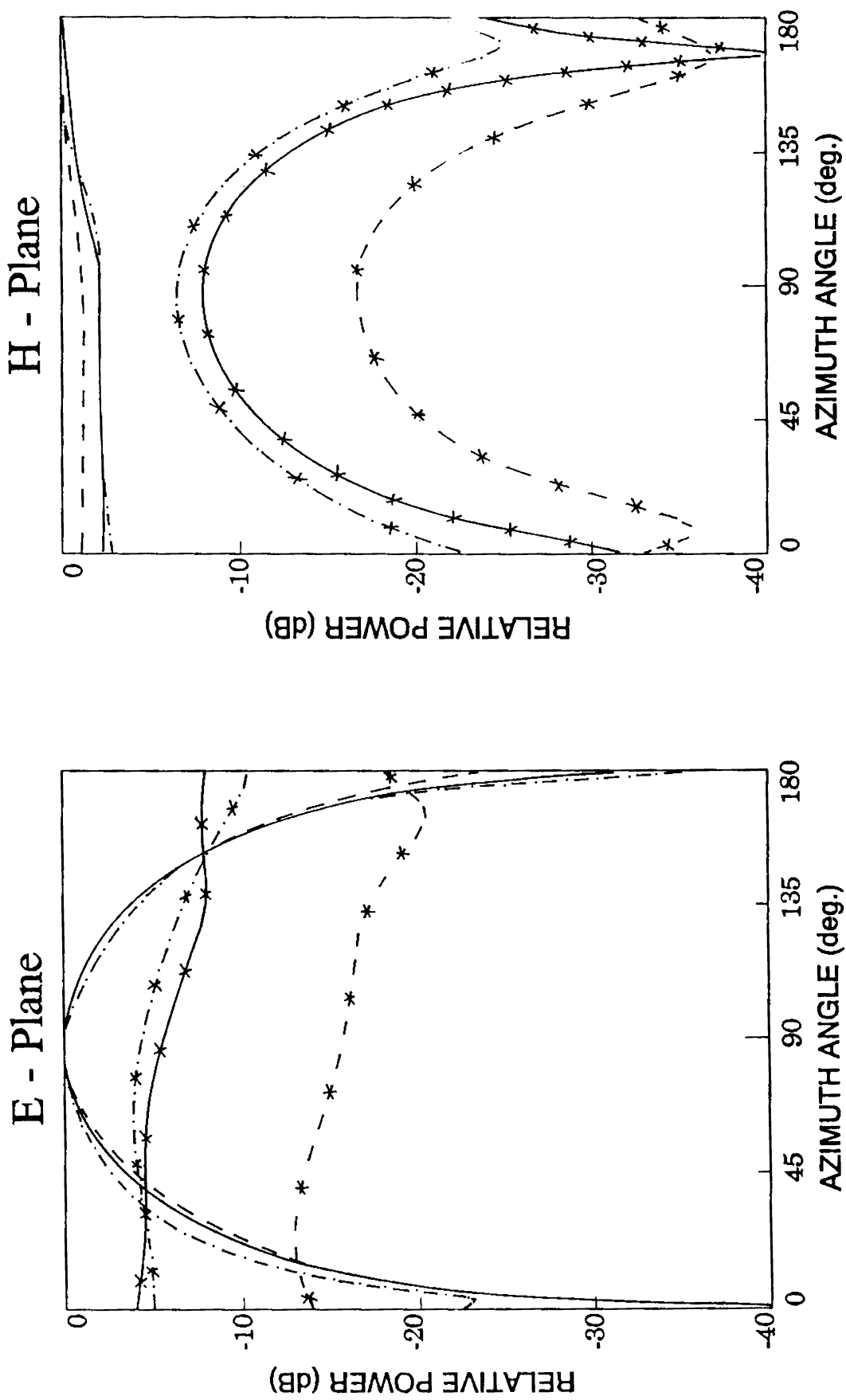


Fig. 4.30 Radiation patterns of PELPDA
 co-polar : - - - - - 1.145 GHz, ——— 1.514 GHz, - - - - - 1.883 GHz
 cross-polar : - - * - - 1.145 GHz, — * — 1.514 GHz, - - * - - 1.883 GHz

The gain of PELPDA is measured by measuring the $|S_{21}|$ of the antenna with respect to the same standard half-wave dipole used for TELPDA. From the $|S_{21}|$ plot (Fig. 4.31), it can be seen that at 1.496 GHz (resonating frequency of standard dipole), the gain of PELPDA is less than that of wire dipole by 1.64 dB.

4.3.1 Cavity backed parallelogram end-loaded printed dipole

Similar to Cavity Backed Triangular End-Loaded Printed Dipole, the effect of reflector plate on the impedance bandwidth of PELPDA is studied. The separation h between the dipole and the reflector plate is varied from 4.5 cm to 6.5 cm in steps of 0.5 cm and the corresponding VSWR plots are given in Fig. 4.32. The VSWR of the antenna is more than 2 in the central part of the frequency band for the separation $h = 5$ cm and increases with the decrease in the separation. The percentage bandwidths and the central frequencies for different separations are given in Table 4.12. Although VSWR bandwidth is maximum for $h = 5.5$ cm, from the corresponding VSWR plot (Fig. 4.32(c)), it can be seen that at 1.4 GHz VSWR is 1.98. This is too close to VSWR = 2 limit. Thus, $h = 6$ cm is selected as the design value, for which VSWR is sufficiently below VSWR = 2 limit in the middle portion of the band of interest.

The impedance plot of Cavity Backed Parallelogram End-Loaded Printed Dipole Antenna (CBPELPDA) with separation $h = 6$ cm is given in Fig. 4.33. The 2:1 bandwidth is 817.34 MHz and the central frequency is 1.489 GHz. This corresponds to 54.85% impedance bandwidth. This is 6% more than PELPDA and 1% more than CBTELPDA.

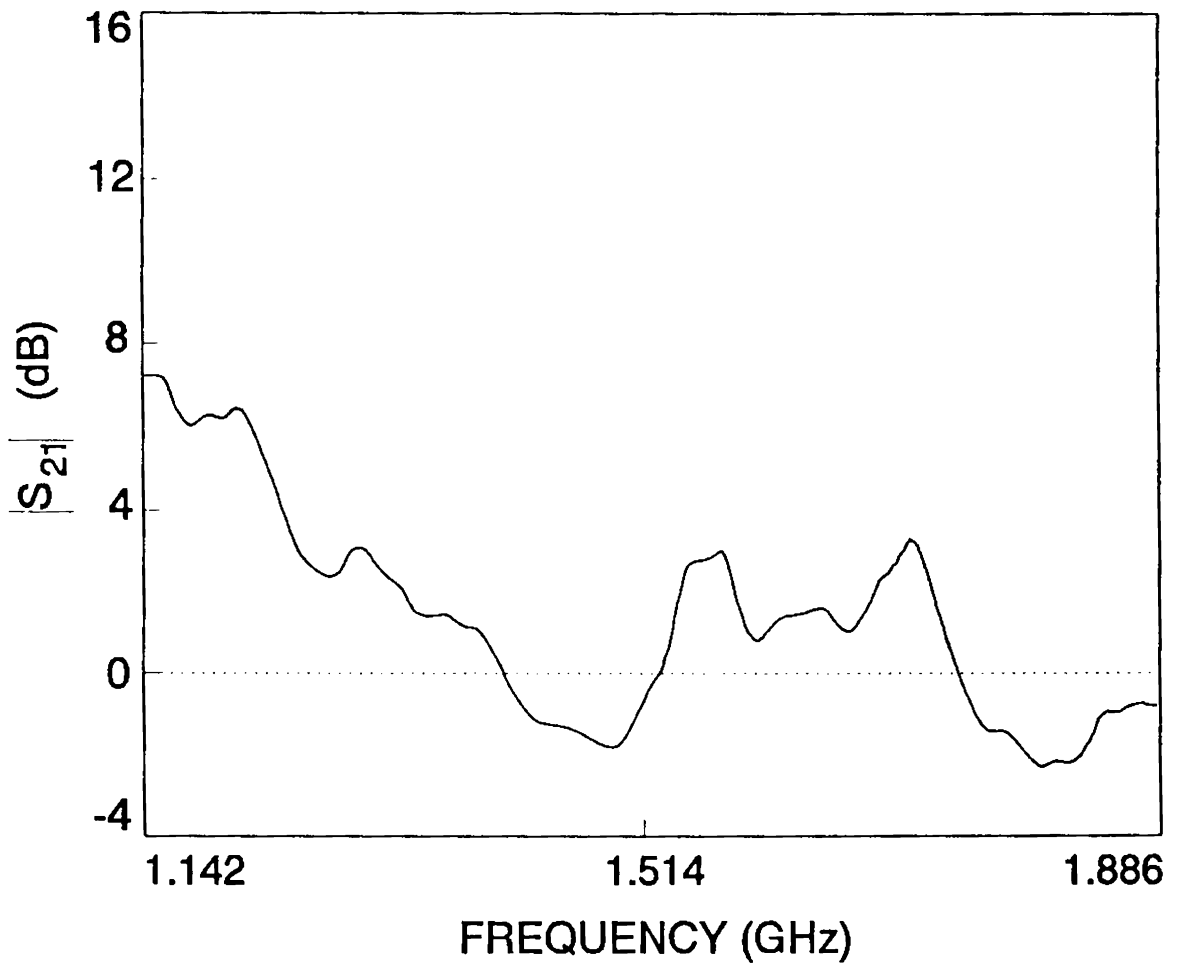
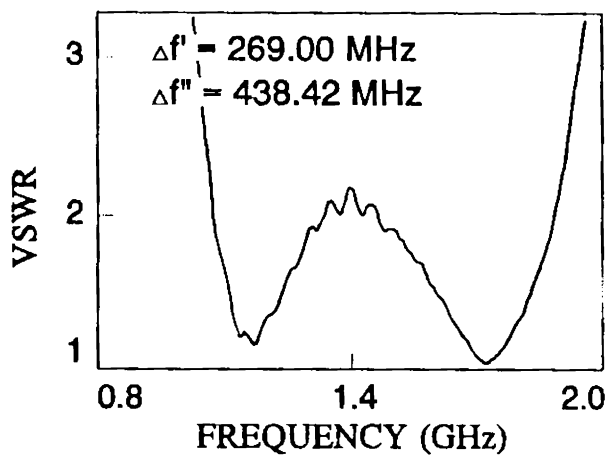
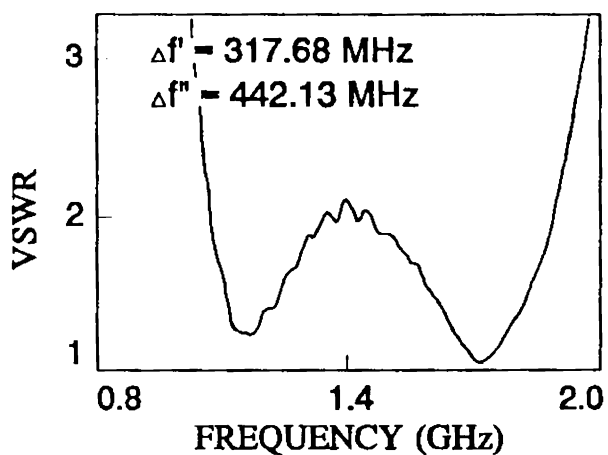


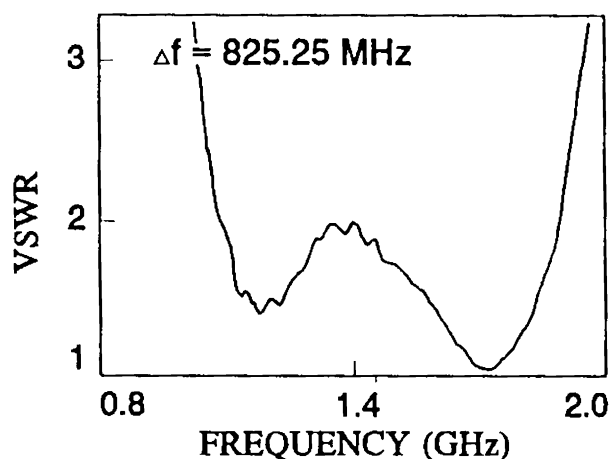
Fig. 4.31 $|s_{21}|$ of PELPDA with respect to half wave wire dipole resonating at 1.496 GHz



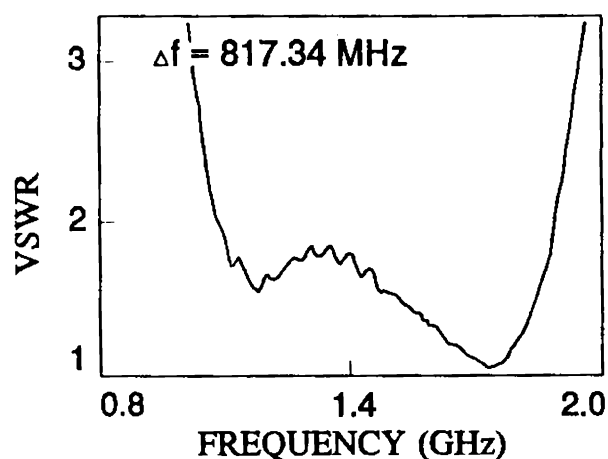
(a)



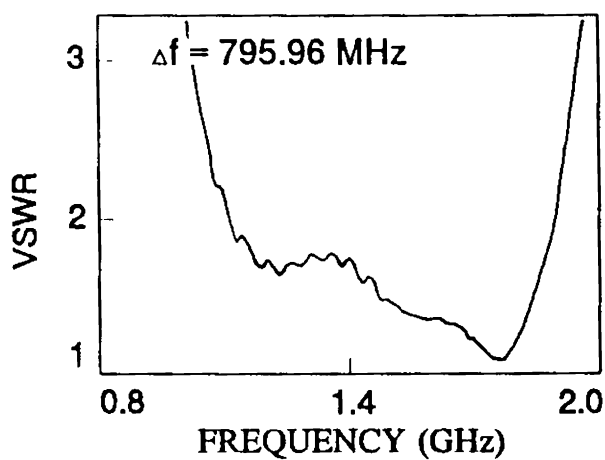
(b)



(c)



(d)

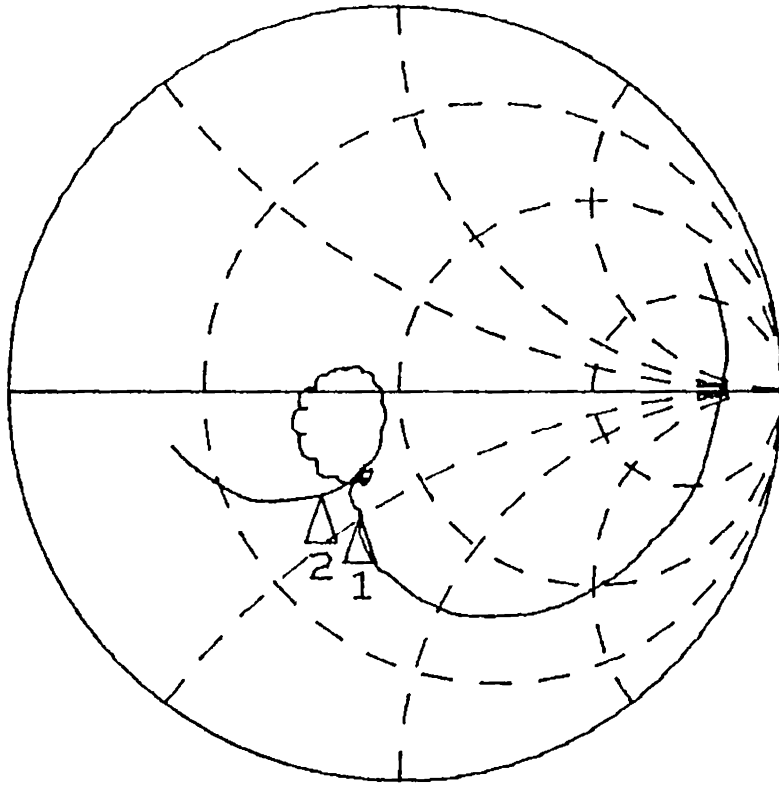


(e)

Fig. 4.32 VSWR plots of cavity backed PELPDA for different separations between the reflector and the dipole

a) $h = 4.5 \text{ cm}$ b) $h = 5.0 \text{ cm}$ c) $h = 5.5 \text{ cm}$ d) $h = 6.0 \text{ cm}$ e) $h = 6.5 \text{ cm}$

MARKER 2-1
817.339118 MHz



START 0.800000000 GHz
STOP 2.000000000 GHz

Fig. 4.33 Impedance loci of CBPELPDA

Table 4.12

Percentage bandwidths and central frequencies of cavity backed parallelogram end-loaded printed dipole for different separations between the dipole and the reflector plate

Separation h (cm)	Percentage bandwidth	Central frequency (GHz)
4.5	22.31 / 26.17	1.205 / 1.677
5.0	25.92 / 25.36	1.227 / 1.677
5.5	55.42	1.488
6.0	54.85	1.489
6.5	53.04	1.502
7.0	49.54	1.526

The principal planes radiation patterns at the start, end and central frequencies of the band of interest are given in Fig. 4.34. The radiation patterns are almost identical to that of CBTELPDA. As compared to PELPDA, cross-polar level is higher for this antenna.

Like previous cases, the same standard wire dipole, resonating at 1.496 GHz, is used to measure the gain of CBPELPDA. The $|S_{21}|$ plot of the antenna with respect to standard wire dipole is given in Fig. 4.35. The gain of the antenna is 3.13 dB more than wire dipole at 1.496 GHz. This is almost 5 dB more compared to PELPDA at 1.496 GHz. The increase in gain is due to the presence of the reflector plate and narrowing of the beamwidth.

4.3.2 Design details

The design criteria of Parallelogram End-Loaded Printed Dipole Antenna have been evolved through experimental iterations, as in the case of Triangular End-Loaded Printed Dipole. The design details of the antenna, shown in Fig. 4.27, are given below in terms of the wavelength (λ_0) corresponding to the central frequency.

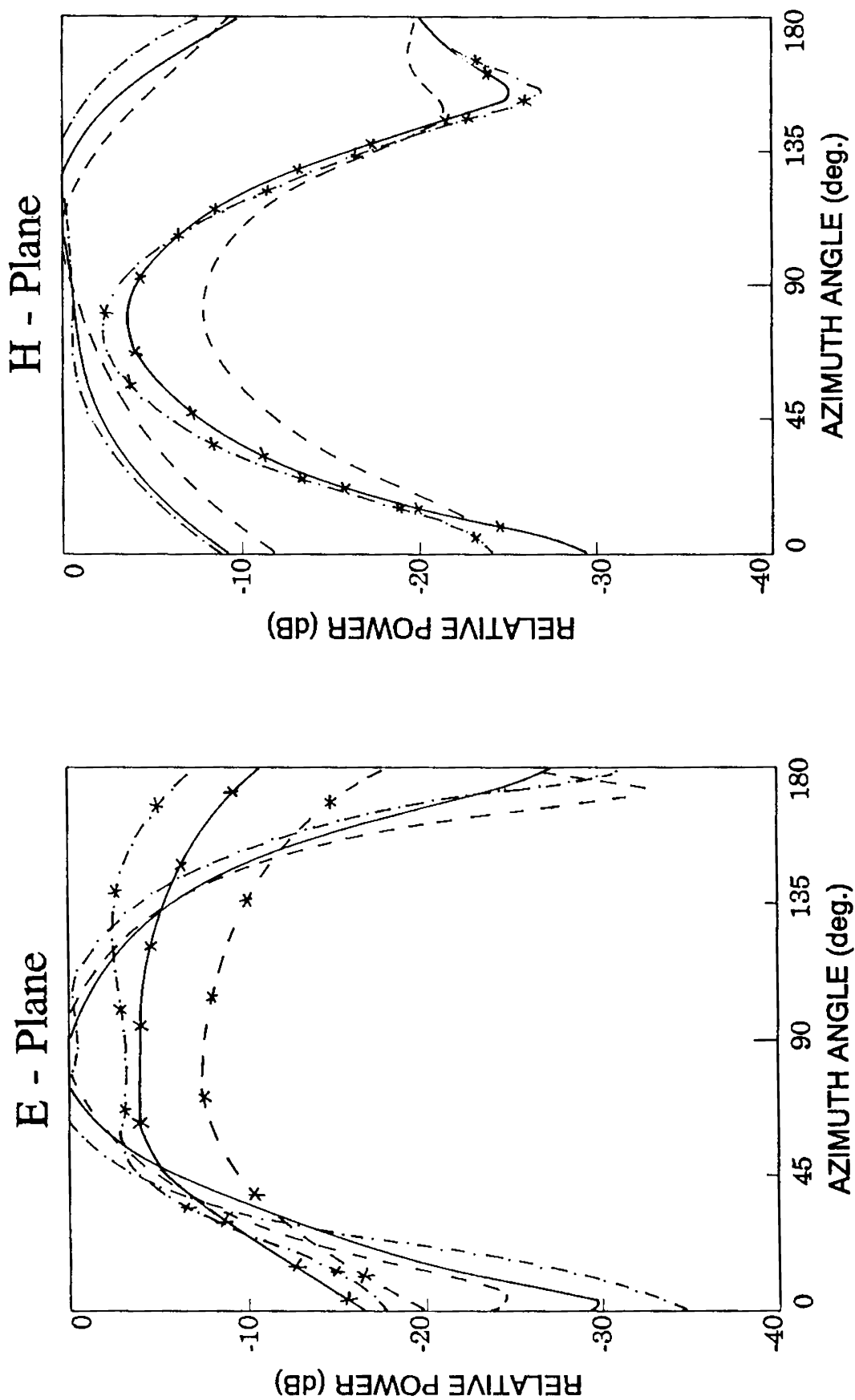


Fig. 4.34 Radiation patterns of CBPELPDA
 co-polar : — 1.081 GHz, - - - 1.490 GHz, - · - · - 1.899 GHz
 cross-polar : · · · 1.081 GHz, - - - - 1.490 GHz, - - - * - - 1.899 GHz

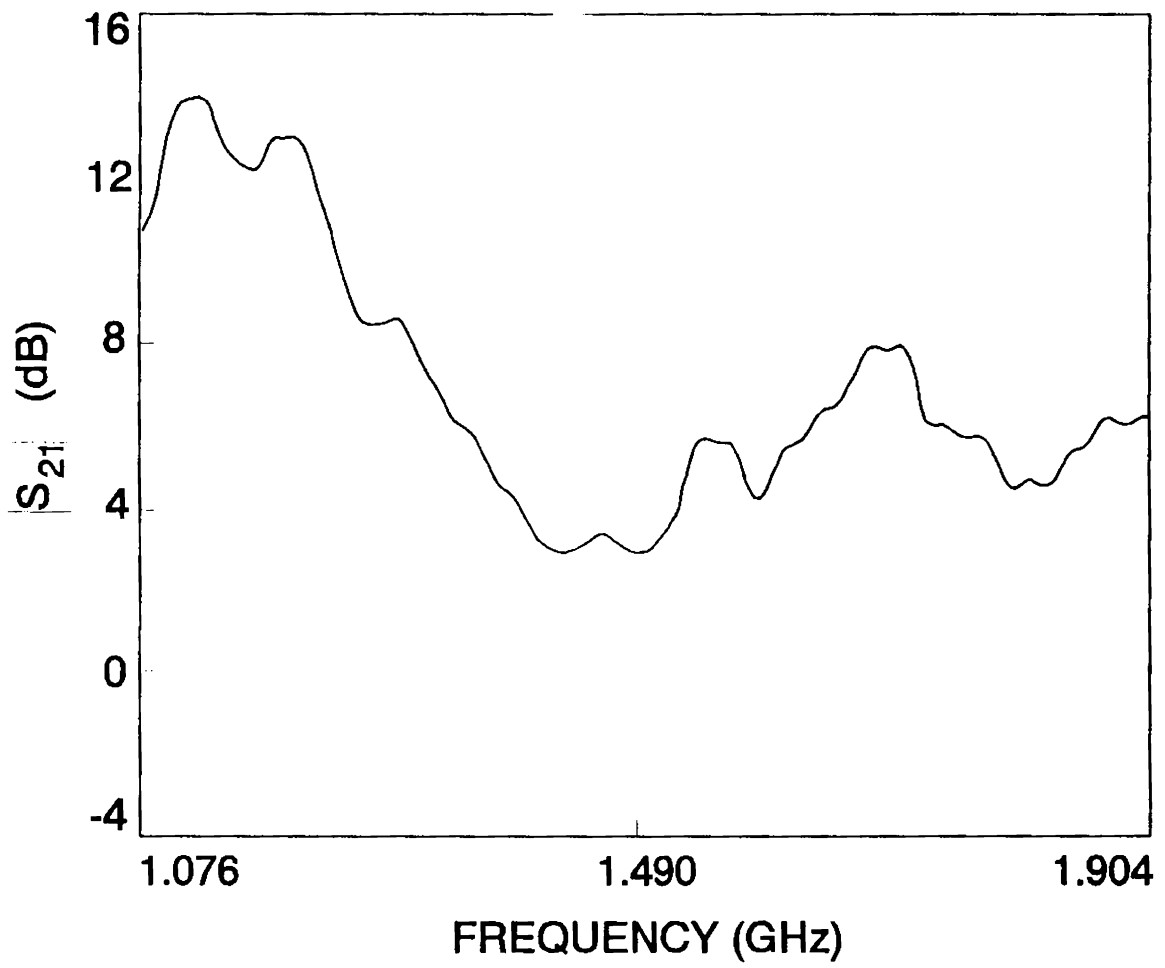


Fig. 4.35 $|S_{21}|$ of CBPELPDA with respect to half wave wire dipole resonating at 1.496 GHz

Main arm length l_m	=	$0.243 \lambda_0$
Bisecting length l_p	=	$0.189 \lambda_0$
Main arm width at feed point w_m	=	$0.050 \lambda_0$
Feed point location l_f	=	$0.025 \lambda_0$
Arms overlapping O_g	=	$0.063 \lambda_0$
Flaring angle θ	=	10°
Angle β	=	120°
Stub length S_t	=	$0.235 \lambda_d$
Stub position S_p	=	$0.118 \lambda_d$
Stub line impedance	=	42Ω
Transformer length l_t	=	$0.55 \lambda_d$
Transformer line impedance	=	42Ω

Ground arm length and the load dimensions are 1.05 times larger than the corresponding main arm values and the ground arm width at feed point is 1.10 times larger than the corresponding main arm value. Here, $\lambda_d = \lambda_0 / \sqrt{\epsilon_{eff}}$ and the effective dielectric constant ϵ_{eff} can be calculated from (1).

The difference in central frequency of PELPDA and CBPELPDA is negligible as compared to the bandwidth of the antennas for all practical purposes. Thus, all design criteria of Parallelogram End-Loaded Printed Dipole Antenna are valid for Cavity Backed Parallelogram End-Loaded Printed Dipole Antenna with a separation between the dipole and reflector of $0.3 \lambda_0$.

Experimental results II: Microstrip dipoles

5

This chapter highlights the outcome of experimental investigations carried out on microstrip dipole antennas. The chapter is divided into two sections:

1. Triangular end-loaded microstrip dipole
2. Triangular microstrip dipole

The procedure adopted for the optimisation of impedance bandwidth of microstrip dipoles are same as that of the printed dipoles. Each design parameter is optimised by varying its value while keeping the other parameters constant.

5.1 TRIANGULAR END-LOADED MICROSTRIP DIPOLE

As described in Chapter 3, wideband microstrip dipole antennas are constructed using the same end-loading technique used for bandwidth enhancement of printed dipoles. Here, triangular shape is selected as the load shape. The dipole arms are etched on a dielectric substrate and placed over another grounded dielectric substrate, shown in Fig. 3.6. Matching of dipoles with 50Ω stripline is done by using impedance matching transformer.

Initial attempts of using the design values of Triangular End-Loaded Printed Dipole to construct microstrip dipole do not yield any good result. The impedance bandwidths of such antennas are found to be very narrow. Thus, all the design values are thoroughly modified through experimental trial and error method.

Fig. 5.1 shows the sketch of the antenna. The initial design values selected are as follows:

Arm width at feed point w	=	0.65 cm
Feed point location l_f	=	0.70 cm
Height of the triangle h_t	=	1.50 cm
Flaring angle θ	=	10°
Apex angle α	=	100°
Ground arm length l_g	=	4.90 cm

Other parameters of the ground arm are same as that of the main arm values.

The effect of three important design parameters on the impedance bandwidth are discussed in detail and are as follows:

1. Main arm length l_m
2. Height of the triangle h_t
3. Apex angle α

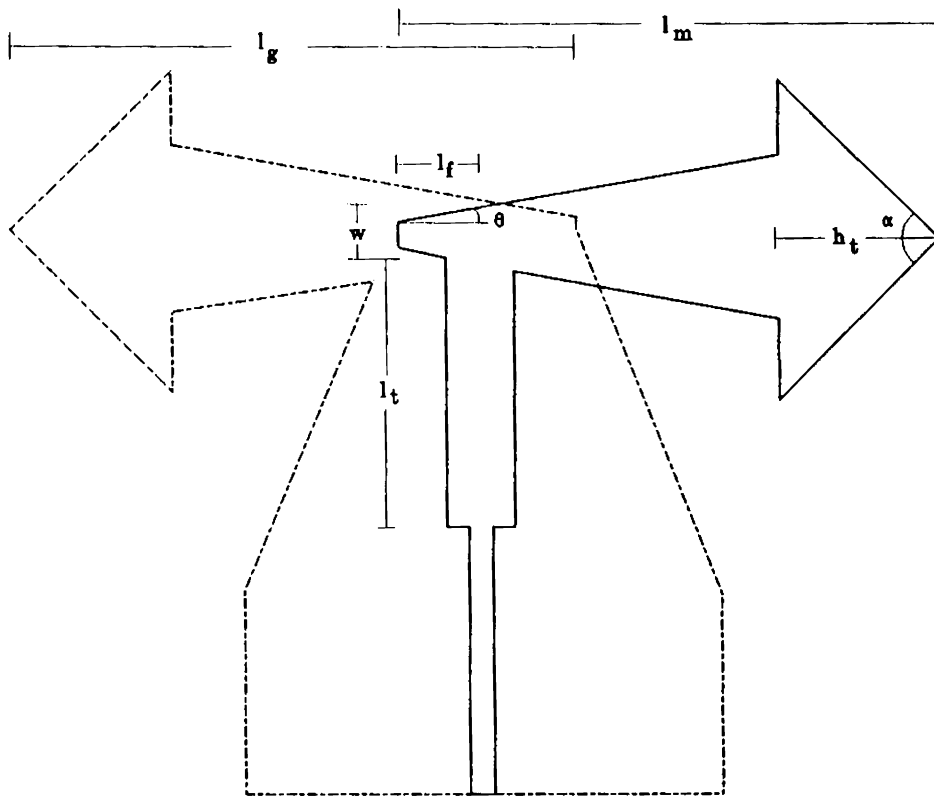
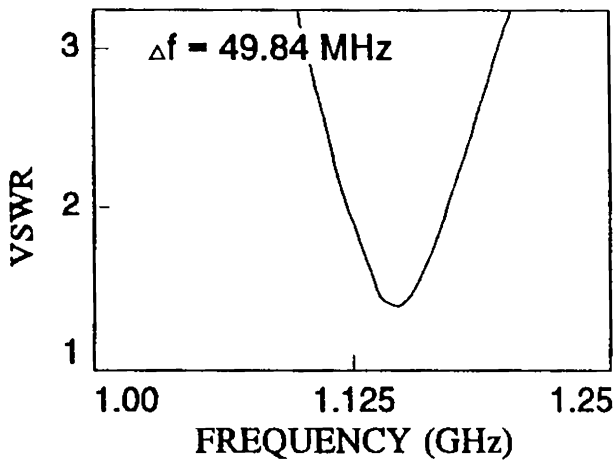


Fig. 5.1 Schematic representation of triangular end-loaded microstrip dipole

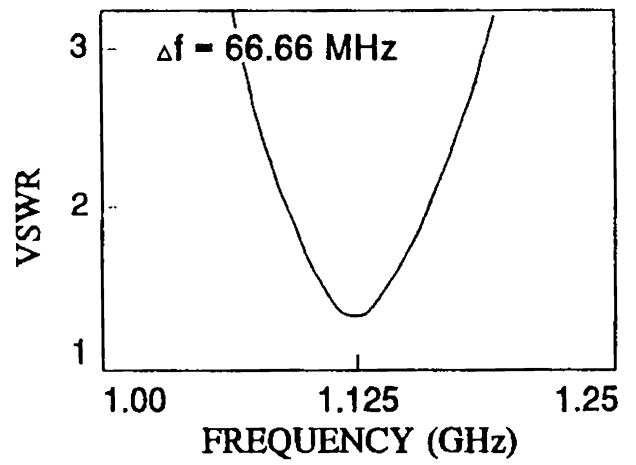
5.1.1 Main arm length

Initial experimental studies show that unlike the case of triangular end-loaded printed dipoles, where the size of ground arm load is 1.05 times larger than the main arm load size, improvement in bandwidth is possible by keeping the size of the load, *ie.*, size of the triangles, same for both arms. Thus, to optimise the arms-ratio, only the main arm length is varied instead of varying the complete arm dimension.

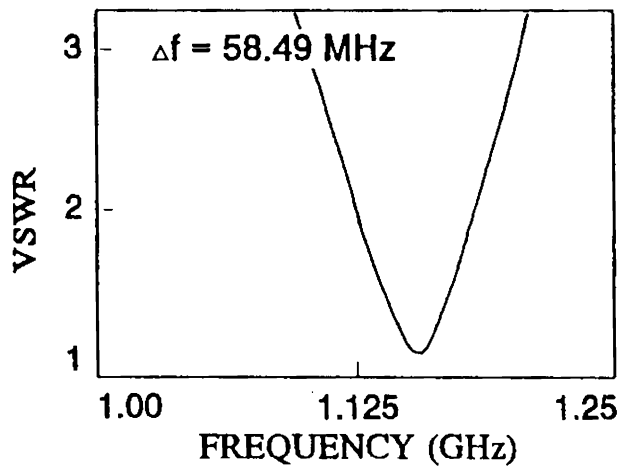
To optimise the main arm to ground arm ratio, antennas are fabricated with different main arm lengths like 4.10 cm, 4.25 cm, 4.45 cm, 4.65 cm and 4.90 cm, while keeping the ground arm length fixed at 4.90 cm. The VSWR plots of the antennas with various main arm lengths are given in Fig. 5.2 and the corresponding percentage bandwidths and the central frequencies with optimum impedance transformer parameters are given in Table 5.1. From the table, it is evident that there is significant improvement in impedance bandwidth of the antenna with decrease in the main arm length, *ie.*, with increase in main arm to ground arm ratio. The percentage bandwidth is maximum when $l_m = 4.25$ cm. From the table, it can also be seen that the impedance bandwidth is very much sensitive to the change in main arm to ground arm ratio. Thus, another set of antennas are fabricated with various main arm lengths, varying around 4.25 cm, in steps of 0.5 mm. The VSWR plots, and the percentage bandwidths and the central frequencies for different antennas are given in Fig. 5.3 and Table 5.2 respectively. From the table, it can be seen that the best value of main arm length is 4.20 cm, corresponding to main arm to ground arm length ratio of 1:1.166. The larger value of arm length ratio, compared to TELPDA, is due to the difference in the effective dielectric constant of the medium surrounding the two arms due to their difference in heights from the ground plane.



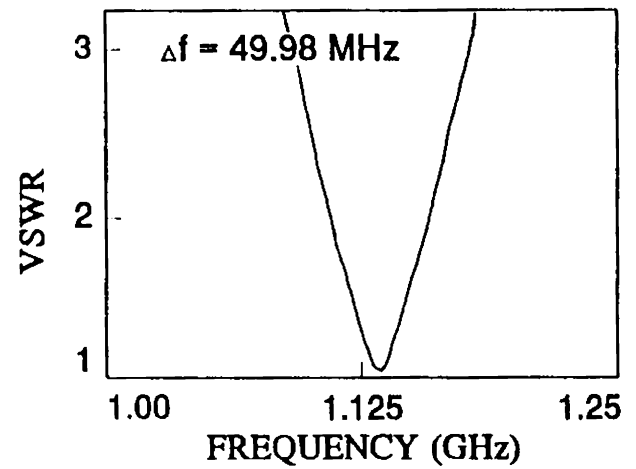
(a)



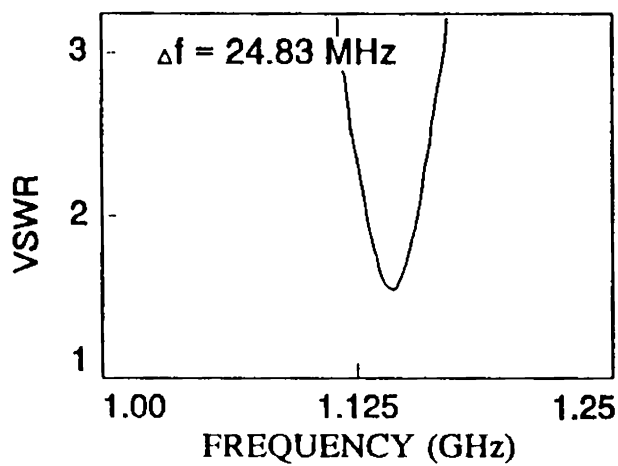
(b)



(c)

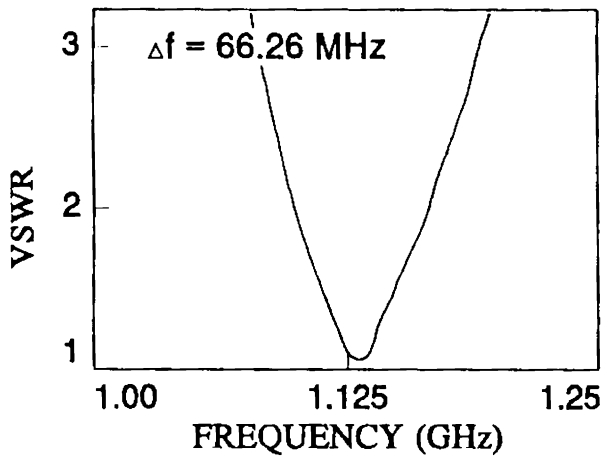


(d)

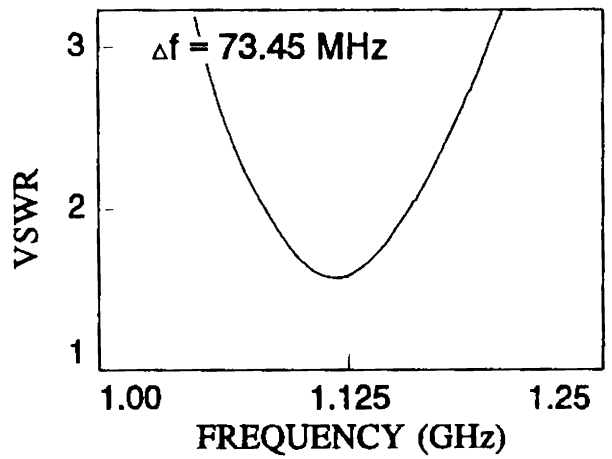


(e)

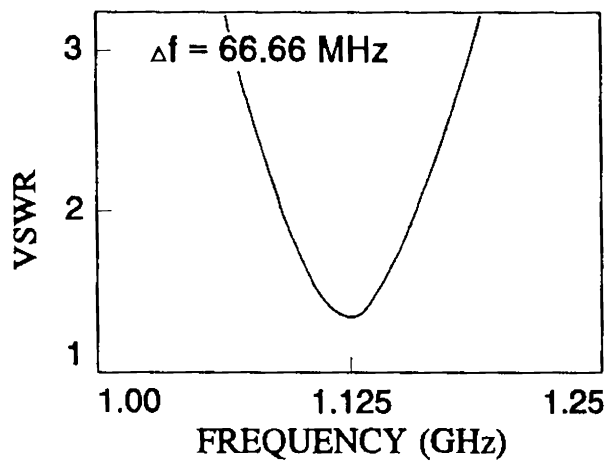
Fig. 5.2 VSWR plots of triangular end-loaded microstrip dipoles for different main arm lengths
 a) $l_m = 4.1$ cm b) $l_m = 4.25$ cm c) $l_m = 4.45$ cm d) $l_m = 4.65$ cm e) $l_m = 4.9$ cm



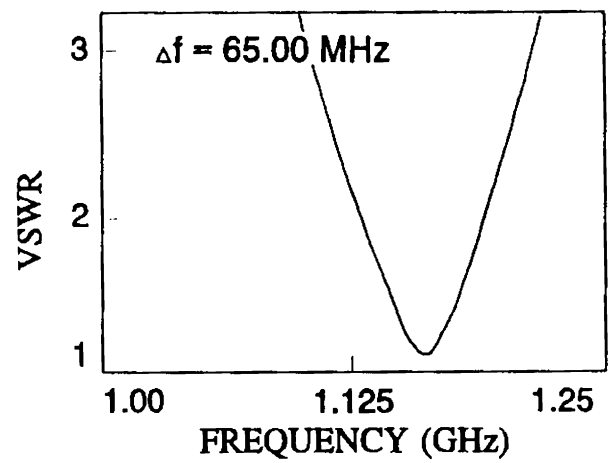
(a)



(b)



(c)



(d)

Fig. 5.3 VSWR plots of triangular end-loaded microstrip dipoles for different main arm lengths
 a) $l_m = 4.15$ cm b) $l_m = 4.20$ cm c) $l_m = 4.25$ cm d) $l_m = 4.30$ cm

Table 5.1

Percentage bandwidths and central frequencies of triangular end-loaded microstrip dipoles of various main arm lengths with optimised impedance transformer parametrs

Main arm length l_m (cm)	Transformer		Percentage bandwidth	Central frequency (GHz)
	length (cm)	impedance (Ω)		
4.10	2.70	21.5	4.34	1.147
4.25	2.60	21.5	5.92	1.124
4.45	2.70	23.5	5.06	1.155
4.65	2.70	21.5	4.40	1.136
4.90	3.00	23.5	2.17	1.141

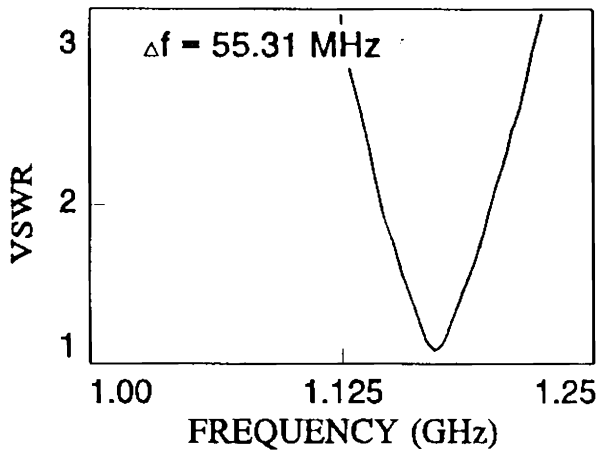
Table 5.2

Percentage bandwidths and central frequencies of triangular end-loaded microstrip dipoles of various main arm lengths with optimised impedance transformer parametrs

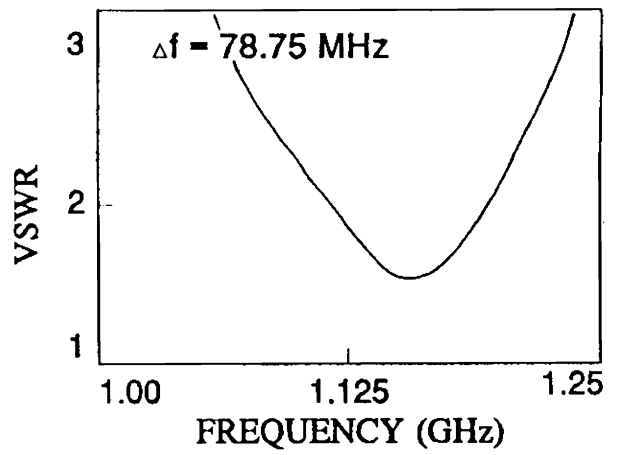
Main arm length l_m (cm)	Transformer		Percentage bandwidth	Central frequency (GHz)
	length (cm)	impedance (Ω)		
4.15	2.80	23.5	5.85	1.133
4.20	2.55	21.5	6.56	1.119
4.25	2.60	21.5	5.92	1.124
4.30	2.70	23.5	5.59	1.162

5.1.2 Height of triangle

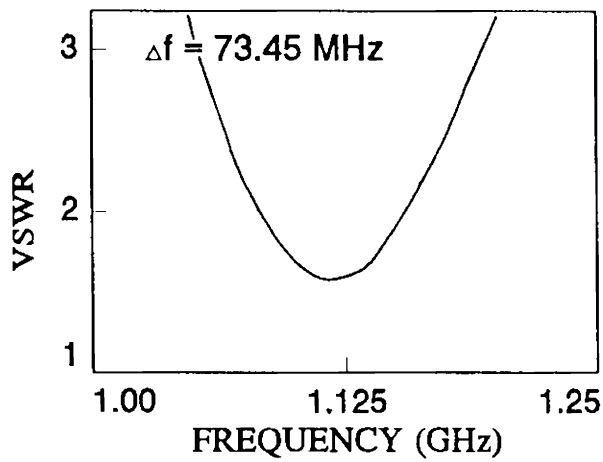
While keeping the main arm length $l_m = 4.20$ cm and other parameters constant, height of the triangle h_t is varied from 1.30 cm to 1.70 cm in steps of 1 mm. The VSWR plots are given in Fig. 5.4 and the percentage bandwidths and the central frequencies with optimum



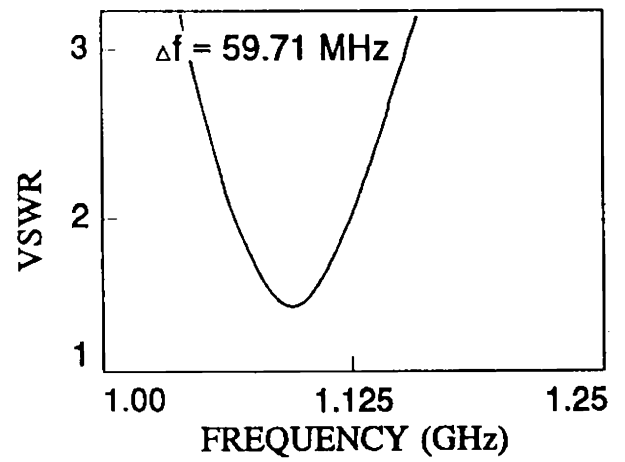
(a)



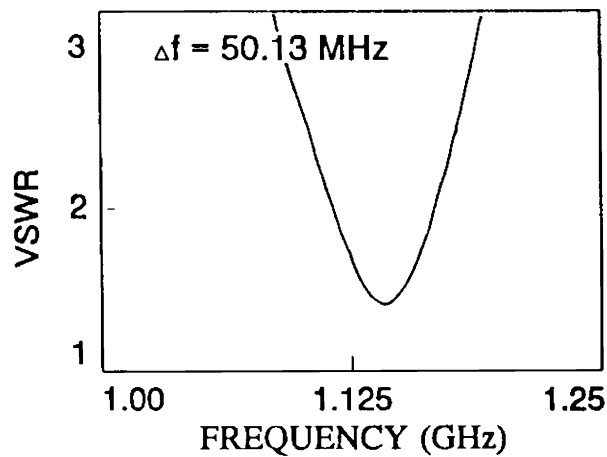
(b)



(c)



(d)



(e)

Fig. 5.4 VSWR plots of triangular end-loaded microstrip dipoles for different heights of triangle
 a) $h_t = 1.3 \text{ cm}$ b) $h_t = 1.4 \text{ cm}$ c) $h_t = 1.5 \text{ cm}$ d) $h_t = 1.6 \text{ cm}$ e) $h_t = 1.7 \text{ cm}$

transformer parameters are given in Table 5.3. From the table, it can be seen that there is not much change in percentage bandwidth with change in the height of the triangle. Also, percentage bandwidth is maximum for $h_t = 1.40$ cm.

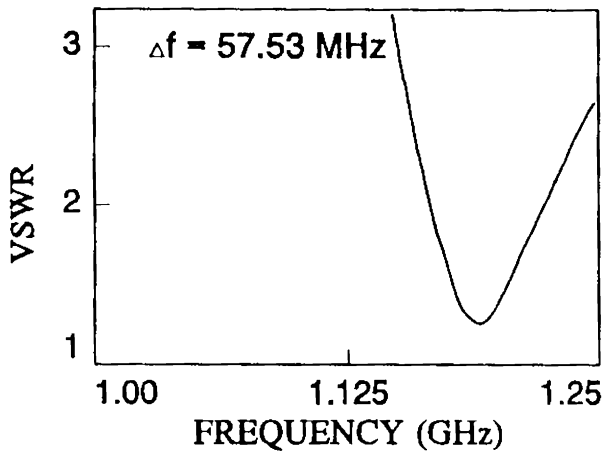
Table 5.3

Percentage bandwidths and central frequencies of triangular end-loaded microstrip dipoles of various heights of triangle with optimised impedance transformer parameters

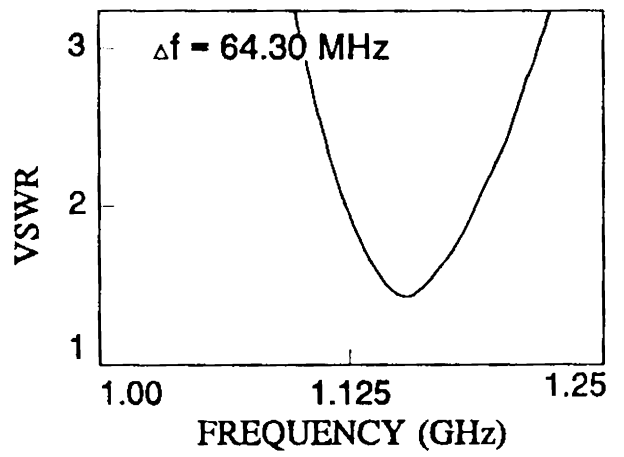
Height of triangle h_t (cm)	Transformer		Percentage bandwidth	Central frequency (GHz)
	length (cm)	impedance (Ω)		
1.30	3.00	21.5	4.71	1.174
1.40	2.70	21.5	6.84	1.155
1.50	2.55	21.5	6.56	1.119
1.60	2.80	21.5	5.45	1.096
1.70	2.95	21.5	4.39	1.142

5.1.3 Apex angle

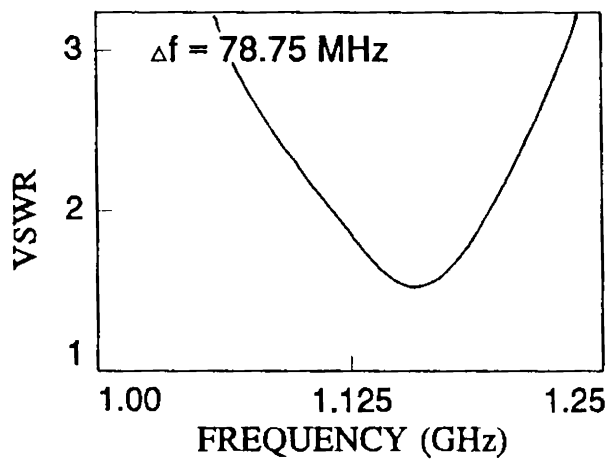
Different antennas are fabricated with various apex angles like 80° , 90° , 100° , 110° and 120° and the corresponding VSWR plots are given in Fig. 5.5. The changes in the percentage bandwidth and the central frequency with apex angle are given in Table 5.4. From the table, it can be seen that the central frequency of the antenna decreases with increase in the apex angle. Also from the table, it can be inferred that the initial selection of $\alpha = 100^\circ$ is the right choice.



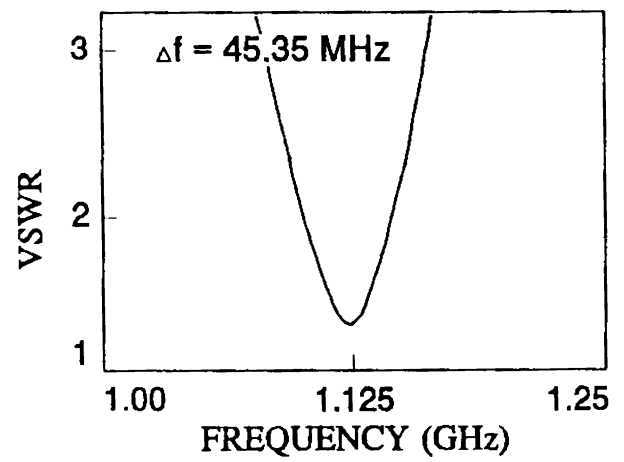
(a)



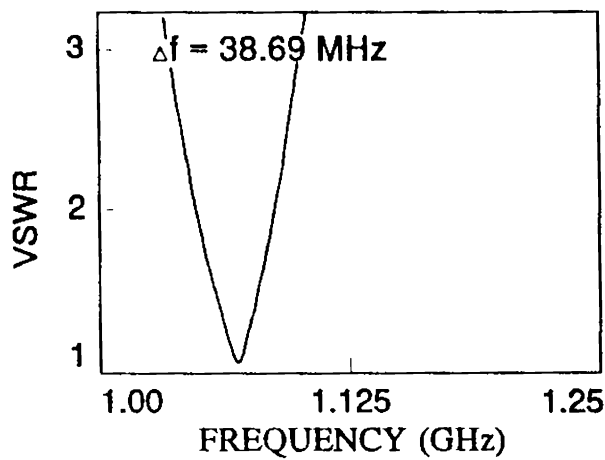
(b)



(c)



(d)



(e)

Fig. 5.5 VSWR plots of triangular end-loaded microstrip dipoles for different apex angles
 a) $\alpha = 80^\circ$ b) $\alpha = 90^\circ$ c) $\alpha = 100^\circ$ d) $\alpha = 110^\circ$ e) $\alpha = 120^\circ$

Table 5.4

Percentage bandwidths and central frequencies of triangular end-loaded microstrip dipoles of various apex angles with optimised impedance transformer parameters

Apex angle α	Transformer		Percentage bandwidth	Central frequency (GHz)
	length (cm)	impedance (Ω)		
80°	2.65	21.5	4.81	1.196
90°	2.60	21.5	5.56	1.156
100°	2.70	21.5	6.84	1.155
110°	3.25	23.5	4.04	1.122
120°	3.65	23.5	3.62	1.069

From the above experimental results, the optimum design values of Triangular End-Loaded Microstrip Dipole Antenna (TELMDA) are as follows:

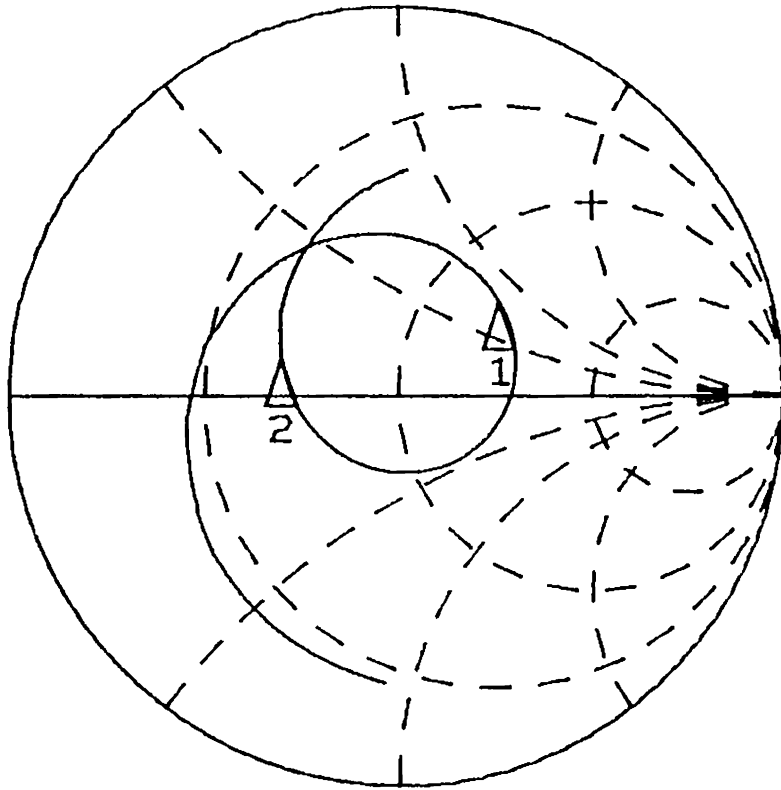
Main arm length l_m	= 4.20 cm
Height of triangle h_t	= 1.40 cm
Transformer length l_t	= 2.70 cm
Transformer line impedance	= 21.5 Ω

The remaining design values are same as that given in Section 5.1.

The impedance plot of the antenna is given in Fig. 5.6. The impedance bandwidth is 78.75 MHz and the central frequency is 1.155 MHz. This corresponds to 6.84% impedance bandwidth.

The E and H-plane radiation patterns of the antenna at the start, end and central frequencies are given in Fig. 5.7. The beam maximum for E-plane patterns are shifted by 10° from the bore-sight direction. But no beam squinting has been observed with frequency. Also, 3-dB beamwidths are narrow compared to that of the conventional microstrip dipole. The H-plane patterns are very broad and resemble the H-plane pattern of the ordinary dipole antenna.

MARKER 2-1
78.75 MHz



START 1.000000000 GHz
STOP 1.250000000 GHz

Fig. 5.6 Impedance loci of TELMDA

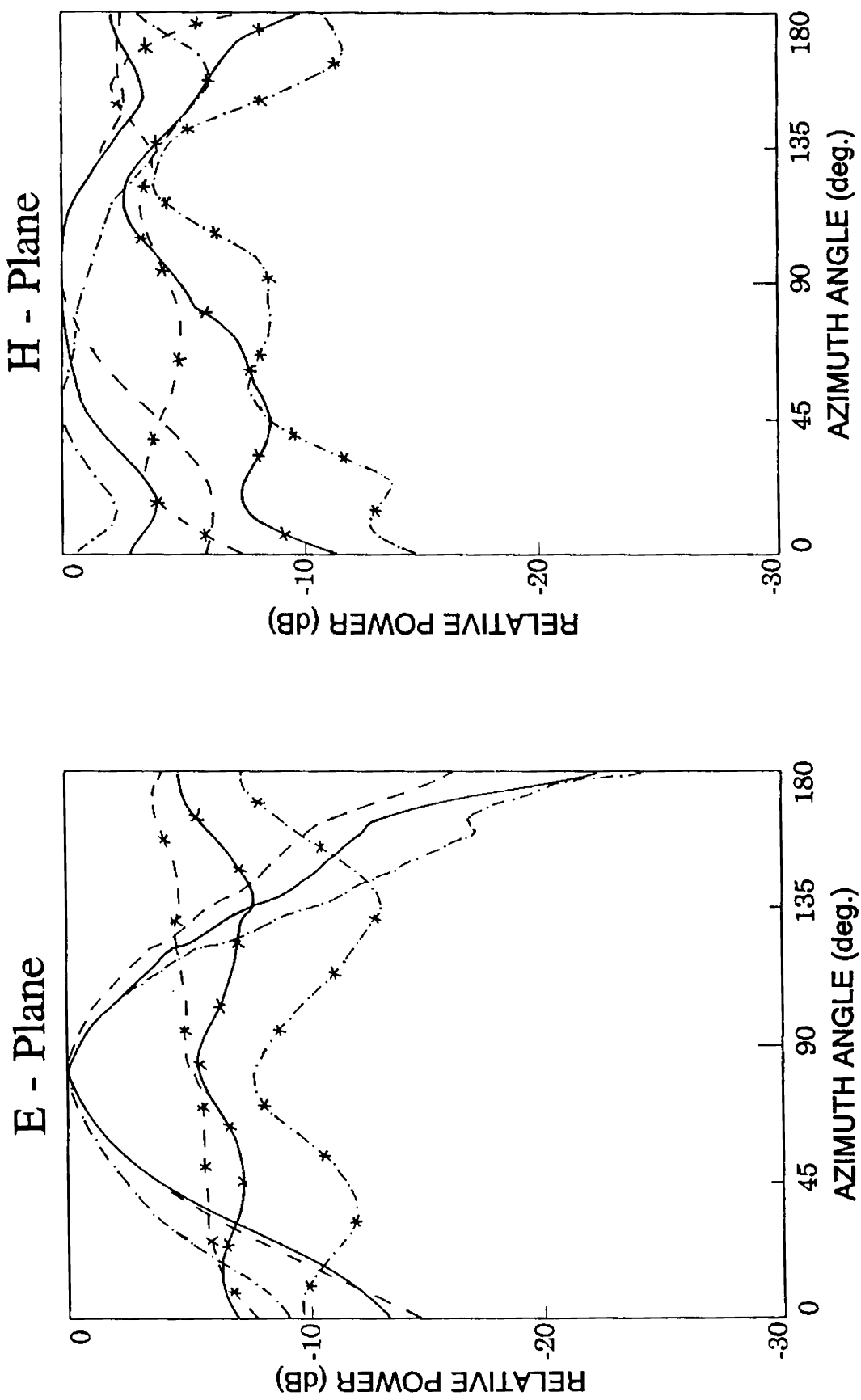


Fig. 5.7 Radiation patterns of TELMDA
 co-polar : - - - - - 1.116 GHz, - - - - - 1.155 GHz, - - - - - 1.195 GHz
 cross-polar : - - * - - 1.116 GHz, - - * - - 1.155 GHz, - - * - - 1.195 GHz

As mentioned earlier, the gain of the antenna is measured by comparing the $|S_{21}|$ of the antenna with a standard rectangular patch antenna resonating at 1.152 GHz, which is almost the center of the frequency band of interest. Fig. 5.8 shows the relative $|S_{21}|$ plot of the antenna with respect to the standard microstrip patch. From the plot, the gain of the antenna is only 0.32 dB less compared to the rectangular patch. This is obvious because of improvement in the impedance bandwidth of the antenna with respect to the patch.

5.1.4 Design details

Like in the case of printed dipoles, empirical design criteria for Triangular End-Loaded Microstrip Dipole Antenna has been developed through experimental iterations. The design details of the antenna, shown in Fig. 5.1, are given below in terms of the wavelength (λ_0) corresponding to the central frequency.

Main arm length l_m	=	$0.302 \lambda_c$
Height of the triangle h_t	=	$0.101 \lambda_c$
Arm width at feed point w	=	$0.053 \lambda_d$
Feed point location l_f	=	$0.050 \lambda_c$
Flaring angle θ	=	10°
Apex angle α	=	100°
Transformer length l_t	=	$0.22 \lambda_d$
Transformer line impedance	=	21.5Ω

The ground arm length is 1.166 times larger than the main arm length. Other parameters of ground arm are same as that of the corresponding main arm parameters.

Here, $\lambda_d = \lambda_0 / \sqrt{\epsilon_r}$ and $\lambda_c = \lambda_0 / \sqrt{\epsilon_{eff}}$. The effective dielectric constant ϵ_{eff} can be calculated using the standard formula [139] given below,

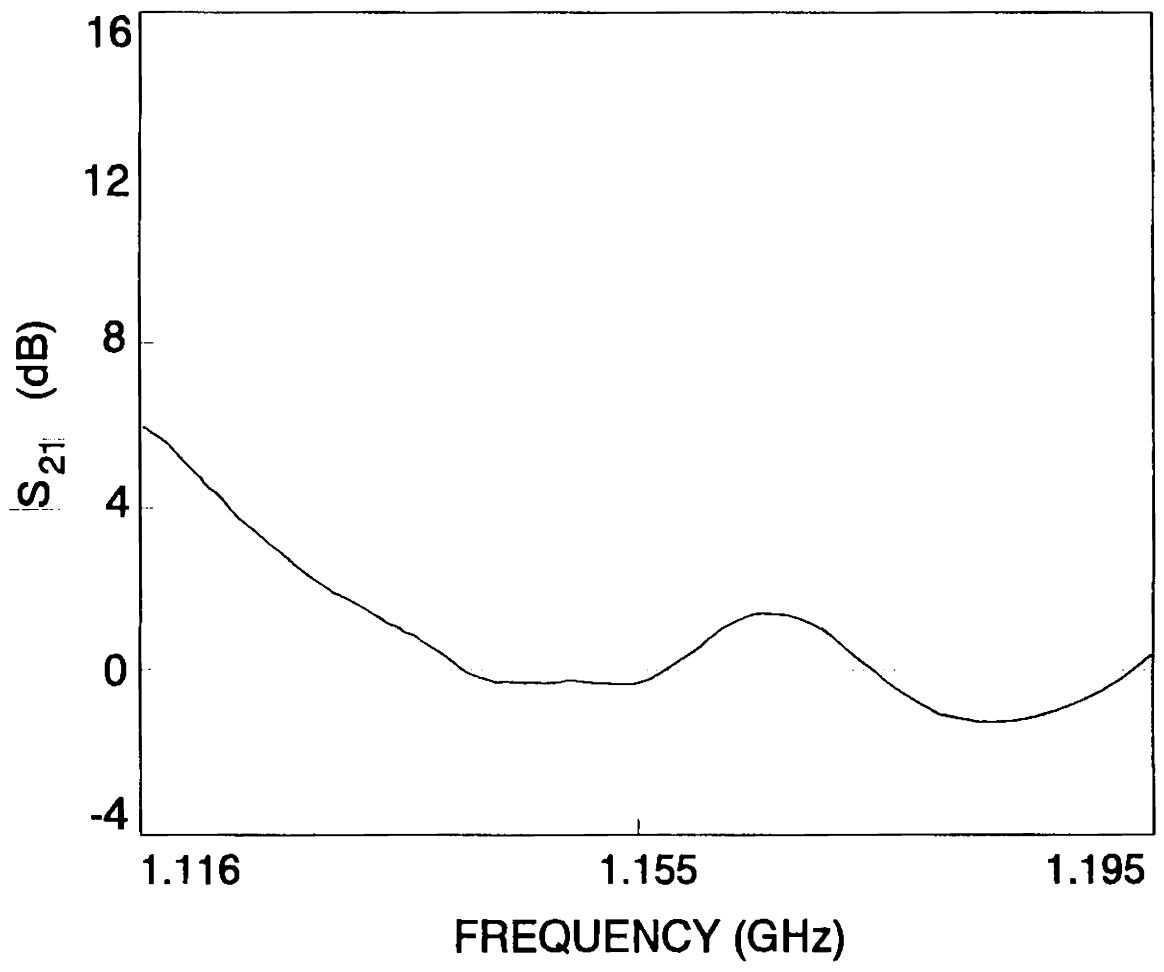


Fig. 5.8 $|S_{21}|$ of TELMDA with respect to rectangular microstrip patch resonating at 1.152 GHz

$$\epsilon_{eff} = \frac{\epsilon_r + 1}{2} + \frac{\epsilon_r - 1}{2} \cdot \frac{\ln \left(\frac{\pi}{2} \right) + \left[\frac{1}{\epsilon_r} \right] \ln \left(\frac{4}{\pi} \right)}{\ln \left(\frac{8h'}{w} \right)} \quad (1)$$

where, h' ($= 3h / 2$) is taken as the average thickness due to the difference in the separation of ground arm and main arm from the ground plane and h is the substrate thickness.

5.2 TRIANGULAR MICROSTRIP DIPOLE

Experimental investigations are also carried out on triangular microstrip dipoles. The basic design of the antenna is adopted by examining the impedance and radiation characteristics data in [140] for flat triangular dipoles.

Sketch of the dipole is given in Fig. 5.9. The dipole is etched along with 50Ω microstrip line on a grounded dielectric substrate. The balanced dipole is matched with unbalanced microstrip line using a short circuited matching balun of line impedance 50Ω .

The initial design values of the antenna are as follows:

Arm length l_m	=	3.10 cm
Arm width at feed point w	=	0.80 cm
Feed point location l_f	=	0.55 cm
Arms separation l_s	=	0.20 cm
Flaring angle β	=	60°

Like the previous case, the bandwidth optimisation is done by studying the effect of various design parameters on the percentage bandwidth of the antenna. The following important design parameters of the antenna are studied in detail:

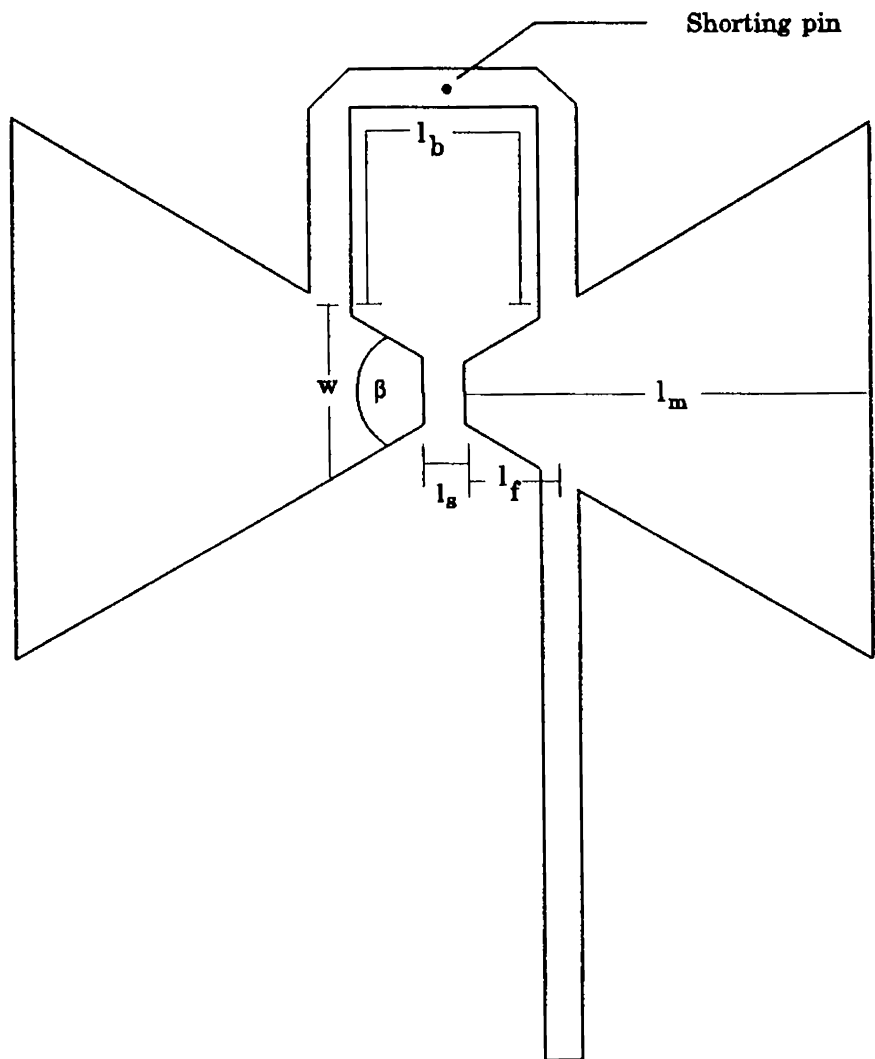


Fig. 5.9 Schematic representation of triangular microstrip dipole

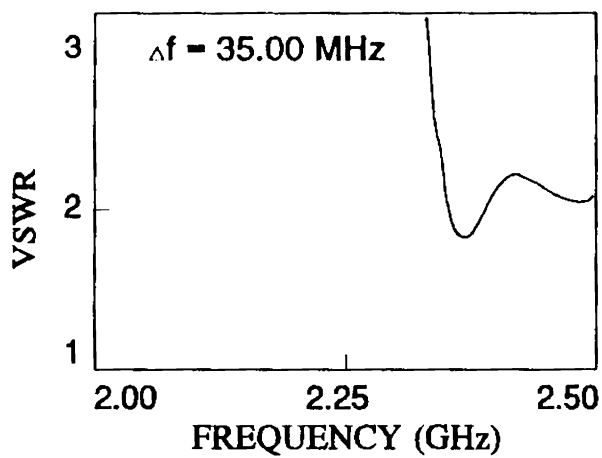
1. Balun length l_b
2. Feed point location l_f
3. Arms separation l_s
4. Flaring angle β

5.2.1 Balun length

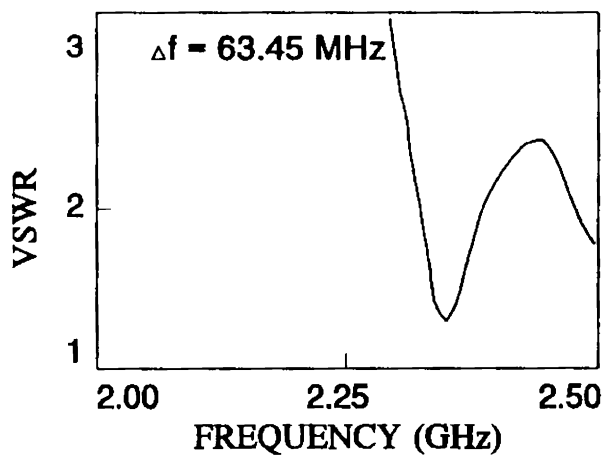
Since the matching of the dipole with 50Ω microstrip feedline mainly depends on the length of balun, the optimisation of balun length is done first. The length of the balun is varied from 5.2 cm to 6.2 cm in steps of 2 mm and the corresponding VSWR plots are given in Fig. 5.10. The VSWR of the antenna is more than 2 in the middle portion of the frequency band for balun length equal to 6.2 cm. The percentage bandwidths and the central frequencies for various balun lengths are given in Table 5.5. The central frequency of the antenna decreases with increase in balun length. Also from the table, it can be seen that the percentage bandwidth is maximum for $l_b = 5.6$ cm and is selected as the optimum balun length.

5.2.2 Feed point location

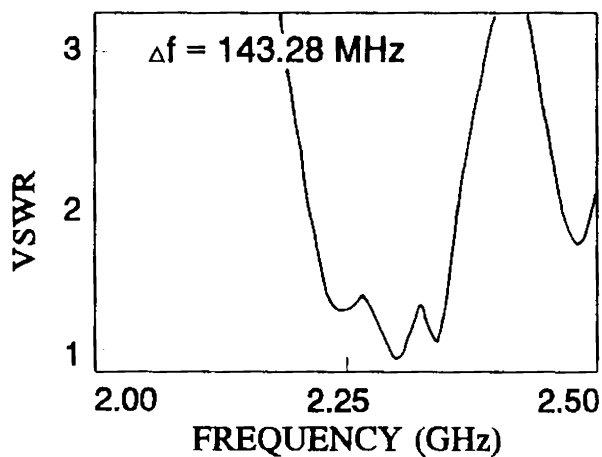
While keeping the balun length fixed at 5.6 cm, the distance of the feed point from the arm end l_f is varied from 4.5 mm to 6.5 mm in steps of 0.5 mm. The VSWR plots, and the percentage bandwidths and the central frequencies are given in Fig. 5.11 and Table 5.6 respectively. From the table, it is clear that the initial selection of $l_f = 5.5$ mm is still the best choice.



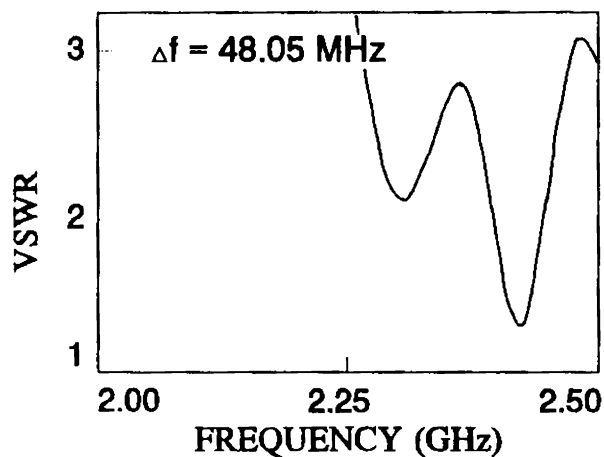
(a)



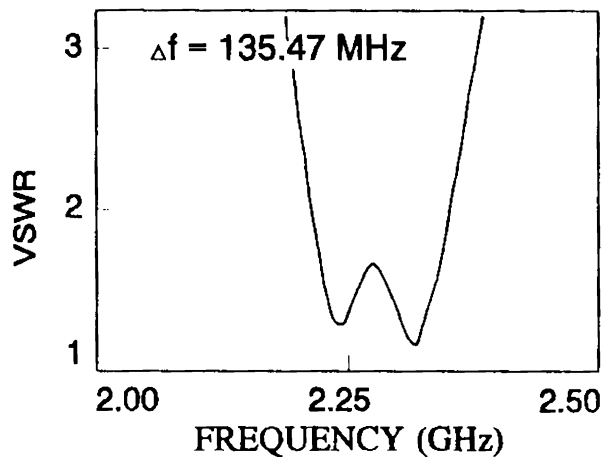
(b)



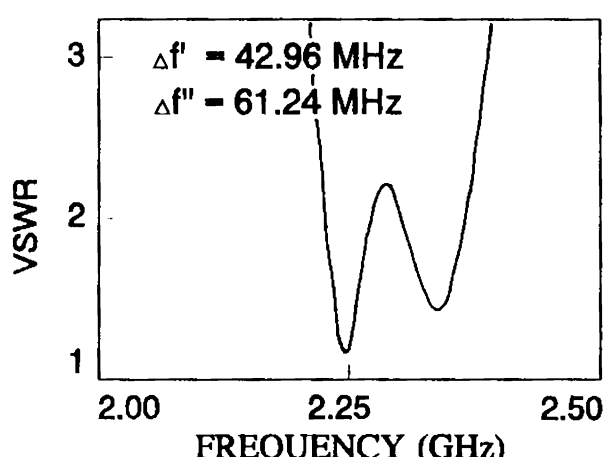
(c)



(d)

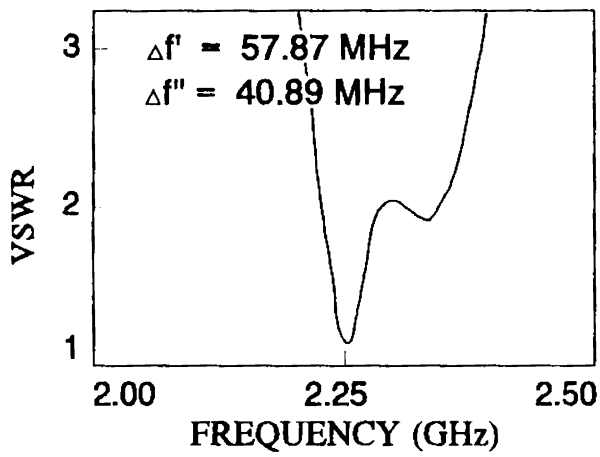


(e)

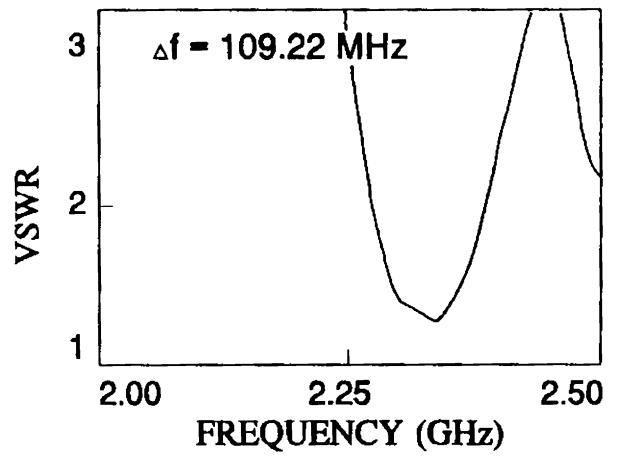


(f)

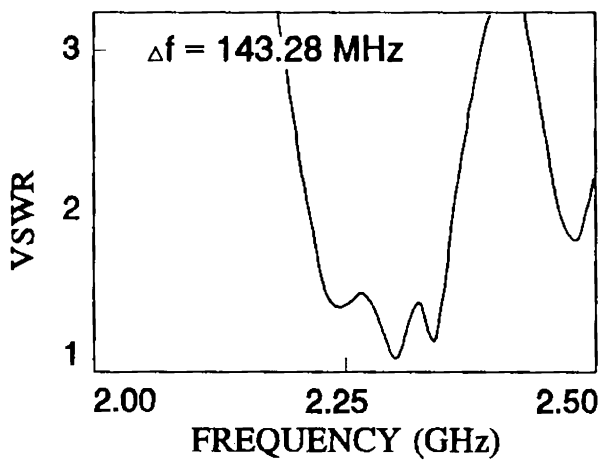
Fig. 5.10 VSWR plots of triangular microstrip dipoles for different balun lengths
 a) $l_b = 5.2 \text{ cm}$ b) $l_b = 5.4 \text{ cm}$ c) $l_b = 5.6 \text{ cm}$ d) $l_b = 5.8 \text{ cm}$ e) $l_b = 6.0 \text{ cm}$
 f) $l_b = 6.2 \text{ cm}$



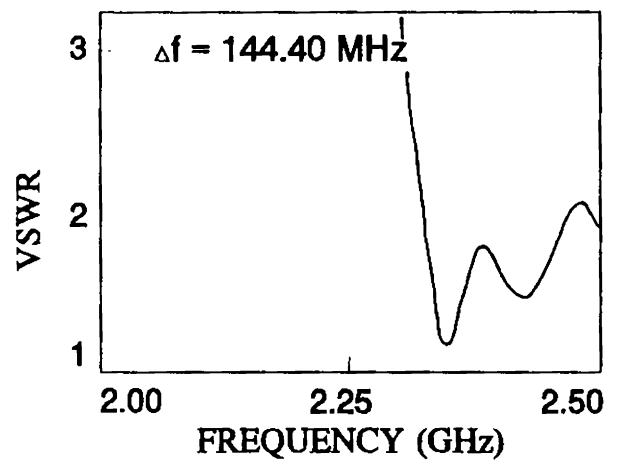
(a)



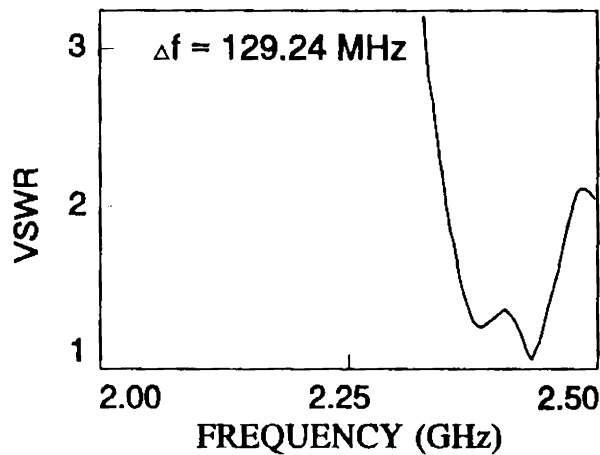
(b)



(c)



(d)



(e)

Fig. 5.11 VSWR plots of triangular microstrip dipoles for different feed points

a) $l_f = 4.5 \text{ mm}$ b) $l_f = 5.0 \text{ mm}$ c) $l_f = 5.5 \text{ mm}$ d) $l_f = 6.0 \text{ mm}$ e) $l_f = 6.5 \text{ mm}$

Table 5.5

Percentage bandwidths and central frequencies of triangular microstrip dipoles of various balun lengths

Balun length l_b (cm)	Percentage bandwidth	Central frequency (GHz)
5.2	1.48	2.371
5.4	2.71	2.360
5.6	6.29	2.291
5.8	1.98	2.422
6.0	5.96	2.282
6.2	1.91 / 2.62	2.251 / 2.337

Table 5.6

Percentage bandwidths and central frequencies of triangular microstrip dipoles of various feed point locations

Feed location l_f (cm)	Percentage bandwidth	Central frequency (GHz)
4.5	2.56 / 1.76	2.265 / 2.334
5.0	4.72	2.330
5.5	6.29	2.291
6.0	6.02	2.397
6.5	5.35	2.412

5.2.3 Arms separation

The effect of the separation between the two arms on the impedance characteristics of the antenna is studied by varying the separation l_s between the dipole arms. l_s is varied from 1 mm to 3 mm and the corresponding VSWR plots are given in Fig. 5.12. The VSWR of

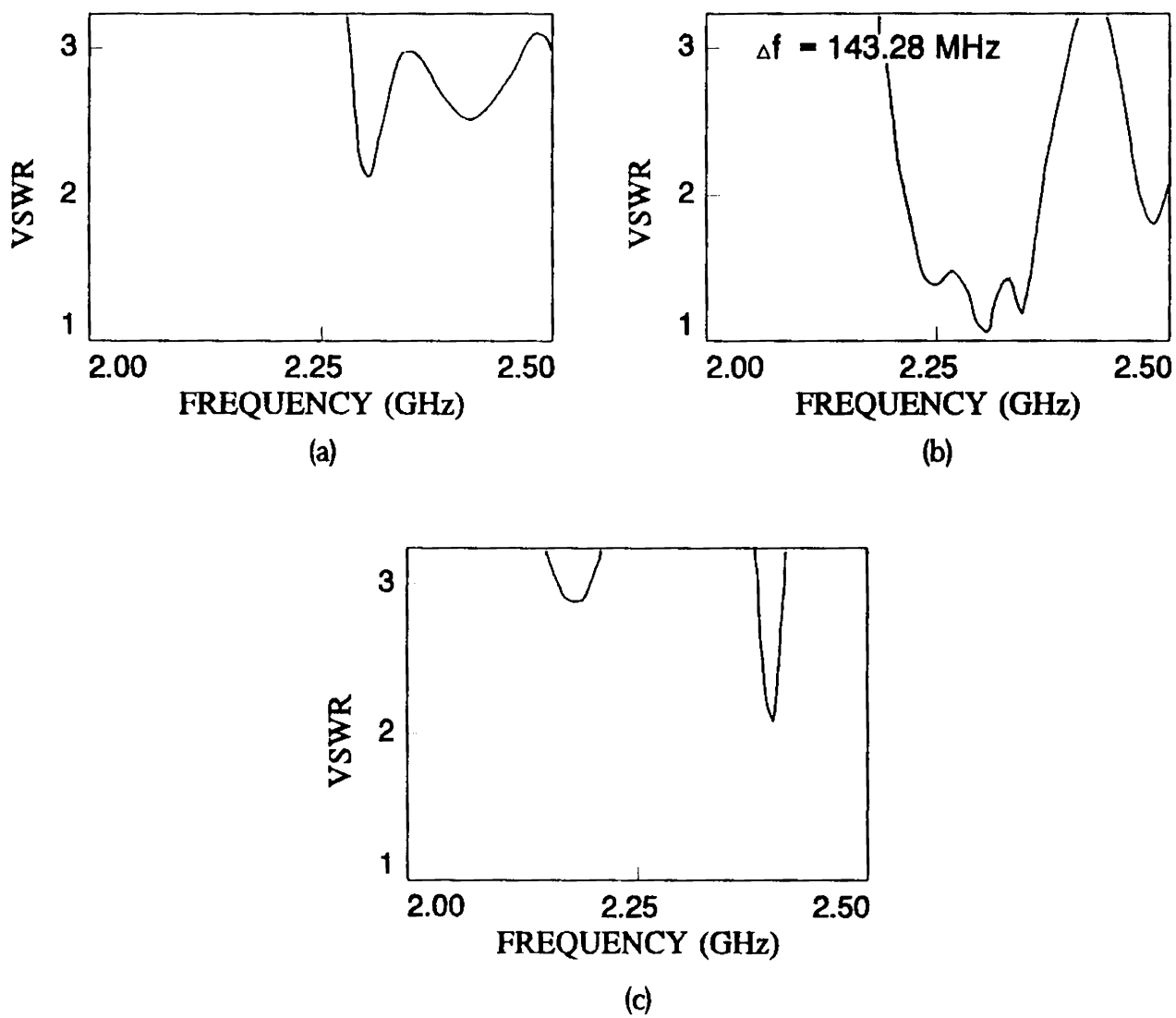


Fig. 5.12 VSWR plots of triangular microstrip dipoles for different arm separations
 a) $l_s = 1.0$ mm b) $l_s = 2.0$ mm c) $l_s = 3.0$ mm

the antennas for $l_s = 1$ mm and $l_s = 3$ mm are more than 2 in the entire band and is less than 2 only for $l_s = 2$ mm.

5.2.4 Flaring angle

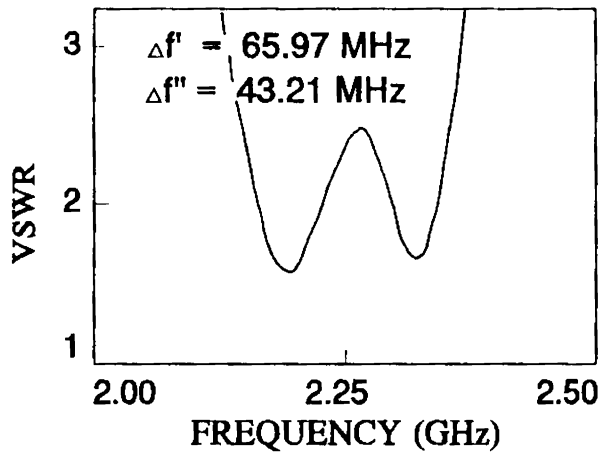
The last parameter studied towards the design optimisation is the effect of flaring to the dipole arms on the percentage bandwidth of the antenna. The flaring angle β is varied from 50° to 70° in steps of 5° . The VSWR plots of different antennas are given in Fig. 5.13. VSWR is more than 2 in the middle of the frequency band for $\beta = 55^\circ$ and increases with the decrease in the flaring angle. The percentage bandwidths and the central frequencies for different flaring angles are given in Table 5.7. From the table, it is clear that the initial selection of β as 60° is a right one.

Table 5.7

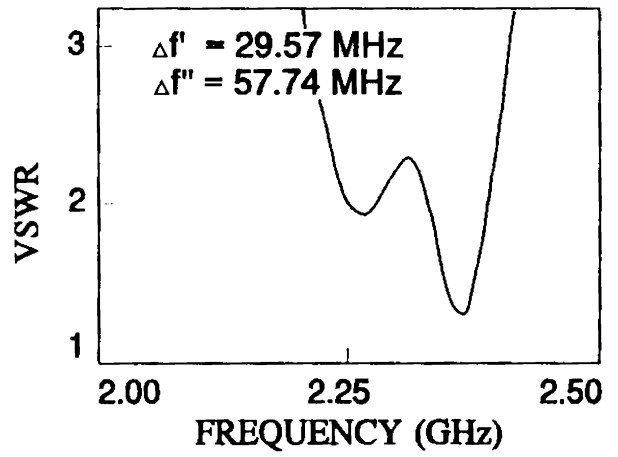
Percentage bandwidths and central frequencies of triangular microstrip dipoles of various flaring angles

Flaring angle β	Percentage bandwidth	Central frequency (GHz)
50°	3.00 / 1.85	2.198 / 2.320
55°	1.32 / 2.41	2.268 / 2.363
60°	6.29	2.291
65°	3.62	2.347
70°	2.47	2.311

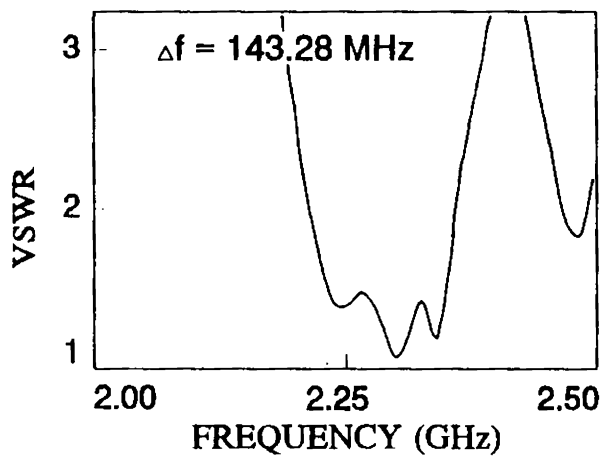
From the above experimental results, it can be concluded that the length of the matching balun depends on the other design parameters. Once the balun length is optimised, any change in any other design parameter will only deteriorate the performance of the



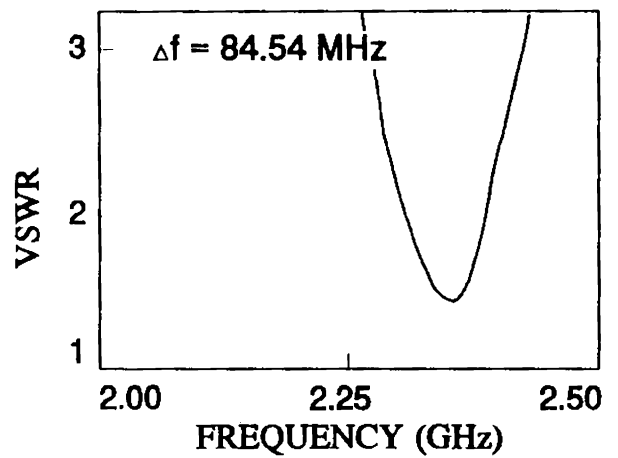
(a)



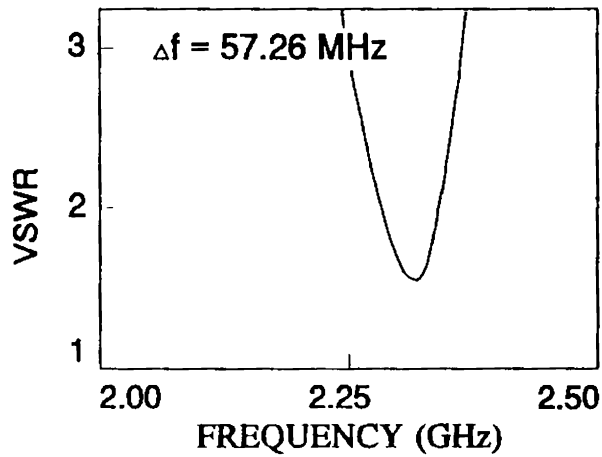
(b)



(c)



(d)



(e)

Fig. 5.13 VSWR plots of triangular microstrip dipoles for different flaring angles
 a) $\beta = 50^\circ$ b) $\beta = 55^\circ$ c) $\beta = 60^\circ$ d) $\beta = 65^\circ$ e) $\beta = 70^\circ$

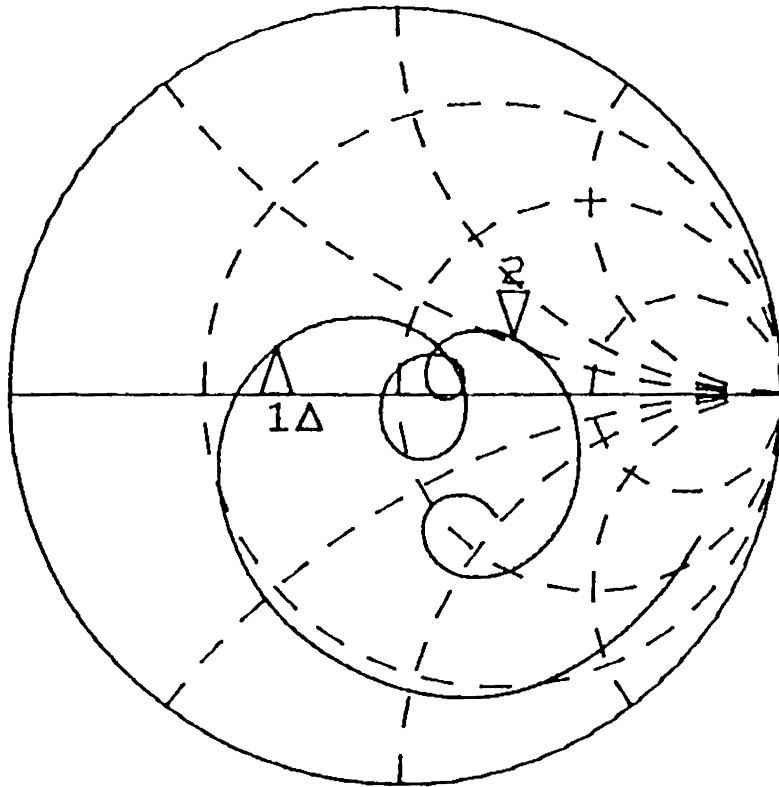
antenna. Thus, the optimum design values of Triangular Microstrip Dipole Antenna (TMDA) are same as that given in Section 5.2, with the balun length $l_b = 5.6$ cm.

The impedance plot of TMDA is given in Fig. 5.14. The 2:1 VSWR bandwidth of the antenna is 143.28 MHz with central frequency at 2.291 GHz. This corresponds to 6.29% impedance bandwidth.

The E and H-plane radiation patterns of the antenna are given in Fig. 5.15. The beam maximum for E-plane patterns is shifted by 30° from the bore-sight direction. The H-plane patterns are broad and resemble the H-plane patterns of the conventional microstrip dipole antenna. The cross-polar level is high at the lower frequency side of the band of interest and improves considerably with frequency.

Like the previous case, gain of TMDA is measured by measuring $|S_{21}|$ of the antenna with respect to a standard rectangular microstrip patch antenna resonating at 2.3 GHz. The $|S_{21}|$ of the antenna with respect to microstrip dipole is plotted in Fig. 5.16. At 2.3 GHz, gain of the antenna is 0.64 dB less than the reference microstrip patch. This reduction in gain is due to large impedance bandwidth of TMDA compared to standard microstrip patch.

MARKER 2-1
143.276969 MHz



START 2.000000000 GHz
STOP 2.500000000 GHz

Fig. 5.14 Impedance loci of TMDA

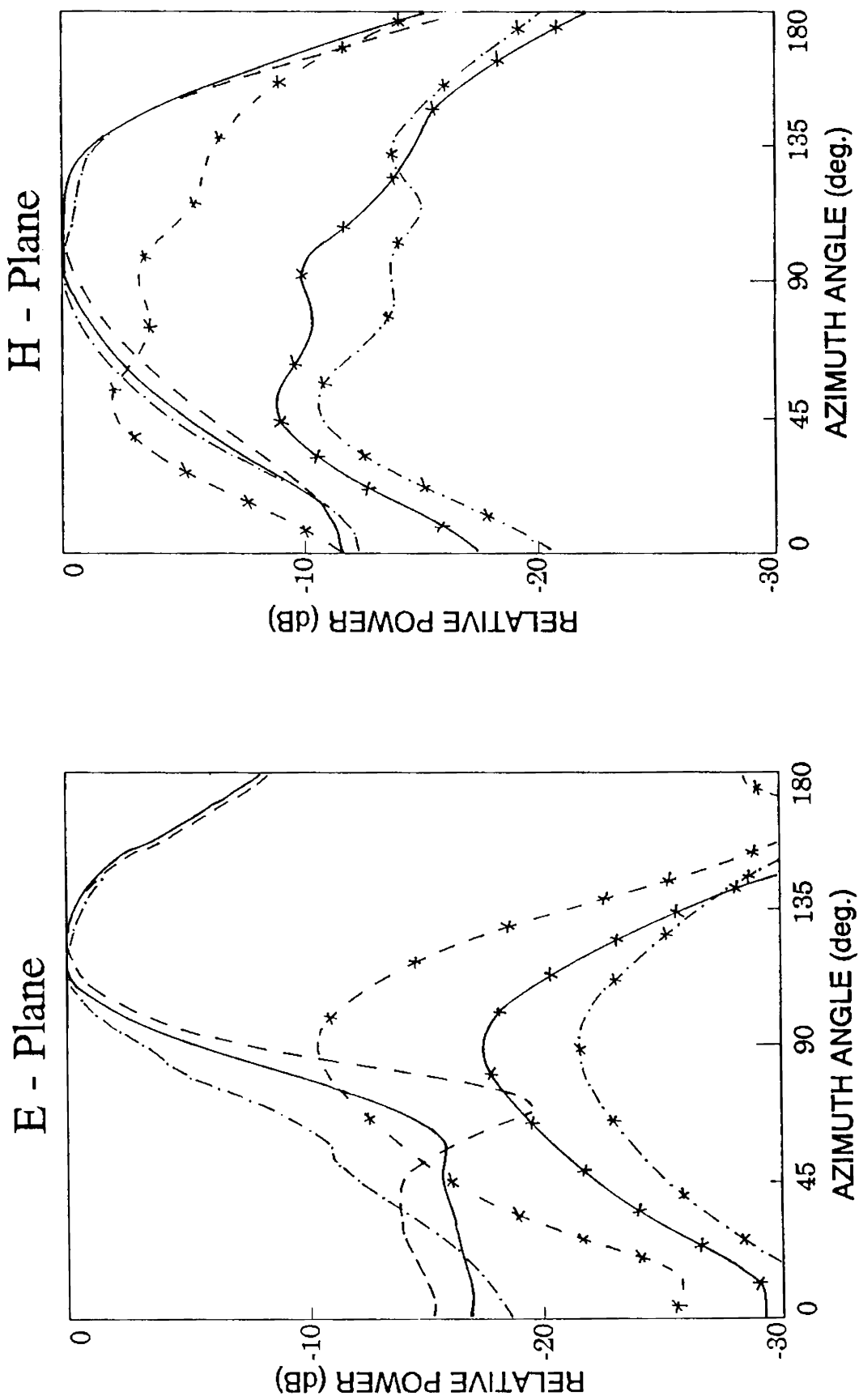


Fig. 5.15 Radiation patterns of TMDA

co-polar : ——— 2.217 GHz, ——— 2.288 GHz, ——— 2.360 GHz
 cross-polar : - - - 2.217 GHz, - - - 2.288 GHz, - - - 2.360 GHz

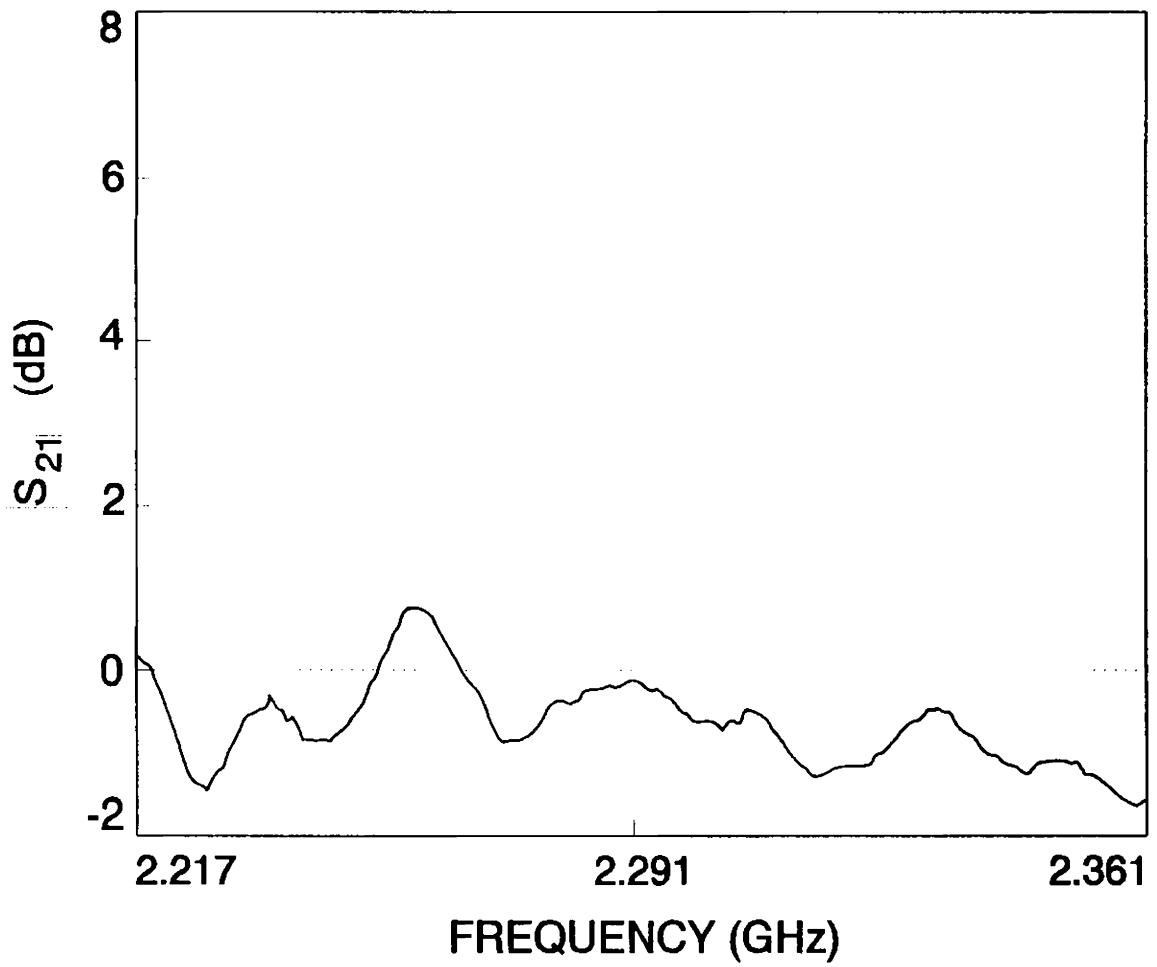


Fig. 5.16 $|S_{21}|$ of TMDA with respect to rectangular microstrip patch resonating at 2.3 GHz

Theoretical analysis

The theoretical analysis of cavity backed printed dipole antennas is presented in this chapter. The cavity backed antenna is assumed as a rectangular microstrip patch with air as dielectric substrate. The theory given by Perlmutter *et al.* [141] for rectangular patch on relatively thick substrate is properly modified to calculate the Quality factor Q and hence the bandwidth of the antenna.

The effect of end-loading, on the impedance bandwidth of the antenna, is incorporated by calculating the Q of the load structure separately and adding it with the Q of the remaining dipole arms. The coupling effect between the dipole arms and the triangles is taken care of by multiplying the Q of the remaining dipole arms with a correction factor.

The experimental results are compared with the computation. A fairly good agreement is obtained, which establishes the validity of the theoretical assumptions.

6.1 RECTANGULAR MICROSTRIP PATCH

The radiation from the microstrip patch is calculated by approximating the surface current distribution and using the potential method. The presence of dielectric material and the ground plane is taken care of by Green's function. This function gives the electric field due to a unit current element on the surface of the dielectric material and actually contains in it the information on the structure of the medium in which the current radiates. When the patch is replaced by the assumed surface current, the geometrical structure in which the current radiates has translational symmetry in two dimensions (the ground plane and the dielectric are assumed infinite) and it is found that the Green's function has an analytic expression in Fourier domain.

The input power to the antenna is then calculated using an analog of the electromotive force (EMF) [142] method. Since the Green's function is known analytically only in Fourier domain, the integration of current density and electric field is carried out in Fourier domain.

6.1.1 Derivation of the Green's function

Fig. 6.1 shows the cross-sectional view of the microstrip structure. The ground plane is at $z=0$ plane and the radiating patch is at $z=h$ plane at the air-dielectric interface.

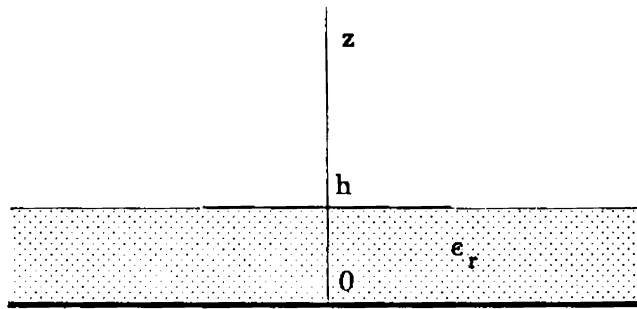


Fig. 6.1 Cross-sectional view of the microstrip antenna

The field equation for electric field is,

$$\nabla^2 \vec{E} + k^2 \vec{E} = 0 \quad (1)$$

where,

$$k^2 = \left\{ \begin{array}{ll} \epsilon_r k_0^2 & \text{if } 0 < z < h \\ k_0^2 & \text{if } z > h \end{array} \right\}$$

k_0 is the free space wave vector and ϵ_r is the relative dielectric constant. The boundary conditions are,

$$\begin{aligned} \hat{z} \times \vec{E}_1 &= 0 && \text{on the plane } z=0 \\ \hat{z} \times (\vec{H}_1 - \vec{H}_2) &= \vec{J} && \text{on the plane } z=h \\ \hat{z} \times (\vec{E}_1 - \vec{E}_2) &= 0 && \text{on the plane } z=h \end{aligned} \quad (2)$$

The subscripts 1 and 2 denote the fields in the region $0 < z < h$ and $z > h$, respectively.

Writing the current \vec{J} and the electric and magnetic fields by their Fourier decomposition,

$$\begin{aligned} \vec{J}(x,y) &= \frac{1}{4\pi^2} \int \int \vec{J}(k_x, k_y) e^{-j(k_x x + k_y y)} dk_x dk_y \\ \vec{E}(x,y) &= \frac{1}{4\pi^2} \int \int \vec{E}(k_x, k_y) e^{-j(k_x x + k_y y)} dk_x dk_y \\ \vec{H}(x,y) &= \frac{1}{4\pi^2} \int \int \vec{H}(k_x, k_y) e^{-j(k_x x + k_y y)} dk_x dk_y \end{aligned} \quad (3)$$

Inserting these expressions into (1) and (2), the Fourier components of electric field can be solved as a function of the corresponding Fourier components of the current.

$$\begin{bmatrix} \vec{E}_x(k_x, k_y) \\ \vec{E}_y(k_x, k_y) \end{bmatrix} = \begin{bmatrix} \tilde{G}_{xx}(k_x, k_y) & \tilde{G}_{xy}(k_x, k_y) \\ \tilde{G}_{yx}(k_x, k_y) & \tilde{G}_{yy}(k_x, k_y) \end{bmatrix} \begin{bmatrix} \vec{J}_x(k_x, k_y) \\ \vec{J}_y(k_x, k_y) \end{bmatrix} \quad (4)$$

where the tilde over the letter denotes the Fourier transform of the variable. The elements of the matrix \tilde{G} are given by,

$$\begin{aligned}
\tilde{G}_{xx} &= C(k_x^2 - k_0^2)\gamma_2 \tan(\gamma_2 h) + j\gamma_1(\epsilon_r k_0^2 - k_x^2) \\
\tilde{G}_{xy} &= C(-k_x k_y(j\gamma_1 - \gamma_2 \tan(\gamma_2 h))) \\
\tilde{G}_{yx} &= C(-k_y k_x(j\gamma_1 - \gamma_2 \tan(\gamma_2 h))) \\
\tilde{G}_{yy} &= C(k_y^2 - k_0^2)\gamma_2 \tan(\gamma_2 h) + j\gamma_1(\epsilon_r k_0^2 - k_y^2) \\
C &= \frac{\eta}{k_0(j\gamma_1 \cot(\gamma_2 h) - \gamma_1)(j\epsilon_r \gamma_1 - \gamma_2 \tan(\gamma_2 h))}
\end{aligned}$$

where η is the free space wave impedance, h is the thickness of the dielectric material and $j = \sqrt{-1}$. Also, $\gamma_1 = \sqrt{k_0^2 - k_x^2 - k_y^2}$ and $\gamma_2 = \sqrt{\epsilon_r k_0^2 - k_x^2 - k_y^2}$

Rewriting (4) in a more compact and convenient form,

$$\tilde{E} = \frac{\eta}{k_0} \left[\frac{k_0^2(\tilde{J}k_t^\perp)k_t^\perp}{j\gamma_2 \cot(\gamma_2 h) - \gamma_1} + \frac{\gamma_1 \gamma_2(\tilde{J}k_t^\parallel)k_t^\parallel}{j\epsilon_r \gamma_1 \cot(\gamma_2 h) - \gamma_2} \right] \quad (5)$$

where,

$$k_t^\perp = -\frac{k_y}{k_t}\hat{x} + \frac{k_x}{k_t}\hat{y}; \quad k_t^\parallel = \frac{k_x}{k_t}\hat{x} + \frac{k_y}{k_t}\hat{y}; \quad k_t = \sqrt{k_x^2 + k_y^2}$$

The first term in (5) is due to plane waves radiating by the current which hit the air-dielectric interface with their electric vector perpendicular to the plane of incidence. The second term is due to waves with polarisation parallel to the plane of incidence.

6.1.2 Calculation of complex power

The complex input power to the antenna is given by,

$$\bar{P} = -\frac{1}{2} \iint \bar{E} \cdot \bar{J}^* ds \quad (6)$$

where the integration is performed over the upper conductor. Writing \bar{P} in Fourier domain and using (5) we get

$$\bar{P} = -\frac{\eta}{8\pi^2 k_0} \iint \left[\frac{k_0 |\bar{J}^\perp|^2}{j\gamma_2 \cot(\gamma_2 h) - \gamma_1} + \frac{\gamma_1 \gamma_2 |\bar{J}^\parallel|^2}{j\epsilon_r \gamma_1 \cot(\gamma_2 h) - \gamma_2} \right] dk_x dk_y \quad (7)$$

where,

$$\bar{J}^\perp = \bar{J} k_i^\perp ; \quad \bar{J}^\parallel = \bar{J} k_i^\parallel$$

The above expression for \bar{P} has real and imaginary parts. The contribution to the real part is due to radiation into space and the radiation in the surface wave modes. The imaginary part is due to energy which is stored in the vicinity of the antenna. Since the bandwidth of the antenna is related to the real part of the expression, no effort has been made to solve the imaginary part.

6.1.3 Space wave radiation

The contribution due to radiation into free space comes mathematically from the range of integration where $(k_x^2 + k_y^2) > k_0^2$, that is from the visible space. The physical meaning is well known; since we decompose the current distribution into two dimensional Fourier components, each component with specific k_x and k_y generates a plane wave with the same k_x and k_y . This wave can contribute to the radiated power if the above condition is satisfied because in this case the wave has a real k_z component. In the other case, where $(k_x^2 + k_y^2) < k_0^2$, the k_z component is imaginary and the wave is evanescent.

Now, transforming the real part of (7) into spherical coordinates by $k_x = k_0 \sin\theta \cos\phi$ and $k_y = k_0 \sin\theta \sin\phi$, we have

$$P_r = \frac{15k_0^2}{\pi} \int_0^{2\pi} \int_0^{\pi/2} \left[\frac{|-\bar{J}_x \sin \phi + \bar{J}_y \cos \phi|^2 \cos^2 \theta}{(\epsilon_r - \sin^2 \theta) \cot^2(hk_0 \sqrt{\epsilon_r - \sin^2 \theta}) + \cos^2 \theta} + \frac{|\bar{J}_x \cos \phi + \bar{J}_y \sin \phi|^2 \cos^2 \theta (\epsilon_r - \sin^2 \theta)}{(\epsilon_r - \sin^2 \theta) + \epsilon_r^2 \cos^2 \theta \cot^2(hk_0 \sqrt{\epsilon_r - \sin^2 \theta})} \right] \cdot \sin \theta \, d\theta \, d\phi \quad (8)$$

6.2 RECTANGULAR PRINTED DIPOLE

Fig. 6.2 shows the sketch of the rectangular printed dipole, kept at a distance h away from a reflector plate (not shown in the figure). The reflector plate acts as a ground plane and forms a cavity backed structure.

The difference of this structure from the experimentally optimised rectangular dipole is in arms overlapping. Here, arms overlapping is kept as minimum as possible, which is not so for experimentally optimised one. This is done because the formulation does not take care of the arms overlapping.

The surface current distribution is assumed as,

$$\bar{J}(x,y) = \left\{ \begin{array}{ll} \hat{x} \frac{V_0}{Z_c w} \sin(\beta x) & 0 < x < l, -\frac{w}{2} < y < \frac{w}{2} \\ 0 & \text{otherwise} \end{array} \right\} \quad (9)$$

where V_0 is the excitation voltage and Z_c is the characteristic impedance of the microstrip line, constituting of the dipole arms. The transverse current is assumed to be constant. The propagation constant β is given by,

$$\beta = \frac{2\pi \sqrt{\epsilon_{eff}}}{\lambda_0} \quad (10)$$

where ϵ_{eff} is the effective dielectric constant and is given by,

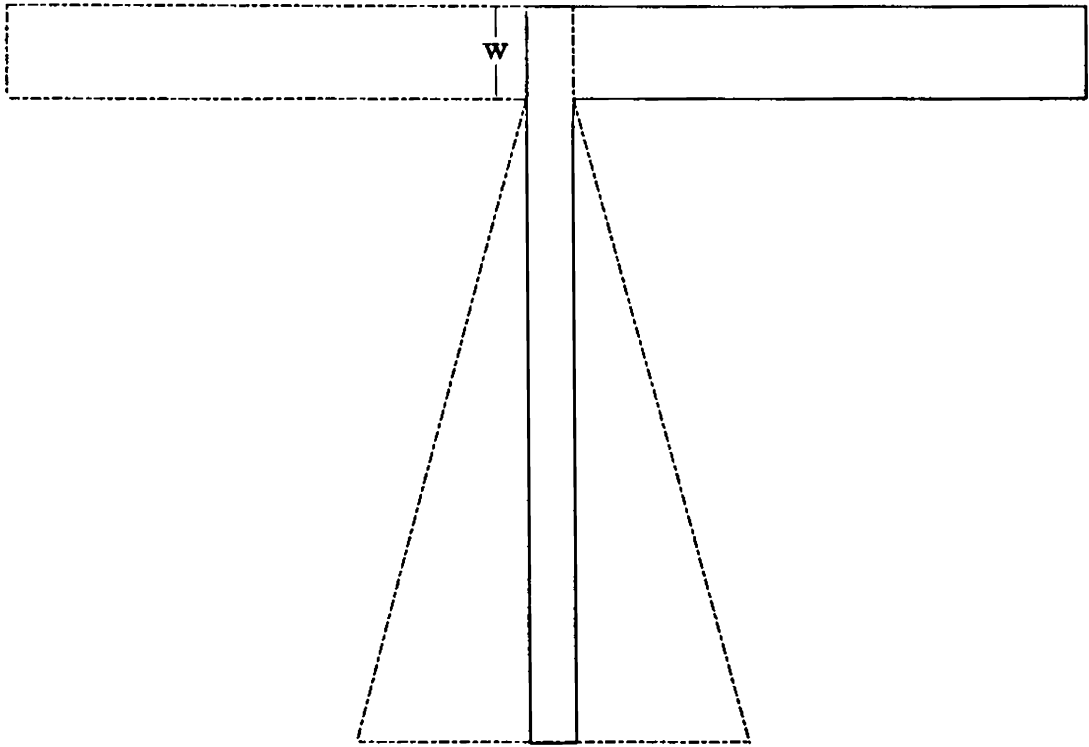


Fig 6.2 Rectangular printed dipole

$$\epsilon_{eff} = \frac{\epsilon_r + 1}{2} + \frac{\epsilon_r - 1}{2} \times \frac{\ln\left(\frac{\pi}{2}\right) + \left(\frac{1}{\epsilon_r}\right) \ln\left(\frac{4}{\pi}\right)}{\ln\left(\frac{8h}{w}\right)} \quad (11)$$

The characteristics impedance Z_c in terms of w , h and ϵ_r is,

$$Z_c = \left\{ \begin{array}{ll} \frac{60}{\sqrt{\epsilon_{eff}}} \ln\left[\frac{8h}{w} + \frac{w}{4h}\right] & \text{if } w < h \\ \frac{120\pi}{\sqrt{\epsilon_{eff}}} \left[\frac{w}{h} + 2.42 - 0.44\frac{h}{w}\right]^{-1} & \text{if } w > h \end{array} \right\} \quad (12)$$

Transforming the current $J(x,y)$ in Fourier domain, we have,

$$\bar{J}(x,y) = \frac{V_0}{Z_c} \frac{2\beta \cos(lk_x/2)}{k_x^2 - \beta^2} \text{sinc}(wk_y/2) \quad (13)$$

where $\text{sinc}(x) = \sin(x)/x$. Transforming (13) to spherical coordinates, we get,

$$\bar{J}(\theta, \phi) = \frac{V_0}{Z_c} \frac{2k_0 \sqrt{\epsilon_{eff}} \cos(\pi l \sin\theta \cos\phi / \lambda_0)}{k_0^2 (\sin^2\theta \cos^2\phi - \epsilon_{eff})} \times \text{sinc}(wk_0 \sin\theta \sin\phi/2) \quad (14)$$

Inserting (14) in (8), we get the expression for the power radiated into space waves,

$$P_r = \frac{V_0^2}{Z_c^2} \frac{60}{\pi} \epsilon_{eff} \int_0^{2\pi} \int_0^{\pi/2} \frac{\cos^2(\pi l \sin\theta \cos\phi / \lambda_0)}{(\sin^2\theta \cos^2\phi - \epsilon_{eff})^2} \cdot \text{sinc}^2(wk_0 \sin\theta \sin\phi/2) \\ \times \left[\frac{\cos^2\theta \sin^2\phi}{(\epsilon_r - \sin^2\theta) \cot^2(hk_0 \sqrt{\epsilon_r - \sin^2\theta}) + \cos^2\theta} \right. \\ \left. + \frac{\cos^2\theta \cos^2\phi (\epsilon_r - \sin^2\theta)}{(\epsilon_r - \sin^2\theta) + \epsilon_r^2 \cos^2\theta \cot^2(hk_0 \sqrt{\epsilon_r - \sin^2\theta})} \right] \cdot \sin\theta d\theta d\phi \quad (15)$$

The normalised power radiated due to unit current ($I_0 = V_0 / Z_c$) can be written as,

$$\begin{aligned}
P_n = & \frac{60}{\pi} \epsilon_{eff} \int_0^{2\pi} \int_0^{\pi/2} \frac{\cos^2(\pi l \sin\theta \cos\phi / \lambda_0)}{(\sin^2\theta \cos^2\phi - \epsilon_{eff})^2} \cdot \text{sinc}^2(wk_0 \sin\theta \sin\phi/2) \\
& \times \left[\frac{\cos^2\theta \sin^2\phi}{(\epsilon_r - \sin^2\theta) \cot^2(hk_0 \sqrt{\epsilon_r - \sin^2\theta}) + \cos^2\theta} \right. \\
& \left. + \frac{\cos^2\theta \cos^2\phi (\epsilon_r - \sin^2\theta)}{(\epsilon_r - \sin^2\theta) + \epsilon_r^2 \cos^2\theta \cot^2(hk_0 \sqrt{\epsilon_r - \sin^2\theta})} \right] \cdot \sin\theta d\theta d\phi
\end{aligned} \tag{16}$$

The radiation resistance R_r of the dipole is then found by,

$$R_r = \frac{V_o^2}{2P_n} = \frac{Z_c^2}{2P_n} \tag{17}$$

and the quality factor Q is given by,

$$Q = \frac{\pi R_r}{2Z_c} \tag{18}$$

The antenna natural bandwidth is,

$$BW = \frac{1}{Q} \tag{19}$$

and the bandwidth for specified VSWR value is,

$$\begin{aligned}
BW_{vswr} &= \frac{vswr - 1}{\sqrt{vswr}} BW \\
&= \frac{vswr - 1}{\sqrt{vswr}} \frac{1}{Q}
\end{aligned} \tag{20}$$

For $vswr = 2$, one gets

$$BW_{vswr=2} = \frac{BW}{\sqrt{2}} = \frac{2\sqrt{2}}{\pi Z_c} P_n \tag{21}$$

Using the above formulation, bandwidth of cavity backed rectangular printed dipole (Fig.6.2) is calculated for two different arm widths. The dipole length is 9 cm (neglecting

the overlapping portion) and is fed by a 50 Ω microstrip feedline. Since the thickness of the dielectric substrate is negligible (thickness=1.6 mm) compared to the separation between the dipole and the reflector plate, the air between the dipole and the plate is only considered as dielectric medium. Thus, the dielectric constant of the medium is taken as unity.

The experimentally obtained and the theoretically computed values of bandwidths for different heights h between the dipole and the reflector plate are given in Table 6.1. From the table, it is clear that the theoretical values agree well with the experimental data. Also, from the analysis, it can easily be interpreted that the bandwidth of the dipole increases with separation h and dipole arms' width w . This is due to decrease in Q with increase in separation h and arms' width w .

Table 6.1

Comparison of experimentally and theoretically obtained percentage bandwidths of rectangular printed dipoles

Separation h (cm)	Percentage bandwidth			
	width $w = 0.75$ cm		width $w = 1.00$ cm	
	Experiment	Theory	Experiment	Theory
2.0	6.83	5.53	6.86	6.13
2.5	7.88	7.65	12.00	8.41
3.0	11.71	9.77	12.68	10.85
3.5	13.53	11.03	13.33	12.96
4.0	15.07	14.38	17.10	15.61
4.5	18.18	16.51	17.95	17.85
5.0	18.28	18.38	20.18	19.79
5.5	19.91	19.89	20.38	21.38

6.3 FLARED PRINTED DIPOLE

Fig 6.3 shows the sketch of flared printed dipole antenna. The dipole is backed by a reflector plate (not shown in figure) to form a cavity backed flared printed dipole antenna. Like the case of rectangular printed dipole, the arms' overlapping is kept at its minimum possible value. The flared arms are approximated as rectangularly shaped arms with an average width of

$$w_{av} = w + \frac{l}{2} \times \tan\theta \quad (22)$$

where w is the width of the dipole arm at the feed point, l is the length of the dipole and θ is the flaring angle. Now by replacing w by w_{av} in the preceding section, the percentage bandwidth of the antenna can be calculated.

Percentage bandwidth of flared dipole is computed for dipoles with two different arm widths at feed point. The length and the flaring angle of the dipoles are 9 cm and 10° respectively. The experimental results and the theoretical values for various separations between the dipole and the reflector plate are given in Table 6.2. As in the previous case, the experimental results agree well with the theoretical predictions.

The enhancement in percentage bandwidth due to flaring is apparent from the analysis. As discussed in the foregoing section, the dipole bandwidth increases with increase in arms width and from (22), it is clear that the flaring of the dipole arms increases the effective width of the dipole. Thus the improvement of bandwidth is a logical consequence.

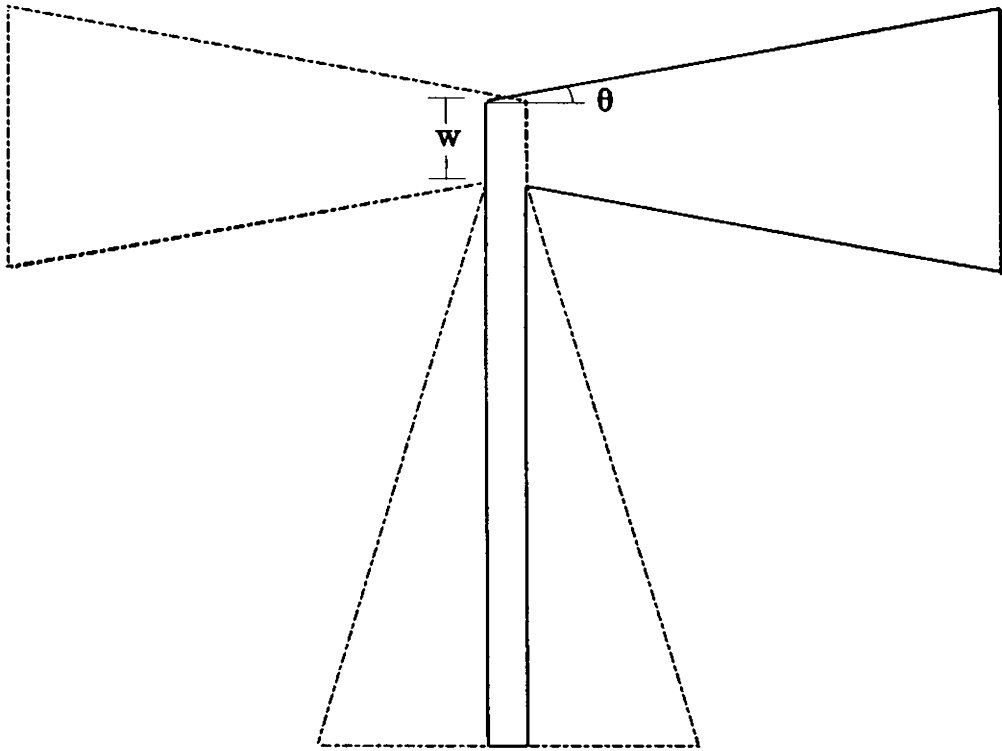


Fig. 6.3 Flared printed dipole

Table 6.2

Comparison of experimentally and theoretically obtained percentage bandwidths of flared printed dipoles

Separation h (cm)	Percentage bandwidth			
	width $w = 0.80$ cm		width $w = 1.00$ cm	
	Experiment	Theory	Experiment	Theory
2.0	5.60	7.02	8.81	8.04
2.5	8.70	9.23	9.25	9.82
3.0	12.49	11.86	12.97	12.45
3.5	14.06	14.49	15.05	15.06
4.0	18.15	17.29	16.20	17.75
4.5	20.88	19.78	18.42	20.37
5.0	24.76	22.27	20.91	22.92
5.5	25.99	24.31	24.94	25.11

6.4 TRIANGULAR END-LOADED FLARED PRINTED DIPOLE

The sketch of triangular end-loaded flared printed dipole antenna is shown in Fig.6.4. The reflector plate used to form the cavity backed structure is not shown in the figure. As mentioned earlier, bandwidth of the antenna is calculated by dividing the antenna into two sections, the flared arm portion (AA') and the remaining triangularly shaped loads. The Q of both portions are calculated separately and then added together in parallel with proper correction factor.

6.4.1 Q of the triangle

The triangular shaped load is considered as an independent patch antenna and the Q of the patch can be calculated from the close form formula given by Kuester and Chang [143] for 45°-45°-90° triangular patch, shown in Fig.6.5. The Q in terms of dielectric constant ϵ_r , the separation h from the reflector plate and the side length a is,

$$Q = \left\{ \begin{array}{ll} \frac{\epsilon_r a}{2h} & \epsilon_r \geq 2 \\ \frac{\epsilon_r a}{2h[1 + (2 - \epsilon_r)/\sqrt{2}]} & \epsilon_r \leq 2 \end{array} \right\} \quad (23)$$

The resultant Q_t due to both the triangles can be written as,

$$\frac{1}{Q_t} = \frac{1}{Q_m} + \frac{1}{Q_g} \quad (24)$$

where Q_m is the Q due to main arm load

Q_g is the Q due to ground arm load.

6.4.2 Q of the remaining dipole

The remaining portion of the dipole (*i.e.*, AA') is the same as flared printed dipole structure, except in the latter case arms' end are open whereas for the former case arms are coupled to the loads, which considerably modifies the Q of the portion AA'. This effect is incorporated by multiplying the unloaded Q of the portion AA' with an empirically selected correction factor and is given as,

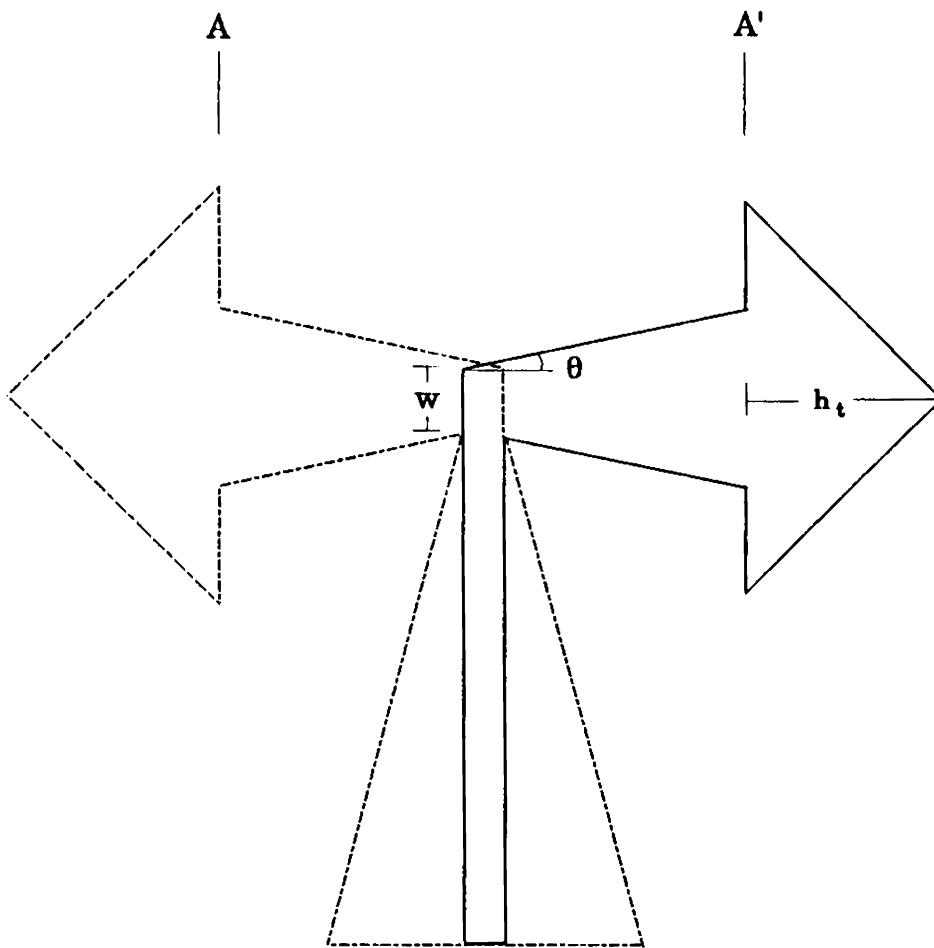


Fig. 6.4 Triangular end-loaded printed dipole

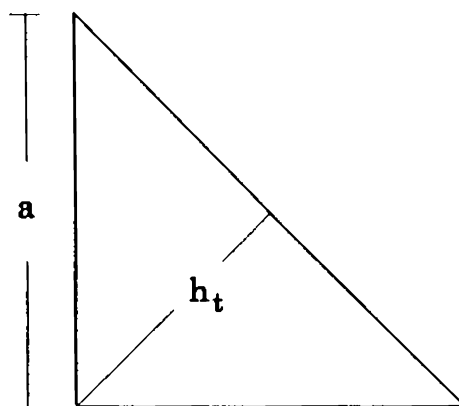


Fig. 6.5 45° - 45° - 90° triangular patch

$$Q_f = Q \times h^{(0.15)} \quad (25)$$

where, h is the separation between the dipole and the reflector plate.

6.4.3 Q of the complete structure

Now, the resultant Q of the antenna structure (Q_d) can easily be calculated by adding Q of both portions in parallel.

$$\frac{1}{Q_d} = \frac{1}{Q_i} + \frac{1}{Q_f} \quad (26)$$

where Q_i and Q_f can be calculated from (24) and (25) respectively.

Once the Q of the system is known, bandwidth of the antenna can easily be calculated using (20). Validity of the assumption made for Q_f is confirmed by fabricating two dipoles with different triangle heights h_t . The length, width and the flaring angle of the dipoles are 9 cm, 0.75 cm and 10° respectively.

Table 6.3 shows the comparison between the experimental and theoretical values for various separations between the dipole and the reflector plate for both the dipoles. Except for a few, the computed values agree quite well with the experimental data. Also from the table, it can be seen that bandwidth is more for larger size of triangle. This is due to the reduction in Q of the flared arm portion (Q_f) due to decrease in the length of the flared arm portion of the dipole. Also from (26), decrease in Q_f means decrease in the Q of the total structure or in other words improvement in the impedance bandwidth.

Table 6.3

Comparison of experimentally and theoretically obtained percentage bandwidths of triangular end-loaded printed dipoles

Separation h (cm)	Percentage bandwidth			
	height $h_t = 2.0$ cm		height $h_t = 2.5$ cm	
	Experiment	Theory	Experiment	Theory
2.5	11.41	13.01	9.91	13.93
3.0	16.42	16.12	19.59	17.55
3.5	18.53	19.18	21.30	20.92
4.0	22.82	22.41	28.19	24.43
4.5	24.79	25.61	29.92	27.72
5.0	25.93	29.10	31.93	30.73
5.5	29.46	31.36	36.58	33.87

Thus, it can be concluded that the theory described here presents a clear inside view of the bandwidth enhancement due to flaring and end-loading of the dipole arms. The small discrepancies between the theoretical and experimental results may be due to the arms' overlapping at the feed point, which is neglected in the theoretical formulation.

This chapter presents the summary of results of the investigations carried out and comments therein. A comparison of the characteristics of various optimised antennas are also given. This chapter concludes with a brief description of various possible applications of these antennas and scope of further work in the field.

7.1 INFERENCES FROM THE EXPERIMENTAL STUDIES

Investigations are carried out on printed dipoles and microstrip dipoles with the aim of enhancing the impedance bandwidth of the antennas without much deterioration in the radiation properties of the antennas.

7.1.1 Printed dipole

The effect of flaring the dipole arms is studied in Section 4.1. It is observed that the flaring modifies the impedance characteristics of the dipole. In particular, the change in the reactive part of the impedance with frequency is controlled considerably. This improves the 2:1 VSWR bandwidth of the antenna. The effect of various other design parameters on the impedance bandwidth of the antenna are also studied. The important conclusion drawn is that, there is considerable improvement in the impedance bandwidth of the dipole when ground arm dimensions are larger than the main arm dimensions. This may be due to the fact that the microstrip line, used for feeding dipole, is an unbalanced structure. Whereas, dipole with equal arms is a balanced structure. The larger size of ground arm provides a good matching and thus improves the bandwidth of the antenna. For the same main arm length, central frequency of Flared Printed Dipole Antenna (FPDA) is much higher compared to Rectangular Printed Dipole Antenna (RPDA). The co-polar patterns of FPDA are almost similar to the patterns of RPDA. Only a slight deterioration in the cross-polar level of FPDA is observed.

From Table 4.5, it can be seen that the impedance bandwidth of the antenna improves considerably by end-loading the dipole arms with proper shapes. The triangular-shape load gives maximum bandwidth and thus is selected for further study. While optimising the dimensions of the triangle, it is seen that the central frequency of the antenna increases with decrease in the size of the triangle. For optimum dimensions of the triangle, the central frequency of the antenna (TELPDA) is much less than that of FPDA, even though both are having same arm length. This lowering in central frequency can be attributed to the specific shape of the load. While optimising the design parameters of the triangular end-loaded printed dipole, it is seen that the optimisation of the size of the load

is related to other design parameters. From Fig. 4.21, the cross-polar level of the antenna increases with frequency. This may be due to effective increase in sides of the triangle with frequency which increases the transverse current. Comparison of the radiation patterns of the antenna with RPDA shows that there is no significant change in co-polar patterns, but the cross-polar level is high for TELPDA.

The effect of reflector plate, which acts as a ground plane, kept at finite distance away from the dipole, on various antenna characteristics is also studied and given in Section 4.2.5. It is observed that below a minimum separation between the dipole and the reflector plate, the VSWR of the antenna is more than 2 in the middle portion of the frequency band of interest and increases with further decrease in separation. The impedance bandwidth of Cavity Backed Triangular End-Loaded Printed Dipole Antenna (CBTELPDA) is more than that of the same dipole without cavity backup. Also central frequency of the antenna increases with increase in separation between the reflector plate and the dipole. The E-plane radiation patterns show slight dip at the bore-sight direction, in the higher frequency side of the band of interest. This may be due to slight cancellation of radiation from the ground plate due to effective increase in the separation between the dipole and the reflector plate with frequency. Also, the cross-polar level of CBTELPDA is slightly higher as compared to TELPDA.

Once again from Table 4.5, the second best load shape is parallelogram. Thus, an attempt has also been made to improve the impedance bandwidth of flared printed dipole using parallelogram shaped load. The optimised design values of Parallelogram End-Loaded Printed Dipole Antenna (PELPDA) are found to be entirely different from the FPDA. In this case, unlike TELPDA, no relationship has been found between the size of the parallelogram and the central frequency of the antenna. Also, for triangular end-loaded

printed dipole, the impedance bandwidth is less for too large and too small sizes of the loads. But in this case, the impedance bandwidth is directly proportional to the size of the load and found to be maximum for largest possible load size. The radiation patterns of PELPDA are same as that of TELPDA. Like TELPDA in this case also the cross-polar level increase with frequency.

The effect of reflector plate on the impedance bandwidth and radiation patterns of PELPDA is also studied and is given in Section 4.3.2. Like the case of cavity backed triangular end-loaded printed dipole, VSWR of the antenna is more than 2 in the middle portion of the frequency band when the separation between the dipole and the reflector plate is less than a certain minimum value. Like CBTELPDA, the E-plane radiation patterns also show a dip of around 0.5 dB at bore-sight direction, in the higher frequency side of the band of interest.

A comparison of various antenna characteristics of Triangular End-Loaded Printed Dipole Antenna (TELPDA) and Parallelogram End-Loaded Printed Dipole Antenna (PELPDA) with and without cavity backup are given in Table 7.1.

From the table, it is clear that the impedance bandwidth of the dipole with both load shapes is almost equal and improves considerably in cavity backup configuration. Also, 3 dB beamwidths of the dipoles are almost same and as expected, the presence of reflector plate makes the beam narrower. The cross-polar level and the gain are better for triangular end-loaded printed dipole antennas. Thus, comparing various antenna characteristics of both the dipoles, it can be concluded that triangular end-loaded printed dipole has an edge over parallelogram end-loaded printed dipole.

Table 7.1

Various characteristics of triangular and parallelogram end-loaded flared printed dipoles with and without reflector plate

Characteristics	Without reflector plate		With reflector plate	
	TELPDA	PELPDA	CBTELPDA	CBPELPDA
Percentage bandwidth	48.55%	48.74%	53.51%	54.85%
Central frequency (GHz)	1.488	1.514	1.469	1.489
3 dB beamwidth				
E-plane	84°	85°	70°	67°
H-plane	180°	180°	100°	118°
Cross-polar level at bore-sight and at central frequency	-12.2 dB	-5.7 dB	-9.4 dB	-4.0 dB
Gain with respect to half wave wire dipole resonating at 1.496 GHz	-0.55 dB	-1.64 dB	4.43 dB	3.13 dB

7.1.2 Microstrip dipole

Keeping in mind the conclusions drawn from the results of the experimentation on printed dipoles, attempts have also been made to enhance the impedance bandwidth of rectangular microstrip dipoles by flaring and triangular shape end-loading of the dipole arms. For this, the design of TELPDA is suitably modified so as to make it amiable to microstrip configuration. It is clear from the antenna structure (Fig. 3.6) that the separations of the two arms from the ground plane are different. Also, surrounding environment of the two arms are not the same. The arm connected to the main feedline is sandwiched between two substrates, whereas the other arm is at the air-dielectric interface. This makes the effective dielectric constant for two arms different. Thus, the effective lengths of the two arms are not same for the same physical lengths and make the dipole an unbalanced structure. The

feedline for this antenna is stripline which is a balanced structure. The dipole is made balanced by increasing the ground arm length sufficiently compared to the main arm length, so that the effective lengths of both arms become equal. This provides a good matching and leading to a better bandwidth.

The different design parameters of the antenna are optimised as explained in Section 5.1. The radiation patterns of optimised Triangular End-Loaded Microstrip Dipole Antenna (TELMDA) are given in Fig. 5.7. The E-plane beam maximum is shifted by 10° . Although the E-plane patterns are similar to that of a rectangular microstrip dipole, the H-plane patterns are much broader compared to those of rectangular microstrip dipole. The gain of the antenna is found to be only 0.33 dB down compared to a standard rectangular patch, etched on same dielectric substrate and resonating almost at the center of the frequency band of interest. This reduction in gain is obvious, due to enhancement in the impedance bandwidth of the antenna.

The triangular end-loaded microstrip dipole antenna requires two dielectric substrates and two photographic exposures. This makes the fabrication of the antenna slightly difficult. To reduce the design complexity, while keeping the impedance bandwidth sufficiently large, a totally new design is attempted. For this, the flat triangular dipole antenna design is suitably tailored for microstrip configuration. The balanced dipole is matched with unbalanced microstrip feedline using a short-circuited matching balun. The final design gives almost the same percentage bandwidth as that of TELMDA, but requires only one substrate and single photographic exposure.

The radiation patterns of the antenna are almost similar to the patterns of ordinary rectangular microstrip dipole. Only the E-plane beam maximum is shifted by 30° from the

bore-sight direction. The gain of the antenna is only 0.64 dB less compared to a standard rectangular microstrip patch resonating at the center of the frequency band of interest.

7.2 CONCLUSIONS FROM THE THEORETICAL ANALYSIS

Theoretical analysis of various cavity backed antennas are given in Chapter 6. The experimental values agree well with the computation. Also the theory gives a clear inside view and explains the reasons for bandwidth enhancement due to flaring and end-loading of the dipole arms. The percentage bandwidth is determined by calculating the Q of the antenna. Since the approach is for the analysis of microstrip antenna on thick grounded substrate, this method cannot be used to predict the impedance bandwidth of the antennas without cavity backup. Also, the structures analysed are simplified versions of the optimised ones. Specially, the arms overlapping is neglected in the analysis. Also, the antennas with symmetrical arms can only be analysed with this theory.

7.3 SOME PRACTICAL APPLICATIONS OF THE PRESENT ANTENNAS

These types of antennas are highly suitable for IFF application, where large impedance bandwidth is required. By selecting proper amplitude and phase distribution, planar array with desired sum and difference pattern along the azimuth and cosecant square pattern along the elevation can easily be achieved. Hence, this can be an ideal substitute for conventional dipole array. Moreover, the switching circuits, power dividers etc. can be integrated with the feeding network on the same substrate.

The E-plane radiation patterns of cavity backed end-loaded printed dipoles show a dip of 0.5 dB along the bore-sight direction. Thus, these antennas are suitable as feed for

reflectors. The dip along the bore-sight direction will reduce the direct reflection from the center of the reflector.

A combination of these types of antennas with corner reflectors can be used as an ideal auxiliary antenna in radar.

For the treatment of large cross-section tumours, the best clinical response has been achieved for antennas with large beamwidth since it has the capability of heating large area uniformly. Since, these new microstrip dipoles produce very broad beamwidth along with other attractive features like, light-weight and easier fabrication on flexible substrates, they can find applications in RF and MW hyper-thermia treatment.

7.4 SCOPE OF FURTHER WORK IN THE FIELD

The studies on planar dipoles reported here, open a few interesting problems for further investigations in this field.

Although the impedance bandwidth of printed dipole is improved considerably by end-loading the dipole arms, the cross-polar level of such an antenna is higher compared to ordinary rectangular printed dipole. So, work can be continued to improve the cross-polar level of the antenna without any decrease in the bandwidth of the dipole. This can be attempted using superstrate with strip-gratings structure or by modifying the load shape.

For both types of microstrip dipoles, the beam maximum is shifted from bore-sight direction. The antenna structure can suitably be modified so as to get the beam maximum along bore-sight direction. Also work can be carried out to develop the design criteria for triangular microstrip dipole.

As discussed in the last section, the theoretical method employed in this thesis is applicable only for simplified structure with cavity backup. A suitable theoretical model, based on moment method, can be worked out, which takes care of the complicated feeding structure and the arms asymmetry.

The effect on impedance bandwidth of these dipoles in different array environments is another interesting subject to study.

Development of an input impedance tunable circular patch antenna

A

A.1 INTRODUCTION

One of the charming features of microstrip antennas is the ease with which they can be formed into arrays. Commonly used radiating elements are rectangular and circular microstrip patch antennas [144-147]. Advantage of circular patch over the rectangular patch is the smallness of the area. The main handicap of circular patch is the high input impedance along the circumference, which restricts the direct use of 50Ω microstrip line as feed for circular patch antennas. Direct match of circular patch to 50Ω feedline is possible only through coaxial feed because matching point always lies within the patch. This increases the fabrication cost and design complexity, and make it unusable for microwave

integrated arrays. In this appendix, a modified design of circular patch to match it with 50Ω microstrip feed is presented.

A.2 ANTENNA GEOMETRY AND EXPERIMENTAL SET-UP

The sketch of the modified circular patch antenna is shown in Fig. A.1. The antenna structure consists of circular patch having a sectoral slot on it and a shunt element across the slot. The antenna is etched on double-side copper cladded substrate having dielectric constant $\epsilon_r = 4.5$ and thickness 0.16 cm. The radius of the patch r is 4.95 cm and the sectoral slot angle is 6° . The position of the shunt element from the center of the patch l is 2.35 cm and the width of the shunt is 0.5 cm. The dimensions of the patch has been arrived at by experimental iterations.

The antenna characteristics are studied using the experimental set-up discussed earlier in Chapter 3.

A.3 EXPERIMENTAL RESULTS AND DISCUSSIONS

The measured input impedance of the antenna at resonance, at various points along the circumference is plotted in Fig. A.2. The angle ϕ is measured from the center of the sectoral slot. The variation in input impedance ranges from 36Ω to 99Ω and is 50Ω when the feed point corresponds to $\phi = 12^\circ$. From the graph, it can also be seen that there is a slight variation of about 6 MHz in resonance frequency with change in feed location.

The variation in input impedance along the circumference is due to the sectoral slot and the shunt which impose structural asymmetry in the circular patch and modifies the current distribution, which otherwise is not possible in the case of ordinary circular patch.

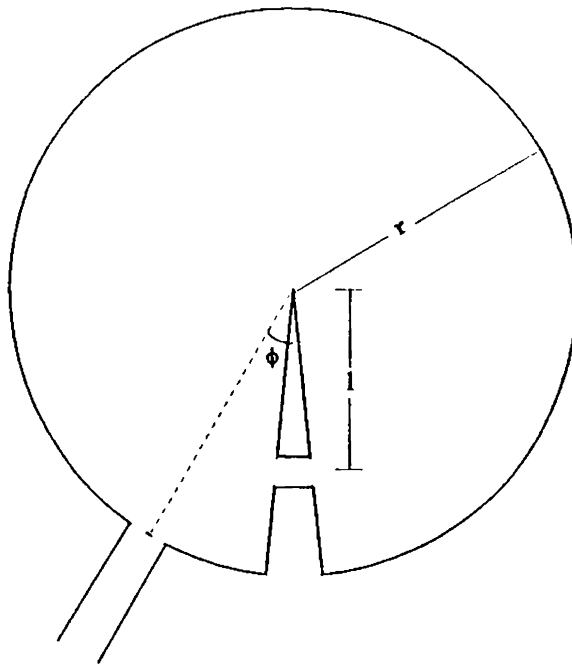


Fig. A.1 Schematic representation of the patch antenna

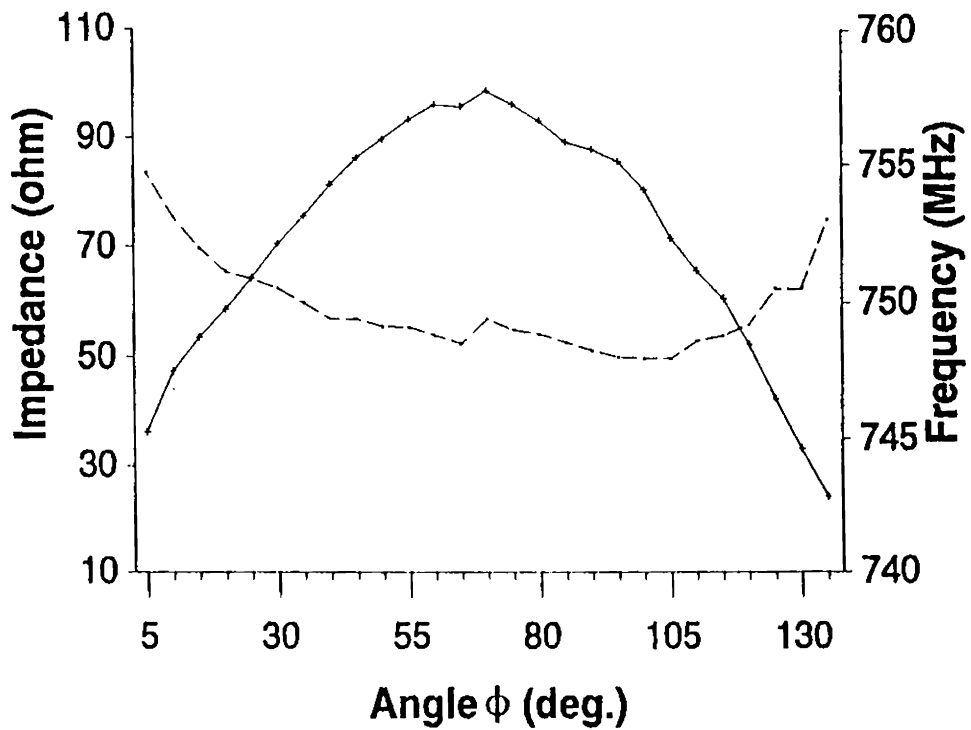


Fig. A.2 Variation of input impedance and resonant frequency with angle ϕ
 ——— impedance, - - - - - frequency

Variation of VSWR with frequency for 50Ω microstrip feedline at $\phi = 12^\circ$ is given in Fig. A.3. The input VSWR of the antenna is 1.05 at 752 MHz. The resonant frequency for the circular patch, having same radius, at the dominant mode is 840 MHz [148]. This decrease in resonant frequency for the new structure is due to effective increase in the length of the circumference, due to the sectoral slot.

The E and H-plane radiation patterns at resonance are shown in Fig. A.4. As in the case of ordinary circular patch, the 3 dB beamwidth of E-plane radiation pattern is slightly more than that of H-plane pattern. The 3 dB beamwidth of E and H-plane patterns are 100° and 85° respectively. The cross-polar patterns are at least 15 dB down compared to co-polar patterns.

A.4 CONCLUSIONS

Employing the modifications in the circular patch as described in this appendix, it is possible to match the antenna with a range of line impedance of microstrip feed, without deteriorating the radiation characteristics. An additional feature of this antenna is that a lower resonant frequency can be achieved with a smaller patch size compared to ordinary circular patch antenna. The input impedance tuning ability of this antenna makes it attractive as a radiative element in large phased arrays incorporating corporate feed networks.

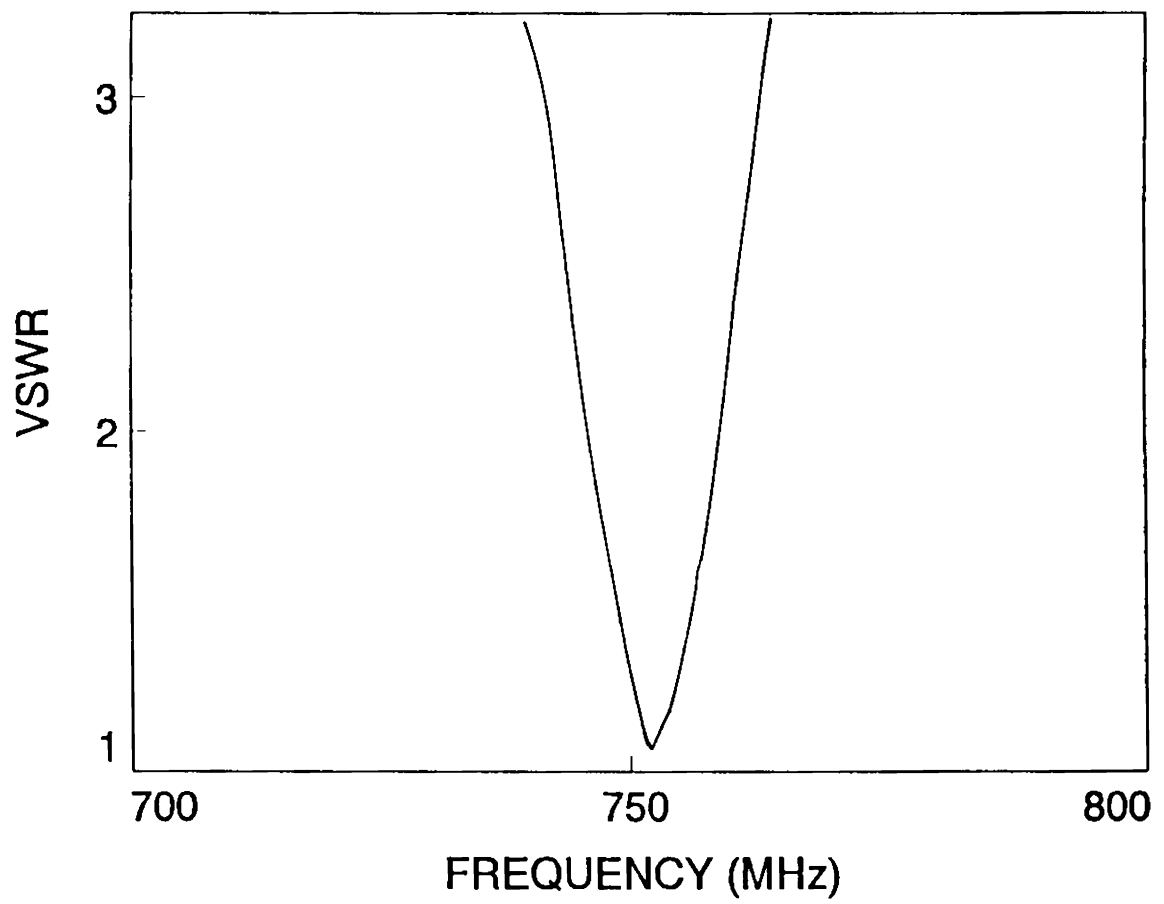


Fig. A.3 VSWR plot for $\phi = 12^\circ$

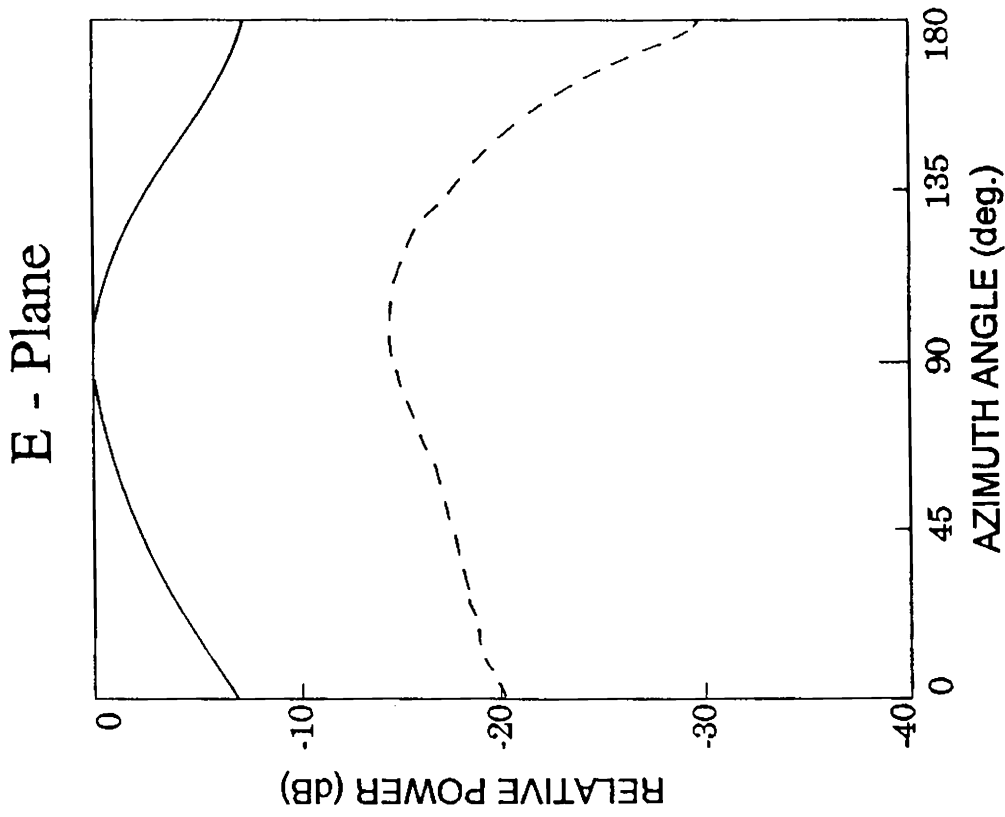
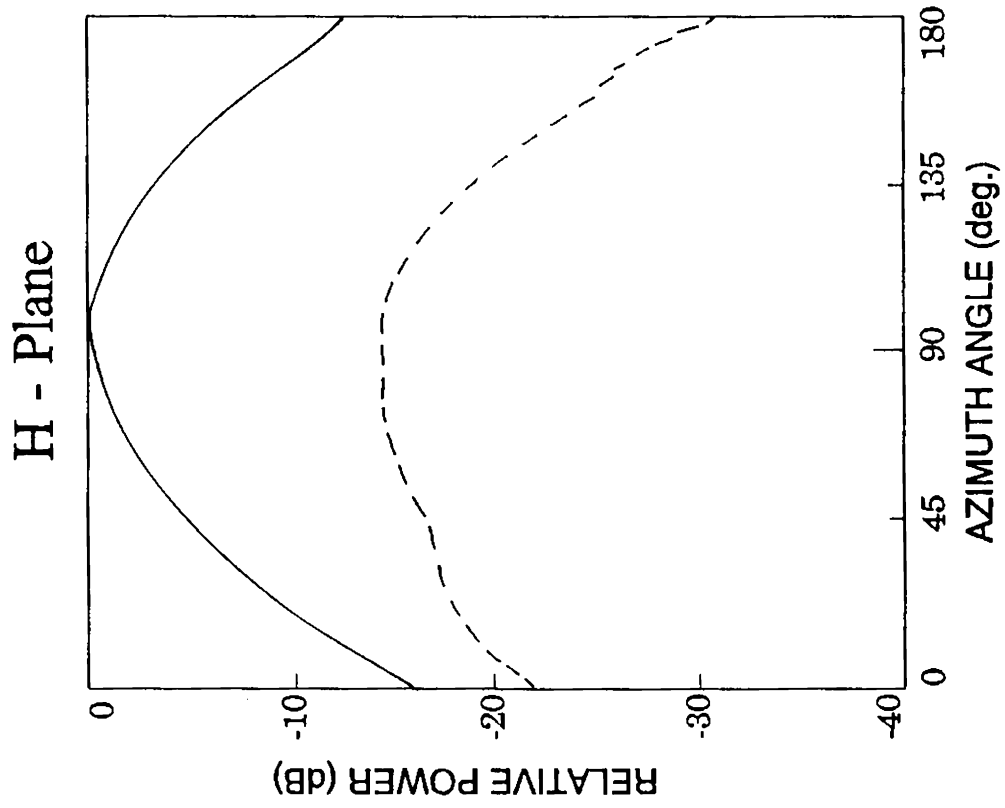


Fig. A.4 Radiation patterns
 — co-polar, - - - cross-polar

Performance study of YBCO superconducting wire loop antenna

B

B.1 INTRODUCTION

The advent of new type of superconducting ceramic materials in 1987 [149,150] with transition temperature above the boiling point of liquid nitrogen (77 K) has generated a great deal of interest with regard to possible engineering applications. One such application is the improvement of antennas and antenna systems. Hansen [151] has suggested six potential applications for such uses of superconductors. These are *super-directive arrays*, *millimeter wave arrays*, *switch-line* or *single-line phasers* for electronic scanning of arrays, *travelling wave type array feeds*, *matching networks* for antennas and *electrically small antennas*.

The first demonstration of superconducting antennas using high T_c materials was done by Khamas *et al.* [54]. Thereafter a number of superconducting antennas have been presented in literature; for example, dipole antennas have been reported by Fujinaka *et al.* [152] and He *et al.* [153] and loop antenna by Wu *et al.* [154].

The effect of using superconductor in constructing an antenna can easily be understood by a careful consideration of the roles of external and internal fields. This can be explained easily by considering the case of a cylindrical dipole antenna. The radiated field and its associated reactance are produced by the current on the surface of the dipole; these are external fields. Fields internal to the dipole cylinder are important only in relating to the conduction loss. Use of superconductor will produce a negligible change in the external fields, hence impedance, pattern and directivity will remain unchanged. Only the internal fields experience main change, leading of course to a zero or extremely low conductor loss. Similar conclusions apply to almost all antennas. All antenna properties except efficiency depend upon external fields and are essentially unchanged by the superconductors. Whereas the low conductor loss reduces the surface resistance of the antenna system and hence improves the radiation efficiency of the antenna. Also, high T_c superconductors has the potential to lower the insertion loss of RF and microwave devices by many dB. All these factors lead to a performance enhancement of the antenna system that justifies the cost and complication of cooling.

In this appendix, the study on the performance of a superconducting loop antenna is presented.

B.2 ANTENNA FABRICATION

The loop antenna is fabricated using Yttrium Barium Copper Oxide ($Y_1Ba_2Cu_3O_{7.5}$), whose transition temperature, from a normal conductor to superconductor, is approximately at 90 K. The antenna fabrication procedure is as follows:

B.2.1 Preparation of YBCO powder

The mixture of nitrates of Yttrium and Barium, and Copper Oxide in 1:2:3 stoichiometry is exposed to microwave of frequency 2.45 GHz and 600 W power for a period of 240 seconds. The nitrates are decomposed and a fine black powder is formed, known as the precursor. The precursor powder is subjected to controlled heating at 800°C initially and then continued to 940°C under flowing Oxygen to phase pure superconducting YBCO powder. The heated mass is further grounded gently to flowable powder.

B.2.2 Fabrication of antenna

The Superconducting wires are drawn from a mixture of polymer and YBCO powder at room temperature for a nonaqueous viscous mass by extraction principle [155]. For this, the finely powdered YBCO is mixed with poly propylene carbonate in acetone medium in the presence of a lubricant by ball milling in a PVC bottle using zirconia balls as the grinding media. The mixture is evaporated gradually until highly viscous mass remained, which is further extruded in a stainless steel extruder having an adjustable nozzle. The antenna can be made by winding these wires on a glass or polyethylene rod of desired diameter and shape. The sample is heat treated at controlled rates and then sintered at 940°C for 10 hours with pre-required conditions.

Using above technique, a superconducting wire loop antenna, with wire diameter 2.2 mm and radius of 7.5 mm, along with short parallel wire transmission line is fabricated. An identical copper wire antenna is also fabricated for comparison. Sketch of the antenna is shown in Fig. B.1. Since the input impedance of the antenna is not equal to 50Ω , a tuning stub is attached to the transmission line to match the antenna with 50Ω feed.

B.3 EXPERIMENTAL SET-UP

Measurements are taken at room temperature with copper antenna and with YBCO antenna placed inside a thermacol dewar containing liquid nitrogen. The radiated field transmits through the walls of the dewar and is then detected by an external wideband antenna with its polarisation aligned with that loop antenna.

B.4 EXPERIMENTAL RESULTS

The return-loss of copper loop antenna at room temperature, is given in Fig. B.2. From the figure it is clear that the return-loss is less than -10 dB in the frequency range 4.54 GHz to 4.99 GHz. Also, the resonant frequency is 4.87 GHz.

The relative radiated power of the copper antenna at room temperature and the superconducting antenna at liquid nitrogen temperature is plotted in Fig. B.3. The superconducting antenna shows a 5 dB improvement in gain compared to the copper antenna in the frequency range of interest.

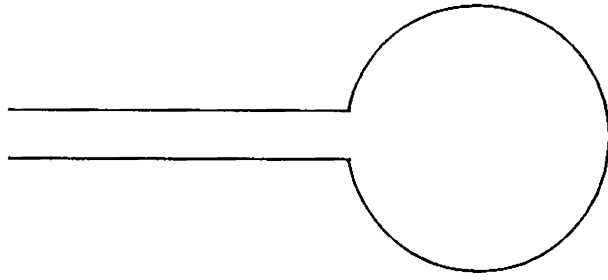


Fig. B.1 Sketch of the loop antenna

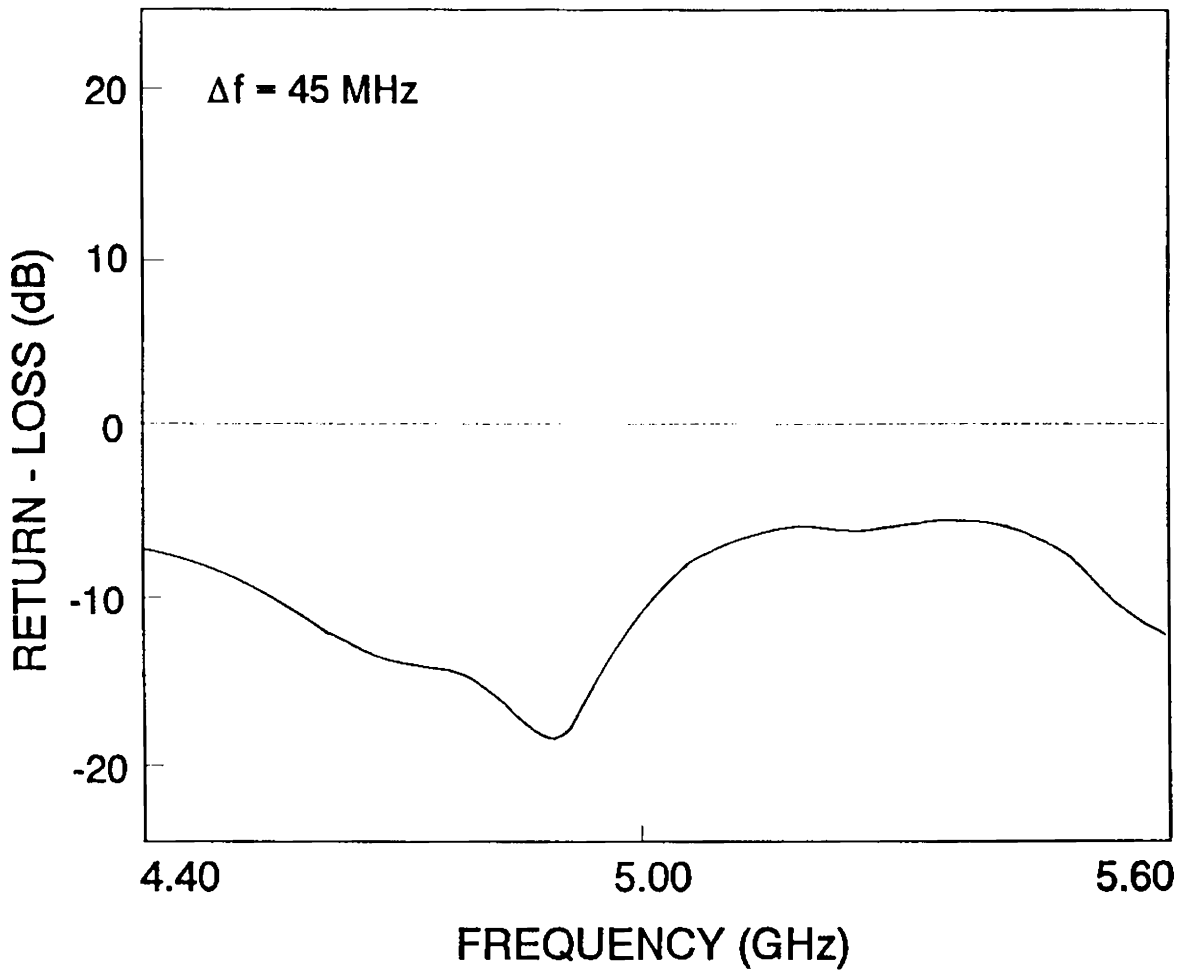


Fig. B.2 Return - loss of copper loop antenna at room temperature

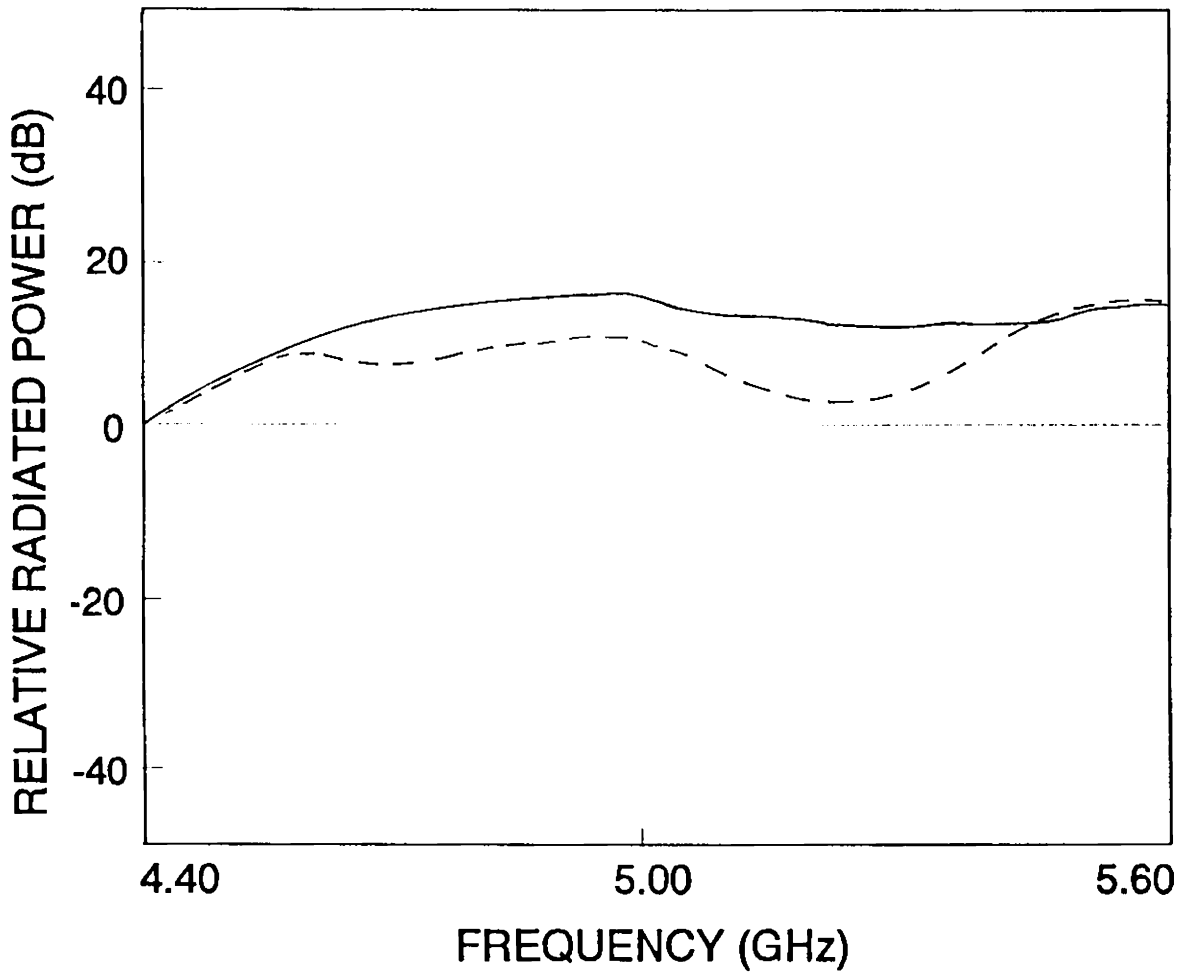


Fig. B.3 Radiated power of superconducting and copper loop antennas
 ———— superconductor at liquid nitrogen temperature
 - - - - - copper at room temperature

B.5 CONCLUSIONS

A superconducting loop antenna is fabricated using cold wire extrusion principle. The cold wire extrusion technique eliminates the common requirement of low loss dielectric substrate for YBCO antennas, which are normally brittle and of low strength. The superconducting loop antenna shows significant improvement in gain over its copper counter part.

1. J. D. Kraus, *Antennas*, McGraw-Hill, New York, p. xxiv, 1988.
2. A. F. Stevenson, "Theory of slots in rectangular waveguides," *J. Appl. Phys.*, vol. 19, p. 24, 1948.
3. A. A. Oliner, "The impedance properties of narrow radiating slots in the broad face of rectangular waveguides, part I and II," *IRE Trans.*, AP-5, p.4, 1957.
4. S. Silver, *Microwave antenna theory and design*, Dover Publication Inc., NEW York, 1965.
5. K. L. Klohn, R. E. Horn, H. Jacobs and E. Freibergs, "Silicon waveguide frequency scanning linear array antenna," *IEEE Trans. Microwave Theory tenhnol.* vol. MTT-26, no. 10, pp. 764-773, Oct. 1978.
6. T. Itoh and A. S. Hebert, "Simulation study of electronically scannable antennas and tunable filters integrated in a quasi - planar dielectric waveguide," *IEEE Trans. Microwave Theory tenhnol.* vol. MTT-26, no. 12, pp. 987-991, Dec. 1978.
7. S. B. Cohn, "Characteristics impedance of shielded-strip transmission line," *IRE Trans.*, vol. MTT-2, no.1, pp. 52-55, 1954.

8. A. A. Oliner, "The radiation conductance of a series - slot in a strip transmission line," *IRE Nat. Conf. Rec.*, Vol. 2, pt. 8, pp. 89-90, 1954.
9. R. W. Berithaupt, "Conductance data for offset series slots in stripline," *IEEE Trans. Microwave Theory tenhno.* vol. MTT-16, no. 11, pp. 969-970, Nov. 1968.
10. W. A. Fritz and P. E. Mayes, "A frequency scanning stripline fed periodic slot array," *Dig. Int. Symp. Antennas Propagat. Soc.*, pp. 278-281, June 1974.
11. R. Hill and D. H. Paul, "A rapid versatile method of designing printed stripline ariel arrays," *Mullard Resh. Lab. Rev.*, pp. 36-37, 1975.
12. R. Yoshimura, "A microstrip line slot antenna," *IEEE Trans. Microwave Theory tenhno.*, vol. MTT-20, no. 12, pp. 760-762, Dec. 1972.
13. W. C. Wilkinson, "A Class of printed circuit antenna," *Dig. Int. Symp. Antennas Propagat. Soc.*, pp. 270-273, June 1974.
14. G. R. Hanley and H. R. Perini, "Column network study for a planar array used with an unattendant radar," RADC-TR-80, final report, RADC, Mar. 1980.
15. E. G. Fubini, J. McDonough and R. Malech, "Stripline radiators," *IRE Nat. Conf. Rec.*, Vol. 3, pp. 51-55, 1955.
16. J. A. McDonough, R. Malech and J. Kowalsky, "Recent developments in the study of printed antennas," *IRE Nat. Conf. Rec.*, Vol. 5, pt. 1, pp. 173-176, 1957.
17. M. J. Sidford, "Performance of an L-band AEROSAT antenna system for aircraft," *Proc. Conf. on Antennas for Aircraft and Spacecraft*, IEE Conf. Publ., 128, pp. 123-129, 1975.
18. G. Dubost, *Handbook of microstrip antennas*, IEE Publ., London, Chap. 7, 1989.
19. W. Rotman and N. Karas, "The sandwich wire antenna: a new type of microstrip wire line source radiator," *IRE Nat. Conf. Rec.*, Vol. 5, pt. 1, pp. 166-172, 1957.
20. R. Graham, "Monopulse aerials for airborne radars," *Proc. 4th European Microwave Conf.*, pp. 362-266, 1974.
21. G. A. Deschamps, "Microstrip microwave antennas," presented at the 3rd USAF symp. on Antennas, 1953.
22. H. Gutton and G. Baissinot, "Flat ariel for ultra high frequencies," French Patent No. 703113, 1955.
23. E. V. Byran, "A new flush - mounted antenna element for phased array application," *Proc. Phased-Array Antenna Symp.*, pp. 187-192, 1970.
24. R. E. Munson, "Single slot cavity antenna assembly," US Patent No. 3713162, Jan. 1973.
25. M. C. Baily, "Broad-band half-wave dipole," *IEEE Trans. Antennas Propagat.*, vol. AP-32, no. 4, pp. 410-412, Apr. 1984.

26. H. G. Oltman, Jr., US Patent no. 4054874, Oct. 1977.
27. L. Stark, "Radiation impedance of a dipole in an infinite planar phased array," *Radio Sci.*, (New series), vol. 1, pp. 361-377, Mar. 1966.
28. P. J. Kahrilas, "HAPDAR-An operational phased array radar," *Proc. IEEE*, vol. 56, no. 11, pp. 1967-1975, Nov. 1968.
29. W. Hersch, "Very slim high gain printed circuit microwave antenna for airborne blind landing aid," *Proc. AGARD Conf. 139 Antennas for Avionics*, pp. 9-1 to 9-2, 1973.
30. R. J. Klensch, "A microwave automatic vehicle identification system," *RCA Rev.*, vol. 34, p. 566, 1973.
31. N. Singh, M. K. Bhattacharjee and I. J. Bhal, "An S-band printed dipole with its feedline," *Int. Jour. of Electron.*, vol. 40, no. 5, pp. 495-498, 1976.
32. R. W. Othius, "Printed circuit antenna for radar altimeter," *IEEE AP-S Int. Symp. Dig.*, pp. 554-557, Oct. 1976.
33. G. Dubost, "Array of flat symmetric dipoles operating at the first antiresonance frequency," *Electron Lett.*, vol. 13, no. 22, pp. 672-673, Oct. 1977.
34. S. Nanbu, "An MIC Doppler module with output radiation normal to substrate plane," *IEEE Trans. Microwave Theory and Technol.* vol. MTT-26, no. 1, pp. 3-5, Jan. 1978.
35. E. H. Newman, "Strip antennas in a dielectric slab," *IEEE Trans. Antennas Propagat.*, vol. AP-26, no. 5, pp. 647-654, Sep. 1978.
36. G. Dubost, "Bandwidth of a dipole near and parallel to a conducting plane," *Electron Lett.*, vol. 14, no. 24, pp. 734-736, Nov. 1978.
37. G. Dubost, J. Samson and R. Frin, "Large-bandwidth flat cylindrical array with circular polarisation and omnidirectional radiation," *Electron Lett.*, vol. 15, no. 2, pp. 102-103, Jan. 1979.
38. G. Dubost, "Theory and experiments of a broadband short-circuited microstrip dipole at resonance," *Proc. Workshop Printed Circuit Antenna Tech.*, pp. 32/1-13, Oct. 1979.
39. K. M. Keen, "A low-blockage dipole array reflector antenna feed for the lower microwave frequencies," *IEEE Trans. Antennas Propagat.*, vol. AP-28, no. 6, pp. 914-916, Nov. 1980.
40. G. Dubost and A. Rabbaa, "Mutual impedance between two short-circuited flat resonant dipoles," *IEEE Trans. Antennas Propagat.*, vol. AP-29, no. 4, pp. 668-671, Jul. 1981.
41. D. B. Rutledge and M. S. Muha, "Imaging antenna arrays," *IEEE Trans. Antennas Propagat.*, vol. AP-30, no. 4, pp. 535-540, Jul. 1982.
42. G. Dubost and C. Vinatier, "Large bandwidth and high gain array of flat folded dipoles acting at 12 GHz," *3rd Int. Conf. Antennas Propagat.*, ICAP, Apr. 1983.

43. N. H. Subhnani and B. V. Rao, "Analysis of a microstrip dipole antenna," *Electron Lett.*, vol. 20, no. 3, pp. 116-118, Feb. 1984.
44. K. Ito, "Circularly polarised printed array antenna composed of end-fed strip dipoles and strips," *Electron. Commun. Japan*, vol. 67-B, pp. 56-69, 1984.
45. G. Dubost and G. Beauquat, "Theoretical radiation admittance of a large bandwidth flat symmetrical folded dipoles," *Electron Lett.*, vol. 20, no. 6, pp. 252-253, Mar. 1984.
46. A. Mohsen, "Representation of the electromagnetic fields of a dipole above an inhomogeneous half space," *Proc. IEE*, vol. 132, pt. H, no. 2, Apr. 1985.
47. R. W. Lampe, "Design formula for an asymmetric coplanar strip folded dipole," *IEEE Trans. Antennas Propagat.*, vol. AP-33, no. 9, pp. 1028-1031, Sep. 1985.
48. A. K. Agrawal and W. E. Powell, "Monopulse printed circuit dipole array," *IEEE Trans. Antennas Propagat.*, vol. AP-33, no. 11, pp. 1280-1283, Nov. 1985.
49. G. Dubost, "Large bandwidth dual polarised multilayered microstrip antenna," *Dig. Int. Symp. Antennas Propagat. Soc.*, pp. 455-458, June 1986.
50. R. S. Chu, K. M. Lee and N. S. Wong, "A network model of a feedthrough phased array lens of printed dipole elements," *IEEE Trans. Antennas Propagat.*, vol. AP-34, no. 12, pp. 1410-1417, Dec. 1986.
51. R. S. Chu, K. M. Lee, "Radiation impedance of a dipole printed on periodic dielectric slabs protruding over a ground plane in an infinite phased array," *IEEE Trans. Antennas Propagat.*, vol. AP-35, no. 1, pp. 13-25, Jan. 1987.
52. R. C. Compton, R. C. McPhedran, Z. Popovic, G. M. Rebeiz, P. P. Tong and D. B. Rutledge, "Bow-tie antenna on a dielectric half space; theory and experiment," *IEEE Trans. Antennas Propagat.*, vol. AP-35, no. 6, pp. 622-631, June 1987.
53. E. Levine, S. Shtrikman and D. Treves, "Double-sided printed arrays with large bandwidth," *Proc. IEE*, vol. 135, pt. H, no. 1, pp. 54-59, Feb. 1988.
54. S. K. Khamas, M. J. Mehler, T. S. M. Madean, C. E. Gouch, N. McN. Alford and M. A. Harmer, "High- T_c superconducting short dipole antenna," *Electron Lett.*, vol. 24, no. 8, pp. 460-461, Apr. 1988.
55. T. J. Athanasas, "Coupling between printed dipole and coplanar strip transmission line," *Dig. Int. Symp. Antennas Propagat. Soc.*, Pt. III, pp. 956-959, June 1988.
56. K. Ito, J. P. Dainel and J. M. Lenormand, "A printed antenna composed of strip dipoles and slots generating circularly polarised conical patterns," *Dig. Int. Symp. Antennas Propagat. Soc.*, Pt. II, pp. 632-635, June 1989.
57. A. J. Parfitt and D. W. Griffin, "The single wire fed dipole on slab: An antenna for integration with monolithic microwave and millimeter wave circuits," *Dig. Int. Symp. Antennas Propagat. Soc.*, Pt. II, pp. 795-798, May. 1990.

58. A. Skalar, T. de. Graauw and H. Stadt, "A planar dipole array antenna with a elliptical lens," *Microwave Opt. Technol. Lett.*, vol. 4, no. 1, pp. 9-12, Jan. 1991.
59. M. C. D. Maddocks and M. S. Smith, "Flat plate steerable antennas for satellite communications and broadcast reception," *Proc. IEE*, vol. 138, pt. H, no. 2, pp. 159-168, Apr. 1991.
60. K. M. Lee and R. C. Chu, "Analysis of mutual coupling between an infinite phased array of horizontal dipole and vertical wires," *IEEE Trans. Antennas Propagat.*, vol. AP-39, no. 5, pp. 591-599, May 1991.
61. J. R. Bayard, M. E. Cooley and D. H. Schaubert, "A general method for treating infinite arrays of antennas printed on protruding dielectric substrates," *Dig. Int. Symp. Antennas Propagat. Soc.*, Pt. II, pp. 600-603, June 1991.
62. J. R. Bayard, M. E. Cooley and D. H. Schaubert, "Analysis of infinite arrays of printed dipoles on dielectric sheets perpendicular to a ground plane," *IEEE Trans. Antennas Propagat.*, vol. AP-39, no. 12, pp. 1722-1732, Dec. 1991.
63. A. J. Parfitt, D. W. Griffin and P. H. Cole, "On the modeling of metal strip antennas contiguous with the edge of electrically thick finite size dielectric substrate," *IEEE Trans. Antennas Propagat.*, vol. AP-40, no. 2, pp. 134-140, Feb. 1992.
64. M. J. Lancaster, Z. Wu, T. S. M. Maclean and Y. Huang, "Super-cooled and superconducting small-loop and dipole antenna," *Proc. IEE*, vol. 139, pt. H, no. 3, pp. 264-270, June 1992.
65. A. J. Parfitt, D. W. Griffin and P. H. Cole, "Mutual coupling between metal strip antennas in finite size electrically thick dielectric substrate," *IEEE Trans. Antennas Propagat.*, vol. AP-41, no. 1, pp. 109-115, Jan. 1993.
66. R. E. Clapp, "A resistively loaded, printed circuit, electrically short dipole element for wideband array applications," *Dig. Int. Symp. Antennas Propagat. Soc.*, Pt. I, pp. 478-481, Jul. 1993.
67. G. V. Eleftheriades and G. M. Rebeiz, "Cavity backed printed dipole arrays with substrate mode using via-hole technology," *Dig. Int. Symp. Antennas Propagat. Soc.*, Pt. II, pp. 592-595, Jul. 1993.
68. A. J. Parfitt, D. W. Griffin and P. H. Cole, "Controlling cross-polarisation radiation from substrate supported metal strip antennas for use in monolithically fabricated arrays," *Dig. Int. Symp. Antennas Propagat. Soc.*, Pt. II, pp. 596-599, Jul. 1993.
69. A. Nestic and I. Radnovic, "Experimental study of the new broadband printed dipole antenna structure," *Proc. URSI*, p.21, Jul. 1993.
70. J. R. James and C. J. Wilson, "Radiation characteristics of stripline antennas," *Proc. 4th European Microwave Conf.*, pp. 484-488, Sep. 1974.
71. J. R. James and C. J. Wilson, "New design techniques for microstrip antenna arrays," *Proc. 5th European Microwave Conf.*, pp. 102-106, Sep. 1975.

72. J. C. Williams, "A 36 GHz printed planar array," *Electron Lett.*, vol. 14, no. 5, pp. 136-137, Apr. 1978.
73. K. Ito, N. Aizawa and N. Goto, "Circularly polarised microstrip antenna," *Report Tech. Group*, IECE of Japan, AP 78-90, pp. 21-26, 1978.
74. D. A. Huebner, "An electrically small microstrip dipole planar array," *Proc. Workshop Printed Circuit Antenna Technol.*, pp. 17/1-16, Oct. 1979.
75. I. E. Rane and N. G. Alexopoulos, "Printed wire antenna," *Proc. Workshop Printed Circuit Antenna Technol.*, pp. 30/1-38, Oct. 1979.
76. N. K. Uzunoglu, G. Alexopoulos and J. G. Fikior, "Radiation properties of microstrip dipoles," *IEEE Trans. Antennas Propagat.*, vol. AP-27, no. 6, pp. 853-858, Nov. 1979.
77. K. S. Lee and G. Eichmann, "Elementary pattern of conformal dipole arrays mounted on dielectrically clad conducting cylinders," *IEEE Trans. Antennas Propagat.*, vol. AP-28, no. 6, pp. 811-818, Nov. 1980.
78. B. A. Panchenko and S. N. Shabunin, "Radiation characteristics of stripline dipoles," *Radio Engg. Electron Phy.*, vol. 26, no. 6, pp. 10-15, Jan. 1981.
79. I. E. Rane and G. Alexopoulos, "Current distribution and input impedance of printed dipoles," *IEEE Trans. Antennas Propagat.*, vol. AP-29, no. 1, pp. 99-105, Jan. 1981.
80. I. E. Rane and G. Alexopoulos, "Mutual impedance computation between printed dipoles," *IEEE Trans. Antennas Propagat.*, vol. AP-29, no. 1, pp. 106-111, Jan. 1981.
81. H. G. Oltman and D. A. Huebner, "Electromagnetically coupled microstrip dipoles," *IEEE Trans. Antennas Propagat.*, vol. AP-29, no. 1, pp. 151-157, Jan. 1981.
82. R. S. Elliott and G. J. Stern, "Design of microstrip dipole arrays including mutual coupling, Part I: Theory," *IEEE Trans. Antennas Propagat.*, vol. AP-29, no. 5, pp. 757-760, Sep. 1981.
83. R. S. Elliott and G. J. Stern, "Design of microstrip dipole arrays including mutual coupling, Part II: Experiments," *IEEE Trans. Antennas Propagat.*, vol. AP-29, no. 5, pp. 761-765, Sep. 1981.
84. V. Hansen, "Approximate equations for the nearfield of a horizontal electric dipole on a grounded dielectric slab," *Proc. IEE*, vol. 129, pt. H, no. 1, pp. 29-31, Feb. 1982.
85. P. B. Katehi and N. G. Alexopoulos, "On the effect of substrate thickness and permittivity on printed circuit dipole properties," *IEEE Trans. Antennas Propagat.*, vol. AP-31, no. 1, pp. 34-39, Jan. 1983.
86. P. B. Katehi and N. G. Alexopoulos, "Real axis integration of Sommerfeld type integrals with applications to printed circuit antennas," *Jour. Math. Phys.*, vol. 24, no. 3, pp. 527-533, Mar. 1983.
87. D. M. Pozar, "Considerations for millimeter wave printed antennas," *IEEE Trans. Antennas Propagat.*, vol. AP-31, no. 5, pp. 740-747, Sep. 1983.

88. S. M. Wright and Y. T. Lo, "Efficient analysis for infinite microstrip dipole array," *Electron Lett.*, vol. 19, no. 24, pp. 1043-1045, Nov. 1983.
89. K. Masanobu and K. Rokushima, "Input impedance and radiation pattern of a printed dipole on a semi-infinite substrate," *Perfect Ser. A.*, vol. 33, no. 2, pp. 89-104, Feb. 1984.
90. M. T. Birand and N. Williams, "Printed dipole millimeter wave array using an insular guide feeder," *Proc. IEE*, vol. 131, pt. H, no. 2, Apr. 1984.
91. D. M. Pozar and D. H. Schaubert, "Scan blindness in infinite phased array of printed dipoles," *IEEE Trans. Antennas Propagat.*, vol. AP-32, no. 6, pp. 602-610, June 1984.
92. N. G. Alexopoulos and D. R. Jackson, "Fundamental superstrate (cover) effects on printed circuit antennas," *IEEE Trans. Antennas Propagat.*, vol. AP-32, no. 8, pp. 807-816, Aug. 1984.
93. A. J. M. Soares, S. B. de. A. Fonseca and A. J. Giarola, "The effect of dielectric cover on current distribution and input impedance of printed dipole," *IEEE Trans. Antennas Propagat.*, vol. AP-32, no. 11, pp. 1149-1153, Nov. 1984.
94. P. B. Katehi and N. G. Alexopoulos, "On the modeling of electromagnetically coupled microstrip antennas - the printed strip dipoles," *IEEE Trans. Antennas Propagat.*, vol. AP-32, no. 11, pp. 1179-1186, Nov. 1984.
95. J. L. Tsulamengas and N. K. Uzunoglu, "Radiation from a dipole in the proximity of a general anisotropic ground layer," *IEEE Trans. Antennas Propagat.*, vol. AP-33, no. 2, pp. 165-172, Feb. 1985.
96. N. G. Alexopoulos, D. R. Jackson and P. B. Katehi, "Criteria for nearly omnidirectional radiation patterns for printed antennas," *IEEE Trans. Antennas Propagat.*, vol. AP-33, no. 2, pp. 195-205, Feb. 1985.
97. D. M. Pozar, "General relation for phased array of printed antennas derived from infinite current sheets," *IEEE Trans. Antennas Propagat.*, vol. AP-33, no. 5, pp. 498-504, May 1985.
98. M. K. Kominami, D. M. Pozar and D. H. Schaubert, "Dipole and slot elements and arrays on semi-infinite substrate," *IEEE Trans. Antennas Propagat.*, vol. AP-33, no. 6, pp. 600-607, June 1985.
99. D. R. Jackson and N. G. Alexopoulos, "Gain enhancement method for printed circuit antennas," *IEEE Trans. Antennas Propagat.*, vol. AP-33, no. 9, pp. 976-987, Sep. 1985.
100. D. R. Jackson and N. G. Alexopoulos, "Microstrip dipoles on electrically thick substrate," *Int. Jour. Microwave Millimeter Wave.*, vol. 7, no. 1, Jan. 1986.
101. R. W. Jackson, "Printed dipoles electromagnetically coupled to coplanar waveguide for linear or circular polarisation," *Electron Lett.*, vol. 22, no. 6, pp. 324-326, Mar. 1986.
102. D. R. Jackson and N. G. Alexopoulos, "Analysis of planar strip geometries in a substrate-superstrate configuration," *IEEE Trans. Antennas Propagat.*, vol. AP-34, no. 12, pp. 1430-1438, Dec. 1986.

103. D. R. Jackson and N. G. Alexopoulos, "An asymptotic extraction technique for evaluating Sommerfeld-type integrals," *IEEE Trans. Antennas Propagat.*, vol. AP-34, no. 12, pp. 1467-1470, Dec. 1986.
104. P. B. Katehi, N. G. Alexopoulos and I. Y. Hsia, "A bandwidth enhancement method for microstrip antennas," *IEEE Trans. Antennas Propagat.*, vol. AP-35, no. 1, pp. 5-12, Jan. 1987.
105. P. Lepeltier, J. M. Flock and J. Citerne, "Complete and rigorous analysis of electromagnetically coupled transverse microstrip dipole," *Electron Lett.*, vol. 23, no. 16, pp. 822-824, Jul. 1987.
106. H. Y. Yang and N. G. Alexopoulos, "Gain enhancement methods for printed circuit antennas through multiple substrates," *IEEE Trans. Antennas Propagat.*, vol. AP-35, no. 7, pp. 860-863, Jul. 1987.
107. D. W. Griffin and M. Kara, "Experimental evidence that microstrip patches and flat dipoles on grounded substrates are same type of element," *Dig. Int. Symp. Antennas Propagat. Soc.*, Pt. II, pp. 458-461, June 1988.
108. S. Barkeshli and P. H. Pathak, "An efficient moment method analysis of finite phased arrays of microstrip dipoles using an asymptotic closed form approximation for the planar microstrip Green's function," *Proc. URSI*, p. 387, June 1988.
109. M. A. Blischke, E. J. Rothwell and K. M. Chen, "Scattering from an impedance loaded printed dipole array," *Proc. URSI*, p.388, June 1988.
110. A. Hoofar, K. C. Gupta and D. C. Chang, "Cross-polarisation level in radiation from a microstrip dipole," *IEEE Trans. Antennas Propagat.*, vol. AP-36, no. 9, pp. 1197-1203, Sep. 1988.
111. P. Russo and M. Ruggieri, "A high gain microstrip array adopting EMC dipoles," *Microwave Opt. Technol. Lett.*, vol. 1, no. 8, pp. 299-304, Oct. 1988.
112. K. M. Lee and R. S. Chu, "Analysis of mutual coupling between finite phased array of dipoles and its feed network," *IEEE Trans. Antennas Propagat.*, vol. AP-36, no. 12, pp. 1681-1699, Dec. 1988.
113. P. B. Katehi, "Mutual coupling between microstrip dipoles in multilayered arrays," *IEEE Trans. Antennas Propagat.*, vol. AP-37, no. 3, pp. 275-280, Mar. 1989.
114. N. K. Das and D. M. Pozar, "Analysis and design of series fed printed dipoles proximity coupled to a perpendicular microstrip line," *IEEE Trans. Antennas Propagat.*, vol. AP-37, no. 4, pp. 435-444, Apr. 1989.
115. M. Gaouyer, J. M. Floch and J. Citerne, "Radome effect on an electromagnetically coupled dipole," *Dig. Int. Symp. Antennas Propagat. Soc.*, Pt. II, pp. 612-615, June 1989.
116. H. Y. Yang, N. G. Alexopoulos, P. M. Lepeltier and G. J. Stern, "Design of transversely fed EMC microstrip dipole arrays including mutual coupling," *IEEE Trans. Antennas Propagat.*, vol. AP-38, no. 2, pp. 145-151, Feb. 1990.

117. D. R. Jackson, A. E. Dinbergs and S. A. Long, "A moment method design procedure for an array of EMC dipoles," *IEEE Trans. Antennas Propagat.*, vol. AP-38, no. 5, pp. 766-770, May. 1990.
118. G. W. Hanson and D. P. Nyquist, "Coupling of impressed radiation to resonant microstrip dipole currents deduced from a Hallen - type integral equation," *Dig. Int. Symp. Antennas Propagat. Soc.*, Pt. II, pp. 652-655, May. 1990.
119. S. L. Dvorak, "Analysis of printed strip dipole antenna used as a hyperthermia applicator," *Proc. URSI*, p. 20, May 1990.
120. P. M. Lipeltier, J. Citerne and J. M. Floch, "On the EMC dipole feedline parasitic radiation," *IEEE Trans. Antennas Propagat.*, vol. AP-38, no. 6, pp. 878-882, June 1990.
121. A. Paul and I. Gupta, "An analysis of log periodic dipole antenna with printed dipoles," *IEEE Trans. Microwave Theory Technol.*, vol. MTT-29, no. 2, pp. 114-117, Feb. 1991.
122. J. H. Clote and W. I. George, "An S-parameter model for the design of arrays of inclined strip dipoles proximity coupled to a microstrip feedline," *Trans. South Afr. Inst. Electronic. Engg.*, vol. 82, no. 1, pp. 1-8, Mar. 1991.
123. P. V. Brennan, "Low cost phased array antenna for land mobile satcom applications," *Proc. IEE*, vol. 138, pt. H, no. 2, pp. 131-136, Apr. 1991.
124. C. J. Alder, C. B. B. Taylor, M. Dixon, R. D. Hodges, L. D. Irving and H. D. Rees, "Microwave and millimeter wave receivers with integral antennas," *Proc. IEE*, vol. 138, pt. H, no. 3, pp. 253-257, June 1991.
125. G. W. Hanson and D. P. Nyquist, "Perturbation formulation for nearly-degenerate microstrip dipole eigenmodes," *Dig. Int. Symp. Antennas Propagat. Soc.*, Pt. I, pp. 80-83, June 1991.
126. T. S. Hong and N. G. Alexopoulos, "Microstrip linear array of EMC dipoles with a corporate feed," *Dig. Int. Symp. Antennas Propagat. Soc.*, Pt. II, pp. 634-637, June 1991.
127. W. Hong, "Mutual impedance analysis of broadband coupled asymmetrical printed dipoles," *Dig. Int. Symp. Antennas Propagat. Soc.*, Pt. II, pp. 844-847, June 1991.
128. N. W. Montgomery and D. R. Wilton, "Analysis of arbitrary conducting periodic structures imbedded in layered media," *Dig. Int. Symp. Antennas Propagat. Soc.*, Pt. III, pp. 1889-1892, June 1991.
129. P. K. Potharazu and D. R. Jackson, "Analysis and design of a leaky-wave EMC dipole," *Proc. Program Elect. Res. Symp.*, p. 288, Jul. 1991.
130. R. R. Crzybowski, R. Bansal and F. C. Jain, "Design and characterisation of travelling wave microstrip dipole antennas," *Proc. Program Elect. Res. Symp.*, p. 687, Jul. 1991.
131. M. A. Hassan, A. Al. Jabri and K. Al. Hakbani, "Point matching method for reduction of anomalous radiation of log-periodic dipole array," *Electron Lett.*, vol. 27, no. 15, pp. 1315-1317, Jul. 1991.

132. J. Seaux, A. Reineix and B. Jecko, "Double resonance antenna", *Microwave Opt. Technol. Lett.*, vol. 4, no. 10, pp. 383-384, Sep. 1991.
133. N. K. Das and D. M. Pozar, "Multiport scattering of general multilayered printed antennas fed by multiple feed ports: Part I-Theory," *IEEE Trans. Antennas Propagat.*, vol. AP-40, no. 5, pp. 469-481, May. 1992.
134. N. K. Das and D. M. Pozar, "Multiport scattering of general multilayered printed antennas fed by multiple feed ports: Part II-Applications," *IEEE Trans. Antennas Propagat.*, vol. AP-40, no. 5, pp. 482-491, May. 1992.
135. A. N. Tulintseff, "Series fed type linear arrays of dipole and slot elements transversely coupled to a microstripline," *Dig. Int. Symp. Antennas Propagat. Soc.*, Pt. I, pp. 128-131, Jul. 1993.
136. R. H. MacPhie, "The impedance of a center-fed strip dipole by the Poynting vector method," *Dig. Int. Symp. Antennas Propagat. Soc.*, Pt. III, pp. 1462-1465, Jul. 1993.
137. B. T. DeWitt and W. D. Burnside, "Electromagnetic scattering by pyramidal and wedge absorbers," *IEEE Trans. Antennas Propagat.*, vol. AP-46, no. 7, pp. 971-984, July 1988.
138. P. Mohanan, C. K. Aanandan, K. A. Jose, K. Vasudavan and K. G. Nair, "Measurement and analysis of radiation pattern using HP 8510B network analyser," *Proc. APSYM*, pp. 424-429, 1992.
139. K. C. Gupta, R. Garg and I.J. Bhal, *Microstrip lines and slot - lines*, Artech House, Dedham, MA, p. 11, 1979.
140. G. H. Brown and O. M. Woodward, Jr., "Experimentally determined radiation characteristics of conical and triangular antennas," *RCA Rev.*, vol. 13, pp. 425-452, Dec. 1952.
141. P. Perlmutter, S. Shtrikman and D. Terves, "Electric surface current model for the analysis of microstrip antennas with application to rectangular elements," *IEEE Trans. Antennas Propagat.*, vol. AP-33, no. 3, pp. 301-311, Mar. 1985.
142. R. F. Harrington, *Time harmonic electromagnetic fields*, McGraw Hills, New York, p. 169, 1981.
143. E. F. Kuester and D. C. Chang, "A geometrical theory for the resonant frequencies and Q-factors of some triangular microstrip patch antennas," *IEEE Trans. Antennas Propagat.*, vol. AP-31, no. 1, pp. 27-34, Jan. 1983.
144. R. Stockton and R. Hockensmith, "Application of spherical arrays - A simple approach.," *Dig. Int. Symp. Antennas Propagat. Soc.*, pp. 202-205, Jul. 1977.
145. G. C. Sandford, "Conformal microstrip phased array for aircraft tests with AT-6," *IEEE Trans. Antennas Propagat.*, vol. AP-26, no. 5, pp. 642-646, Sept. 1978.
146. C. H. Chen, A. Tulintseff and R. M. Sorbello, "Broadband two layer microstrip antenna," *Dig. Int. Symp. Antennas Propagat. Soc.*, pp. 251-254, Jul. 1984.

147. J. Kinzel, B. J. Edward and D. Rees, "V-band space-based phased array antenna," *Microwave J.*, pp. 89-102, Jan. 1987.
148. I. J. Bhal and P. Bhatia, *Microstrip antennas*, Artech House, Dedham, MA, p. 119, 1981.
149. M. K. Wu, J. R. Ashburn, C. J. Torng, P. M. Hor, R. L. Meng, L. Gao, Z. J. Huang, Y. Q. Wang and C. W. Chu, "Superconductivity at 93 K in a new mixed-phase YBaCuO compound system at ambient pressure," *Phys. Rev. Lett.*, vol.58, no. 9, pp. 908-910, Mar. 1987.
150. J. G. Bednorz and K. A. Muller, "Possible high T_c superconductivity in the BaLaCuO system," *Z. Phys. B. Condens. matter*, vol. 64, pp. 189-193, 1986.
151. R. C. Hansen, "Superconducting antennas," *IEEE Trans. Aerop. Electron. Syst.*, vol. 26, no. 2, pp. 345-355, Mar. 1990.
152. M. Fujinaka, T. Ishida, T. Goto, K. Takel and T. Maehara, "Trial manufacture of dipole antenna using YBCO ceramic wire," *Int. J. Electron.*, vol. 67, no. 2, pp. 245-250, Feb. 1989.
153. Y. S. He, A. S. He, X. X. Zhang, C. S. Shi, N. Lu, B. Tian, D. R. Lu, M. L. Zhou and W. G. Wang, "Progress in High T_c superconducting ceramic antenna," LT19 Conf., U.K., 1990.
154. Z. Wu, T. S. M. Maclean, M. J. Lancaster, C. E. Gough and N. McN. Alform, "Supercooled and superconducting small loop antenna," IEE Colloquium on Microwave applications of High Temperature Superconductors, No. 1989/16, Oct. 1989.
155. H. K. Verma, P. Mukundan, K. G. Warriar and A. D. Damodaran, "Nonaqueous cold extrusion as a route for Yttrium Barium Copper oxide wires," *J. Am. Ceram. Soc.*, vol. 73, no. 10, pp. 3100-3102, Oct. 1990.

Index

Agrawal	21	Array	
Alder	39	cavity backed printed	8
Alexopoulos	28-30, 32-35, 39	circularly polarised	27, 30
Anechoic chamber	50	cylindrical	28
Antenna		dielectric waveguide	5
cavity backed printed	6	EMC dipole	36, 39
circular patch	186	flat	23
electrically small	192	linear	30
Franklin	8, 16	log periodic microstrip dipole	38, 40
leaky wave	40	microstrip dipole	27
lens	22	millimeter wave	192
microstrip	10, 186	monopulse	21, 27, 30
rectangular patch	12, 159, 186	phased	189
sandwich wire	10	planar dipole lens	22
slot	2, 34	resonant	2, 27
superconducting	193	series-fed-type	41
superconducting loop	25, 193	steerable	24
trapezoidal slot	26	super-directive	192
triplate	5	travelling wave	2, 27, 192
waveguide	2	triplate slotted	6
Anti-resonance	18	waveguide	3
Aperture blockage	20	Athanasas	23

Babinet's principle	3	Gaouyer	37
Baily	21	George	38
Baissinot	10	Graham	10
Barkeshli	36	Green's function	160
Bayard	24	Griffin	24, 36
Beauquat	21	Gulton	10
Berithaupt	5	Gupta	38
Birand	31	Hallen's equation	38
Blischke	36	Hanley	19
Bloch-wave analysis	40	Hansen	30
Brennan	39	Hanson	38, 39
Byron	10	Harsch	17
Characteristics impedance	167	Hassan	40
Chi	36	Hong	39
Chu	22, 24	Huebner	27, 29
Circular polarisation	8	Insular guide	31
Clapp	26	Ito	20, 23, 27
Clate	38	Jackson	32, 34, 35, 37, 40
Compton	22	James	27
Conformal transformation technique	20	Kahrilas	17
Contour integral	32	Kara	36
Corner reflector	183	Katehi	30, 32, 35, 37
Cosecant square pattern	183	Keen	19
Crzybowski	40	Khamas	23
Das	37, 40	Kominami	34
Deschamps	10	Kraus	1
Dielectric lens	24	Lampe	21
Dipole		Lancaster	25
cylindrical	193	Lee	22, 24, 28, 36
flat triangular	147	Levine	23
Hertzian	28, 29, 32	Linear polarisation	8
Hertzian magnetic	3	Lipeltier	38
microstrip	12, 27, 47, 181	Lo	31
printed	6, 16, 43, 178	MacPhic	41
short superconducting	23, 25, 193	Maddocks	24
Dipole moment	12	Masanobu	31
Dolph-Chebyshev pattern	39	McDonough	8, 17
Doppler module	18	Microstrip dipole	
Dubost	8, 14, 18-22	asymmetric	39
Dvoark	38	EMC	27, 29, 30, 32, 35, 37, 38, 40
Effective dielectric constant	166	triangular	47, 147
Eichmann	28	triangular arm	131
Electromotive force method	160	triangular end-loaded	47, 131-132
Eleftheriades	26	Mohsen	21
Elliott	30	Montgomery	39
Extraction principle	194	Muha	20
Floquet mode	17, 33	Munson	10
Fourier domain	160	Nanbu	18
Fourier transformation technique	33	Network analyser	52
Fredholm integral equation	30	Newman	19
Fubini	8, 16	Nyquist	38, 39

Oliner	3, 5	Schiffman	8
Oltman	14, 27, 29	Schiffman balun	19
Othius	18	Schockly detector diode	20
Panchenko	28	Seaux	40
Paraboloidal reflector	19	Series waveguide feed	3
Parfitt	24, 25	Shabunin	28
Pathok	36	Sidford	8, 18, 19
Paul	38	Singh	18
Perini	19	Skalar	24
Perlmutter	159	Smith	24
Perturbation technique	28, 39	Soares	32
Pocklington's equation	29, 32, 34	Spectral domain	31
Potential method	160	Stark	17
Potharazu	40	Stationary phase integration	28
Powell	21	Steepest descent technique	38
Poynting theorem	22	Stern	30
Pozar	31, 33, 37, 40	Stevenson	3
Prafitt	25, 26	Strip-gratings structure	184
Printed dipole		Subhnani	20
asymmetric folded	21	Superconducting ceramic material	192
bow-tie	20, 22	Superdirectivity	20
capacitive-coupled	17	Surface wave modes	165
cavity backed	26	Time Domain	31
cavity backed parallelogram		Tsulamengas	33
end-loaded	123	Tulintseff	41
cavity backed triangular		Uzunoglu	28, 33
end-loaded	106	Variational method	28
fan	21	Vinatier	20
flared	43, 66, 171	Watson transformation method	28
flared triangular	21	Waveguide simulator	24, 25, 32
flat folded	19-22, 24, 25	Wilkinson	6, 17
parallelogram end-loaded	43, 114	Williams	27, 31
rectangular	43, 166	Wilson	27
resistively loaded triangular	26	Wilton	39
superconducting	23	Wright	31
trapezoidal	26	Yang	35, 37
triangular	26		
triangular end-loaded	43, 84, 172		
triangular with cap	26		
Quality factor	159		
Rabbaa	20		
Radnovic	26		
Rane	28, 29		
Rao	20		
Rebeiz	26		
Rokushima	31		
Ruggieri	36		
Russo	36		
Rutledge	20		
Scan blindness	25, 26, 32, 33		
Schaubert	31		

LIST OF PUBLICATIONS OF THE AUTHOR

Journal Papers

1. "Wide-band printed dipole antenna", *Microwave and Optical Technology Letters*, USA, vol.4, no.10., pp. 417-419, Sep. 1991.
2. "Wideband Microstrip dipole", *Microwave and Optical Technology Letters*, USA, vol.5, no.12, pp. 709-712, Dec. 1992.
3. "A Modified Circular Microstrip Antenna", *Electronics Letters*, UK, vol.29, no.12, 1126-1127, June 1993.
4. "Wideband printed dipole antenna", *Journal of IETE*, vol. 10, no. 3, pp. 225-228, May-June 1993.

Symposium Papers

1. "Bandwidth enhancement by flared microstrip dipole antenna", *Dig. Int. Symp. Antennas Propagat. Soc.*, USA, pp. 342-345, Jul. 1991.
2. "Novel wideband Microstrip dipole antenna", *Proc. of the National Symp. on Antennas and Propagation APSYM-92*, pp. 252-255, Dec. 1992.
3. "A New Circular Microstrip Antenna", *Dig. Int. Symp. Antennas Propagat. Soc.*, USA, pp. 976-979, Jul. 1993.
4. "Performance of a YBCO superconducting wire loop antenna", *Dig. Int. Symp. Antennas Propagat. Soc.*, USA, pp. 1516-1519, Jul. 1993.
5. "Synthesis and microwave characterisation of $Ba_{1-x}Sr_x(B_{1/2}^{3+}Nb_{1/2}^{5+})O_3$ [$B^{3+} = Sm, Gd, Er$] dielectric resonators", *Proc. IV Int. Symp. on Recent Advances in Microwave Tech.*, pp. 565-568, Dec. 1993.

REPRINTS OF PAPERS PUBLISHED
IN JOURNALS

BY THE AUTHOR

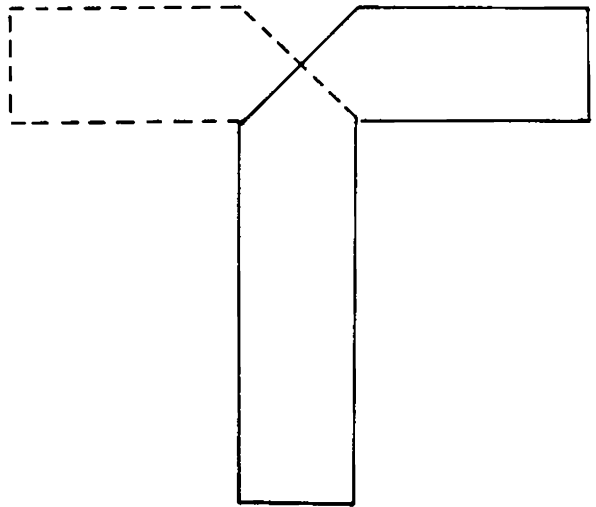


Figure 1 Schematic diagram of conventional printed dipole antenna. Dotted line shows the ground arm etched on the other side of the substrate

Recently the authors have developed a wideband printed dipole with an impedance bandwidth of 30% without using a cavity backup [5]. A further enhancement of radiation efficiency and impedance bandwidth of a printed dipole with no cavity backup has been reported in this article. Its design considerations and experimental details are also presented.

DESIGN APPROACH

A conventional printed dipole is shown in Figure 1. It was experimentally observed that a considerable increase in impedance bandwidth is possible by proper inductive loading. A detailed experimental investigation was carried out with various shapes and sizes. The antenna with triangular loading, having 100° apex angle, is found to be optimum for impedance bandwidth and radiation pattern. To compensate the inductive part, a stub is also used. It was also observed that antenna parameters are too sensitive to stub parameters. Incorporating these factors, the new optimum antenna design is as shown in Figure 2.

WIDE-BAND PRINTED DIPOLE ANTENNA

Supriyo Dey, C. K. Aanandan, K. A. Jose, P. Monahan, and K. G. Nair
 Department of Electronics
 Cochin University of Science and Technology
 Cochin 682 022, India

KEY TERMS

Antennas, printed dipoles, impedance bandwidth

ABSTRACT

The design and development of an L-band printed dipole antenna, optimized for wide-band applications near first resonance, is reported. This design has achieved more than 48% impedance bandwidth (VSWR 2:1), without degrading its overall radiation efficiency.

INTRODUCTION

Microstrip antennas are fast replacing conventional antennas due to such merits as low cost, light weight, small size, and convenience for mass production. However, there is an inherent disadvantage of very narrow impedance bandwidth for these antennas. Bandwidth enhancement is reported using electromagnetically gap-coupled parasitic elements [1, 2] or by traveling-wave technique [3]. However, in both cases, bandwidth enhancement was achieved at the expense of efficiency. Bailey [4] has reported a cavity-backed printed dipole having an impedance bandwidth of 37%.

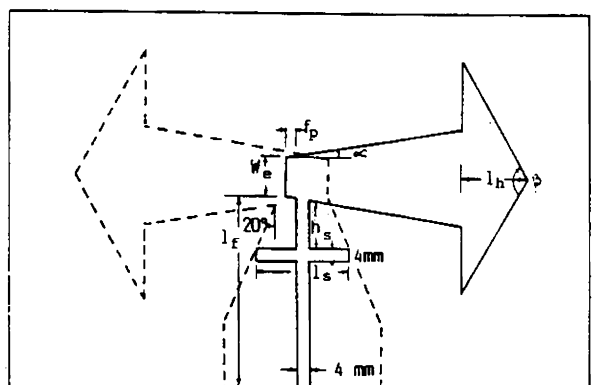


Figure 2 Schematic diagram of new antenna. Dotted line shows the ground arm etched on the other side of the substrate

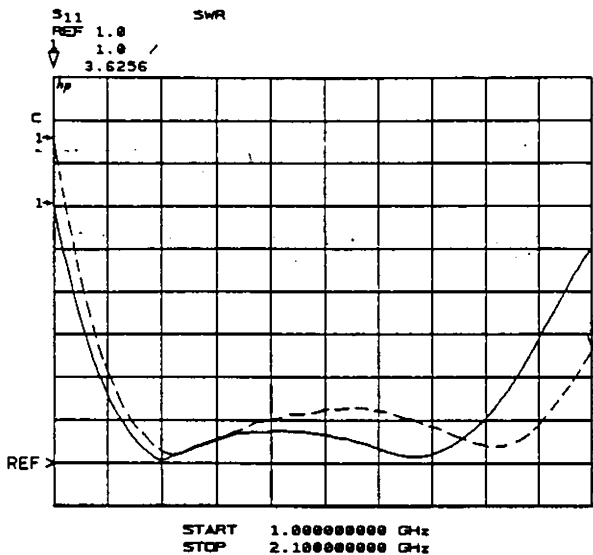


Figure 3 Variation of impedance with frequency. Solid line, $h_1 = 1.4$ cm; dashed line, $h_1 = 1.2$ cm

DESIGN DETAILS

The design details of the optimum antenna, as shown in Figure 2, are

Main arm length	$l_1 = 0.475 \lambda_d$
Altitude	$h_1 = 0.209 \lambda_d$
End width	$W_e = 0.076 \lambda_d$
Feed separation from end	$f_p = 0.021 \lambda_d$
Stub separation from patch	$h_2 = 0.119 \lambda_d$
Stub length	$l_2 = 0.307 \lambda_d$
Feed line length	$l_f = 0.553 \lambda_d$
Flare angle	$\alpha = 8^\circ$
Apex angle	$\beta = 100^\circ$

where $\lambda_d (= \lambda/\sqrt{\epsilon_r})$ represents the wavelength in the dielectric material. Here ϵ_r is the dielectric constant of the substrate and λ is the free-space wavelength corresponding to the central frequency.

Except for flare angle and apex angle, all other parameters

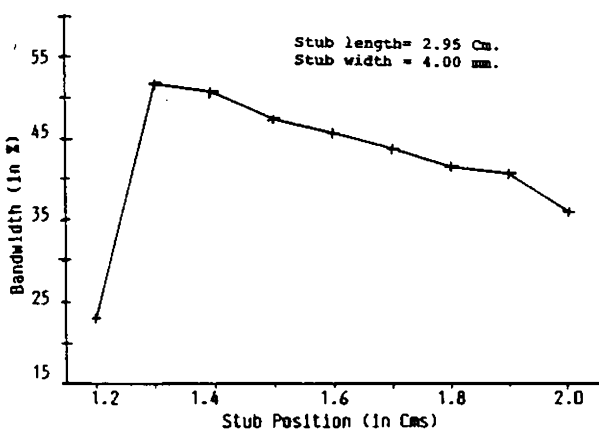


Figure 4 Variation of bandwidth with stub position (h_1)

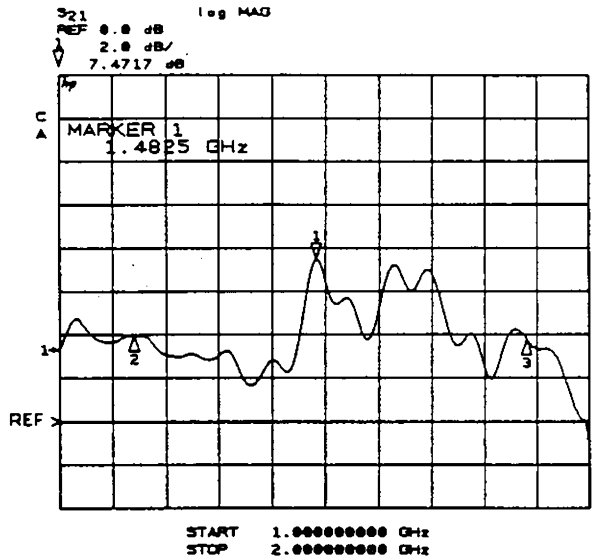


Figure 5 Variation of the S_{21} of new antenna with frequency compared to a standard dipole. REF is for conventional dipole and the trace is of the new antenna

of the ground arm, which is on the other side of the main arm, are kept 1.05 times larger than those of the respective main arm parameters, for optimum bandwidth. The same flares and apex angles for both arms show better radiation patterns.

EXPERIMENTAL RESULTS

An antenna is fabricated over a dielectric substrate ($\epsilon_r = 4.2$) to operate at a central frequency of 1.5 GHz. Typical variations of impedance with frequency for two stub positions are

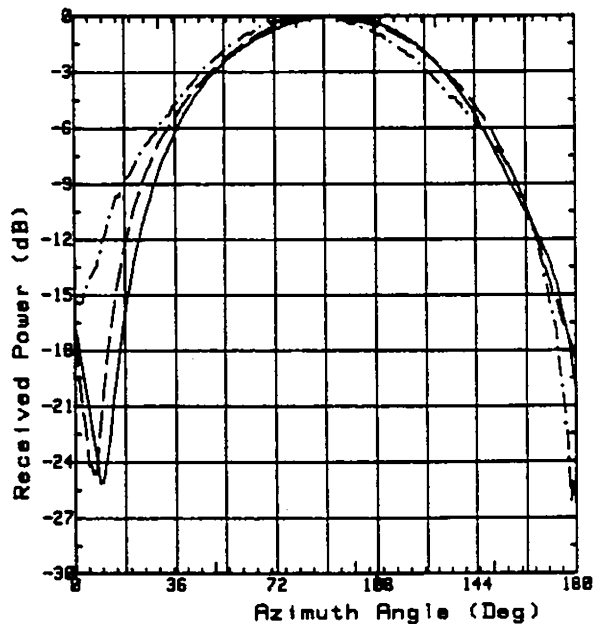


Figure 6 E-plane radiation patterns. Solid line, 1.14 GHz; dashed line, 1.50 GHz; dash-dotted line, 1.88 GHz

shown in Figure 3. From the figure it is clear that the impedance bandwidth of the antenna is 50.52% when the stub position is 1.4 cm. Variation of bandwidth with stub position is shown in Figure 4. The bandwidth is maximum for a stub position of 1.3 cm.

From the preceding it is clear that a slight shift in the stub position toward the antenna arm deteriorates the impedance bandwidth. When the stub position is 1.3 cm from the radiating arm, the central part of the VSWR trace just grazes the $VSWR = 2$ line. Hence for a safer design, h_s is selected as 1.4 cm in the present study. The other two parameters of the stub, namely, stub width and stub length, are also optimized after extensive experimental iterations.

A comparison of the gain of new antenna (Figure 2) with a conventional one (Figure 1), having the same physical area and operating frequency of 1.5 GHz, is presented in Figure 5. In Figure 5, the above figure, markers 2 and 3 represent the start and end frequencies of the operating bandwidth. In this band, the gain of the new antenna is found to be greater than 2 dB and at the design frequency, the gain is 6 dB more than the conventional one. This confirms the bandwidth enhancement of the antenna without any kind of ohmic losses.

The E -plane radiation patterns, plotted using a time-gating technique with HP8510B-based instrumentation for three different frequencies are shown in Figure 6. The radiation patterns confirm that the antenna is not exhibiting beam squinting with frequency.

CONCLUSION

Design, development, and experimental data on a broadband printed dipole antenna are reported. It has been shown that an impedance bandwidth of more than 48% can be achieved without affecting the radiation efficiency. This antenna can be used in a wideband phased array or as a primary feed for reflectors.

ACKNOWLEDGMENT

The authors wish to acknowledge the University Grants Commission (U.G.C.) and the Ministry of Human Resource Development (MHRD), Government of India, for financial assistance.

REFERENCES

1. C. K. Aanandan and K. G. Nair, "Compact Broad Band Microstrip Antennas," *Electron. Lett.*, Vol. 22, 1986, pp. 1064-1065.
2. G. Kumar and K. C. Gupta, "Non-Radiating Edges and Four Edges Gap Coupled with Multiple Resonator, Broadband Microstrip Antennas," *IEEE Trans. Antennas Propagat.*, Vol. 33, No. 2, 1985, pp. 173-178.
3. J. L. Drewniak and P. E. Mayers, "ANSERLIN a Broad-band Low Profile, Circularly Polarized Antenna," *IEEE Trans. Antennas Propagat.*, Vol. 37, No. 3, 1989, pp. 281-288.
4. M. C. Bailey, "Broad-Band Half Wave Dipole," *IEEE Trans. Antennas Propagat.*, Vol. 32, No. 4, 1984, pp. 410-412.
5. S. Dey, P. Venugopalan, K. A. Jose, C. K. Aanandan, P. Mohanan, and K. G. Nair, "Bandwidth Enhancement by Flared Microstrip Dipole Antenna," Accepted for presentation in 1991 IEEE AP-S Int. Symp., Canada.

Received 5-22-91

WIDEBAND MICROSTRIP DIPOLE

Supriyo Dey, C. K. Aanandan, K. A. Jose, P. Mohanan, and

K. G. Nair

Department of Electronics

Cochin University of Science & Technology

Cochin—682 022, India

KEY TERMS

Antenna, microstrip dipole, impedance bandwidth

ABSTRACT

The design details of a new wideband half-wave microstrip dipole antenna, suitable for low-frequency operation, having more than 5% 2:1 VSWR bandwidth, are presented. The bandwidth enhancement is achieved by proper end-loading of the dipole arms. The design includes stripline feeding mechanism to avoid unwanted radiation from the feeding structure. © 1992 John Wiley & Sons, Inc.

INTRODUCTION

Antennas printed on thin and grounded dielectric substrates are becoming increasingly important for electronically scanned antenna systems. Such antennas present many advantages like light weight, low production cost, small size, and convenience in flush mounting configurations over the conventional antennas. Dipoles are highly amiable in printed array configurations.

In the past few years properties of microstrip dipoles have been extensively studied in the literature [1–3]. However, the impedance bandwidth of such dipoles is extremely narrow. The antenna described here is the result of an attempt to optimize the impedance bandwidth of microstrip dipoles.

DESIGN APPROACH

The impedance bandwidth of a conventional dipole is restricted due to rapid variation of impedance near the resonance. In the earlier work (4) done by the authors on printed dipoles, it was observed that impedance variation can be restricted considerably by end-loading of the dipole. In the case of microstrip dipoles, like printed dipoles, it is found that triangular loading at the arm ends gives better impedance bandwidth compared to any other shape.

Figure 1 shows the complete antenna structure, consisting of two layered substrates. The dipole arms are etched on either side of a substrate and placed over a grounded substrate. The ground arm of the dipole is shown by the solid line and the main arm by the dotted line. The ground arm

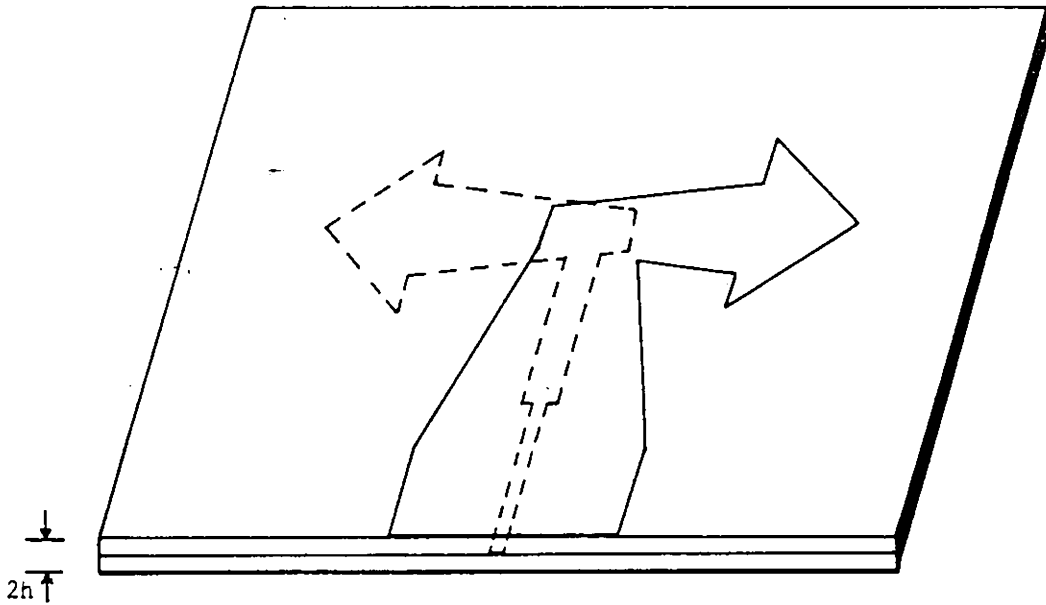


Figure 1 Top view of the complete dipole

feed line is electrically coupled to the ground plane to form stripline feed.

Further bandwidth enhancement is achieved by keeping the main arm 1.165 times shorter than the ground arm. Apparently the feeding mechanism to the antenna and the difference in the separation of the arms from ground plane effectively increases the main arm length. An impedance transformer (T) of 21.5Ω is also used to match the low dipole impedance with $50\text{-}\Omega$ feed line (F).

DESIGN DETAILS

The antenna schematic is shown in Figure 2. The design details are

$$W = 0.053 \lambda_d,$$

$$l_g = 0.352 \lambda_e,$$

$$l_m = 0.302 \lambda_e,$$

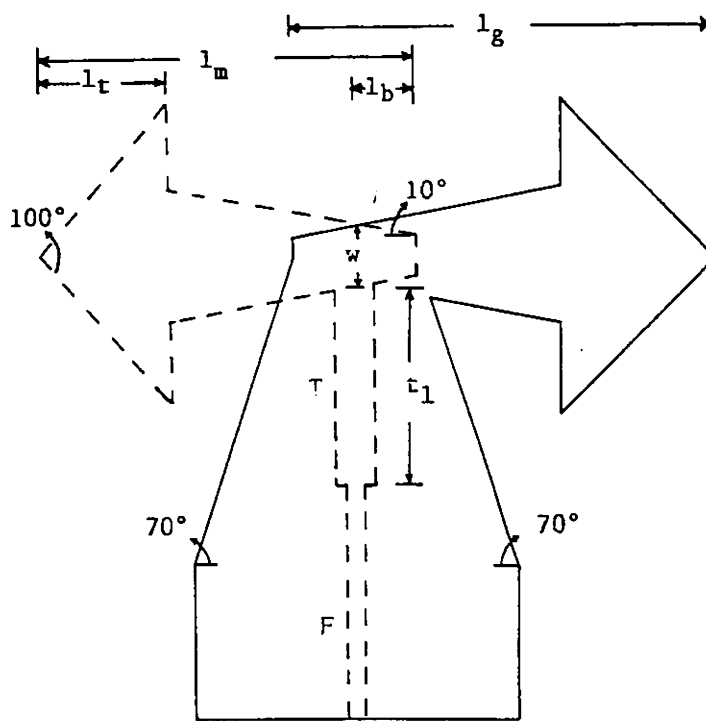


Figure 2 Schematic of the dipole

$$l_b = 0.05 \lambda_e$$

$$l_t = 0.101 \lambda_e$$

$$t_1 = 0.22 \lambda_d$$

where $\lambda_d = \lambda/\sqrt{\epsilon_r}$ and $\lambda_e = \lambda/\sqrt{\epsilon_{eff}}$. The effective dielectric constant ϵ_{eff} is calculated using the conventional microstrip formula (5) and is given as

$$\epsilon_{eff} = \frac{\epsilon_r + 1}{2} + \frac{\epsilon_r - 1}{2} \times \frac{\ln(\pi/2) + (1/\epsilon_r) \ln(4/\pi)}{\ln(8h'/W)} \quad (1)$$

Here h' ($=3h/2$) is taken as the average substrate thickness due to the difference in the separation of ground arm and main arm from the ground plane. Other ground arm parameters are same as that of the corresponding main arm parameters.

RESULTS

An antenna is fabricated over a dielectric substrate ($\epsilon_r = 4.5$ and thickness $h = 1.55$ mm) to operate at a central frequency of 1.15 GHz.

Figure 3 shows the variation of input VSWR of the microstrip dipole with frequency. From figure it is clear that 2:1 VSWR bandwidth is from 1.114 GHz to 1.194 GHz.

The E -plane radiation patterns at the central and at the two end frequencies are shown in Figure 4. Radiation patterns show that there is a slight shift in beam maximum of around 14° . This can easily be corrected in phased arrays by a proper progressive phase shift between the elements. The 3-dB beamwidth of 71° at central frequency confirms the broad radiation characteristics of dipole.

The radiation efficiency of the antenna is compared with a conventional microstrip patch having the same physical area, etched on the same dielectric substrate and resonating at the

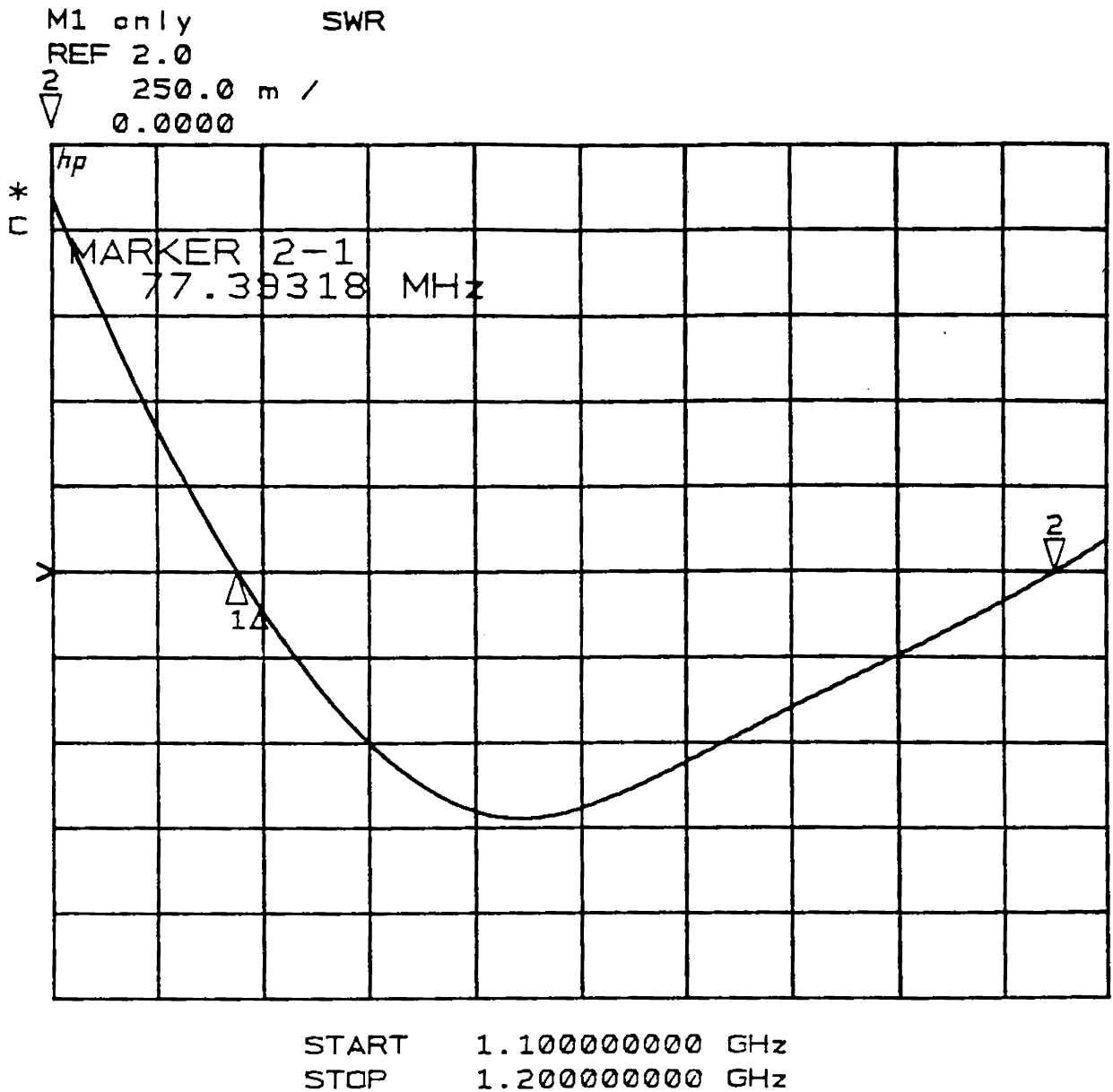


Figure 3 Variation of input VSWR with frequency

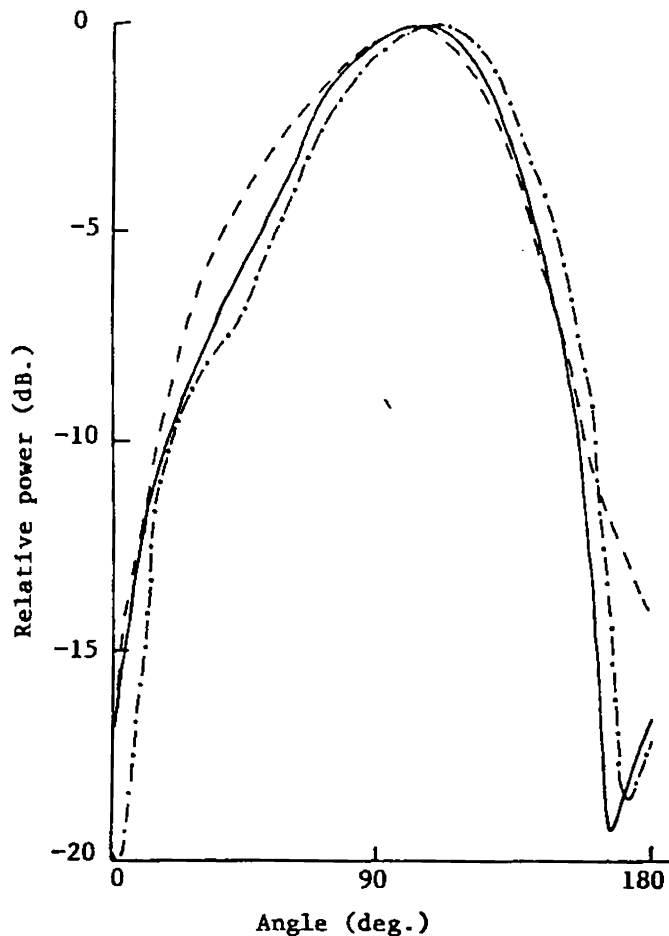


Figure 4 E-plane radiation pattern. Dashed line, 1.114 GHz; solid line, 1.5 GHz; dash-dot line 1.194 GHz

central frequency of the new dipole antenna. The gain of the new antenna is only 0.5 dB less compared to the microstrip patch. This confirms that the bandwidth enhancement is achieved without much degradation in radiation efficiency.

CONCLUSION

The design details and the experimental observations of a wideband microstrip dipole are presented. This newly developed dipole has better impedance bandwidth compared to the microstrip dipoles reported earlier. The antenna design includes stripline feed to avoid the unwanted radiation from feed structure. This dipole can replace the conventional dipoles or the existing microstrip antennas in phased array applications.

ACKNOWLEDGEMENT

One of the authors, Supriyo Dey, acknowledges the University Grants Commission for providing a Research Fellowship.

REFERENCES

1. I. M. Rana and N. G. Alexopoulos, "Current Distribution and Input Impedance of Printed Dipoles," *IEEE Trans. Antennas Propagat.*, Vol. AP-29, No. 1, Jan. 1981, pp. 99-105.
2. P. B. Katehi and N. G. Alexopoulos, "On the Effect of Substrate Thickness and Permittivity on Printed Circuit Dipole Properties," *IEEE Trans. Antennas Propagat.*, Vol. AP-31, No. 1, Jan. 1983, pp. 34-39.
3. K. C. Gupta and A. Hoorfar, "Cross-Polarisation Level in Radiation from a Microstrip Dipole Antenna," *IEEE Trans. Antennas Propagat.*, Vol. AP-36, No. 9, June 1988, pp. 1197-1203.
4. S. Dey, C. K. Aanandan, K. A. Jose, P. Mohanan, and K. G. Nair, "Wideband Printed Dipole Antenna," *Microwave Optical Technol. Lett.*, Vol. 4, No. 10, Oct. 1991, pp. 112-114.
5. K. C. Gupta, R. Garg, and I. J. Bhal, *Microstrip Lines and Slotlines*, Artech House, Dedham, MA, 1979.

Received 7-8-92

Microwave and Optical Technology Letters, 5/13, 709-712
 © 1992 John Wiley & Sons, Inc.
 CCC 0895-2477/92/\$4.00

The variation of input impedance along the circumference can be explained as follows. An ordinary circular patch

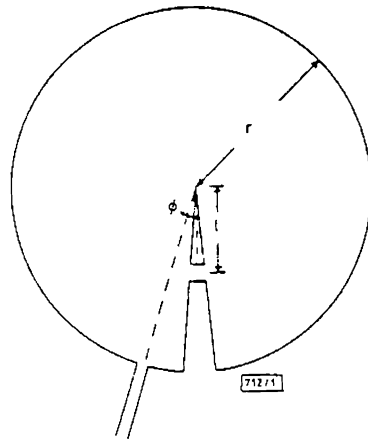


Fig. 1 Schematic diagram of antenna

MODIFIED CIRCULAR PATCH ANTENNA

S. Dey, C. K. Aanandan, P. Mohanan and K. G. Nair

Indexing terms: Antennas, Microstrip

A circular microstrip antenna with a modified structure is presented. By adjusting the feed location along the circumference of the patch it is possible to match the antenna with a microstrip line of any impedance. The impedance bandwidth and radiation characteristics are unaffected by this structural modification.

Introduction: Owing to their excellent properties such as light weight, conformal nature and low production cost, microstrip antennas are widely used as radiating elements in phased arrays. Commonly employed microstrip radiating elements are rectangular and circular patches [1, 2]. The advantage of the circular patch over the rectangular patch is the smallness of the area. However, the high input impedance along the circumference restricts the direct use of 50 Ω microstrip line as a feed for circular patch antennas. Direct matching of a circular patch to a 50 Ω feed line is possible only through a coaxial feed because the matching point always lies within the patch. This increases the fabrication cost and design complexity and makes it unsuitable for microwave integrated arrays.

In this Letter, a modified design of the circular patch rectifying the above defect is presented. A sectoral slot with a shunt element offers a wide variation in input impedance along the circumference of the patch. Thus by simply adjusting the location of the feed point, this antenna can be matched to a microstrip feed line of any impedance, as in the case of a rectangular patch, without deteriorating the radiation characteristics.

Design and experimental details: The schematic diagram of the proposed microstrip antenna configuration is shown in Fig. 1. A sectoral slot is cut on the circular patch and the slot is shunted by a conducting strip, which acts as a perturbing element and modifies the current distribution on the patch surface. The location of the feed is specified in terms of angle ϕ with respect to the centre of the slot.

The antenna is fabricated on a dielectric substrate having thickness $h = 0.16$ cm and dielectric constant $\epsilon_r = 4.5$. The radius of the patch r is 4.95 cm and the sectoral slot angle is 6°. The position of the shunt from the centre of the circle is 2.35 cm and the width of the shunt is 0.5 cm.

The measured input impedance of the patch antenna at resonance, at various points along the circumference, is shown in Fig. 2. The variation in input impedances ranges from 36 to 99 Ω and is 50 Ω when the feed point corresponds to $\phi = 12^\circ$. It is possible to obtain an input impedance of 50 Ω at different values of ϕ depending on the slot angle and the shunt position. From the graph it can also be seen that there is a slight variation of ~ 6 MHz in resonance frequency with feed location.

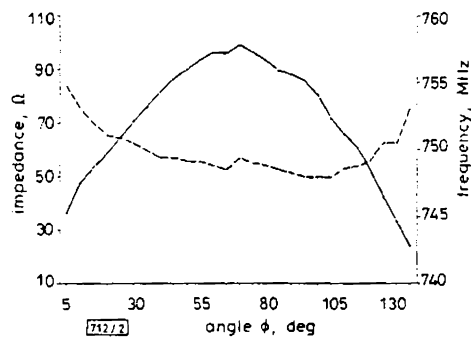


Fig. 2 Variation of input impedance and resonance frequency with angle ϕ

— impedance
- - - frequency

antenna is always symmetric with respect to the feed located on the circumference. Hence the impedance for the dominant mode varies only along the radius. However, in this case, owing to the slot and the shunt element, the structure is asymmetric so that the variation in impedance also depends on the position of the feed point along the circumference.

Fig. 3 shows the variation of VSWR with frequency for a 50 Ω feed line with $\phi = 12^\circ$. From the Figure, the input VSWR of the antenna at 752 MHz is 1.05. The resonance frequency for a circular patch, having the same radius, at the dominant mode is 840 MHz [3]. The decrease in resonance frequency for the new structure is due to the effective increase in circumference of the patch due to the slot.

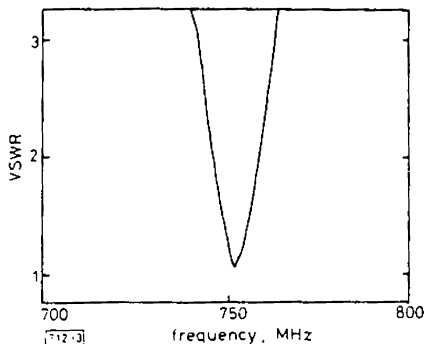


Fig. 3 Variation of VSWR with frequency for $\phi = 12^\circ$

E and H-plane radiation patterns, at resonance are shown in Fig. 4a and b, respectively. As in the case of the circular

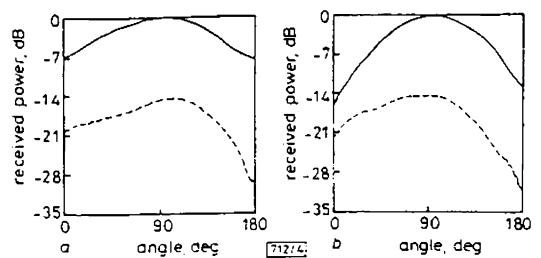


Fig. 4 Radiation patterns

— copolar
 - - - crosspolar
 a E-plane
 b H-plane

patch, the 3 dB beamwidth of the E-plane radiation pattern is slightly more than that of the H-plane pattern. The 3 dB beamwidths of E and H-plane patterns are 100 and 85°, respectively. In both the cases, crosspolar patterns are at least 15 dB down compared to the corresponding copolar patterns. Thus, the experimental results show that there is not much deviation in the radiation characteristics of this antenna compared to the conventional circular patch antenna.

Conclusion: A modified design of a circular patch antenna, showing wide variation in input impedance along the circumference of the patch, is presented. The impedance tuning capability of the circular patch is achieved without deteriorating the antenna radiation characteristics. This antenna can be used as a radiating element in large phased arrays implementing a corporate feeding structure.

Acknowledgment: S. Dey acknowledges the University Grants Commission, Govt. of India, for providing a research fellowship. The authors acknowledge the UGC and MHRD, Govt. of India, for financial support.

© IEE 1993

14th April 1993

S. Dey, C. K. Aanandan, P. Mohanan and K. G. Nair (Department of Electronics, Cochin University of Science & Technology, Kochi 682 022, India)

References

- 1 SANFORD, G. G.: 'Conformal microstrip phased array for aircraft tests with ATS-6', *IEEE Trans.*, 1978, AP-26, pp. 642-646
- 2 BAILEY, M., and PARKS, F.: 'Design of a microstrip disc antenna arrays', NASA Tech., 1978, Memo 78631
- 3 BHAL, I. J., and BHATRIA, P.: 'Microstrip antennas' (Artech House, Dedham, MA, 1981)

Novel Wide Band Printed Dipole Antenna

SUPRIYO DEY, C K AANANDAN, P MOHANAN AND K G NAIR, FIETE

Department of Electronics, Cochin University of Science & Technology, Kochi 682 022, India

Design, development and experimental observations of a L-band printed dipole antenna is presented. Bandwidth enhancement is achieved by end-loading of the dipole arms. Using the present technique impedance bandwidth can be enhanced up to 50% without degrading the efficiency of the antenna.

A simple dipole is of great interest not only historically but also as a feed for reflector antennas with low aperture blockage. Dipoles are also commonly used as building blocks in phased array technology.

This is an era of microstrip antennas because of their excellent properties like low profile, light weight and smallness in size. They can be made conformal to the nozzle of the missiles and rockets and can be easily mass produced with very high precision at a low cost with photo-etching techniques.

In the past few years, dipoles etched on the same side or on either side of a dielectric substrate, with or without reflector has drawn the attention of many researchers [1,2]. Printed dipoles provide minimum aperture blockage and due to their light weight nature, they can be used as an ideal radiating element in electronically scanned phased arrays. Bailey [3] has reported a cavity backed printed dipole antenna having 37% impedance bandwidth. The rigid requirement of the cavity restrict the use of this antenna in certain applications. Recently, the authors have reported a new printed dipole antenna offering an impedance bandwidth of 42% without any cavity backup [4]. This paper is the extension of the above work for further enhancement of the impedance bandwidth.

DESIGN APPROACH

As reported in [4], considerable enhancement in impedance bandwidth is possible by end-loading the dipole arms using triangular shape at the end of the dipole arms. Experimental investigation shows that a rectangular end-loading instead of a triangular one gives better impedance bandwidth. Further enhancement is achieved by keeping the main arm slightly shorter than the ground arm.

Figure 1 shows the schematic of the antenna structure, with solid line as main arm and dotted line as ground arm, etched on either side of a dielectric substrate. The low input impedance of the dipole is matched with 50 Ω feedline using an impedance transformer. To compensate the inductive part, due to endloading, a stub is also used. The antenna can be placed over a reflector plate, acting as cavity, to produce unidirectional pattern.

DESIGN DETAILS

For clarity the main arm and the ground arm are shown

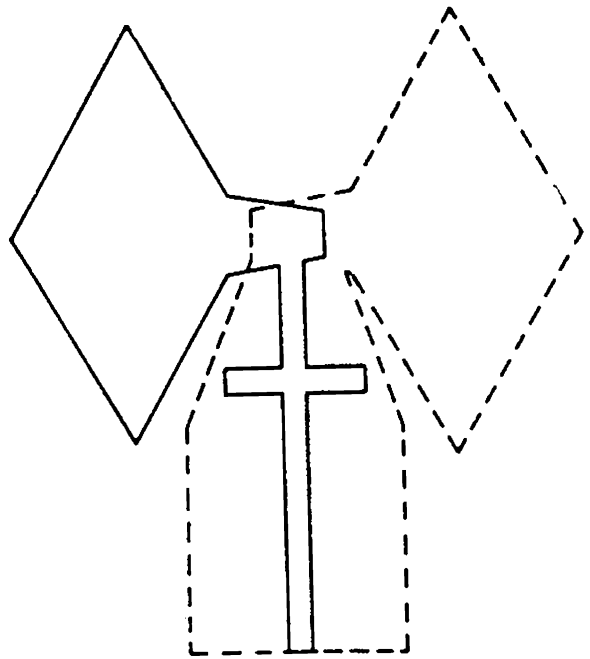


Fig 1 Schematic of the dipole (dotted line shows the ground arm etched on the other side of the substrate)

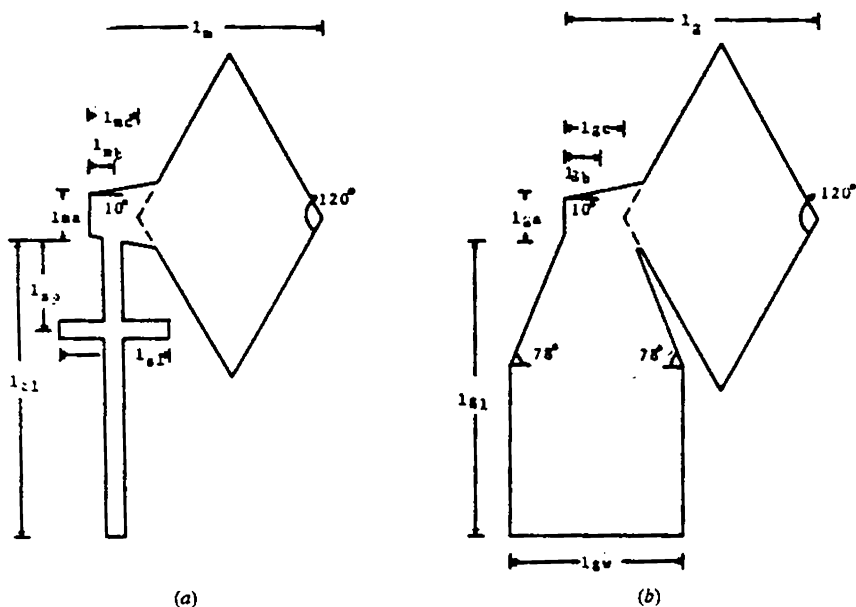


Fig 2 Schematic of the dipole (a) main arm (b) ground arm

separately in Fig 2a and 2b. The experimentally optimized design data are given in Table 1.

TABLE 1 Design data for a dipole antenna

Main arm	Ground arm
$l_m = 0.2425 \lambda_0$	$l_g = 0.256 \lambda_0$
$l_{ma} = 0.05 \lambda_0$	$l_{ga} = 0.055 \lambda_0$
$l_{mb} = 0.025 \lambda_0$	$l_{gb} = 0.0375 \lambda_0$
$l_{mc} = 0.055 \lambda_0$	$l_{gc} = 0.06 \lambda_0$
$l_{md} = 0.055 \lambda_0$	$l_{gd} = 0.545 \lambda_0$
$l_{me} = 0.23 \lambda_0$	$l_{ge} = 0.19 \lambda_0$
$l_{mf} = 0.135 \lambda_0$	

Here λ_0 is the free space wavelength at central frequency and $\lambda_d = \lambda_0 / \sqrt{\epsilon_r}$ is the wavelength inside the substrate. Both the transformer and the stub are having the line impedance of 42 Ω . The above design data are same for both type of dipoles, with and without reflector. The optimum spacing between the antenna and the reflector is found to be $0.3 \lambda_0$.

EXPERIMENTAL DETAILS

An antenna is fabricated over a dielectric substrate ($\epsilon_r = 4.5$, thickness $h = 1.6$ mm) to operate at the central frequency of 1.5 GHz. The central frequency of the antenna with reflector is found to be 1.506 GHz and that without reflector is 1.51 GHz.

Figure 3 shows the input VSWR variation of the antenna with and without reflector. The 2:1 VSWR bandwidth of the antenna with and without reflector are 51% and 48% respectively.

The E and H-plane radiation patterns of the antenna with and without reflector are given in Fig 4a, 4b, 4c and 4d. The deviation of the H-plane radiation patterns of the antenna from conventional half-wave dipole may be due to the radiation from feed structure. As evident from Fig 4c and 4d, there is a slight depression in the patterns at bore-sight at higher frequencies in the case of antenna with reflector. This is due to increase in the effective separation between the antenna and the reflector with increase in frequency.

The gain of the antenna with reflector is compared with a rectangular microstrip patch of same physical area and etched on same dielectric substrate. The microstrip patch antenna is matched at 1.5 GHz. The gain of the dipole is

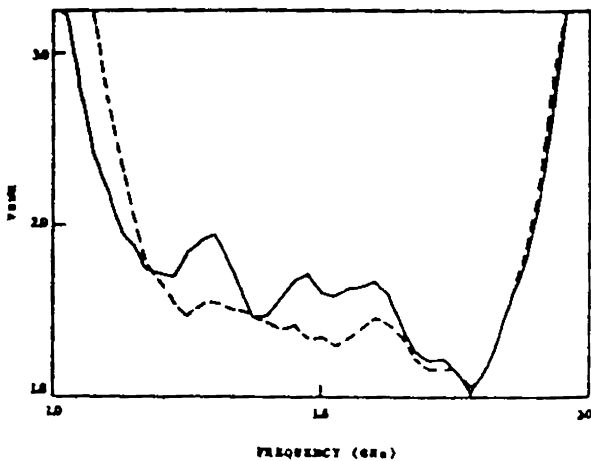


Fig 3 Variation of VSWR with frequency — with reflector, --- without reflector

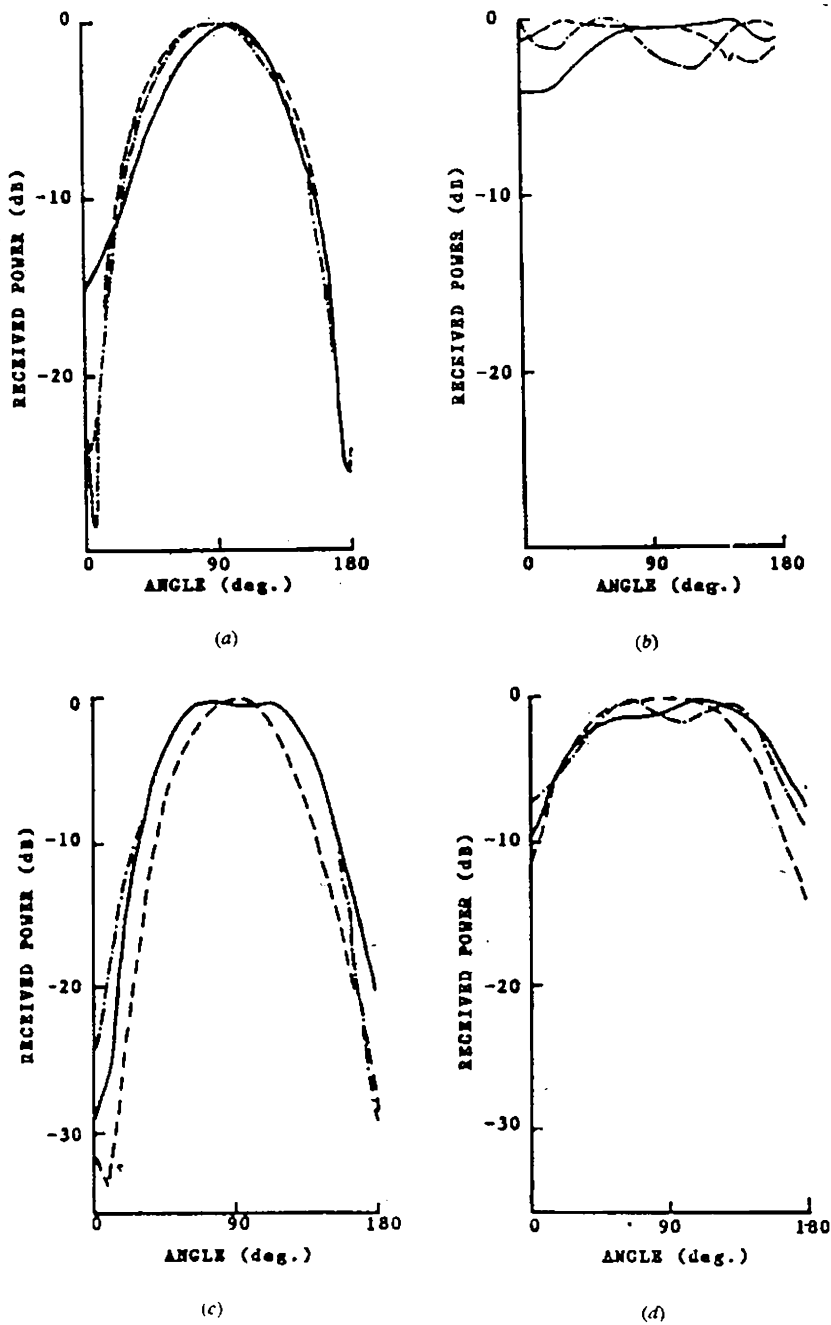


Fig 4 Radiation patterns of the antenna at different frequencies
1.15 GHz, ——— 1.5 GHz, - - - 1.8 GHz.
 (a) E-plane, without reflector (b) H-plane, without reflector
 (c) E-plane, with reflector (d) H-plane, with reflector

found to be 1 dB more than that of microstrip patch.

CONCLUSION

The design and experimental details of an L-band printed dipole antenna with more than 48% impedance bandwidth

are given after extensive exploration. The bandwidth enhancement is achieved without sacrificing the radiation efficiency of the antenna. This antenna can be used as radiating elements in phased array applications and also as a primary feed in deep reflectors.

ACKNOWLEDGEMENT

One of the authors, Supriyo Dey acknowledges University Grants Commission, Govt of India, for providing a research fellowship. The research work is carried out by the financial support under COSIST programme.

REFERENCES

1. W C Wilkinson, A class of printed circuit antennas, *Dig Int Symp Antenna Propagat Soc.*, Atlanta GA, pp 270-273, June 1974.
2. R W Othius, Printed circuit antenna for radar altimeter, *Dig Int Symp Antenna Propagat Soc.*, Amhorst MA, pp 554-557, Oct 1976.
3. M C Bailey, Broad-band half wave dipole, *IEEE Trans. Antenna, Propagat.*, vol 37, pp 410-412, Apr 1984.
4. Supriyo Dey, K A Jose, C K Aanandan, P Mohanan & K G Nair, Wide-band printed dipole antenna, *Microwave and Optical Tech. Letts.*, vol 4, pp 417-419, Sep 1991.